AFRL-MN-EG-TR-2000-7017

ENVIRONMENTAL EFFECTS OF TUNGSTEN AND TANTALUM ALLOYS

Dr. Arend Meijer
Mr. Gregory Wroblicky
Ms. Sarah Thuring
Mr. Michael W. Marcell
GCX, Inc.
3821 Anderson Ave. SE
Albuquerque, NM 87108-4304

Program Manager: Ms. Tonya Cheek
AFRL/MNMI
101 West Eglin Blvd
Eglin AFB, FL 32542-6810

CONTRACT NO. FO8630-95-C-0071 and FO8630-96-C-0024

October 1998

FINAL REPORT FOR PERIOD: JUNE 1995-OCTOBER 1998

APPROVED FOR PUBLIC RELEASE, DISTRIBUTION UNLIMITED

AIR FORCE RESEARCH LABORATORY, MUNITIONS DIRECTORATE

Air Force Materiel Command ■ United States Air Force ■ Eglin Air Force Base

20000410 061

NOTICE

WHEN GOVERNMENT DRAWINGS, SPECIFICATIONS, OR OTHER DATA ARE USED FOR ANY PURPOSE OTHER THAN IN CONNECTION WITH A DEFINITE GOVERNMENT-RELATED PROCUREMENT, THE UNITED STATES GOVERNMENT INCURS NO RESPONSIBILITY OR ANY OBLIGATION WHATSOEVER. THE FACT THAT THE GOVERNMENT MAY HAVE FORMULATED OR IN ANY WAY SUPPLIED THE SAID DRAWINGS, SPECIFICATIONS, OR OTHER DATA IS NOT TO BE REGARDED BY IMPLICATION, OR OTHERWISE IN ANY MANNER CONSTRUED, AS LICENSING THE HOLDER, OR ANY OTHER PERSON OR CORPORATION; OR AS CONVEYING ANY RIGHTS OR PERMISSION TO MANUFACTURE, USE, OR SELL ANY PATENTED INVENTION THAT MAY IN ANY WAY BE RELATED THERETO.

Small Business Innovation Research Program (SBIR)
GOVERNMENT PURPOSE LICENSE RIGHTS LEGEND
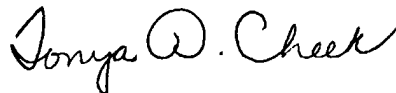Contract Numbers: FO8630-95-C-0071 and FO8630-96-C-0024
Contractor: GCX, Inc.

For a period of four (4) years after the delivery and acceptance of the last deliverable item under the above contract, all technical data contained in this report shall be subject to the restrictions contained in the definition of "Limited Rights" in DFARS clause 252.227-7013 (Oct. 1988). After the four-year period, the data shall be subject to the restrictions contained in the definition of "Government Purpose Rights" in DFARS clause 252.227-7013 (Oct. 1988). The Government assumes no liability for unauthorized use or disclosure by others. This legend, together with the indications of the portions of the data which are subject to such limitations, shall be included on any reproduction hereof which contains any portions subject to such limitations and shall be honored only as long as the data continues to meet the definition on Government purpose license rights.

This technical report has been reviewed and is accepted under the provisions of the Small Business Innovation Research Program.

AARON D. BRINSON
Technical Director
Ordnance Division

TONYA D. CHEEK
Program Manager

Even though this report may contain special release rights held by the controlling office, please do not request copies from the Air Force Research Laboratory, Munitions Directorate. If you qualify as a recipient, release approval will be obtained from the originating activity by DTIC. Address your request for additional copies to:

Defense Technical Information Center
8725 John J. Kingman Road, Ste 0944
Ft Belvoir VA 22060-6218

This report is published in the interest of the scientific and technical information exchange. Publication of this report does not constitute approval or disapproval of the ideas or findings. Do not return copies of this report unless contractual obligations or notice on a specific document requires its return.

REPORT DOCUMENTATION PAGE

Form Approved
OMB No. 0704-0188

1. AGENCY USE ONLY (Leave blank)	2. REPORT DATE October 1998	3. REPORT TYPE AND DATES COVERED Final; June 1995-October 1998

4. TITLE AND SUBTITLE
Environmental Effects of Tungsten and Tantalum Alloys

5. FUNDING NUMBERS
Contract #: F08630-95-C-0071 and
F08630-96-C-0024
JONs: 30055330 (1998) and 30055331
(1996)

6. AUTHOR(S)
Dr. Arend Meijer, Mr. Gregory Wroblicky, Ms. Sarah Thuring and Mr. Michael W. Marcell

7. PERFORMING ORGANIZATION NAME(S) AND ADDRESS(ES)
GCX, Inc.
3821 Anderson Ave. SE
Albuquerque, NM 87108-4304

8. PERFORMING ORGANIZATION REPORT NUMBER

N/A

9. SPONSORING/MONITORING AGENCY NAME(S) AND ADDRESS(ES) (Program Mgr Name & Ph #)
Air Force Research Laboratory, Munitions Directorate
AFRL/MNMI
101 West Eglin Blvd., Ste. 258
Eglin AFB, FL 32542-6810
POC: Ms. Tonya Cheek, (850) 476-4173 ext. 2248, cheekt@eglin.af.mil

10. SPONSORING/MONITORING AGENCY REPORT NUMBER

AFRL-MN-EG-TR-2000-7017

11. SUPPLEMENTARY NOTES
Report encompasses Phase I and Phase II studies

12a. DISTRIBUTION/AVAILABILITY STATEMENT
Approved for public release - Distribution unlimited

12b. DISTRIBUTION CODE
(Leave this block blank)

13. ABSTRACT:
Report developed under SBIR contract (covers Phase I and Phase II studies).
The purpose of this study was to evaluate the potential environmental impacts of the testing of tungsten alloy and tantalum penetrator munitions at Test Site C-64 A on Eglin AFB, FL. The tungsten alloys that were investigated in this study contained iron, nickel, cobalt, copper, and/or manganese as alloying elements. Data on physical, chemical, and biological site conditions were obtained from field studies and published reports. These data were used to design and carry out leaching/corrosion studies on the penetrator alloys in the laboratory. The data obtained in the laboratory studies were combined with additional site data to quantify the potential environmental impacts of munitions testing at Site C-64 A through the use of a computer code called the Multimedia Environmental Pollutant Assessment System (MEPAS) developed by Pacific Northwest National Laboratory. The results obtained from the MEPAS code indicate that the tungsten alloy containing cobalt will have the least impact, while the alloy containing copper would have the greatest impact. The conclusions assume that the deposition rate of metal/alloy on the site is less than or equal to 500 lbs/yr. The calculations further indicate that testing of the tungsten alloy or tantalum penetrator munitions on the C-64 A test site would not pose unacceptable risks to humans or the environment.

14. SUBJECT TERM
Environmental impacts of tungsten/tantalum, tungsten alloys, tantalum, tungsten leach rates, SBIR Report

15. NUMBER OF PAGES
~~287~~ 286 p

16. PRICE CODE
N/A

17. SECURITY CLASSIFICATION OF REPORT UNCLASSIFIED	18. SECURITY CLASSIFICATION OF THIS PAGE UNCLASSIFIED	19. SECURITY CLASSIFICATION OF ABSTRACT UNCLASSIFIED	20. LIMITATION OF ABSTRACT UL

NSN 7540-01-280-5500

Standard Form 298 (Rev. 2-89)
Prescribed by ANSI Std. 239-18

TABLE OF CONTENTS

TABLE OF CONTENTS

(Continued)

TABLE OF CONTENTS

(Continued)

TABLE OF CONTENTS

(Continued)

LIST OF FIGURES

LIST OF FIGURES

(Continued)

LIST OF FIGURES

(Continued)

LIST OF FIGURES

(Continued)

LIST OF FIGURES

(Continued)

LIST OF FIGURES

(Continued)

LIST OF FIGURES

(Continued)

LIST OF TABLES

LIST OF TABLES

(Continued)

LIST OF TABLES

(Continued)

ACRONYMS

ACGIH	American Conference of Government Industrial Hygienists
AET	actual evapotranspiration
AFB	Air Force Base
AFRL	Air Force Research Laboratory
AT	averaging time
BW	body weight
CFS	cubic feet per second (ft^3/sec)
DO	dissolved oxygen
ED	exposure duration
EDXA	Energy Dispersed X-ray Analysis
EF	exposure frequency
Eh	oxidation-reduction potential
EPA	Environmental Protection Agency
Gf	gastrointestinal tract absorption fraction coefficient
GI	gastrointestinal
HI	hazard index
HQs	hazard quotient
ICP-MS	Inductively Coupled Plasma Mass Spectrometry
IR	intake rate
IRIS	Integrated Risk Information System (EPA)
K_d	sorption coefficient
MEPAS	Multimedia Environmental Pollutant Assessment System
mya	million years ago
NADP	National Atmospheric Deposition Program
Ne	effective porosity
NIOSH	National Institute for Occupational Safety and Health
OSHA	Occupational Safety and Health Administration

ACRONYMS

(Continued)

PET	potential evapotranspiration
R_f	retardation factor
RfD	reference dose
RME	reasonable maximum exposure
SAF	soil accumulation factor
SCS	Soil Conservation Service
SEM	Scanning Electron Microscope
STEL	short-term exposure limit
THI	temperature humidity index
TLV	threshold limit value
TWA	time weighted average
USDA	United States Department of Agriculture
USEPA	United States Environmental Protection Agency
V/S	volume/surface area

EXECUTIVE SUMMARY

The purpose of this study was to evaluate the potential environmental impacts of the testing of tantalum and/or tungsten alloy penetrator munitions at the Test Area C-64A on Eglin AFB, Florida. The tungsten alloys are composed primarily of tungsten (88-92%) and nickel (5.0-6.6%). In addition, each alloy contains several percent of either cobalt, copper, or manganese. The potential environmental impacts of the testing of these alloys at Test Area C-64A were quantified using the computer code called Multimedia Environmental Pollutant Assessment System (MEPAS) developed by Pacific Northwest National Laboratory. To calculate the potential environmental impacts with this code, data are required on the physical, chemical and ecologic conditions at the site, the local climate, the leaching/ corrosion and migration behavior of the metals in the alloys in waters and soils from the site and surrounding area, and on population density and agricultural production in the surrounding region. These data were obtained either from published sources or through field studies and direct experiments.

Field studies were carried out to better define the hydrologic regime at the Test Area C-64A. Experimental studies were carried out to quantify the leaching/corrosion behavior of the alloys in water compositions representative of the site and to derive sorption coefficients for the metals of interest on soils from the site. Both immersion tests and drip tests were conducted to derive leach rates for the different metals as a function of pH, water composition and time. The results of leaching/corrosion studies indicate that the copper containing tungsten alloy is leached most readily whereas tantalum metal is least readily leached or corroded. Compounds containing the metals of interest precipitated in many of the long-term immersion experiments and impacted metal concentrations in solution. However, the fact that rainwater has a short residence time (minutes to hours) in the soil zone at the site suggests metal concentrations in waters infiltrating below the soil zone will reflect primarily leaching reactions unhindered by compound formation. Sorption experiments indicate that tantalum and tungsten are strongly bound on mineral grains in the soil zone and will remain in this zone indefinitely. The other metals will gradually be leached into the vadose zone eventually to groundwater.

Of the metals contained in the alloys, only nickel is potentially carcinogenic to humans. Copper, cobalt, and manganese are associated with various human and ecologic impacts at sufficiently high doses. Tungsten and tantalum appear to have minimal human and ecologic impacts based on the available data. The potential human risks associated with the testing of the different penetrator alloys at Test Area C-64A were estimated using the MEPAS computer models with appropriate inputs of physical, chemical, climatic, agricultural, and demographic data. The calculated risk factors indicate that any of the four alloys could be used in munitions testing at Test Area C-64A without unacceptable human or ecologic risk. If testing occurred at the rate assumed in this study and if humans were to inhabit the site in the future, the calculations suggest that the use of the copper-containing alloy (HD-17) in testing would pose the highest risk. This risk results primarily from copper in the alloy that would be taken up by agricultural products grown and consumed on the site. The use of tantalum would pose the smallest future human risk while the use of tungsten alloys containing manganese (alloy WL-1) and cobalt (alloy NS) would pose somewhat higher risks. The potential risk associated with the use of manganese alloys may be slightly greater than that associated with the use of cobalt alloys. Analysis of potential ecologic risks indicates no unacceptable risks will result from the use of tantalum and/or tungsten alloys in the testing of penetrator munitions at Test Area C-64A on Eglin AFB.

1.0 INTRODUCTION

Over the past few years, the AFRL Munitions Directorate has begun to promote the development of "green munitions" for the future Air Force arsenal. "Green" weapons are considered to be weapons in which more environmentally sound materials are used to replace hazardous materials used in the body of a weapon. By developing more environmentally sound materials, the risk of adverse environmental effects associated with the research, development and testing of these munitions can be minimized or even eliminated. Two such materials proposed for use in kinetic energy penetrators and other munitions are Tungsten and Tantalum. Part of the evaluation process for the testing of munitions containing these alloys will consist of open field tests of prototype munitions. It is assumed in this report that many of these tests will be carried out at Test Area C-64A on Eglin AFB (Figure 1.1). The tungsten alloys are considered to contain other metals that are potentially toxic to humans and/or other organisms at high concentrations. Since such a risk may be unacceptable for a "green munition", an evaluation of the potential environmental impacts of the use of these alloys on test ranges at Eglin AFB was solicited. The results from this report can be used to rank the alloys in terms of potential environmental risks associated with their dispersal on test ranges.

In order to evaluate the potential environmental impacts of the use of tungsten alloys on open test ranges, a multi-pathway risk analysis was performed. This type of analysis required various types of experimental and environmental input data. For example, data were required on the composition, form and mass of alloy material to be dispersed on the test ranges. Data were also required on the corrosion and dissolution behavior of these alloys under the environmental conditions at the test ranges. Additional data were required on the hydrology and environmental conditions at the test ranges. All of these data were combined to identify possible exposure pathways and exposure concentrations. Finally, the potential exposure concentrations were evaluated in light of potential risk factors and regulatory constraints.

Figure 1.2 provides a flowchart of the data and analysis required to complete the risk analysis and impact assessment. Because information on certain characteristics of the test sites

(e.g., climate data, water chemistry, soil types, precipitation rates, etc.) was required to carry out the laboratory analyses on the alloys, this information is discussed first in Section 2. The results of laboratory corrosion and dissolution tests on alloy compositions are discussed in Section 3. This discussion provides the basis for a source term calculation. Also reported in this section are the results of tests to determine the extent to which the metals in the alloys are bound by the soils at the sites. The parameter determined in these tests is the sorption coefficient. Section 4
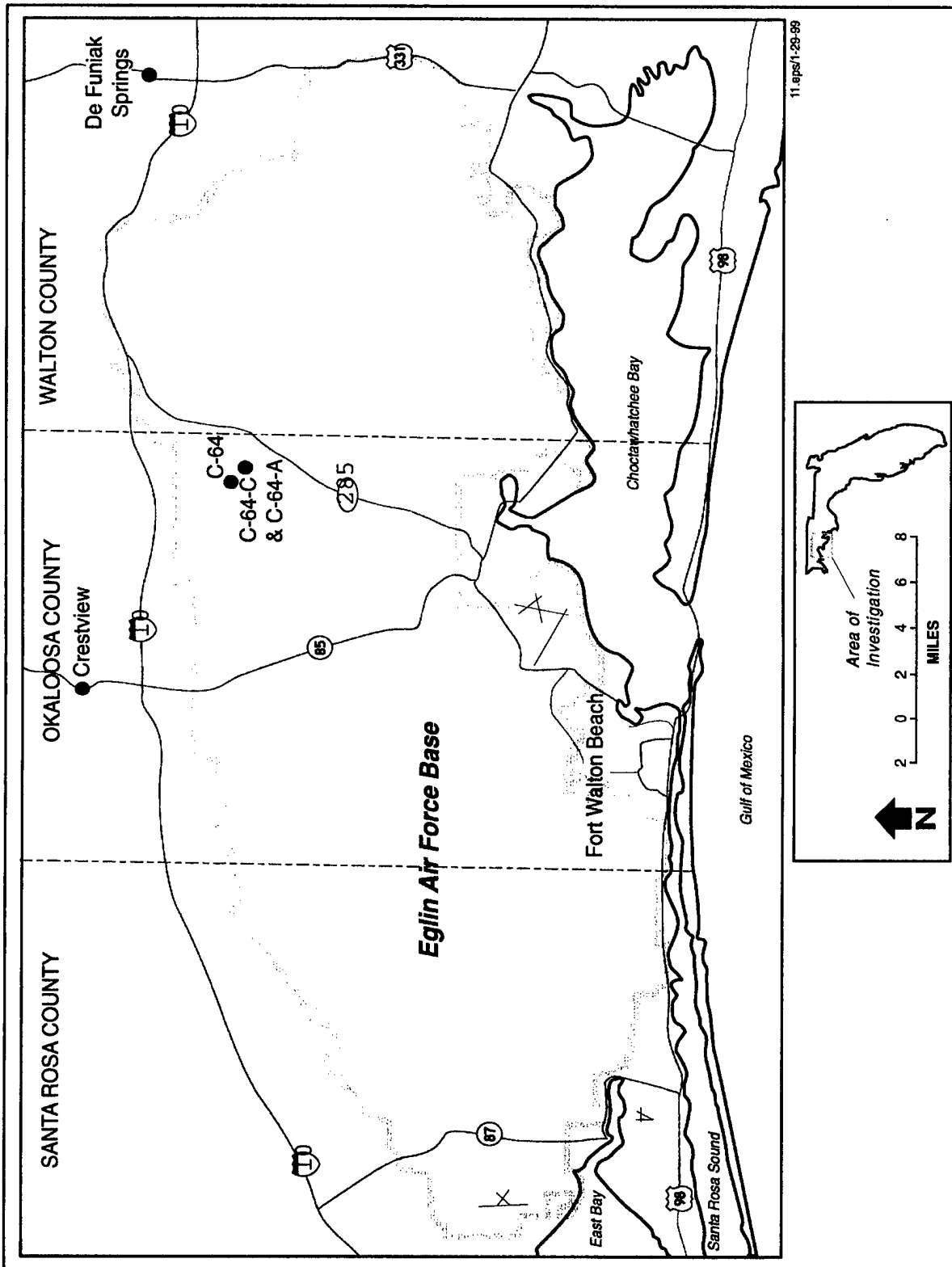
Figure 1.1. Location map of Eglin Air Force Base and munition Test Area C-64A.
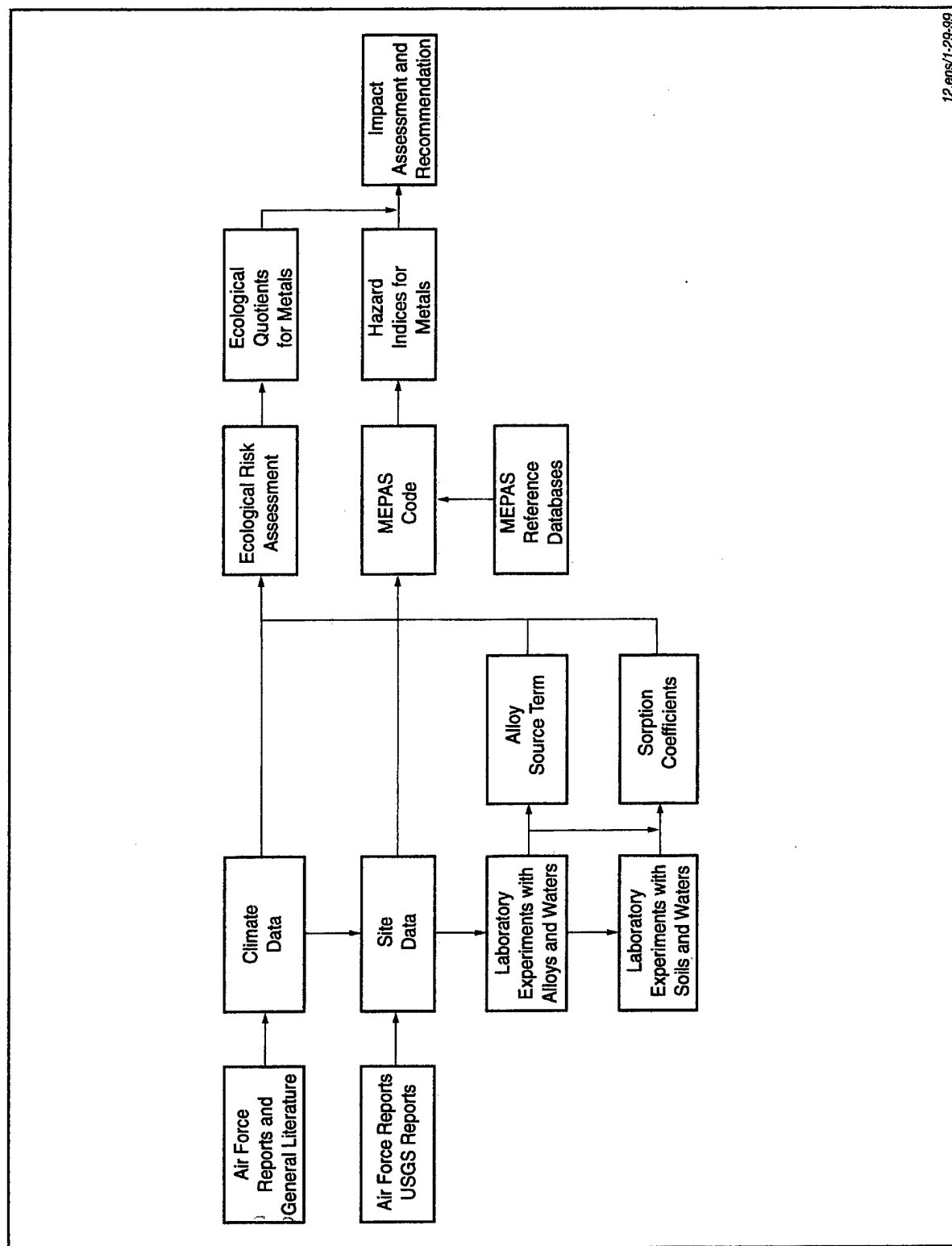
Figure 1.2. Flowchart of the data and analysis required to complete the risk analysis and impact assessment.

discusses information available on the toxicology of the metals contained in the alloys. The source term data are combined in Section 5 with the sorption coefficient data, toxicologic data, and other data for the sites that are required to perform human and ecologic risk analyses. These analyses are used to calculate hazard indices and ecological quotients for the testing of tantalum and tungsten alloy munitions at the Eglin site. These indices and quotients are used in Section 6 to develop a long-term impact assessment for the dispersal of the different alloys on the test sites. Based on this assessment, recommendations are made in Section 7 regarding the use of different alloys in the testing programs. The data for various laboratory analyses and calculations are provided in several appendices.

2.0   SITE CHARACTERISTICS

2.1   Physiography

Test Area C-64A is located in the Western Highlands, one of three divisions of the Gulf Coastal Plain Physiographic Province, including the Coastal Lowlands and the Coastal Barrier Island Chain, which are occupied by Eglin AFB (US Air Force, 1995). The Western Highlands in the vicinity of Test Area C-64A consist of sandhills characterized by highly permeable sands which exhibit high infiltration, low runoff and drainage density, and high stream base flow runoff.

2.2   Climate

Southern Okaloosa and Walton Counties have a humid, subtropical climate characterized by an abundance of sunshine and rainfall, warm and humid summers, and mild winters. Table 2.1 presents climatic data collected at Eglin AFB Main Weather Station.

Winters at Eglin AFB are mild, with occasional frost from November through February. Annual rainfall averages approximately 61.6 inches, and occurs primarily in the summer and late winter or early spring. Average rainfall in excess of potential evapotranspiration ranges between 15 and 20 inches in Northwest Florida, the highest in the state (Fernald et al., 1992). Average rainfall ranges from 3.3 inches in October to 7.9 inches in July. Most of the summer rainfall results from scattered showers and thunderstorms that are often heavy and last only 1 or 2 hours. Average daily temperatures in the hottest months, July and August, may range from a low of 74° F to a high of 90°F, with an average of approximately 82°F. From December through February, the coldest months, the average daily temperature ranges from a low of 42°F, to a high of 63°F, with an average around 52°F. Relative humidity is high throughout the year. The temperature-humidity index (THI) goes up to 79 by early June and remains between 79 and 81 during most of the afternoon hours until late September.

Table 2.1. Climatic data, Eglin AFB.

Month	Temperature					Precipitation				Average number of days		Relative Humidity (Percent)		Wind Speed (Knots)		Average Sky Cover in 10ths
	Average			Extreme		Average	Max. monthly	Min. monthly	Max. in 24 hrs.	Precipitation	Thunder-storms	Average		Mean Wind	Max. Wind	
	Daily max.	Daily min.	Monthly	Max.	Min.					>0.01 in.		Min. Daily	Max. Daily			
	°F	°F	°F	°F	°F	In	In	In	In							
Jan.	60	42	51	78	9	4.3	9.9	0.2	5.5	9	2	51	88	5.69	43	6.4
Feb.	63	44	54	80	12	4.2	12.7	.3	5.4	9	3	49	86	5.99	54	6.3
Mar.	68	50	60	89	19	6.0	14.4	.4	4.9	10	5	51	89	6.36	44	6.2
Apr.	76	58	67	94	29	4.5	12.1	.3	6.1	6	4	49	89	6.13	47	5.6
May	83	65	74	102	40	3.7	11.8	.0	5.2	7	6	53	90	5.48	51	5.4
June	88	72	80	103	52	5.2	12.3	.9	5.8	10	11	55	89	4.65	40	5.6
July	89	74	82	106	60	7.9	19.9	1.0	5.9	14	17	57	90	4.13	57	6.3
Aug.	90	74	82	104	62	6.9	14.2	2.0	5.6	13	16	58	92	4.12	52	5.9
Sept.	86	70	79	97	43	7.3	23.3	1.3	8.6	9	7	55	90	4.81	58	5.4
Oct.	79	59	69	95	33	3.3	15.0	.0	6.7	5	2	48	86	5.19	100	4.2
Nov.	69	49	59	89	17	3.6	11.9	.2	3.2	7	2	51	87	5.54	35	5.1
Dec.	63	44	53	79	9	4.7	16.6	.6	7.7	9	2	52	87	5.61	38	6.1

1) Data for Eglin AFB Main Weather Station 1939 – 1981 (USDA, 1995), except relative humidity and wind speed, 1973 – 1996 (AFCCC, 1998), and cloudiness, 1938-1996 (AFCCC, 1998)

2) The symbol > means more than; < means less than)

The occurrence of rainfall over the study area can be associated with two types of weather systems, the convective type and the frontal type. The frontal type weather system results from the interaction of low- and high-pressure systems produced by the convergence of polar and tropical air masses and is particularly active during winter when the general atmospheric circulation system is shifted southward. This system is responsible for the occurrence of a peak in rainfall during the period of December through March (Figure 2.1).

The other weather system is of the convective type, more commonly referred to as late afternoon and evening thunderstorms. Convective storms are produced by vertical overturning of air masses; overturning is caused by the rising of warmer, lighter air over colder, denser surrounding air. Convective weather systems are most active in the summer, when solar radiation strikes the earth's northern hemisphere more directly and supplies great amounts of heat for the warming of air masses at the earth's surface. Convective showers are at their peak during the summer months from July through September (Figure 2.1).

Convective storms are characterized by strong, localized showers of relatively short duration as compared to winter frontal storms that are distinguished by less intense showers of longer duration that cover a greater area. Summer rainfall is the highest of the year and also the most variable (Figure 2.1). In September, for example, the record shows that rainfall can vary from a minimum of 1.3 to a maximum of 23.3 inches, a difference of about 22 inches. While July through September are the wettest months, October and November are the driest.

Prevailing winds usually come from the north in winter and from the south in summer. March is the windiest month based on average hourly velocity, while August has the lowest average velocity winds. During summer a moderate sea breeze usually blows off of the Gulf of Mexico, and occasional strong winds are associated with thunderstorms. Figure 2.2 presents an annual wind rose for Eglin AFB located at 30 degrees 29 minutes north latitude and 86 degrees 32 minutes west longitude (US Air Force, 1995).
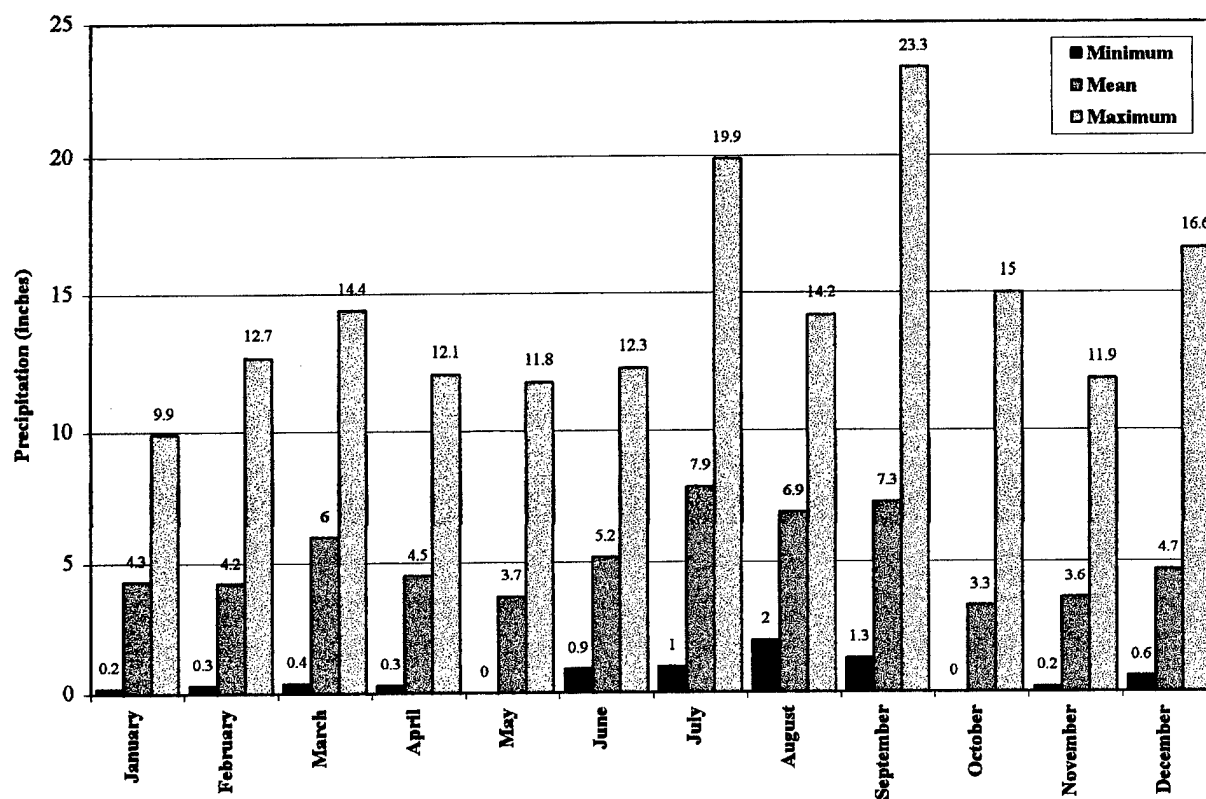
Figure 2.1. Monthly precipitation at Eglin AFB main weather station, 1939-1981.

N

14%
12%
10%
8%
6%
4%
2%

W

E

S

Calm Winds 19.9%

1-4   5-9   10-14   15-19

Wind Speed Classes
(Knots)

Notes: Diagram of the frequency of occurrence for each wind direction.
Wind direction is the direction from which the wind is blowing.
Example-Wind is blowing from the north 13.2 percent of the time.

adapted from U.S. Air Force (1995).

22.eps-9/02/98
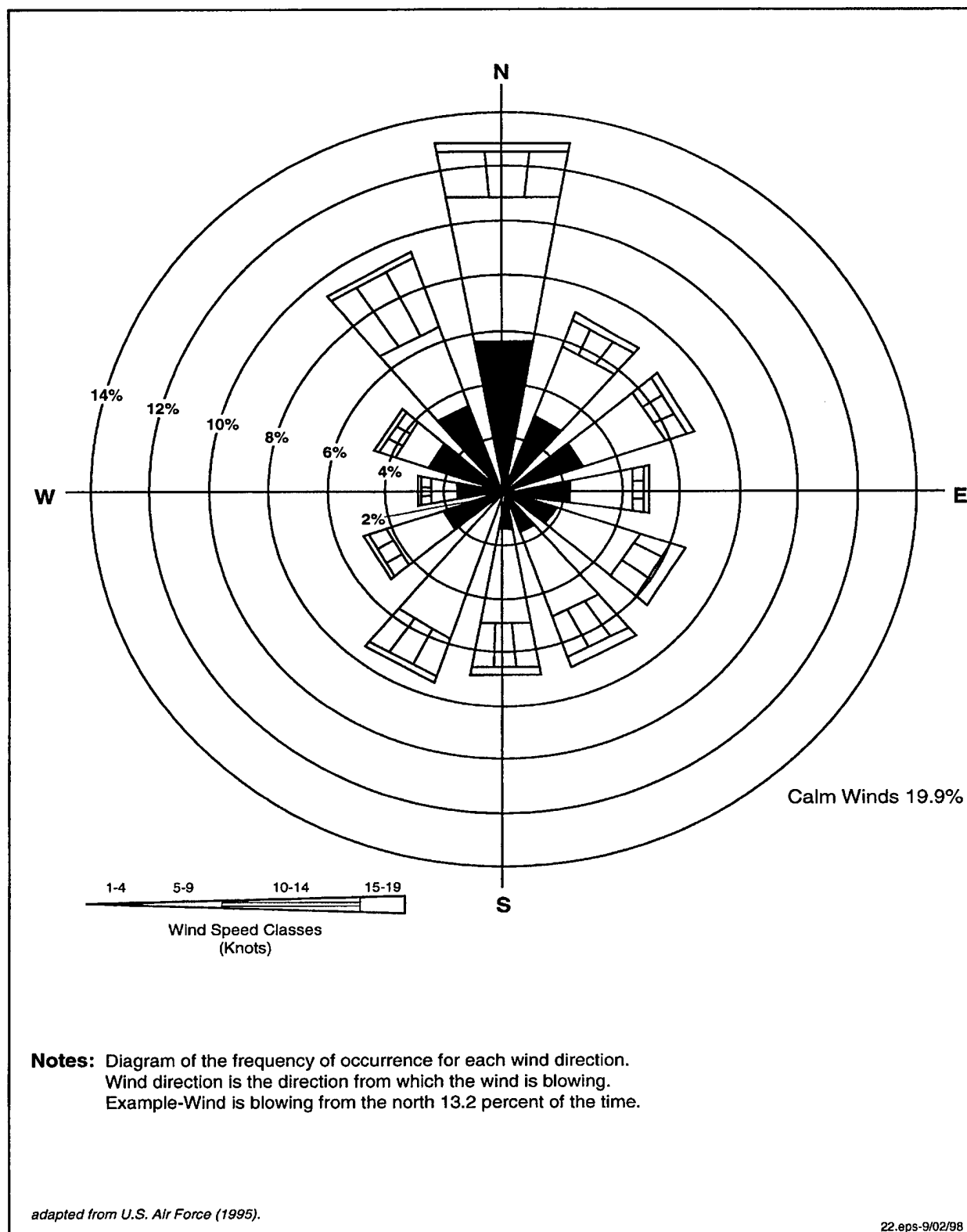
Figure 2.2. Representative wind rose for Eglin AFB: 1983-1992.

2.3 Soils and Geology

2.3.1 Soils

Eglin AFB contains eight major soil associations, with the majority of the base (78%), including Test Area C-64A, covered by Lakeland Series soils. Lakeland Series soils consist of very deep, excessively drained, highly permeable soils that formed in thick, sandy sediments, principally on high elevation ridge tops associated with the sandhills (US Air Force, 1995, USDA, 1995). Other soil series found on Eglin AFB are associated with lower lying drainage areas, flatwoods, and swamps, and exhibit soil textures which range from loamy sand to muck. (US Air Force, 1995)

Lakeland soils are classified as thermic, Typic Quartzipsamments. Figure 2.3 depicts soil type distributions at Test Area C-64A, whereas Table 2.2 presents some physical characteristics typical of Lakeland soils at Test Area C-64A. Lakeland soils are described as dark grayish brown, turning to brownish yellow, yellowish brown, and then yellow at depth, and consist of medium to fine Sand containing 5 to 10 percent silt and clay. Lakeland soils are highly permeable, with very low available water capacity, resulting in almost no runoff. These soils exhibit low natural fertility, and are generally unsuitable to most cultivated crops (USDA, 1995). Due to low clay content, Lakeland series soils lack a Bt horizon and have a very low shrink-swell potential. The designation Bt reflects a soil mineral horizon in which mineral particles accumulated by transport downward from overlying horizons.

LAKELAND
SAND

RAMER

LAKELAND
SAND

C-64C

TROUP
SAND

CREEK

LAKELAND
SAND

C-64A
TEST AREA

TROUP
SAND

C-64A

C-64B

LAKELAND
SAND

TROUP
SAND

0   200' 400'   800'   1600'

N

1" = 800'-0"

FIG2_3.DWG 02/08/99
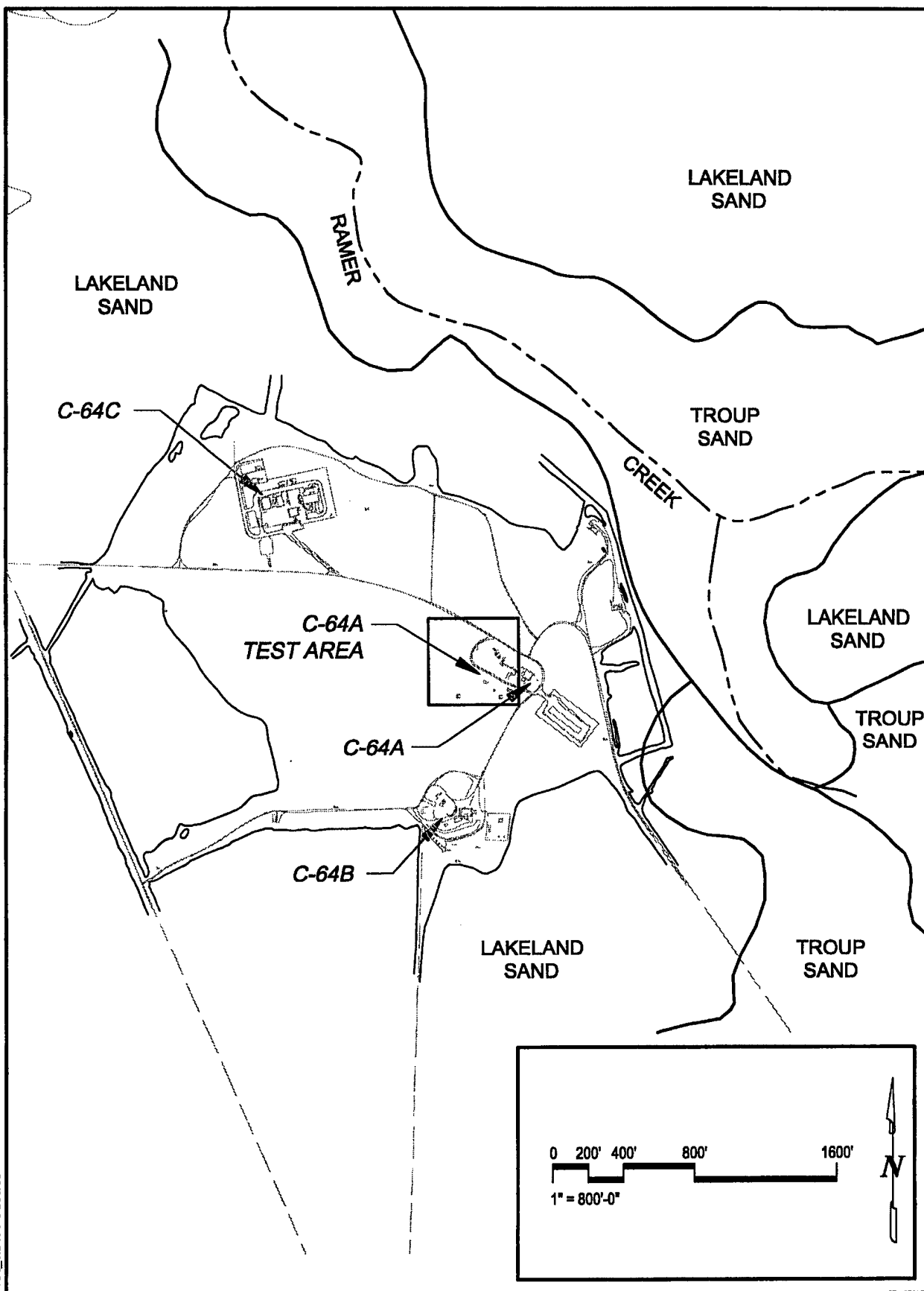
Figure 2.3. Soils near Test Area C-64A.

Table 2.2. Physical characteristics of Lakeland sand soils.

Composition		Range (percent)	Mean %
Sand (2 – 0.05 mm)		90.5 – 94.9	93
Silt (0.05 – 0.002 mm)		2.8 – 5.8	4
Clay (<0.02 mm)		2.3 – 3.7	3
Physical Characteristics			
Depth	in	0 – 80	
Bulk Density (field moist)	g/cm^3	1.35 – 1.65	
Permeability	cm/hr	15 – 48	
Hydraulic Conductivity	cm/hr	35 – 67	
Available Water Capacity	in/in	0.02 – 0.09	
Organic Matter	%	0.04 – 1.02	
pH		4.5 – 6.0	
Soil is Non-plastic, with Low Shrink Swell Potential			

Data from USDA (1995)

Nearby soils associated with Lakeland Series soils include the Chipley, Dorovan, Foxworth, Lucy, and Troup soils. Chipley and Foxworth soils are less well drained with a seasonal high water table within 72 inches of the surface, and occupy lower landscape positions. Dorovan soils are organic and associated with low elevation swamps. Lucy and Troup soils exhibit a Bt (clay rich) horizon which is lacking in Lakeland soils.

2.3.2 Geology

Test Area C-64A and Eglin AFB are located on the Gulf Coastal Plain geosyncline, a thick sequence of unconsolidated to semiconsolidated sedimentary rocks of Jurassic to Holocene age (200 million years ago [mya] to present) that were deposited in fluvial, marginal marine, and shallow marine environments. At Eglin AFB, Gulf Coastal Plain sediments are deposited on an older basement rock complex composed of a complicated mosaic of lower Mesozoic, middle to lower Paleozoic, and upper Precambrian sedimentary, igneous, and metamorphic rocks.

Overall, the configuration of the Gulf Coastal Plain sequence is that of a wedge of sediments that dips and thickens seaward. Superimposed on this wedge are a series of gentle folds that created major headlands and embayments along the coastline over geologic time. Coastal plain sediments beneath Eglin AFB dip and thicken to the southwest and are deposited in the Conech Embayment, a structural low created during regional folding (Miller, 1988; Miller and Johnston, 1988; Fernald et al., 1992). The principle sedimentary lithologic units underlying Eglin AFB are listed in Table 2.3. The locations of several geologic and hydrogeologic sections that depict sedimentary lithologic units underlying Eglin AFB and Southern Okaloosa County are shown in Figure 2.4. The geologic cross-section A-A[1] is presented in Figure 2.5.

Uppermost in the stratigraphic sequence and blanketing the Western Highlands portion of Eglin AFB is the Plio-Pleistocene Citronelle Formation (5 mya to Present). The Citronelle Formation ranges from 50 to 250 ft thick and consists predominantly of nonmarine quartz Sands with relatively thin and discontinuous beds of clay or gravel that are generally not well correlated between outcrops. Two types of sandy clay units have been found in the Citronelle Formation. One is a gray, massive, plastic clay that contains only a small amount of quartz sand. The other unit is generally gray-mottled red and gray and contains more sand. The clay is kaolinitic in both units. The distribution and character of the Citronelle sediments suggest that they represent deposits of several early rivers that emptied into the Gulf of Mexico (US Air Force, 1995).

Soil borings drilled near Test Area C-64C, and in a borrow pit northwest of Test Area C-64 near the outlet of the Bull Creek watershed, revealed sands and silty sands of the Citronelle Formation down to a depth of approximately 100 feet. Distinct sandy clay units were not found in any of the soil borings. Sediments beneath Test Area C-64C near the top of the broad ridge separating Bull and Ramer Creeks are generally coarse-medium sands, along with some silty and clayey silty sands (Figure 2.6). Their average composition based on grain size analysis was 93 percent sand, 4 percent silt and 3 percent clay. These sands ranged in color from brown near the surface to white, pink, tan, yellow, and orange at depth. Occasionally, white chalk was also noted. Sediments in the borrow pit northwest of Test Area C-64 are generally poorly graded

Table 2.3. Geologic units in the southern parts of Okaloosa and Walton Counties and their hydrogeologic equivalents.

Series	Formation or Group	Thickness (feet)	Hydrogeologic Unit
Holocene to Pliocene	Unnamed Holocene to Pliocene Sands and Citronelle Formation, undifferentiated	50-250	Sand-and-Gravel aquifer
Miocene	Miocene coarse clastics	50-200	Pensacola Clay confining bed
	Intracoastal Formation	0-360	
	Alum Bluff Group (northern part only)	0-300	
	Pensacola Clay	0-190	
	Bruce Creek Limestone	20-220	Upper limestone of the Floridan aquifer
Oligocene	Tampa Limestone equivalent and Chickasawhay Limestone, undifferentiated	30-260	
	Bucatunna Formation	0-130	Bucatunna clay confining bed
Eocene	Ocala Limestone	165-600	Lower limestone of the Floridan aquifer
	Lisbon and Tallahatta Formations	345-500 170-300	Lisbon-Tallahatta confining unit

Adapted from Barr et al., (1985).
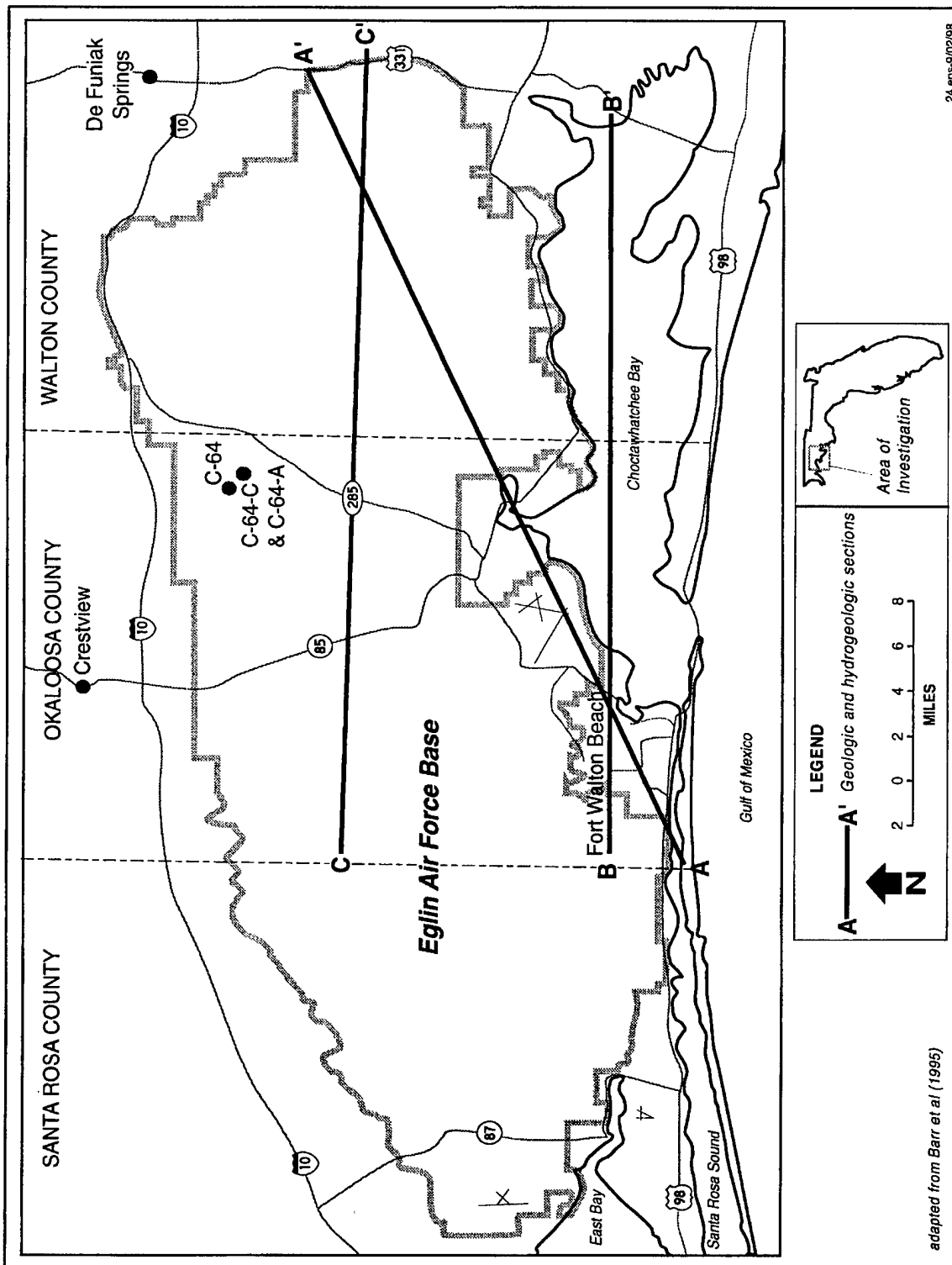
Figure 2.4. Approximate locations of geologic and hydrogeologic cross-sections in Okaloosa and Walton Counties.
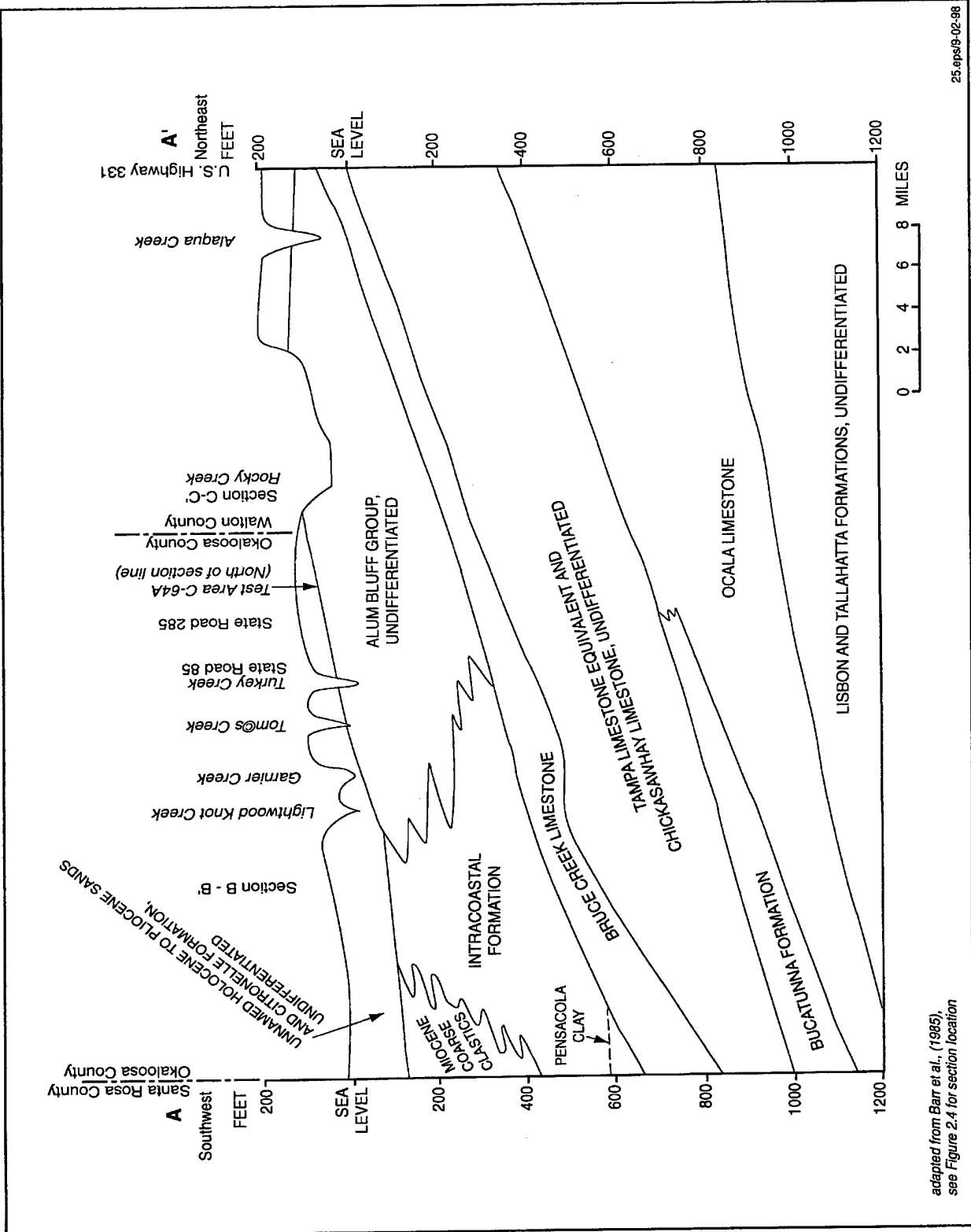
Figure 2.5. Geologic section A – A¹, southwest to northeast through Okaloosa and Walton Counties.

DEPTH Feet	USCS Symbol	Soil Profile	Description
0	SM		Brown Silty Sand
5	SP		Light Brown Sand
10 15 20	SP		Tan Sand
25 30	SM		Orange Silty Sand
35 40	SM		Redish Orange Silty Sand
45	SM		Tan Silty Sand
50	SP		Yellow Sand
55 60	SP		White Sand
65 70	SP		Tan Sand
75	SP		Pinkish Tan Sand
80 85	SP		White and Orange Sand Mixed
90	SM		Orange Clayey Silty Sand with White Lumps of Chalk
95	SP		Orange Sand
100	SP		Pinkish Tan Sand
105	SP		Tan Sand
110 115 120	SP		White Sand
			Boring terminated at 120 feet.

adapted from original log

26.eps/8-20-98

Figure 2.6. Lithologic log of monitoring well MW-3 at Site C-64C.

fine sands, with occasional thin layers of silty sand (15% silt, estimated visually). Colors range from pale to strong brown, to yellow, reddish-yellow, and pink at depth.

The Citronelle Formation is underlain by up to 300 feet of undifferentiated middle to late Miocene aged (5 to 15 mya) Alum Bluff Group sediments. These sediments consist of well sorted thin beds of sand, clay, and shell, with a clay or carbonate matrix. Beneath the Alum Bluff Group lie more than an 1000 feet of early Eocene to middle Miocene (15 to 55 mya) marine limestones. These include, with increasing depth, the Bruce Creek Limestone, the Tampa Limestone equivalent and undifferentiated Chickasawhay Limestone, the Ocala Limestone, and the undifferentiated Lisbon and Tallahatta Formations. These are generally clastic, sometimes fossiliferous, ocassionally chalky or phosphatic, interbedded limestone and some dolomites.

2.4 Hydrogeology

Two principal aquifers underlie the upland areas of Eglin AFB in the vicinity of Test Area C-64A: the Sand and Gravel aquifer, and the Floridan aquifer. These aquifers have been delineated by dividing the sequence of stratigraphic units underlying Eglin AFB into hydrogeologic units with distinct hydrologic characteristics as depicted in Table 2.4. With increasing depth below the surface, hydrogeologic units underlying Test Area C-64A are the Sand and Gravel aquifer, the Pensacola Clay confining bed, the Floridan aquifer, and the Lisbon-Tallahatta confining bed (Figure 2.7). Closer to the coast, the Floridan aquifer is divided into upper and lower aquifers by the Bucatunna Clay confining bed (Bucatunna Clay Member of the Byram Formation) (Figure 2.8), however, this unit is absent in the Western Highlands beneath Test Area C-64A (Hayes and Barr, 1983).

2.4.1 Sand and Gravel Aquifer

The Sand and Gravel aquifer is the uppermost aquifer beneath the site. It consists of Citronelle Formation and overlying unnamed terrace deposits and contains clean fine to coarse grained sands and gravelly sands with local occurrences of silt, silty clay, and peat layers. The Sand and Gravel aquifer thickens from east to west, ranging from less than 25 feet thick in

Table 2.4. Lithology and water-bearing properties of geologic and hydrogeologic units in the southern parts of Okaloosa and Walton Counties.

Geologic Unit	Lithology	Hydro-geologic Unit	Water-bearing Properties
Holocene to Pliocene Sands	Unconsolidated, white to light gray, fine to medium quartz sand. Accessories include heavy minerals and phosphate.	Sand-and-Gravel aquifer	Water mainly unconfined. In Fort Walton Beach, includes surficial unconfined unit and lower leaky artesian unit. Yields range from less than 20 gal/min in coastal lowlands of Walton County to 1,000 gal/min in uplands of western Okaloosa County. Tapped by shallow wells for domestic supply and a few larger capacity wells for irrigation. Currently not used by municipal systems for public consumption.
Citronelle Formation	Predominantly nonmarine quartz sands with thin stringers of clay or gravel discontinuous over short distances.		
Miocene coarse clastics	Present in Okaloosa County, the Miocene coarse clastics comprise poorly consolidated sand, silt, clay, and beds of shells.	Pensacola clay confining bed	Restricts vertical movement of water because of thickness and comparatively low permeability. In the area of investigation grades laterally from predominantly dense clay and sandy clay in western part to predominantly clayey, silty sand in the eastern part. Not a source of water.
Intracoastal Formation	Upper and lower carbonate layers separated by a phosphatic sand. The carbonate is a poorly consolidated, sandy, clayey, micro-fossiliferous limestone.		
Alum Bluff Group (northern part only)	Mixture of sand, clay, and shell in relatively well-sorted thin beds. The matrix material is commonly clay or carbonate cement.		
Pensacola Clay	Present only in Okaloosa County in the coastal area, the Pensacola Clay interfingers with the Intracoastal Formation and Alum Bluff Group. The Pensacola is predominantly a bluish gray to olive gray, dense, silty clay.		

Geologic Unit	Lithology	Hydro-geologic Unit	Water-bearing Properties
Bruce Creek Limestone	Light gray to white, moderately indurated, granular, and occurs as a clastic limestone. Accessories include a sand fraction that increases north and east.	Upper limestone of the Floridan aquifer	Principal source of water in Okaloosa and Walton Counties. Yields large quantities of freshwater under confined conditions. Yields range from 250 gal/min to over 1,000 gal/min. Sustained yields are generally lowest immediately adjacent to the coast in Okaloosa County. Individual zones vary greatly in permeability and vertical connection. Contains over 250 mg/L chlorides in parts of southeastern Walton and southwestern Okaloosa Counties.
Tampa Limestone Equivalent	Lithologically similar to Chickasawhay Limestone but slightly less dolomitic. Silt and clay content increase toward the top.		
Chickasawhay Limestone	Primarily a tan sucrosic dolomite but may also occur as a cream to buff fossiliferous limestone. The gradations between the limestone and the dolomite occur both vertically and laterally within the formation.		
Bucatunna Formation	Medium brown to dusky, yellowish-brown calcareous clay. Accessories include up to 10 percent quartz sand and up to 1 percent phosphate. The top contact is sharp and well defined from the overlying limestone.	Bucatunna clay confining bed	Where present, restricts vertical movement of water between overlying and underlying hydrogeologic units. Generally present in coastal Walton and Okaloosa Counties but absent in northern sections of the counties. Not a source of water.
Ocala Limestone	A white to light gray, chalky, fossiliferous relatively pure calcium carbonate limestone. Occasionally the limestone is interlayered with thin streaks of light brown to tan dolomite layers.	Lower limestone of the Floridan aquifer	Comprises a separate hydrogeologic unit in coastal Walton and Okaloosa Counties. In other parts, cannot be hydrologically distinguished from upper limestone aquifer. Not used as a source of freshwater in the southern parts of Okaloosa and Walton Counties.
Lisbon and Tallahatta Formations	Massive shaly to chalky limestones often dark gray to brownish gray to cream in color. Thin shaly beds predominate with specks of glauconite in the more calcareous parts. Foraminifera are abundant.	Lisbon-Tallahatta confining unit	Predominantly impermeable strata. Comprises the base of the freshwater flow system.

Adapted from Barr et al., (1995).

Figure 2.7. Hydrogeologic section C-C[1], west to east through the southern parts of Okaloosa and Walton Counties, and south of Test Area C-64A.

adapted from Barr et al., (1985),
see figure 2.4 for location of section

27.eps/9-02-98

adapted from Barr et al., (1985),
see Figure 2.4 for location of section

28.eps/9-02-98
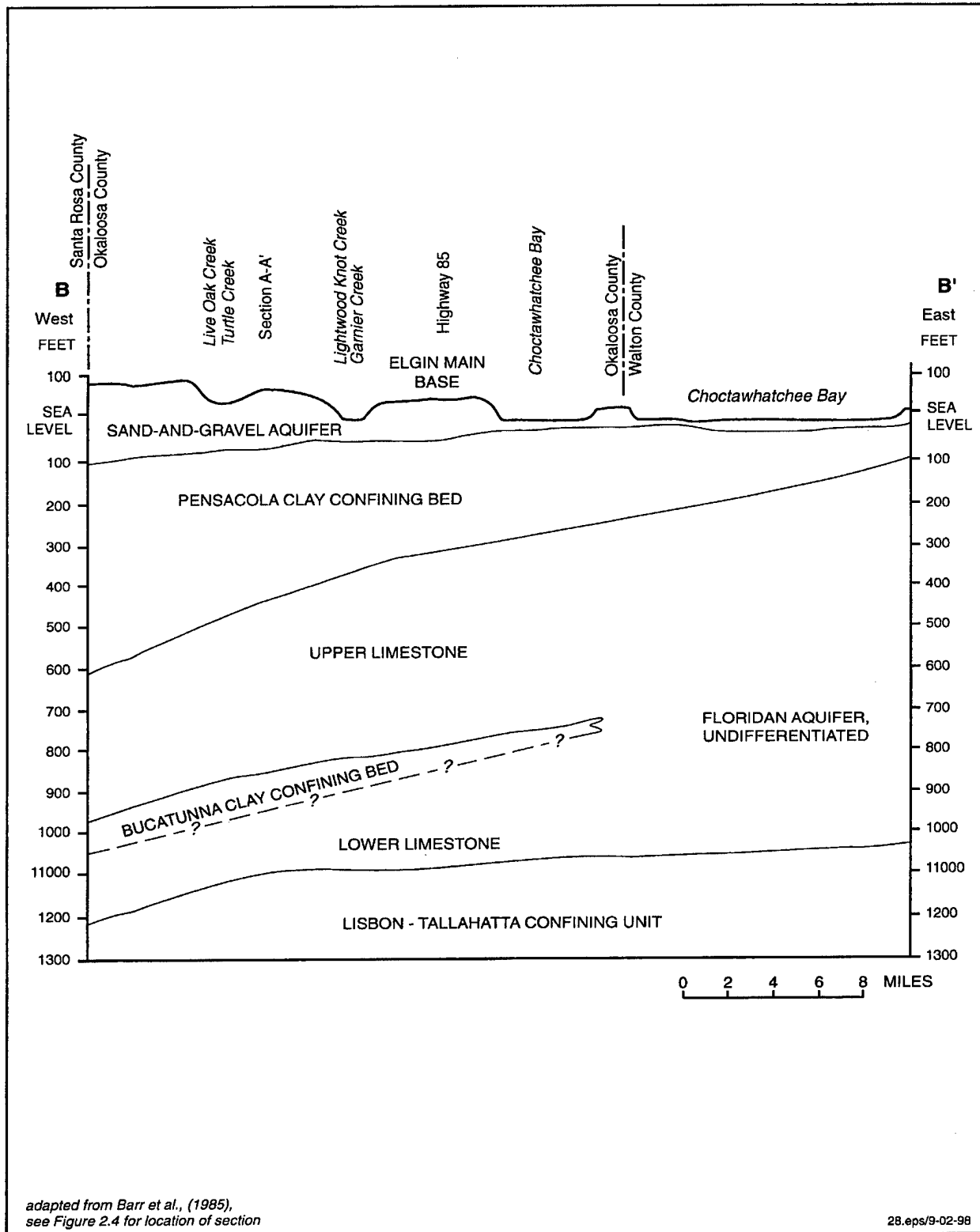
Figure 2.8. Hydrogeologic section B-B^1, west to east through the southern parts of Okaloosa and Walton Counties near the coast.

south-central Walton County to over 200 feet in southwestern Okaloosa County. Beneath the Test Area C-64A, Hayes and Barr (1983) estimate its thickness at approximately 150 feet.

Hayes and Barr (1983) recognize two water-producing zones in the Sand and Gravel aquifer. The uppermost or surficial water table zone is the shallowest water-bearing zone and consists of moderately sorted fine to medium sands approximately 20 to 60 feet thick under unconfined conditions. This zone is underlain by an intermediate confining layer ranging from 10 to 65 feet thick and consisting of clays, sandy clays, and clayey sands. Beneath the confining clay unit lies the main water producing zone made up of 10 to 85 feet of medium to coarse grained sands and fine gravel. This deep water-producing zone exists under confined or artesian conditions and is separated from the surficial water table zone by the confining clay layer as depicted in Figure 2.9.

The middle confining layer noted by Hayes and Barr (1983), may not be present in all localities. Boring logs of monitoring wells installed near Test Area C-64C do not indicate the presence of a clear intervening clay layer at depth. Some boring logs indicate a clayey silty sand unit between depths of approximately 20 and 35 feet, however, it is not noted in all the boring logs, and perched groundwater was not reported above this layer during installation of the monitoring wells. The lack of existence of a confining clay layer beneath the site indicates that only one permanent water bearing zone, equivalent to the main water producing zone of Hayes and Barr (1983) is present beneath Site C-64C, and nearby Test Area C-64A.

Groundwater in the Sand and Gravel aquifer occurs under unconfined conditions with the water table generally taking the form of a subdued replica of surface topography. The aquifer is recharged annually by precipitation in excess of evaporation, Vecchioli et al. (1990), on the basis of base flow separation techniques, estimate recharge to range between 14.7 and 50.7 inches/year, with recharge throughout Okaloosa County averaging more than 10 inches/year. Groundwater in the upper Sand and Gravel aquifer is in hydrologic connection with and discharges to local streams and lakes before being transported to local bays.

Depth Below Ground Surface (feet)

0

Surficial zone

Sand-and-Gravel Aquifer

Sand, white to light-gray to light-brown, fine to medium grained, subrounded to angular, moderately sorted.

20

40

Intermediate zone

Clay, dark-gray, slightly silty, contains shell fragments and some organic material.

Sand, white to light-orange, very fine to medium grained, subrounded to angular, poorly sorted, upper section contains large amounts of greenish clay with abundant shell fragments and organic material.

60

Sand, white to light-brown, fine to medium grained, subrounded, moderately sorted, in places contains slight to moderate amounts of greenish-gray clay with shell fragments and organic material.

80

Sand, white to light-orange, very fine to very coarse grained, subrounded to angular, poorly sorted, contains moderate to large amounts of dark-gray, silty clay with organic material.

100

Main producing zone

Sand, white to light-orange to light-brown, medium to coarse grained with some fine gravel,subrounded to subangular, moderately to well sorted; this zone is capable of yielding over 300 gal/min of generally high-quality water (the exceptions being a low pH and a possible high total iron concentration).

120

140

Pensacola Clay Confining Bed

Clayey sand, dark-gray to dark-bluish-green, fine to coarse grained sand, poorly sorted, contains shell fragments and organic material.

Clay, dark-gray to bluish-green, contains interbedded clayey sand and gravel, varying amounts of silt, and some shell fragments in upper part.

160

29.eps/7-22-98

adapted from Hayes and Barr, (1983)

Figure 2.9. Generalized stratigraphic description of the sand-and-gravel aquifer and the upper most part of the underlying Pensacola clay confining bed, Fort Walton Beach area, southern Okaloosa County.

Groundwater levels measured in monitoring wells located at Site C-64C indicate that the water table occurs at a depth of approximately 90 feet. Groundwater beneath the site flows northeast towards the nearest stream, Ramer Creek (Figure 2.10), under a hydraulic gradient of 0.001 to 0.003 ft/ft. Groundwater encountered and sampled during drilling of soil borings near Bull Creek also confirm a flow direction toward the nearest stream, in this case northwest, towards Bull Creek. Similar conditions are expected to occur under nearby Test Area C-64A with groundwater flowing to the northeast and discharging to Ramer Creek.

According to Hayes and Barr (1983), potential yields of wells screened in the main water-producing zone of the Sand and Gravel aquifer generally range from 200 to 400 gallons per minute. Although the hydraulic conductivity of sediments beneath Test Area C-64A have not been measured directly, aquifer tests performed in the Sand and Gravel aquifer near Fort Walton Beach found transmissivities ranging from 400 to 6200 ft^2/day. Dividing these transmissivities by the test well screen lengths indicates hydraulic conductivities ranging between 20 and 150 ft/day as presented in Table 2.5. These estimates are similar to those obtained from data on Lakeland Series soils provided in USDA (1995) which indicate hydraulic conductivites ranging between 12 and 53 ft/day. Typical hydraulic conductivities for unconsolidated medium to coarse sands reported in Fetter (1988) range between 30 and 150 ft/day.

Based on hydraulic gradients measured beneath Site C-64C, and assuming that hydraulic conductivity of subsurface sediments ranges between 10 and 150 ft/day, groundwater flow velocities beneath Test Area C-64A are estimated to range between approximately 0.01 and 0.45 ft/day. Assuming an effective porosity (n_e) of 0.25 typical of unconsolidated sands (Fetter, 1988), groundwater pore velocities beneath Test Area C-64A are estimated to range between 0.04 and 1.8 ft/day.
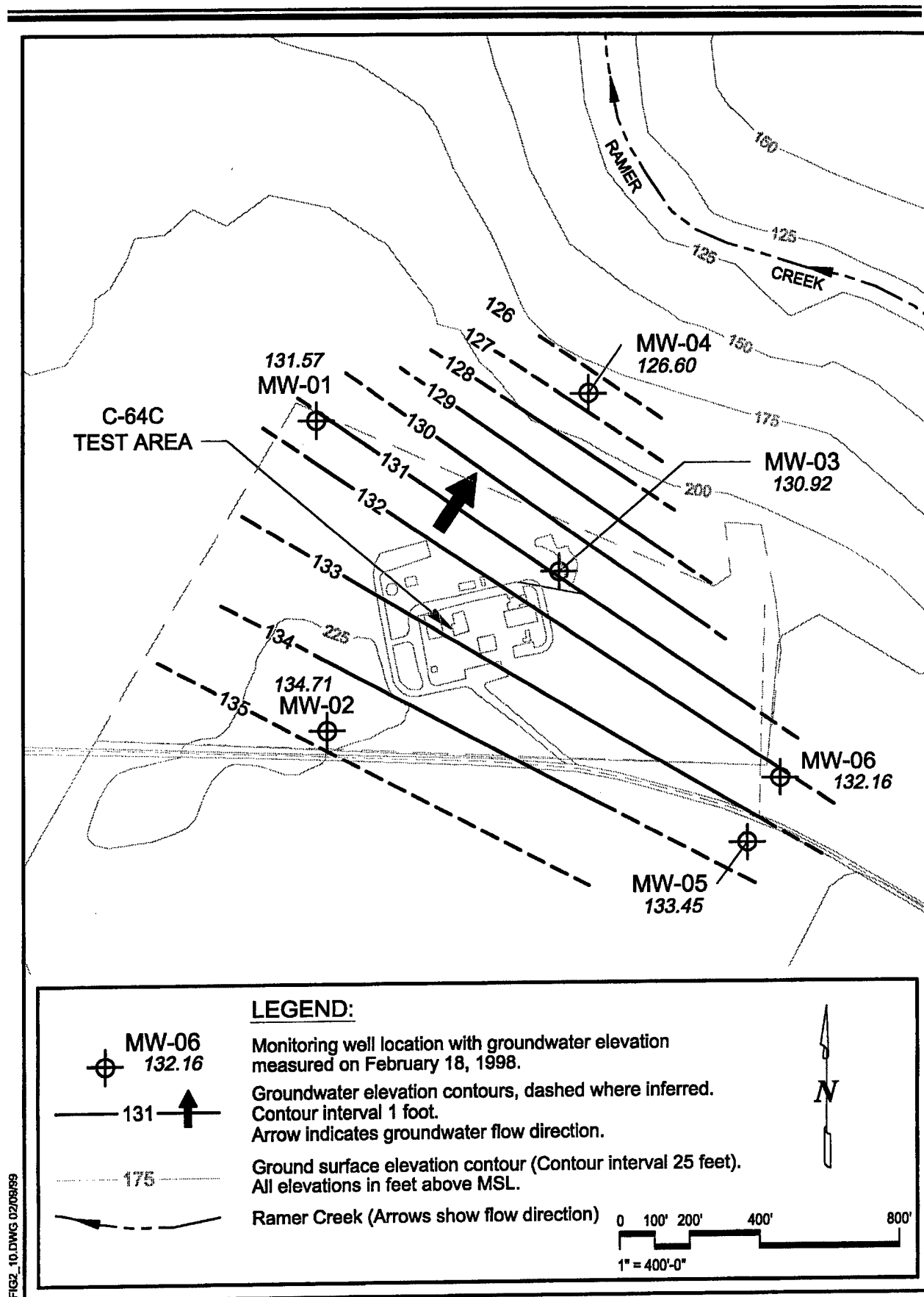
Figure 2.10. Groundwater surface elevations beneath Site C-64C, Eglin AFB.

Table 2.5. Hydrogeologic parameters for sand and gravel aquifer beneath Test Area C-64A and Site C-64C.

Hydraulic Conductivity (ft/day)	Low	High
Lakeland Soils (ft/day)[1]	27	53
Sand and Gravel Aquifer Tests (ft/day)[2]	20	150
Groundwater Velocity	**Low**	**High**
Hydraulic Gradient (ft/ft)[3]	0.001	0.003
Groundwater Darcy Velocity (ft/day)[4]	0.02	0.45
Groundwater Pore Velocity (ft/day)[4]	0.08	1.80

Notes:

[1]Lakeland Soil Data from USDA (1995)

[2]Sand and Gravel Aquifer Test Data from Hayes and Barr (1983), hydraulic conductivities (ft/day) calculated by dividing reported transmissivities (ft²/day) by test well screen lengths (ft)

[3]Hydraulic gradient determined from monitoring wells at Site C-64C

[4]Groundwater velocities calculated for hydraulic conductivities of 20 and 150 ft/day and an assumed effective porosity (n_e) of 0.25

2.4.2 Pensacola Clay Confining Bed

The Sand and Gravel aquifer is separated hydraulically from the underlying Floridan aquifer by the Pensacola Clay confining bed. Stratigraphically, the Pensacola Clay is not present beneath Test Area C-64A. However, Alum Bluff Group sediments are present beneath the site (Figure 2.5), and are included as part of the Pensacola Clay confining bed (Table 2.4) because they serve to restrict vertical movement of water between the sand and Gravel and Floridan aquifers. Barr et al., (1985) estimate that the Pensacola Clay confining bed averages about 350 feet thick in Okaloosa County, grading laterally from dense clay and sandy clay in the west to sandy clay, clayey sand and limestone in the east. The top of the confining bed dips south-southwest at about 15 feet per mile, ranging from about 140 feet above sea level in northeastern Walton County to more than 125 feet below sea level in southwestern Okaloosa County. Beneath Test

Area C-64A, the top of the confining bed occurs at a depth between 75 and 100 feet, and is between 200 and 250 feet thick. The average vertical hydraulic conductivity of Pensacola Clay confining bed sediments ranges between 1E-02 and 1E-06 ft/day, with an average of 1E-05 ft/day in Okaloosa County and 1E-03 ft/day in Walton County (Barr et al., 1981).

2.4.3 Floridan Aquifer

The Floridan aquifer is the principle source of drinking and irrigation water for Eglin AFB and Okaloosa and Walton counties with well yields ranging from 250 to more than 1,000 gallons per minute. It consists of a thick sequence of interbedded limestones and dolomites deposited from Eocene to Miocene times. In some areas, it is separated into an upper and lower aquifer by Bucatunna Clay confining bed. However, this confining unit wedges out about twelve to fifteen miles north and east of Ft. Walton Beach and is not present beneath Test Area C-64A (Barr et al., 1985).

The overall thickness of the Floridan aquifer, including the Bucatunna Clay confining bed, ranges from 850 feet thick in east central Walton County where the Bucatunna confining bed is absent, to about 600 feet in the southwest Okaloosa County where it is present and approximately 125 feet thick. The top of the Floridan aquifer dips southwest at 15 to 20 feet per mile and ranges from about 50 feet above sea level in east-central Walton County to more than 600 feet below sea level in southwestern Okaloosa County. Beneath Test Area C-64A, the top of the Floridan aquifer occurs at an altitude of about 150 feet below sea level and is approximately 750 feet thick. At approximately 900 feet below sea level, the bottom of the Floridan aquifer beneath Test Area C-64A is marked by the Lisbon-Tallahatta confining bed (Barr et al., 1985).

The Floridan aquifer is a confined aquifer, with groundwater storage and movement taking place in interconnected, intergranular pore spaces, small solution fissures, and larger solution channels and cavities. Regionally, groundwater in the Floridan aquifer flows to the south, discharging to the Gulf of Mexico. The principle source of recharge to the Floridan aquifer is rainfall in the northern portions of Okaloosa and Walton Counties and in southern Alabama, where the sedimentary rocks which comprise the aquifer outcrop at the surface.

Beneath Test Area C-64A, the presence of the Pensacola Clay confining bed prevents significant recharge of the Floridan aquifer from the overlying Sand and Gravel aquifer. Analyses of aquifer tests performed by Barr et al., (1981) indicate no significant leakage between the Floridan aquifer and Sand and Gravel aquifer over short pumping durations. Vecchioli et al., (1990) report on recent modeling studies which estimate average recharge to the underlying Floridan aquifer from the overlying Sand and Gravel aquifer at less than or equal to 5 inches/year.

2.5 Surface Hydrology

Three hydrologic basins, the Choctawhatchee Bay, Yellow River, and Pensacola Bay basins lie within the boundaries of Eglin AFB. Test Area C-64A straddles the divide between the Bull Creek and Ramer Creek watersheds (Figure 2.11), both of which are located in the Yellow River Basin. Most of the drainage systems within the Yellow River Basin are characterized by U-shaped channels and trellis-type drainage patterns.

Bull and Ramer Creeks are perennial first-order streams which drain north into Titi Creek. Titi Creek drains west into the Shoal River, and then the Yellow River. The Yellow River continues west and empties along the northwestern boundary of Eglin AFB into Blackwater Bay, a tributary arm of Pensacola Bay and the Gulf of Mexico.

Table 2.6 presents data on average annual discharge and baseflow estimates at stream sites within the Yellow River Basin for which partial or extended records are available from the United States Geological Survey (Figure 2.12). Baseflow, representing streamflow derived from groundwater discharge, ranges from 62 percent to approximately 100 percent of total discharge. Thus, surface runoff from these watersheds can range from zero to as much as one third of total precipitation falling on these watersheds.
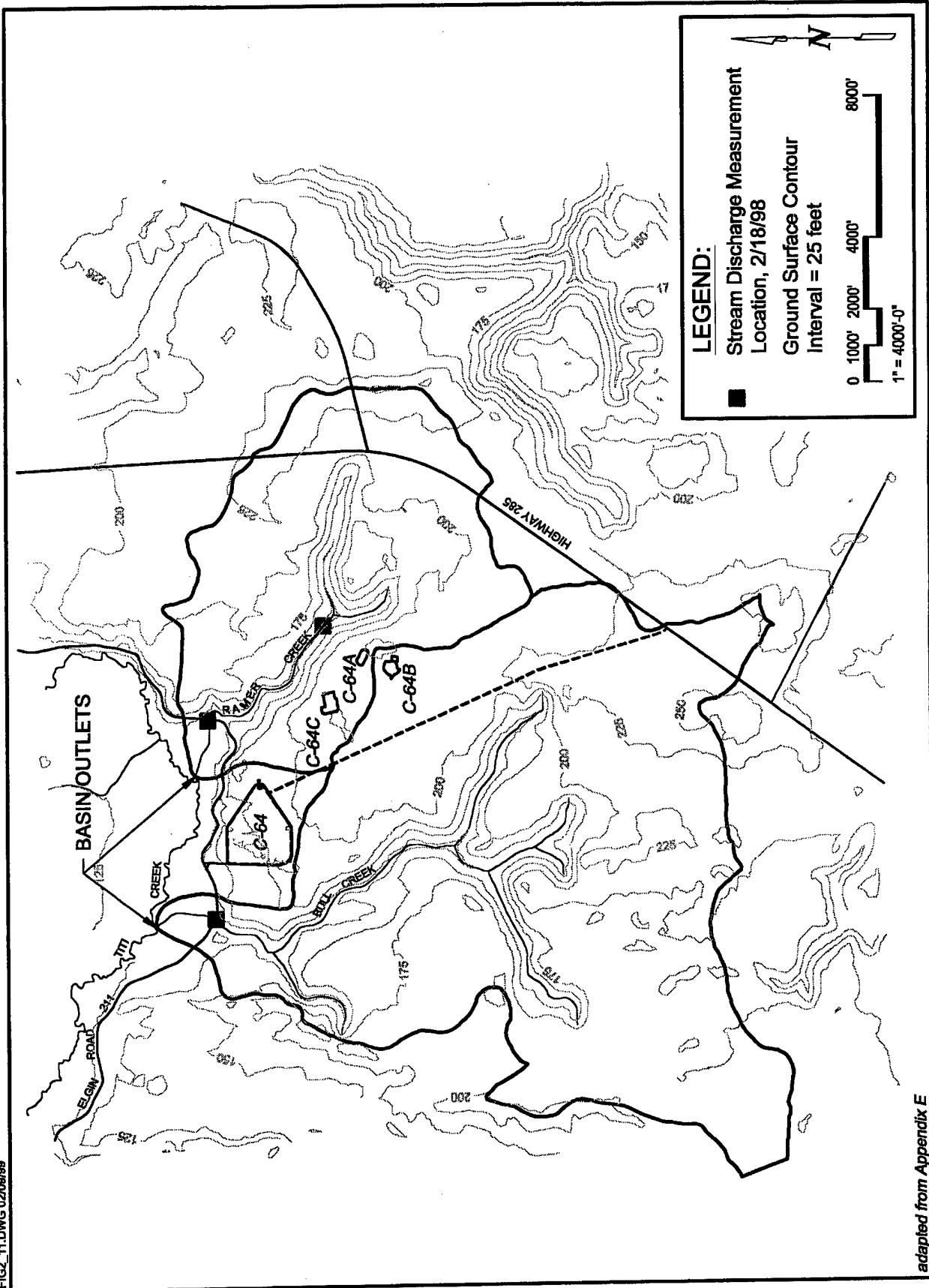
Figure 2.11. Bull and Ramer Creek drainage basins.

Table 2.6. Yellow River Basin streamflow data.

	Drainage Area (mi^2)	Average Discharge cfs	Maximum Discharge (cfs)	Minimum Discharge (cfs)	Average Annual Runoff (in/yr)	Baseflow (cfs)	(in/yr)	Baseflow as Percent Runoff	Period of Record
Yellow River at Milligan	624	1143	28000	136	25	708	15.4	0.62	1939-67
Baggett Creek near Milligan	7.8	21.7	368	7.8	37.7	17.9	31.1	0.82	1964-67
Shoal River near Mossey Head	123	238	10500	42	26.4	166	18.3	0.69	1952-67
Pond Creek near Dorcas	94.8	113	2500	12	15	97.6	14	0.93	1966-68
Pond Creek at Dorcas	96.5	NA	NA	NA	NA	79.8	11.2	—	1966-68
Titi Creek near Crestview	62.9	134	1450	69	29	134	28.9	0.99	1966-68
Shoal River near Crestview	474	1120	23500	240	32.1	737	21.1	0.66	1939-96
Yellow River near Holt	1210	2400	NA	NA	27	1820	20.4	0.76	1933-41 1966-68
Shoal River at Dorcas	319	NA	NA	NA	NA	350	14.9	—	1966-68

Data from Trapp et al., (1977), Vecchioli et al., (1990), and Franklin and Meadows, (1997).

adapted from Vecchioli et al. (1990)

212.eps/8-17-98
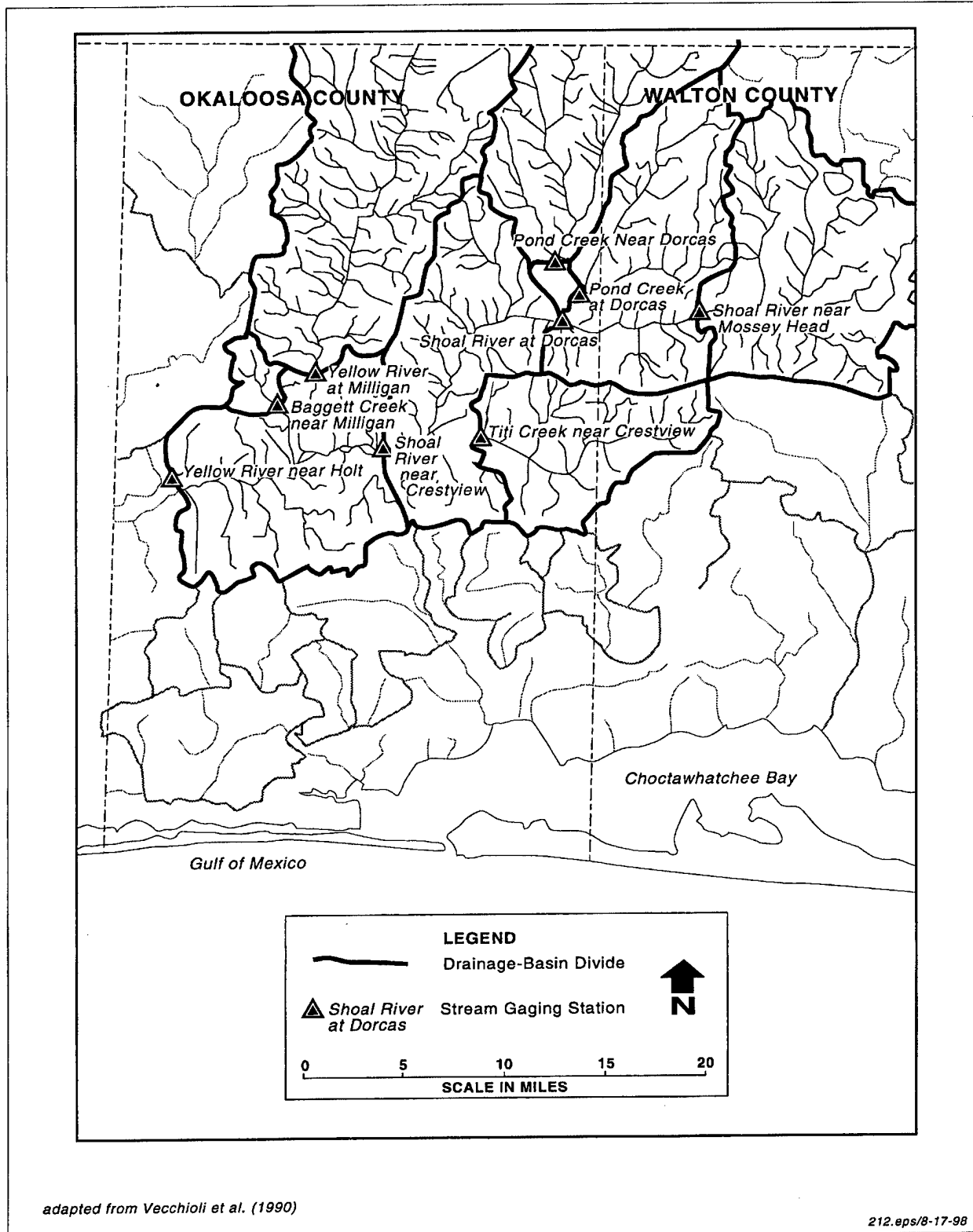
Figure 2.12. Location of streamflow record sites and respective drainage basins in and around Okaloosa County.

Streamflow data on small watersheds such as Bull and Ramer Creek have not historically been collected. In order to estimate discharge from these basins, data on average annual discharge and drainage area listed in Table 2.6 were plotted and the resulting linear relationship (Figure 2.13) was used to predict average annual discharge from the Bull and Ramer Creek watersheds (Table 2.7). Discharge from Bull and Ramer Creeks was also measured on February 18, 1998 during a period of high discharge following an extended period of above average rainfall (Table 2.7). Discharge observed at the site in February 1998 was approximately twice that estimated from the discharge-drainage area relationship, except for the upper stream sampling location on Ramer Creek. This suggests that most of the source areas for precipitation draining into Ramer Creek may be located along the lower reaches of the creek, below the confluence of the two upper tributaries.

Note: Data for regression from Trapp et al., (1977), Vecchioli et al., (1990), and Franklin and Meadows, (1997).
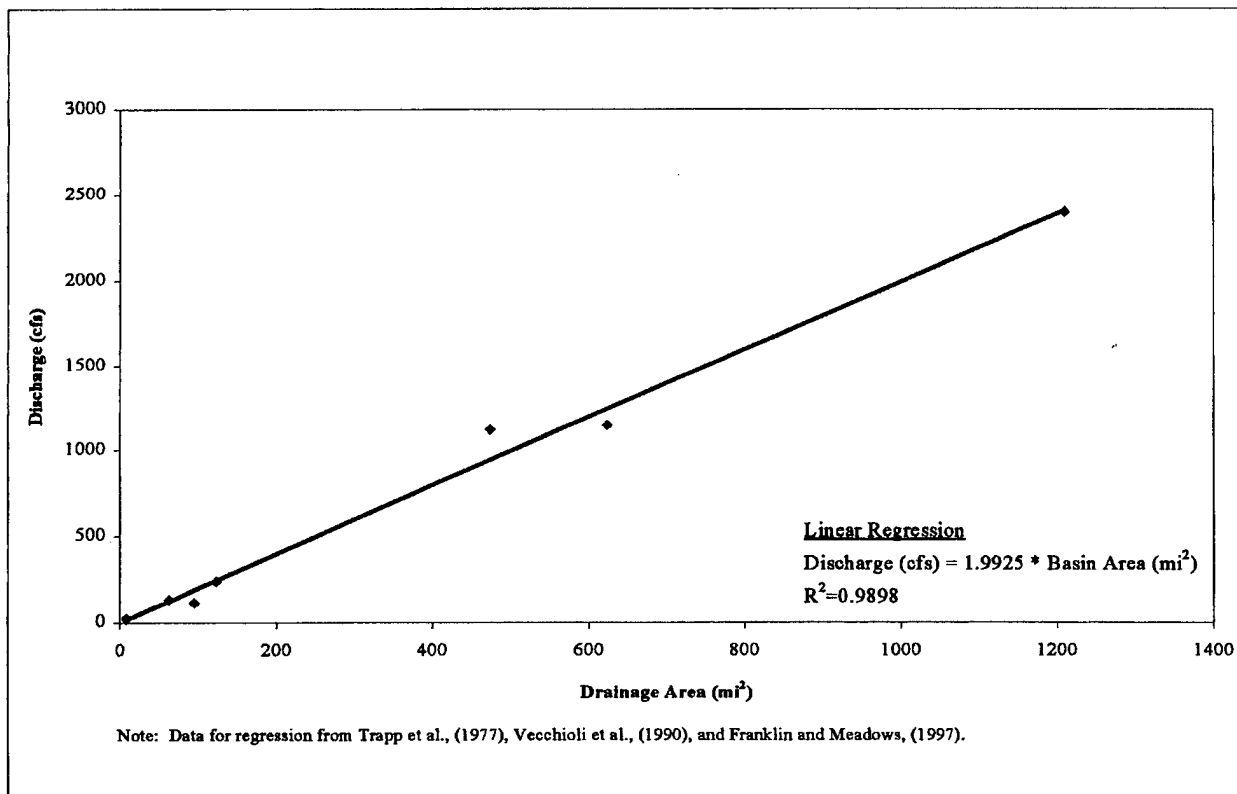
Figure 2.13. Linear regression of discharge vs. drainage area for the Yellow River Basin.

Table 2.7. Streamflow discharge, Bull and Ramer Creek watersheds.

Watershed	Location	Basin Area (mi^2)	Estimated Average Annual Discharge (cfs)	Discharge Measured 2/18/98
Bull Creek	1) At Eglin Rd. 211	6.2	12.4[1]	25.7
Ramer Creek	1) At Eglin Rd. 211	2.8	5.6[1]	10.1
	2) 1 mile upstream of Eglin Rd. 211 below confluence	--	2.3[2]	2.6

[1] Discharge (cfs) = 1.9925 x Basin Area (mi^2) – see Figure 2.13.

[2] Based on assumption that discharge increases 3.3 cfs per mile along Ramer Creek and distance from stream head water to location 2 on Ramer Creek is 0.7 miles. 3.3 cfs per mile obtained by dividing average annual discharge at basin outlet (5.6 cfs) by total length of streambed (1.7 mi.).

2.6 Hydrochemistry

The chemical compositions of surface and ground waters present in the Test Area C-64A are important parameters in this assessment because they largely determine the rates at which alloy fragments from the testing of penetrator munitions will be leached and otherwise degraded. The alloy fragments exposed at the surface will initially come into contact with rainwater. Analyses of rainwater are not available for the C-64A site. However, the National Atmospheric Deposition Program (NADP) maintains a collection site at Quincy, Florida. Rainwater from this site has been collected and analyzed on a quarterly basis. Data are available for the years 1984 through 1991. The average values for each major constituents reported are listed in Table 2.8.

With time, the alloy fragments could migrate into the soil profile at Test Area C-64A. Analyses of soil waters from the site are not available. However, the waters in Ramer Creek and Bull Creek are likely to have compositions that approximate the soil water compositions in as much as the waters in these creeks have likely passed through the soil zone. An analysis of water from Bull Creek is listed in Table 2.8.

The compositions of ground waters from the Sand and Gravel aquifer at various locations in Okaloosa and Walton Counties were reported by Hayes and Barr (1983). The mean value reported by these authors for the main producing zone is listed in Table 2.8. One of the locations included in the evaluation by Hayes and Barr (1983) is close to the Test Area C-64A. Although the complete analysis for water samples from this well are not provided in the Hayes and Barr (1983) report, values for chloride, iron and pH are given as 3.5 and 0.13 mg/L and 6.1, respectively.

Although not present at the Test Area C-64A, the composition of seawater is included in Table 2.8 because it was included in the experimental matrix for the immersion experiments.

Table 2.8. Chemical analysis of natural waters.

Ion	Sea Water (1*	Surface Water (2*	Ground Water (3*	Rain Water (4*
SiO2	<0.8	2.5	5.1	N/A
Mg	1225	0.2	0.7	0.04
Ca	406	0.15	1.5	0.08
Na	9400	1.55	3.3	0.26
K	365	0.008	0.4	0.22
CO3	<0.1	<0.1		N/A
HCO3	132	<0.1	7	N/A
F		<0.1	0.1	N/A
Cl	18025	2.18	4.4	0.46
SO4	2940	0.95	2	1.08
NO3		0.59	1.4	0.59
Fe		<0.02		
pH	8.2 – 8.4	4.8	6.1	4.7

1*)   From Kester et al. (1968).
2*)   Bull Creek water analyzed by J. Hussler, University of New Mexico (5/97).
3*)   From Hayes and Barr (1983).
4*)   NADP Database (1997). (N/A = Not Available)

2.7 Biological or Natural Resources

A detailed evaluation of the biologic resources on Eglin AFB is presented in Appendix L of the Eglin Environmental Baseline Study US Air Force (1995). The discussion in this section provides a brief synopsis of the information assembled in Appendix L of the Baseline Study.

Potential receptors and receptor habitats have been identified in previous surveys of the site (USAF, 1972; 1976a; 1976b; 1983). Ecological surveys of the area have identified 17 common mammal and 22 common bird species near the test sites (USAF, 1972). Dominant species, which were observed more than 80% of the time, include the beach or old field mouse (*Peromyscus polionotus*), white-tailed deer (*Odocoileus virginianus*), and eastern meadowlark (*Sturnella magna*). These species are all potential receptors for metals dispersed on the test site. Terrestrial habitats on the test sites are primarily grasslands, which have been described as dominated by switchgrass (*Panicum virgatum*) and broomsedge bluestem (*Andropogon virginicus*). Adjacent to the test area, the terrestrial habit is oak-pine forest dominated by turkey oak (*Quercus laevis*), sand pine (*Pinus clausa*), and longleaf pine (*Pinus palustris*)(USAF, 1976a).

Adjacent to the test sites, previous surveys have identified diverse fish and macroinvertebrate communities in Bull Creek and Ramer Creek (USAF, 1976b; 1983). These surveys identified 12 species of fish, but this does not include the Okaloosa darter (*Etheostoma okaloosae*), which has been identified as a species of concern in streams elsewhere on Eglin Air Force Base. A diverse macroinvertebrate community has also been identified in these streams and includes orders Diptera, Trichoptera, Coleoptera, Odonata, Plecoptera, Hemiptera, and Decapoda (USAF, 1983).

3.0 EXPERIMENTAL PROGRAM AND DATA

Samples of tungsten penetrator alloys were obtained from AFRL Munitions Directorate at Eglin AFB. The alloys were used in this experimental program to determine the rate at which they would leach metals into the soil profile at Test Area C-64A on Eglin AFB. The experimental program was separated into two major tasks. The objective of the first task was to obtain a source term representing the leach rates of each of the alloys in the test range soils. This task involved the experimental determination of the rate of leaching/corrosion of three tungsten alloys and tantalum metal in three water compositions. The objective of the second task was the determination of sorption coefficients for the metals in the alloys on soils from the test range at Eglin. A sorption coefficient (K_d) quantifies the degree to which the metals composing the alloys are bound by soils.

3.1 Alloy Compositions and Preparation of Alloy Samples

Samples of three penetrator alloys were received from Eglin Air Force Base in the form of rod stock of different diameters and labeled as HD-17, WL-1 and NS. The compositions of these samples were provided by AFRL Munitions Directorate and are listed in Table 3.1 along with the rod diameters. The latter were used to confirm the identity of the alloy in the various experiments conducted during the course of this study. Disks of 1/8" thickness were cut from the rod stock and a single 1/32" hole was drilled into each disk near the edge to allow them to be suspended in a solution. Details of the procedure used to cut and clean the alloy disks are provided in Appendix A.

In addition to the tungsten alloys, a sample of tantalum metal was tested for leaching/corrosion behavior. The composition of this alloy is also listed in Table 3.1. The tantalum metal was cut into plates that were 0.5 X 0.7 X 0.125 inches in size. A hole was drilled into the plates along one edge. These plates were cleaned using the procedure described in Appendix A.

Table 3.1. Tungsten and tantalum penetrator compositions in weight percent, including rod diameters.

	Alloy Composition							Rod
Sample	W	Ni	Fe	Cu	Co	Mn	Ta	Diameter
HD-17	89.80%	6.00%	0.00%	4.20%	0.00%	0.00%	0.00%	1.025 in
WL-1	87.60%	6.60%	4.30%	0.00%	0.00%	1.50%	0.00%	1.151 in
NS	92.10%	4.95%	1.45%	0.00%	1.50%	0.00%	0.00%	1.283 in
Ta	0.00%	0.00%	0.00%	0.00%	0.00%	0.00%	100.00%	*

* Tantalum stock is square 0.5 X 0.7 X 0.125 inches

3.2 Waters and Soils

Because the corrosion/leaching behavior of metal alloys is known to be sensitive to water composition and pH (Camp and Meserve, 1963), experiments were conducted with each of the water compositions with which alloy fragments might come into contact at various Eglin test sites. The three types of water used in the corrosion/leach tests were: surface water, ground water, and sea water. The surface water composition was intended to represent soil water at Test Area C-64A. This is the water composition most likely to contact the alloy fragments that may be dispersed at the site. A sample of surface water was obtained from Bull Creek at the location shown in Figure 3.1. Ground water and sea water compositions were included in the experiments to provide a more general understanding of the leaching/corrosion behaviors of the alloys and to enlarge the database of information on the leaching/corrosion behavior of the alloys in other potential testing environments. A sample of shallow ground water was obtained from a well behind Chapel II on Eglin AFB and seawater was obtained on the beach near Destin, Florida.

In most of the corrosion/leaching tests, "artificial" waters were used instead of natural waters from the Eglin area. The compositions of the artificial waters were formulated to represent the three major water compositions. The use of these artificial waters simplified the interpretation of the corrosion/leaching data obtained in this study; the natural waters can
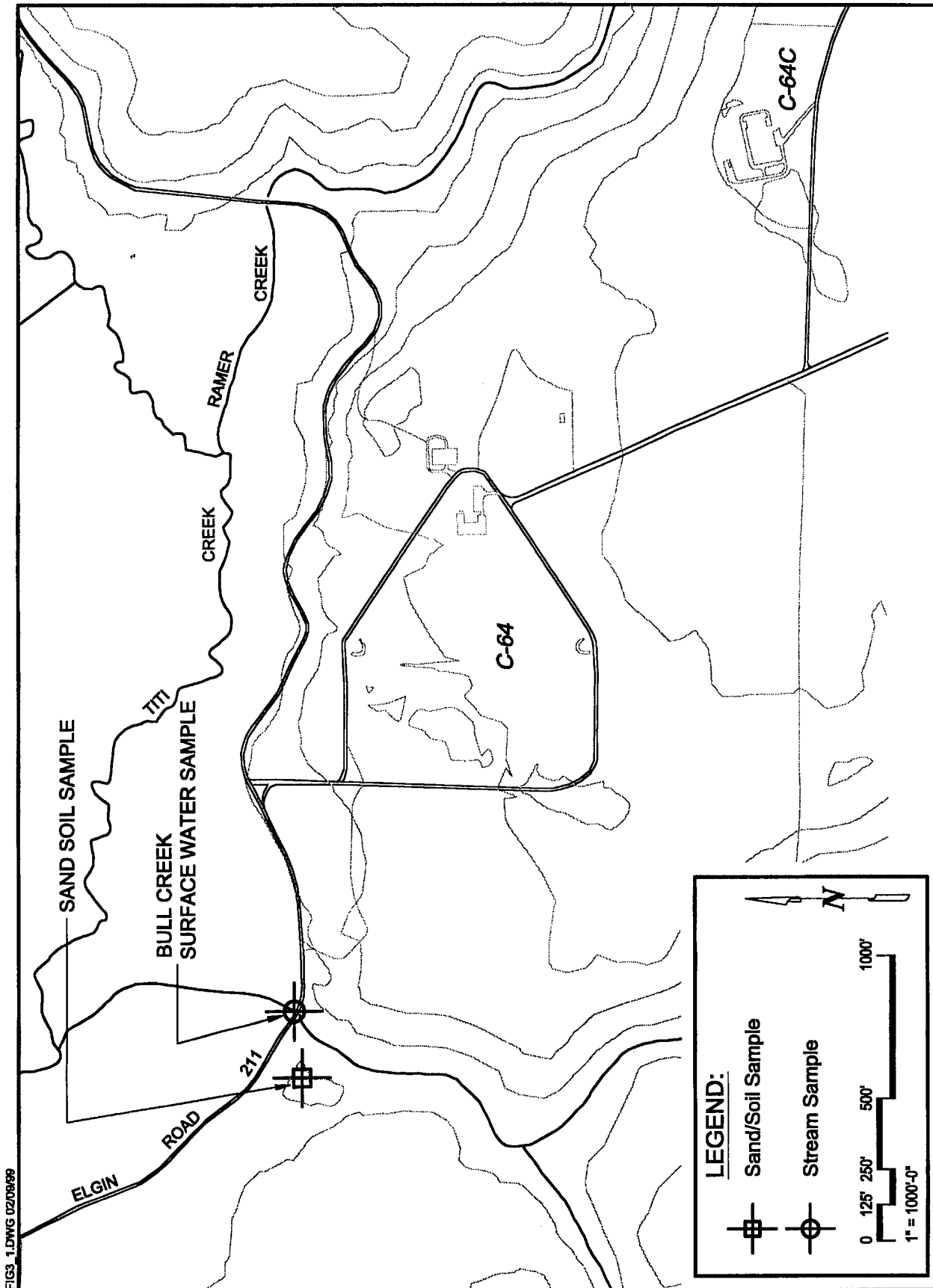
Figure 3.1. Soil and surface water sample location map.

contain biologic materials that may enhance or inhibit leaching/corrosion behavior in the laboratory tests in ways that are not representative of the natural field sites. Nonetheless, natural waters were used in some tests to gauge the possible influence of biologic materials.

The compositions of the artificial waters were obtained by averaging the available analyses of the different water types. For example, the ground water composition was derived by averaging the analyses of waters from the shallow portion of the sand and gravel aquifer reported for the Eglin region by Hayes and Barr (1983). The surface water composition was obtained by averaging analyses of rain compositions for the region as reported by the National Atmospheric Deposition Program (NADP). The seawater composition was obtained from Kester et al. (1968). The detailed water compositions are presented in Table 3.2. Detailed procedures for the formulation of the artificial waters are presented in Appendix A. Note that two separate batches of artificial waters were formulated because the first batch was exhausted with the immersion tests. The two batches are somewhat different in composition. The differences are not significant.

3.3   Corrosion/Leaching Experiments and Source Term

Two different types of corrosion experiments were conducted: immersion and drip experiments. In the immersion experiments, alloy samples were immersed in each of the three main water types for durations of several weeks to months. These experiments were carried out over weeks to months because it was originally believed it would take this long to leach measurable quantities of metals into solution. This turned out not to be the case. At the completion of each immersion experiment, the alloy sample was removed from the experimental vessel and the remaining water was analyzed for each of the metals known to be in the alloy. In order to properly analyze for all of the constituents of interest, at least 500 ml of water was required. The technique used for the analysis of these water samples was inductively coupled-plasma-mass-spectrometry (ICP-MS).

Table 3.2. Artificial and natural water compositions.

Analysis of Waters: Immersion Corrosion				Natural	Natural	Natural
	Artificial Sea Water	Artificial Surface Water	Artificial Ground Water	Gulf Water	Surface Water	Ground Water
Ions	mg/L*	mg/L*	mg/L*	mg/L**	mg/L**	mg/L**
Si	<0.8	<0.8	<0.8	<0.8	2.5	180
Mg	1130	0.16	2.29	1225	0.2	0.62
Ca	376	<0.5	12	406	0.15	<0.5
Na	9250	1.8	14	9400	1.55	3
K	325	<0.1	1.2	365	0.008	<0.1
Br	<0.5	<0.5	<0.5	<0.5		<0.5
CO3	<0.1	<0.1	<0.1	<0.1	<0.1	<0.1
HCO3	66.4	2	15.6	132	<0.1	3.2
F		0.08	0.01		<0.1	0.05
Cl	16550	2.2	18.3	18025	2.18	3.3
SO4	3140	1.1	8.5	2940	0.95	1.56
NO3		<0.5	0.5		0.59	1.42
Fe					<0.02	
Analysis of Waters: Sorption/ Drip Experiments						
	Artificial Sea Water	Artificial Rain Water Surface Water	Artificial Ground Water			
Ions	mg/L*	mg/L*	mg/L*			
Si	4.1	3.3	2.7			
Mg	1180	0.16	2.4			
Ca	445	1.3	16			
Na	10700	7.9	20			
K	340	<0.1	1.1			
Br	1.3	<0.5	<0.5			
CO3	<0.1	<0.1	<0.1			
HCO3	35.6	25.6	69.6			
F		0.23	0.3			
Cl	19150	0.58	20			
SO4	3350	1.68	9.36			
NO3		<0.5	<0.5			
Fe						
* Waters analyzed by John Husler analyst, University of New Mexico, Department of Geologic Sciences						
** From literature references, see text						

The metal concentrations in these water samples represent the integrated result of all the leaching and corrosion reactions that occurred during the time the alloys were in the water. Therefore, these samples are called integral water samples.

As a check on the corrosion rate of the alloys, nickel concentrations were determined in small aliquots of water taken from many of the ongoing experiments. These analyses were carried out with field kits specific for nickel. The water aliquots were too small to analyze for all the metals of interest by ICP-MS. In some experiments, these analyses followed a schedule whereby the time between analysis was roughly doubled between each subsequent analysis starting with several minutes and ending with several weeks. These are called time-series analysis. In other experiments, the analyses were carried out on an irregular basis. The intent of these analyses was to develop curves in time-concentration space that reflected the corrosion/dissolution reaction(s) involved in each alloy-water system.

Although the amounts of corrosion products (i.e., secondary phases) formed during most of the experiments were very limited, evidence of the precipitation of nickel was obtained in some experiments from the time-series data. Identification of the phase(s) precipitating on alloy samples in the immersion experiments was difficult because of the small masses involved (i.e., 5-25 mg spread over the surface of an alloy disk). To promote the formation of corrosion products, at the end of each immersion test, the alloy disks were put into small (15 ml) polyethylene containers ("pillboxes") with 10 ml of the final test solution. The low water volume/alloy surface area (V/S) ratio in these containers caused the metal concentrations in solution to increase more rapidly leading to the precipitation of corrosion products. The corrosion products that formed in these containers were analyzed by scanning electron microscopy (SEM) and energy dispersive analysis using X-rays (EDX). Although the water compositions in these containers may have been somewhat altered in terms of pH and oxidation-reduction potential (Eh) as a result of the ongoing corrosion reactions, the compounds identified by these analyses can be used to derive upper bound estimates of the metal concentrations to be expected in immersion tests and in the soil environments at the Eglin sites.

Because the residence time of water in the soil zones at Eglin is likely to be in the range of only hours to days, the leach rates calculated from the long-term immersion tests may not be fully representative of the leaching/corrosion environment in the soil zones. To more directly duplicate the conditions under which alloy fragments could be leached and corroded in the soil

zones at the Eglin site, drip experiments were carried out. These experiments were designed to also represent the effects of intermittent rainfall on the leach rate of metals from alloy fragments lying on the surface and buried in soil. In the drip experiments, water was dripped onto alloy samples and collected for immediate analysis. The amounts of water recovered in these experiments were limited to 10-20 ml given the experimental design. These quantities of water allowed the analysis of only 1-2 metals in each sample.

3.3.1 Immersion Tests

Experimental Design and Metals Analysis Procedures

The immersion test vessel is shown in Figure 3.2. The test vessel was a polyethylene terephthalate jar with a polyethylene screw cap. The polyethylene terephthalate composition was chosen because it is a clear plastic which allows a clear view of the specimen. The volume of the vessels used in the various experiments ranged from 0.5-4 liters. Most experiments were carried out in 1.0 or 2.0 liter vessels. The larger volume vessels were required for experiments in which several samples of solution were to be removed during the experiment for subsequent ICP-MS analysis. The alloy specimen was suspended by a monofilament polyethylene line threaded through the cap and tied off. The cap also had a vent hole to allow air exchange with the atmosphere and access for an air bubbler. The test vessels were kept in a room maintained at a nominal temperature of 25°C. Dissolved oxygen (DO) and pH were measured on a regular basis during some of the tests. For experiments in which pH was to be maintained at a constant value, acid (HCl) or base (NaOH) were added as needed.

The concentrations of the metals leached from the alloys into the solutions were measured at the end of each experiment by ICP-MS in a commercial laboratory. Because these analyses required a major portion of the solution contained in many of the experiments, they could only be done at the end of these experiments. A limited number of experiments were carried out in 4 liter vessels so that several samples could be obtained during the experiment. Details of the sampling and analysis procedure are given in Appendix A. The results of these analyses provide time-averaged leach rates for all the metals of interest.

Monofilament
Line

Air Vent

Polyethylene
1 L Jar

Aqueous
Solution

Air
Pump

Attachment
Hole

Alloy Disc

32.eps/9-02-98
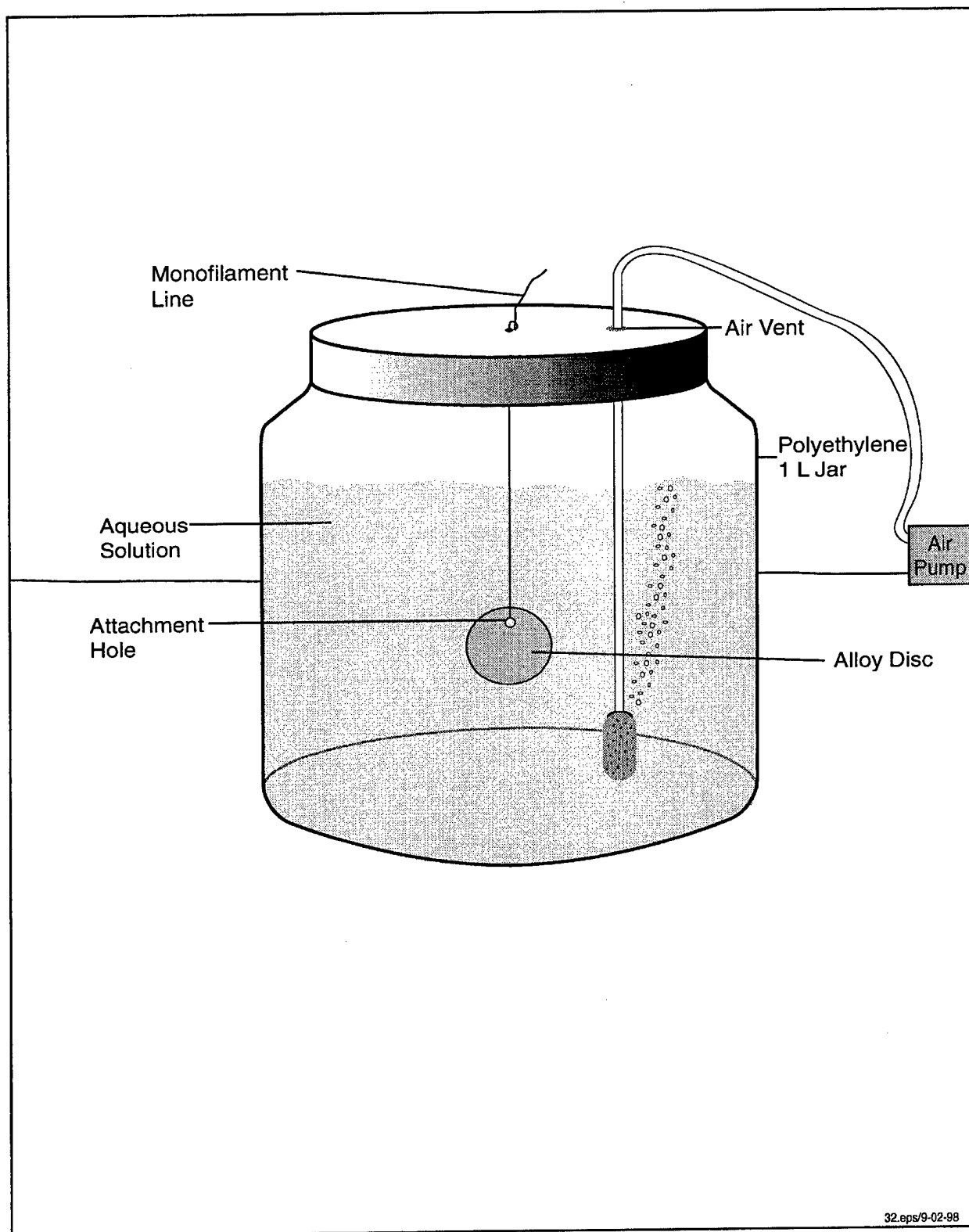
Figure 3.2. Immersion test vessel setup.

Information on short-term variations in the nickel dissolution rates of the various alloy/water combinations was obtained by measurement of the concentration of nickel in small aliquots taken from each experiment. These nickel analyses were carried out with a test kit as described in Appendix A. Some analyses of cobalt and copper were also carried out using test kits.

3.3.1.1 Experimental Matrix

An experimental matrix was developed to address (1) the alloy compositions to be tested, (2) the water compositions to be tested, (3) the pH values to be tested and (4) test durations. Table 3.3 shows the experimental matrix including each alloy with each water type at several nominal pH values. Each water type except Gulf Water was tested over a range of pH values to determine the effect of this parameter on the leaching/corrosion rates. The tests with Gulf Water were carried out at ambient pH and no acid or base were added during the tests with this water. The target pH values for the other tests were 5.0, 6.0, 7.0, and ambient. Time of immersion ranged from 20 to 138 days. Time was varied to determine if corrosion rates changed over time. The volumes listed in Table 3.3 are the volumes remaining in each test vessel at the end of the test. Note that most of the tests were initiated with either 960 or 1800 ml of water (see Appendix B).

Table 3.3. Immersion corrosion experimental matrix.

Water	Alloy	pH	Initial mass (g)	Immersion Time (days)	Final Volume (mL)
Gulf Water	WL-1	ambient	18.4945	138	600
A-SEA	WL1	5	18.5655	49	460
			18.4589	20	1458
			18.5113	30	1335
		7	18.4573	49	450
		ambient	18.4034	49	800
			18.4252	49	800

Water	Alloy	pH	Initial mass (g)	Immersion Time (days)	Final Volume (mL)
A-GRD	WL-1	5	18.4947	49	435
			18.5479	20	1515
			18.3741	30	1407
		7	18.3108	43	630
		ambient	18.3488	91	760
			18.3971		
A-SUR	WL-1	5	18.5522	53	1019
		6	18.7126	53	1063
		7	18.5124	34	1380
		ambient	18.4865	32	960
			18.4231		
			18.4544	47	960
Gulf Water	NS	ambient	22.3269	138	600
A-SEA	NS	5	22.6646	49	250
			22.6646	30	1149
			22.599	20	1525
		6	22.5344	51	375
			22.4087	30	1306
			22.5398	20	1468
			22.6146	48	875
		7	22.337	51	380
		ambient	22.6035	90	700
A-GRD	NS	5	22.3949	49	410
			22.568	20	1566
			22.3813	30	1464
		6	22.4329	51	300
			22.2369	20	1486
		7	22.6361	47	515
			22.4636	34	1620
		ambient	22.5707	87	660

Water	Alloy	pH	Initial mass (g)	Immersion Time (days)	Final Volume (mL)
A-SUR	NS	5	22.3929	53	1000
		6	22.4595	53	1016
		7	22.3368	34	1410
		ambient	22.3021	32	960
			22.4417	47	960
			22.5129		
Gulf Water	HD-17	ambient	13.8962	138	570
A-SEA	HD-17	5	13.7803	49	540
		6	13.8754	49	570
			13.8991	20	640
			14.1802	44	865
		7	13.9364	49	620
		ambient	14.2208	92	600
A-GRD	HD-17	5	13.7397	49	400
			13.9526	20	1480
			14.1066	30	1470
		6	14.0758	50	450
			14.2243	20	1510
			13.9271	21	1520
			13.9364	27	882
		7	13.826	44	630
		ambient	13.8546	92	570
A-SUR	HD-17	5	13.525	53	970
			13.9452	50	721
		6	13.3304	53	820
			13.9993	62	703
		7	14.1369	34	1390
			14.2843	43	827

Water	Alloy	pH	Initial mass (g)	Immersion Time (days)	Final Volume (mL)
		ambient	13.7315	32	960
			13.9004	47	960
			13.9741	104	695
Gulf Water	Ta	ambient	10.5524	138	690
A-SEA	Ta	5	10.4722	76	530
		6	10.4728	76	580
			10.7638	20	640
		7	10.5146	76	550
		ambient	10.475	90	690
A-GRD	Ta	5	10.6066	76	590
		6	10.5282	76	300
			10.7002	20	450
		7	10.4478	69	570
		ambient	10.5188	90	650
A-SUR	Ta	5	10.5463	54	1320
		6	10.3846	54	1260
		7	10.4453	36	760
		ambient	10.598	47	960

3.3.1.2   Corrosion Rate Data - Introductory Discussion

Before discussing the experimental results in detail, it is necessary to describe the procedure adopted for data reduction. Because various aliquots of water were removed from most of the test vessels for pH, DO and metal analysis over the course of the tests, the ratio of the volume of the solution to the alloy surface area (V/S) changed during the tests. This complicates the interpretation of the dissolution behavior of a given alloy/water system. To account for this, dissolution experiment data are reported in terms of the mass lost from the dissolving phase (i.e.,

alloy) per unit time normalized to unit surface area (e.g., mg/hr-cm^2). This type of data reporting requires that various parameters be recorded during the test including time, the volume of the remaining solution after each aliquot of solution is removed, and the surface area of the alloy specimen. Values of these parameters are given for each test in Appendix B. The details of the calculations required to correct for changes in the volume/surface area ratio are presented in the Appendix B.

Because time-series data were obtained primarily for nickel, the corrosion rate data for nickel will be discussed in more detail. This discussion will provide the framework within which data for the other metals can be evaluated. In the following discussion, the nickel data will be presented in terms of cartesian diagrams or scatter plots in which parameters related to the metal content (i.e., concentration, mass, leach rate) are plotted against time.

A diagram in which metal concentration is plotted against time initially shows a trend which reflects only the initial leach rate because the original solutions are essentially free of the metals of interest. With time, the leach rate may vary as a function of a variety of factors including variations in the chemistry of the surrounding solution, changes in the solution volume to alloy surface area ratio, changes in the detailed structure of the alloy surface, changes in the chemical composition of the alloy surface (i.e., incongruent dissolution effects), precipitation of secondary compounds on the alloy surface and/or in the solution, as well as other less well defined factors. In the following discussion, plots are presented that reflect some of these factors. In some cases, the factor responsible for the trend in a plot is clear while in other cases the responsible factor(s) may be obscure.

If the leach rate remains constant and the V/S ratio changes only due to withdrawal of fluid, the rate of change in the concentration of the metal in solution should increase with time assuming there is no precipitation of a nickel-bearing phase(s). An example of this type of trend is shown in Figure 3.3. Note that the trend of Ni concentration with time is concave upwards. A plot of mass dissolved into solution with time should show a linear trend if the leach rate is constant regardless of the V/S ratio of the solution as long as the surface area of the alloy sample remains nearly constant. An example of this type of trend is shown in Figure 3.4. These two
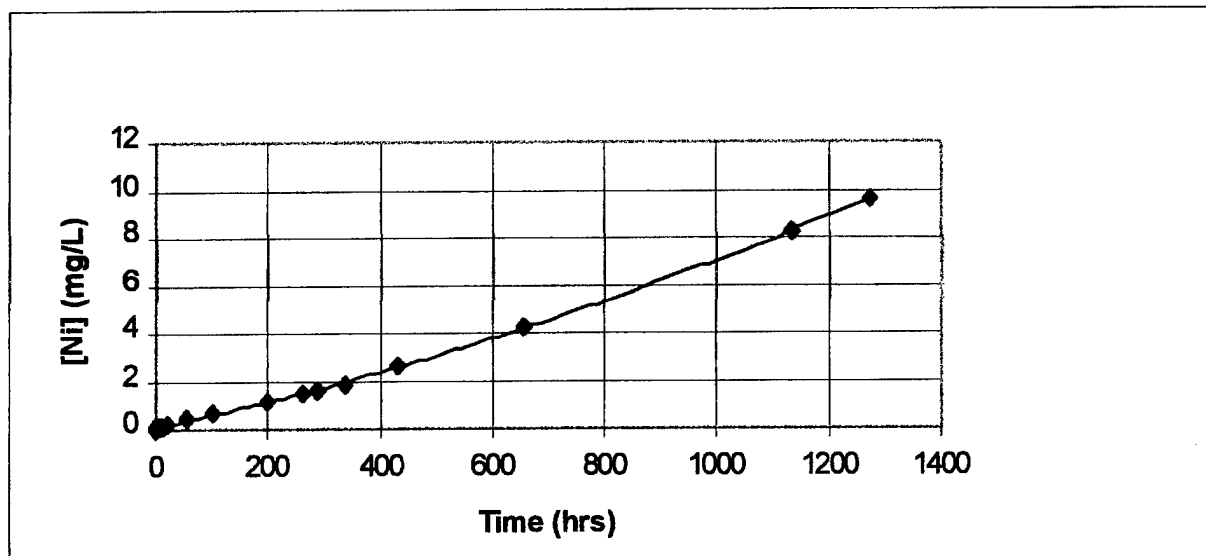
Figure 3.3. Ni concentration measurements vs. immersion time (Sample NS-22.3929) in artificial surface water at pH = 5.
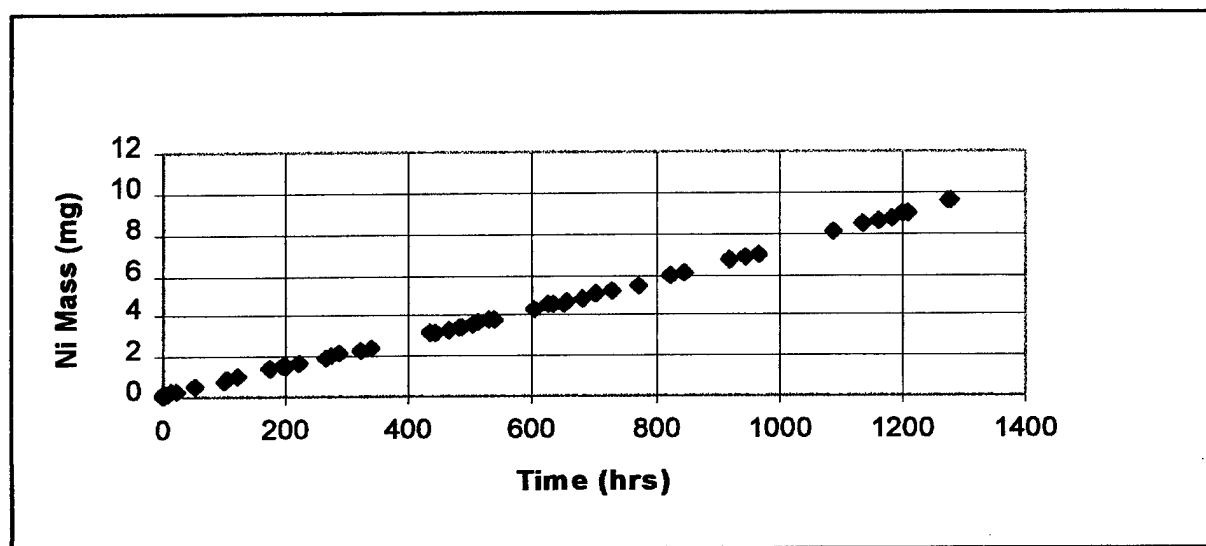
Figure 3.4. Cumulative Ni mass vs. immersion time (Sample NS-22.3929) in artificial surface water at pH = 5.

plots suggest the leach rate for the NS alloy sample is essentially constant up to 1280 hours in artificial surface water at a pH=5. Note that the additional points plotted on Figure 3.4 relative to Figure 3.3 represent interpolated concentration values (see Appendix B).

The trend of the data plotted in Figure 3.4 implies that secondary nickel phases (e.g., corrosion products) have not formed in this system even though the nickel concentrations reached approximately 8 ppm at the end of the experiment. The data also suggest that the surface area of the alloy sample remained nearly constant with time.

Evidence of the formation/precipitation of secondary compounds is found in the nickel concentration trends for many of the systems investigated. The data shown in Figure 3.5 for alloy HD-17 in surface water at pH=5 is an example. In this case, the concentration of Ni increased up to 480 hours at which time the concentration started to decrease in a nearly linear fashion. Note that the concentration reached a maximum value of only 1.44 mg/L before it started to decline. In this case, the decrease in concentration was associated with the formation of a corrosion layer on the surface of the alloy disk. This corrosion layer could be easily removed by scraping thereby revealing virgin alloy. The identity of corrosion products is discussed in the following section.

As shown in Figure 3.6, the time-averaged nickel leach rate never exceeded 0.00025 mg/hr-cm^2 in this experiment and the short-term rate was closer to 0.00015mg/hr-cm^2. These data suggest that this alloy corrodes more slowly in surface water at pH=5 than the NS alloy. However, consideration of the leach rates of the other metals (e.g., tungsten) and the thickness of the corrosion product layer suggests this conclusion is not correct as further discussed in the following section.

3.3.1.3   *Discussion of Long-Term Leaching Behavior of Nickel in Different Alloy/Water Systems*

This discussion is intended to summarize the data reported in Appendix B on the leaching behavior of nickel in tungsten alloy/water systems. The discussion is structured first in terms of alloy types, second in terms of water types and third in terms of pH.
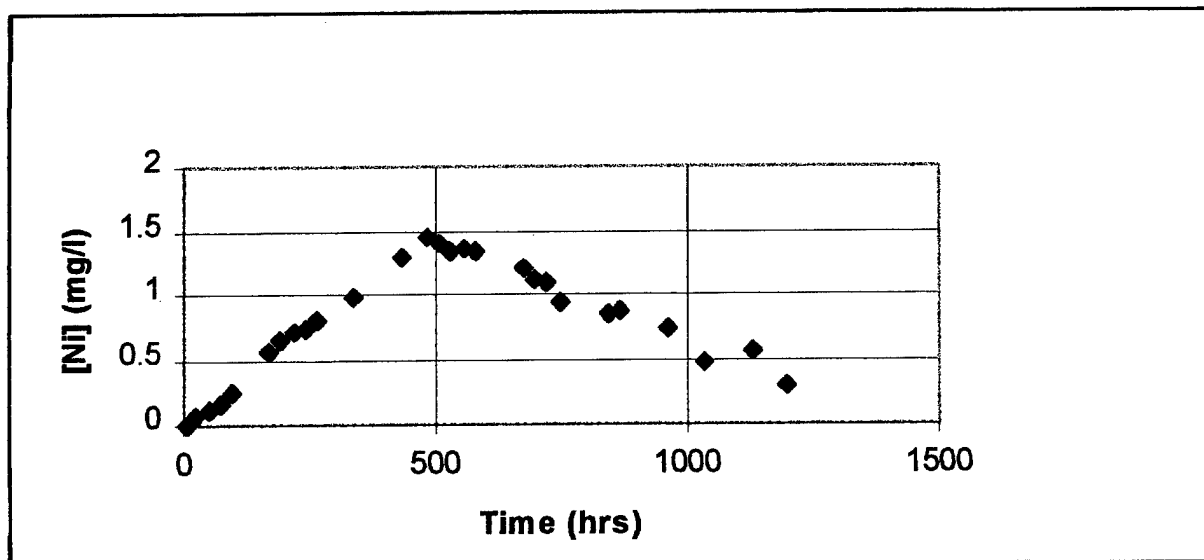
Figure 3.5. Ni Concentration vs. time (Sample HD-17-13.9452) in artificial surface water at pH = 5.
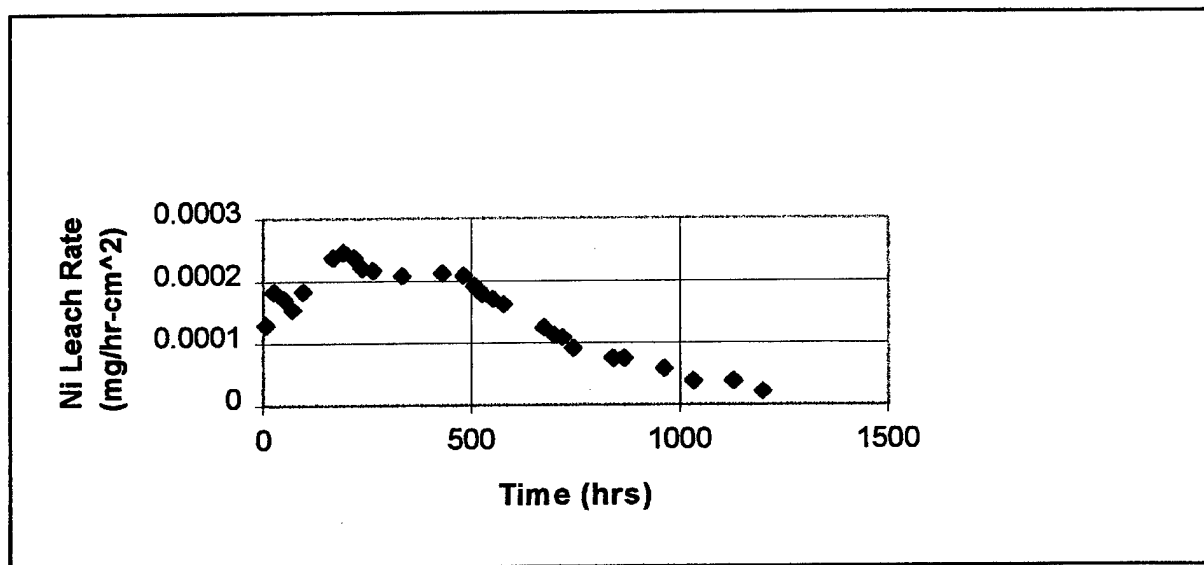
Figure 3.6. Cumulative Ni leach rate average vs. time (Sample HD-17-13.9452) in artificial surface water at pH = 5.

Alloy WL-1

The leaching behavior of this alloy appears to be relatively consistent in most of the experiments. In artificial seawater, the trends of nickel mass dissolved per unit surface area are generally concave upward or linear as a function of time as shown in Figure 3.7. The nickel leach rate was generally higher at lower pH. There is little evidence to suggest a nickel compound precipitated in these experiments over the time frame represented by the trends. However, the observation of red-brown corrosion products on the surfaces of the alloy specimens after several hundred hours (Figure 3.8) suggests iron oxides/hydroxides did precipitate from these experiments with time. The total mass of the corrosion products was generally small but their color made them particularly evident. Attempts to characterize the corrosion products by X-ray diffraction spectrometry were unsuccessful because of their amorphous nature. An EDX analysis of this material is shown in Figure 3.9. Note that the minor amounts of other elements shown on the figure may result from other phases within or upon the iron oxide/hydroxide phase or from the fact that the X-ray beam penetrated beneath the oxide/oxyhydroxide phase into virgin alloy. The formation of these corrosion products indicates that the binder phase was at least partly dissolved (i.e., acting as an anode). Note that acid had to be added to the WL-1 experiments to maintain constant pH (Appendix B).

The WL-1 samples kept in "pillboxes" for several months showed some interesting features. These specimens were generally covered by a layer of powdery iron and nickel oxides, hydroxides, and/or tungstates. The iron oxides/hydroxides tended to occur directly in contact with the alloy while the nickel oxides/hydroxides/tungstates were found as a fine grained deposit on the underlying iron phases. Nickel and iron phases may also have coprecipitated as oxides and/or hydroxides. The dissolution of the binder phase left pure tungsten grains largely intact as shown in Figure 3.8.

Figure 3.7. Cumulative Ni mass vs. time for immersion experiments with alloy WL-1 in artificial sea water at various pH values. The data plotted for the "Ambient #7" represents and experiment in which the pH was allowed to drift.
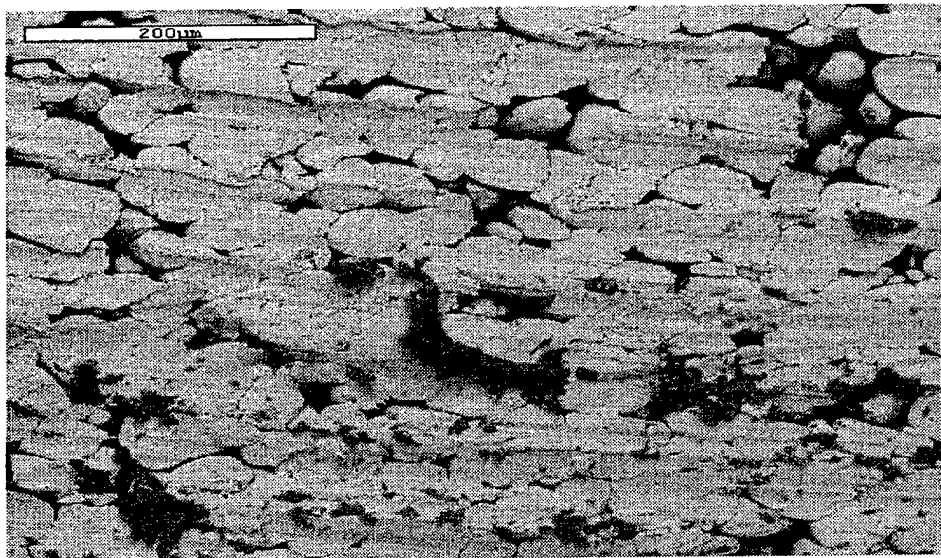
Figure 3.8. SEM photo of sample WL-1-18.4573 reacted in seawater at nominal pH=7.0. Tungsten grains remain after preferential dissolution of binder. Dark gray material is probably ferric hydroxide or oxyhydroxide.
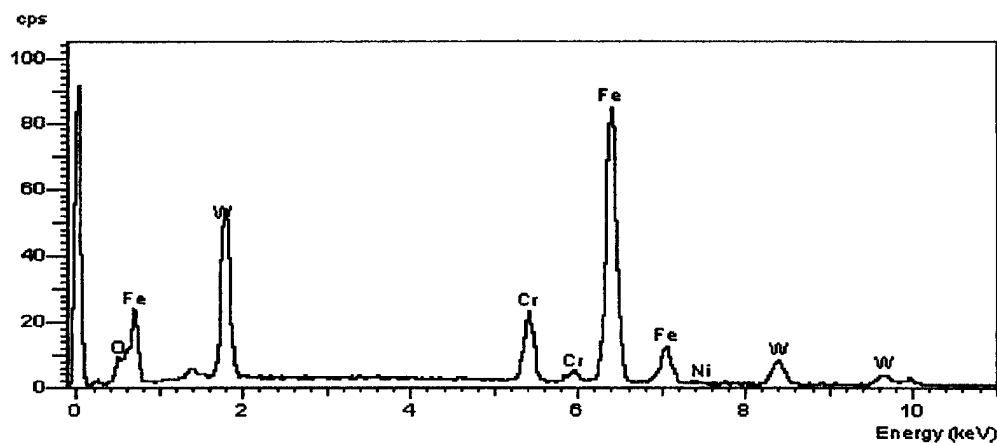
Figure 3.9. EDX analysis of iron hydroxides shown in Figure 3.8.

The SEM observations suggest that the binder phase was anodic (i.e., leached) during the reaction of alloy WL-1 with seawater. Anodic reactions for iron in the binder phase would likely include the following:

$$Fe + 2OH^- \Rightarrow Fe(OH)_2 + 2e^- . \qquad (3.1)$$

$$\text{and} \quad Fe + 1/2 \ O_2 + 2 \ H_2O \Leftrightarrow Fe(OH)_3 + H^+ + e^-. \qquad (3.2)$$

As these equations indicate, the precipitation of ferric oxide/hydroxide generally leads to the production of acidity or the consumption of hydroxide ions. The fact that acid had to be added to the WL-1 experiments to maintain constant pH (see Appendix B) suggests the precipitation of ferric hydroxide was not a dominant corrosion reaction.

For nickel in the binder phase, the dominant anodic reaction would likely be:

$$Ni \Leftrightarrow Ni^{2+} + 2e^-. \qquad (3.3)$$

Because the binder phase also contained some tungsten, an anodic reaction for tungsten might also be expected. This reaction would likely be:

$$W + 4H_2O \Rightarrow WO_4^{2-} + 8 H^+ + 6e^-. \qquad (3.4)$$
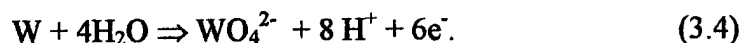
With the binder phase anodic, it is likely that the pure tungsten grains in the alloy were cathodic and that a galvanic corrosion cell was set-up. The dominant cathodic reactions likely would be the following:

$$2H^+ + 2e^- \Leftrightarrow H_2 \qquad (3.5)$$

$$\text{or} \qquad 2H_2O + O_2 + 4e^- \Leftrightarrow 4OH^- \qquad (3.6)$$

These reactions consume hydrogen ions or produce hydroxide ions and would cause the pH to increase with time as observed. The cathodic behavior of pure tungsten metal can be explained by the fact that pure tungsten tends to be more noble (i.e., less tendency to oxidize) than the binder in the WL-1 alloy under the conditions of the experiments as discussed further below.

The leaching behavior of this alloy in artificial ground water (Figure 3.10) was similar to the behavior observed in artificial seawater. There is slight suggestion of curvature in the nickel mass versus time trends suggesting some precipitation occurred during the tests. Alternatively, the leach rates are affected by the formation of a corrosion layer on the alloy. SEM photomicrographs suggest that there is less preferential dissolution of the binder phase in ground water compared to seawater (Figure 3.11).

In artificial surface water, the dissolution trends for this alloy also showed slight deviations from linearity in some of the experiments (Figure 3.12). Visual observation of these samples indicates that the surfaces of the samples are partly coated with corrosion products after
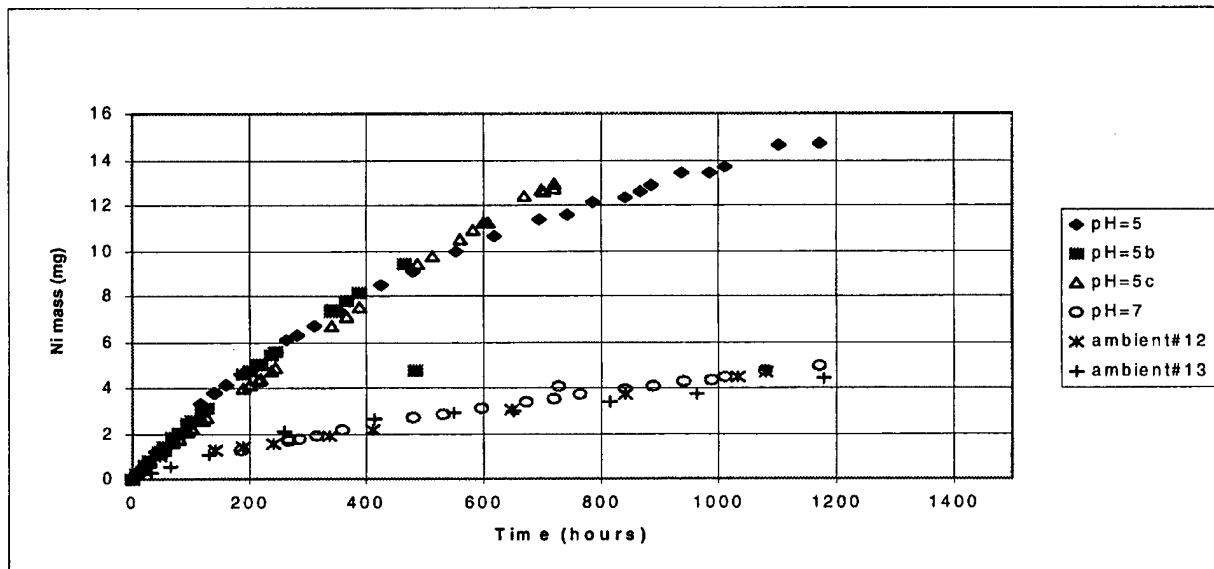
Figure 3.10. Cumulative Ni mass vs. time for immersion experiments with alloy WL-1 in artificial groundwater at various pH values. "Ambient #12" and "Ambient #13" represent experiments in which the pH was allowed to drift.
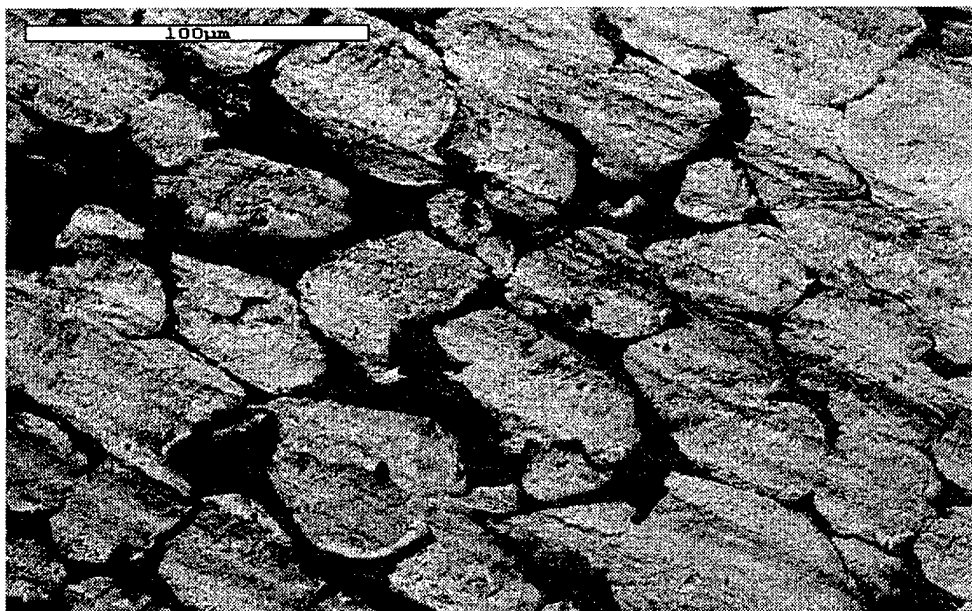
Figure 3.11. SEM photograph of sample WL-1-18.3108 reacted in artificial groundwater at nominal pH=7.0. Note that binder phase (dark gray) is largely intact. Grayish-white grains are pure tungsten.
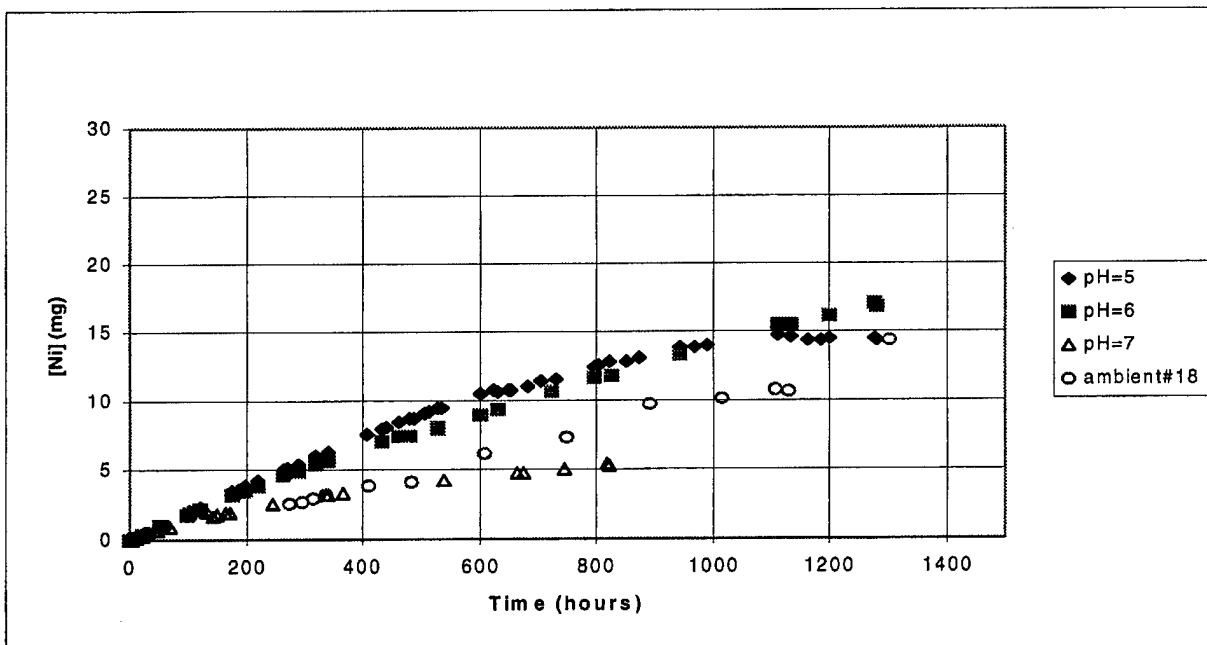
Figure 3.12. Cumulative Ni mass vs. time for immersion experiments with alloy WL-1 in artificial surface water at various pH values. The "Ambient #18" represents an experiment in which the pH was allowed to drift.

several hundred hours. SEM analysis of "pillbox" samples, indicated that the dominant corrosion products are fine-grained iron and nickel oxides/hydroxides and what appear to be iron-nickel tungstates. The texture of these corrosion products is shown in Figure 3.13. An EDX analysis of the fine-grained ground mass is shown in Figure 3.14. An EDX analysis of the angular grain in the center of Figure 3.13 is shown in Figure 3.15. This grain appears to be a nickel-iron tungstate compound.

<u>NS Alloy</u>

The corrosion behavior of this alloy is generally similar to the corrosion behavior of WL-1 but not the same. As with WL-1, acid had to be added to maintain constant pH for all experiments involving this alloy. The leach rates generally decrease with increasing pH as also observed in the experiments with WL-1. In detail, however, the mass vs. time trends are more
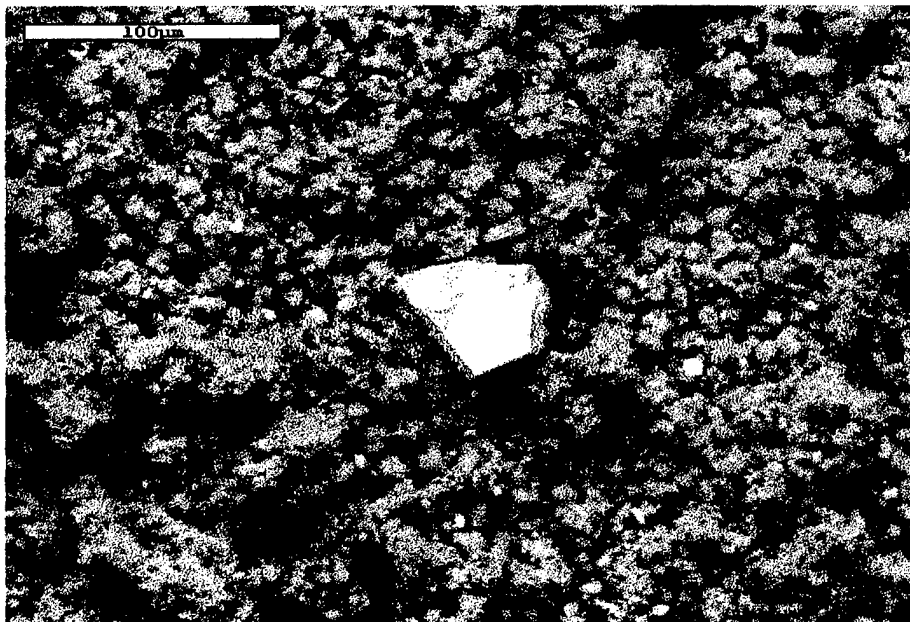
Figure 3.13. SEM photograph of sample WL-1-18.5522 reacted in artificial surface water with a nominal pH=5.0. Corrosion product formed in a pillbox.
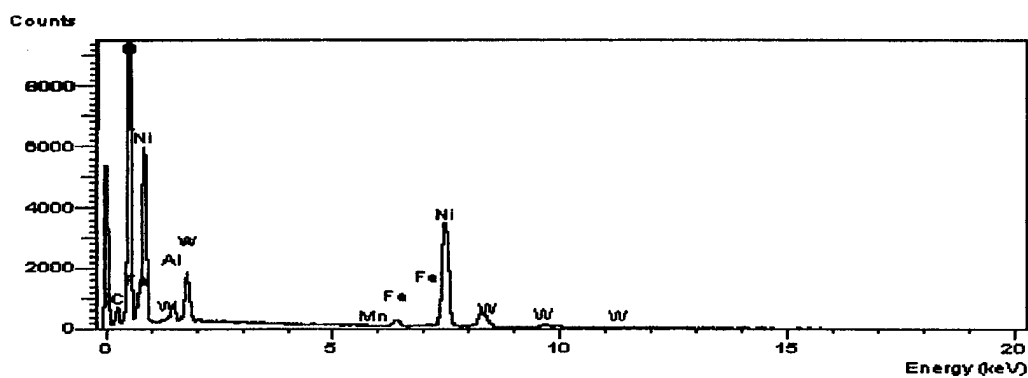
Figure 3.14. EDX analysis of grayish fine grained mass in sample WL-1-18.5522, Figure 3.13. Corrosion products formed in pillboxes.
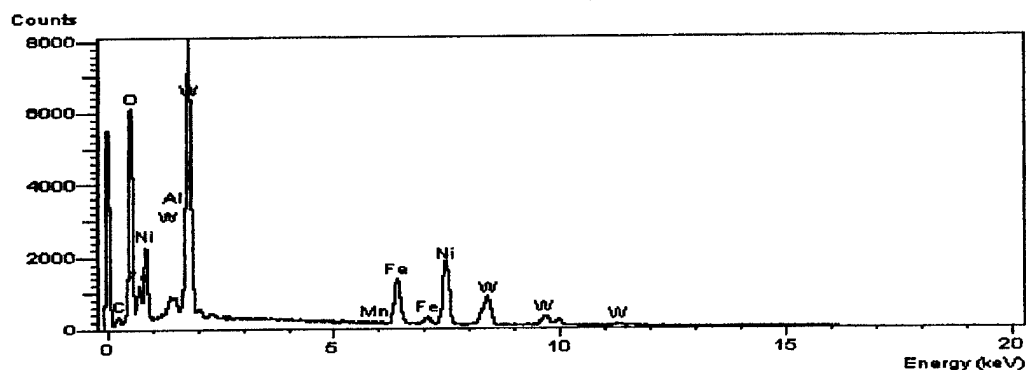
Figure 3.15. EDX analysis of white crystal in Figure 3.13. Corrosion product formed in a pillbox.

complex particularly after 100 hours (Figure 3.16). For example, at pH = 5 and 400 hours, the Ni masses in solution vary by approximately a factor of 2. At pH = 6, the Ni masses in solution vary by approximately a factor of 4 at 400 hours. Further, the masses observed in 2 of the pH=6 experiments exceed the masses in all the pH=5 experiments, contrary to expectation.

It is thought these inconsistencies reflect differences in the nucleation and precipitation rates of corrosion products in the different experiments. These rates are known to be sensitive to the detailed surface structure of corrosion specimens (Trethewey & Chamberlain, 1988).

As with alloy WL-1, the visible corrosion products in artificial seawater are commonly red-brown in color and probably include iron oxide/hydroxide. Minor black colored corrosion products are also visible along the edges of the red-brown products. As is discussed in more detail below, the ending solution compositions in these experiments are generally supersaturated with nickel and cobalt tungstate compounds.
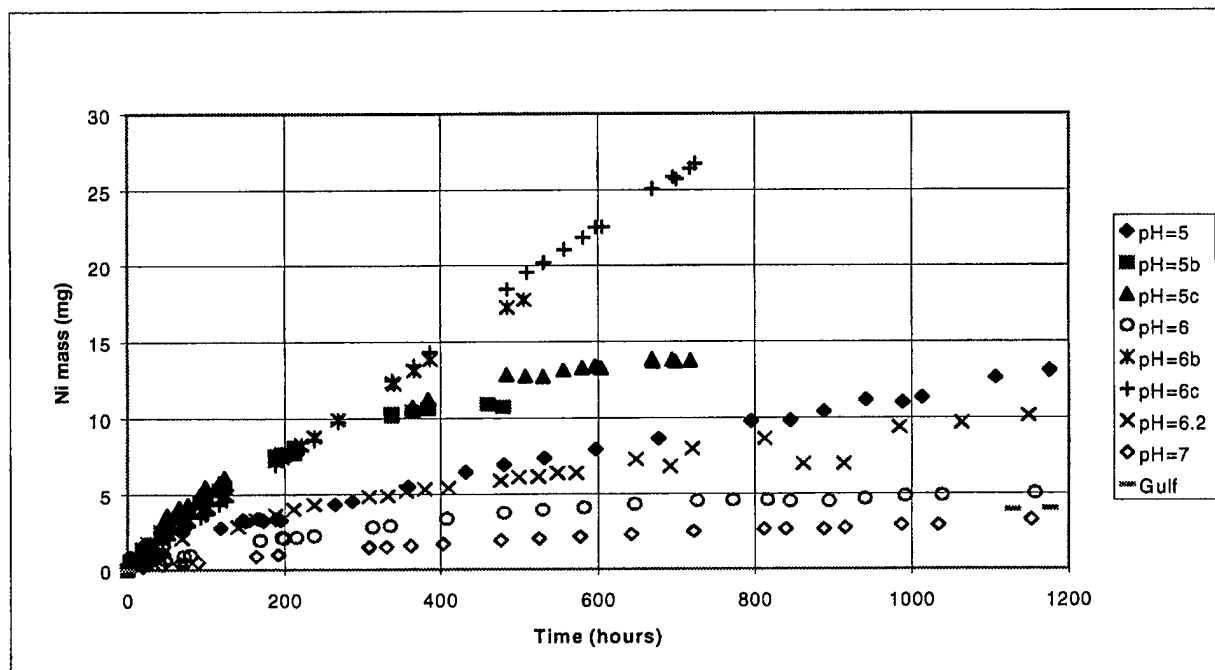
Figure 3.16. Cumulative Ni mass vs. time for immersion experiments with alloy NS in seawater at various pH values. The data points plotted for "Gulf" represent natural sea water. All other data points are for artificial sea water.

In the experiments carried out with this alloy in artificial ground water, mass versus time graphs also show slopes decreasing with time (Figure 3.17). In addition, it appears that the slopes change earlier in the lower pH experiments compared to the higher pH experiments. The amounts of corrosion products formed in these experiments is generally small and some areas on the alloy specimens have no covering of corrosion products. As with seawater, the initial corrosion products are commonly red-brown in color and are probably dominated by iron hydroxide or oxyhydroxide. Black colored corrosion products occasionally occur as patches within the red-brown products. The black patches appear to be more firmly fixed to the alloy substrate than the red-brown patches. Calculations (Appendix E) indicate the ending solutions in these experiments are also saturated with nickel and cobalt tungstate compounds.
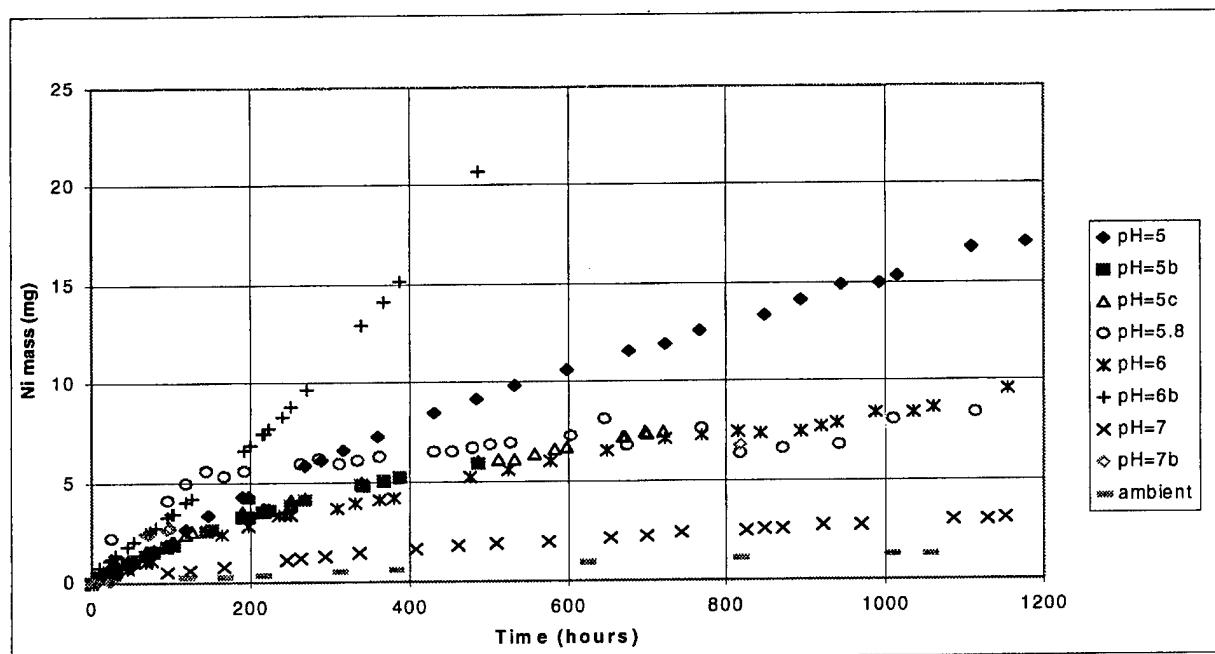
Figure 3.17. Cumulative Ni mass vs. time for immersion experiments with alloy NS in artificial groundwater at various pH values. The data points plotted for "Ambient" represent an experiment in which the pH was allowed to drift.

In artificial surface waters, this alloy corrodes similarly to the way it corrodes in artificial ground waters but it corrodes less. The trends of nickel mass versus time are nearly linear (Figure 3.18) at low pH (4-6) but show decreasing slopes at higher pH suggesting the formation of precipitates. The dominant corrosion products are patches of red-brown iron hydroxide/oxyhydroxides with rare patches of a black solid. The ending solutions in these experiments are also saturated with nickel and cobalt tungstate compounds.

In the "pillbox" samples, corrosion products were present on the NS alloy samples although much of the surface of the specimens remained clear of corrosion products. A photomicrograph of a typical patch of corrosion products is shown in Figure 3.19. An EDX scan of the grayish mass located in the top-center of the figure is shown in Figure 3.20. This scan suggests the mass is a Ni-Fe-Co oxide or hydroxide phase with a minor amount of tungsten. Note that the sizes of the tungsten peaks on a scan such as this are not proportional to
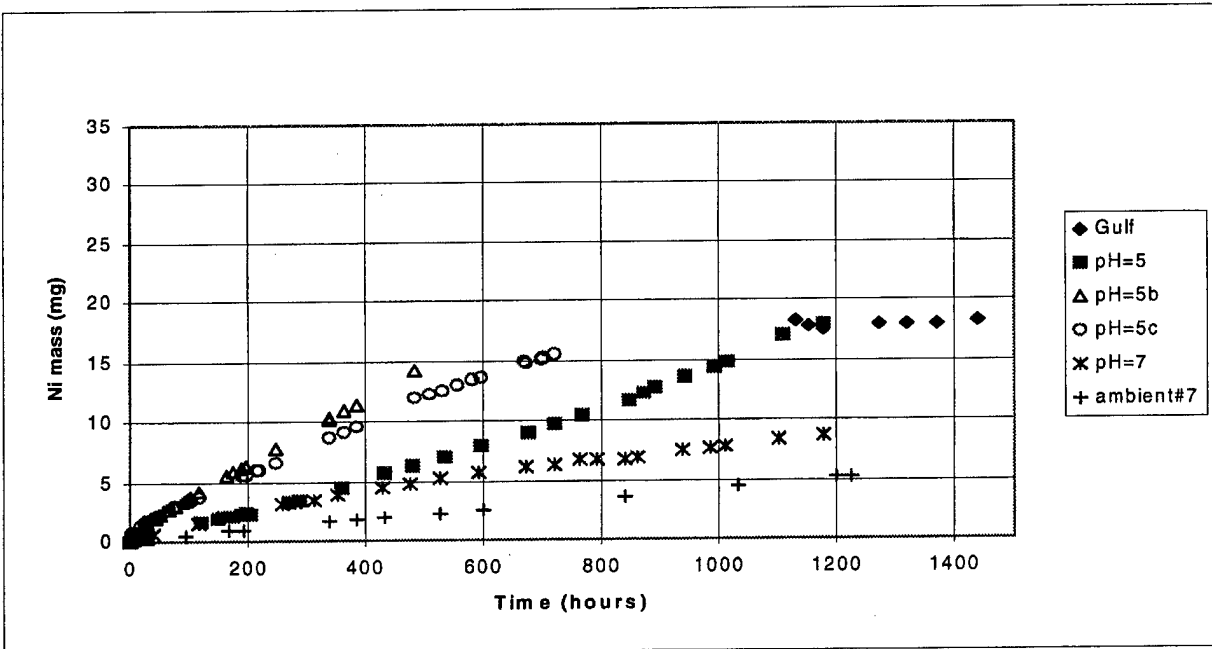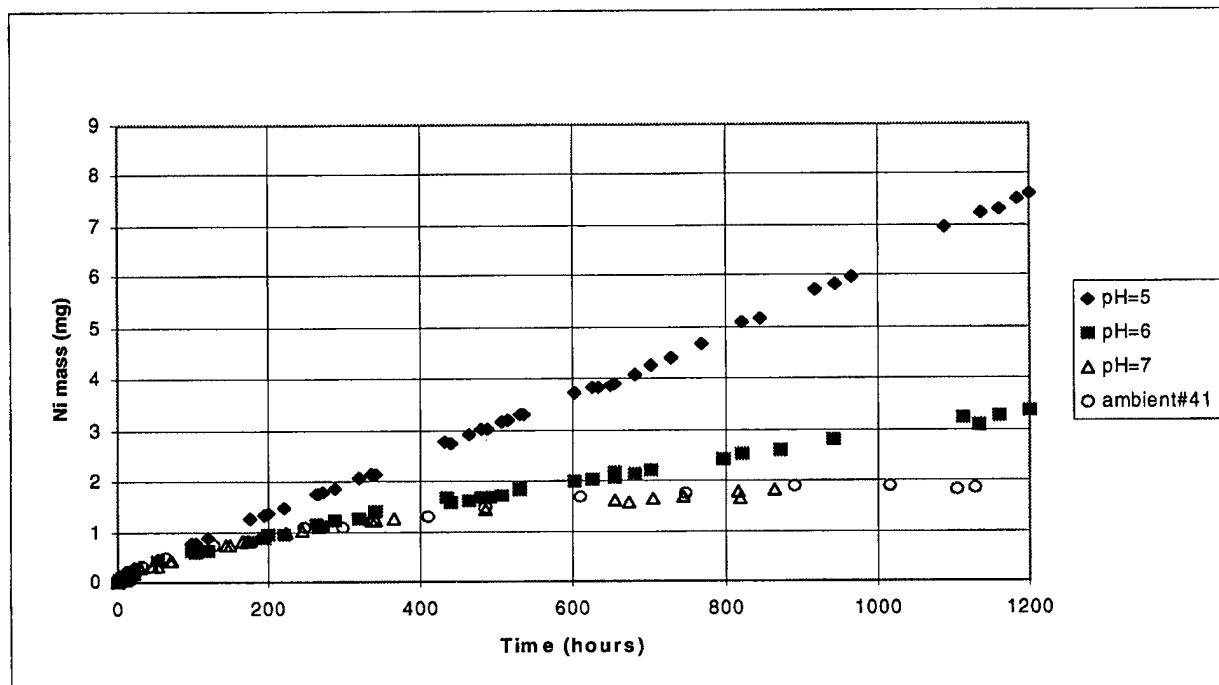
Figure 3.18. Cumulative Ni mass vs. time for immersion experiments with alloy NS in artificial surface water at various pH values. The data points plotted for "Ambient #41" represent an experiment in which the pH was allowed to drift.
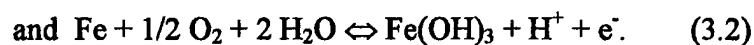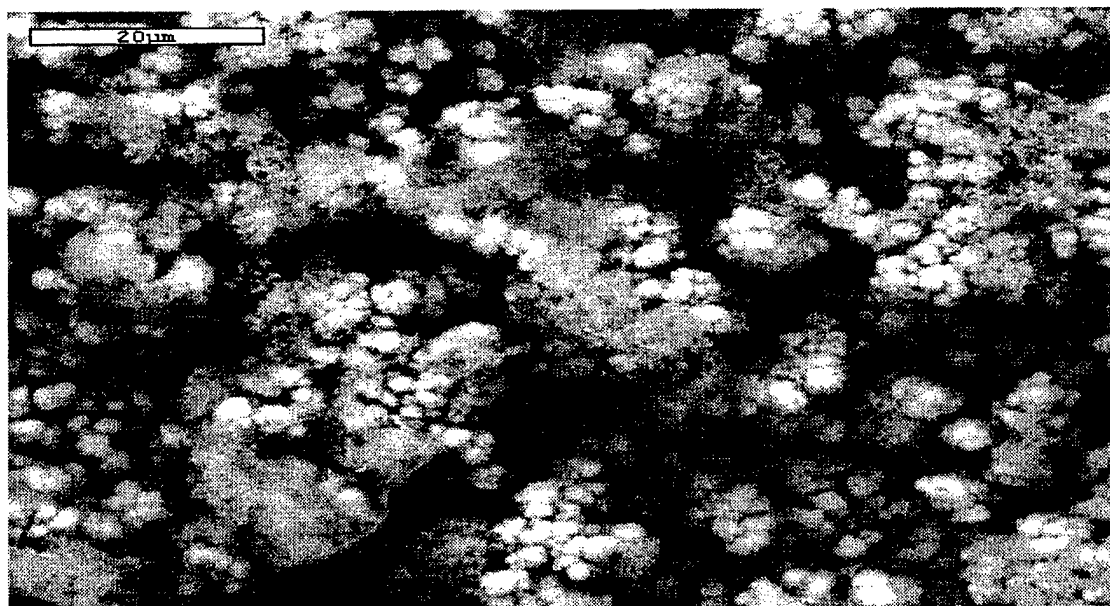

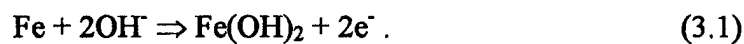**Figure 3.19. SEM photograph of sample NS-22.3929 corrosion product. Typical NS-corrosion products formed in a pillbox.**
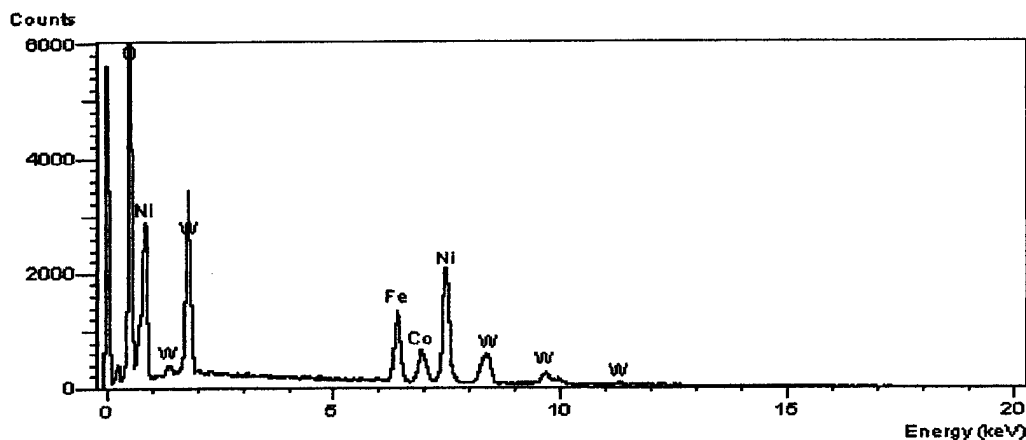
Figure 3.20. EDX analysis of gray mass in top center of Figure 3.19. Ni-Fe-Co oxide or hydroxide corrosion product formed in a pillbox.

concentration because the atomic mass of tungsten is much greater than the atomic masses of nickel, iron and cobalt. For the latter metals, the size of the peaks is approximately proportional to concentration. An EDX scan of the lighter colored "balls" in Figure 3.19 is shown in Figure 3.21. The "balls" are apparently enriched in iron over nickel, cobalt and tungsten compared to the "grayish mass" in Figure 3.19. Both the "gray mass" and the lighter colored "balls" are likely amorphous in structure.

Alloy HD-17

The dissolution behavior of this alloy is the most complex of the alloys investigated. As explained further below, the main reason for this appears to be the fact that the alloy contains copper. For most of the experiments carried out with artificial sea water, the mass versus time graphs (Figure 3.22) are almost linear although this is in part due to the fact that some trendlines represent only 2-3 actual data points. In any case, these trends are consistent with
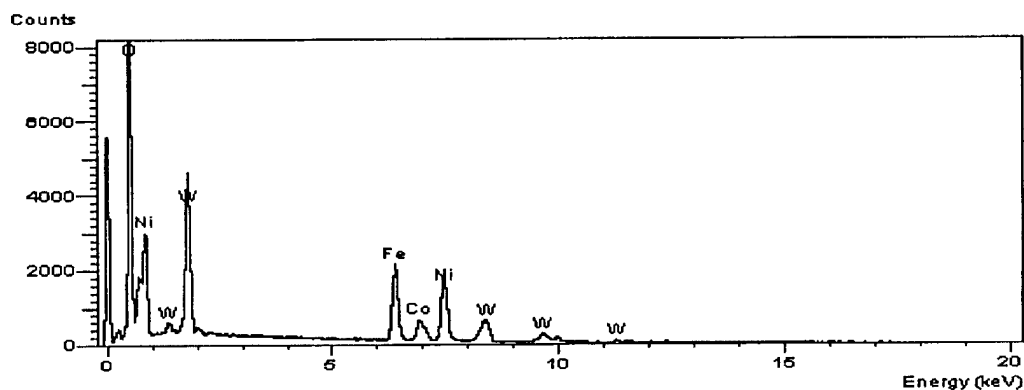
Figure 3.21. EDX analysis of white balls in Sample NS-22.3929, shown in Figure 3.19. Corrosion products formed in a pillbox.
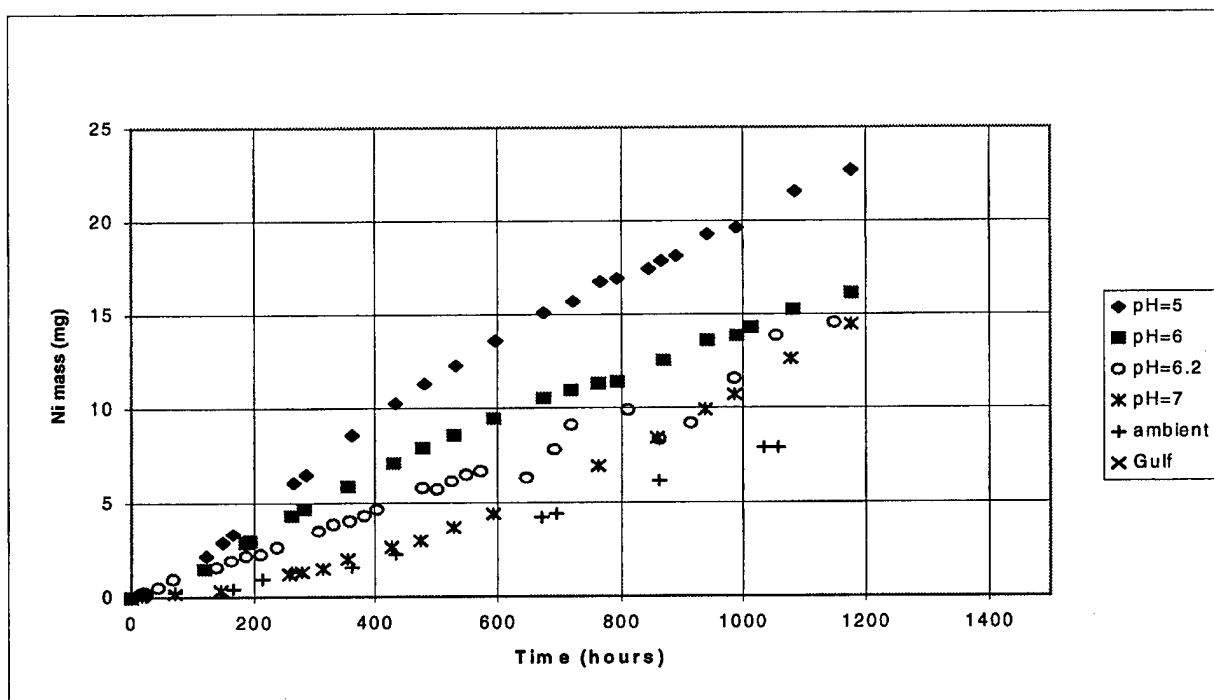
Figure 3.22. Cumulative Ni mass vs. time for immersion experiments with alloy HD-17 in seawater at various pH values. The data points plotted for "Gulf" represent natural sea water. All other data points are for artificial sea water.

simple leaching (i.e., corrosion without precipitation). The experiments at higher pH (> 7.0) show mass versus time graphs that are concave upward. This apparently reflects enhanced pitting corrosion which causes the surface areas and thereby the dissolution rates of the alloy samples to increase with time. Abundant pits are evident in these two samples compared to other samples. Acid was added to maintain constant pH in these seawater experiments. This suggests that the corrosion behavior of this alloy in seawater is similar to the corrosion behavior of alloys WL-1 and NS in seawater with the binder phase anodic and the pure tungsten grains cathodic.

In SEM photomicrographs of "pillbox" samples for HD-17 in seawater, it appears the binder phase dissolves preferentially as shown on the far right hand side of Figure 3.23. Although there is no evidence of the precipitation of nickel compounds in these experiments, copper and tungsten compounds did precipitate in the experiments. Figure 3.23 shows a phase that appears to be a copper/nickel tungstate according to the EDX scan shown in Figure 3.24. Figure 3.25 shows an interesting crystal of tungstite ($WO_3 \cdot 2H_2O$) that crystallized on top of remnant tungsten metal grains in a "pillbox" sample. Note that these crystals probably would not have crystallized during the immersion experiments in which the solutions were much less concentrated compared to the "pillbox" samples.

The leaching/corrosion behavior of the HD-17 alloy in artificial ground water is quite different from its behavior in artificial seawater. The most significant difference is that the amount of nickel and copper leached into solution is much less for the ground water experiments. At pH < 6.0, the nickel concentration versus time and mass versus time trends are nearly constant in slope. At higher pH values, these trends reach a maximum and sometimes even decrease with time (Figure 3.26). The negative slopes are a clear indication that nickel phases are precipitated during these experiments. However, visual observation of the disks during the experiments indicate only a slight discoloration of the alloy specimens to a black or brownish-black "corrosion product." The porosity of the alloy specimens, particularly in areas near the circumference of the disks, appears to have increased with time.
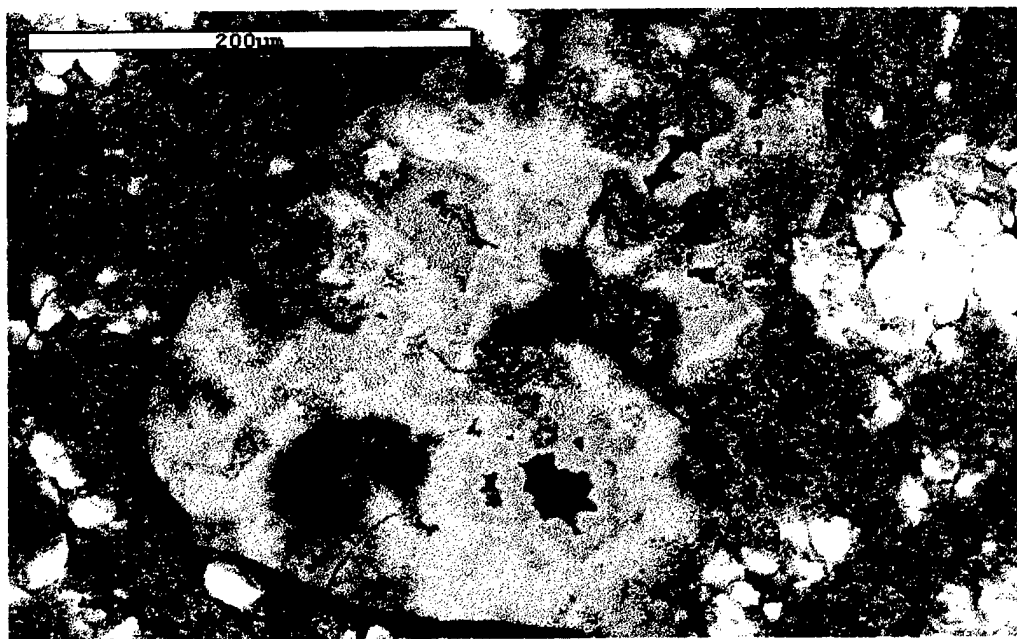
Figure 3.23. SEM photomicrograph of corrosion products in sample HD-17-13.7441. The large grain is apparently a copper-nickel tungstate. White grains are pure tungsten.
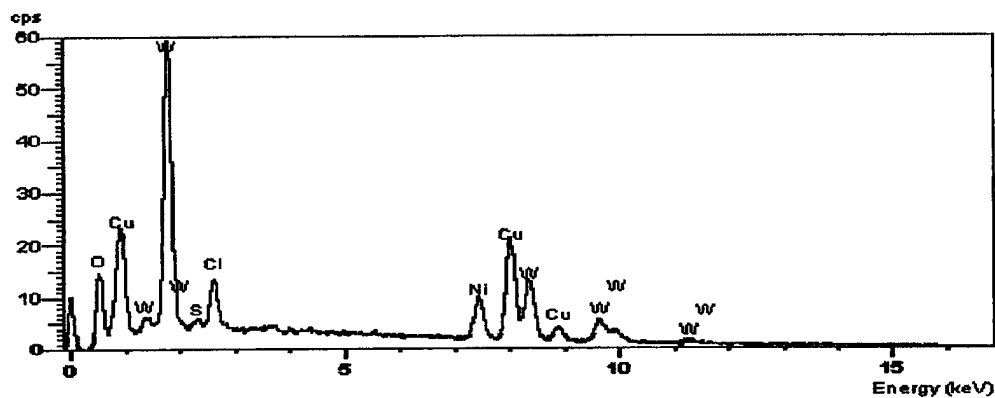
Figure 3.24. EDX analysis of corrosion product shown in Figure 3.23. Probably Cu, Ni tungstate.
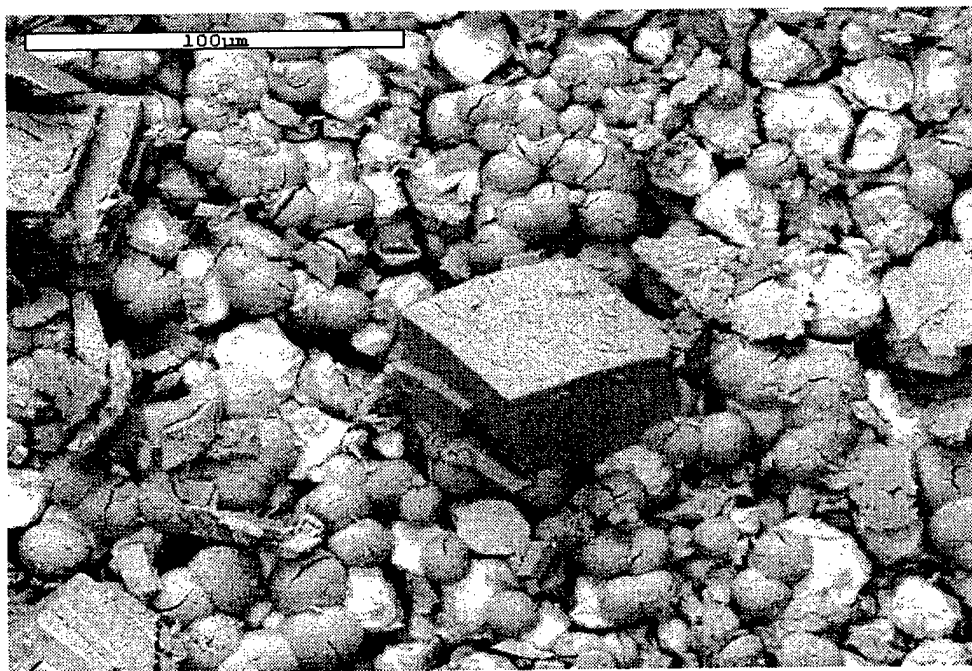
Figure 3.25. SEM photomicrograph of corrosion products on surface of alloy disk HD-17-13.7441. Block appears to be tungsten oxide. White grains are pure tungsten metal. Pillbox sample.
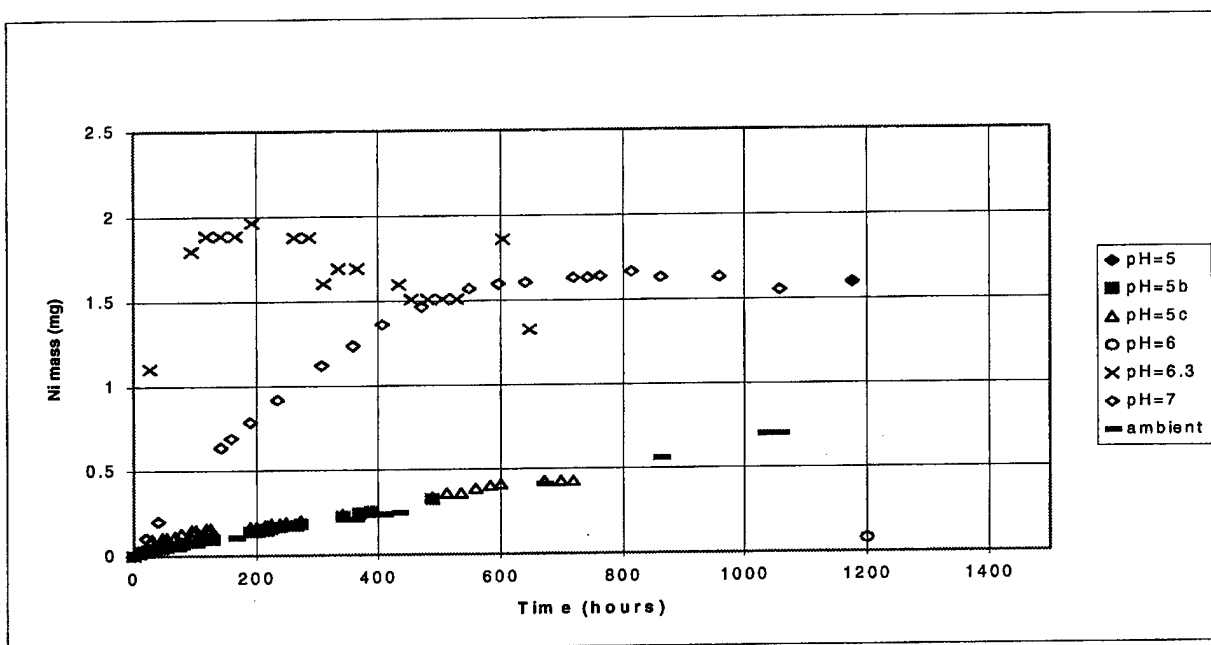
Figure 3.26. Cumulative Ni mass vs. time for immersion experiments with alloy HD-17 in artificial groundwater at various pH values. The data points plotted for "Ambient" represent an experiment in which the pH was allowed to drift.

SEM analysis shows that, in ground water, the pure tungsten grains in this alloy are preferentially dissolved. A photomicrograph of sample HD-17 13.9364 (immersed in ground water at pH = 6.3) is shown in Figure 3.27. This photomicrograph clearly shows the binder phase intact with the near-surface tungsten grains largely dissolved out. Note that tungsten grains some distance into the interior of the sample also appear to have dissolved. This is not a "pillbox" sample. An elemental scan of the binder phase is shown in Figure 3.28. The small oxygen peak suggests that the binder is not oxidized to a significant degree. This implies that the low overall concentrations (<2 mg/L) of nickel and copper dissolved from this sample are the result of the binder acting as a cathode in the ground water immersion experiments while the pure tungsten grains act as anodes.

Figure 3.29 shows copper crystals that grew on top of the binder phase in sample HD-17-14.2243 after this sample had resided in a "pillbox" for several months. This indicates that copper was dissolved from the binder at least under the chemical conditions predominating in the "pillbox."
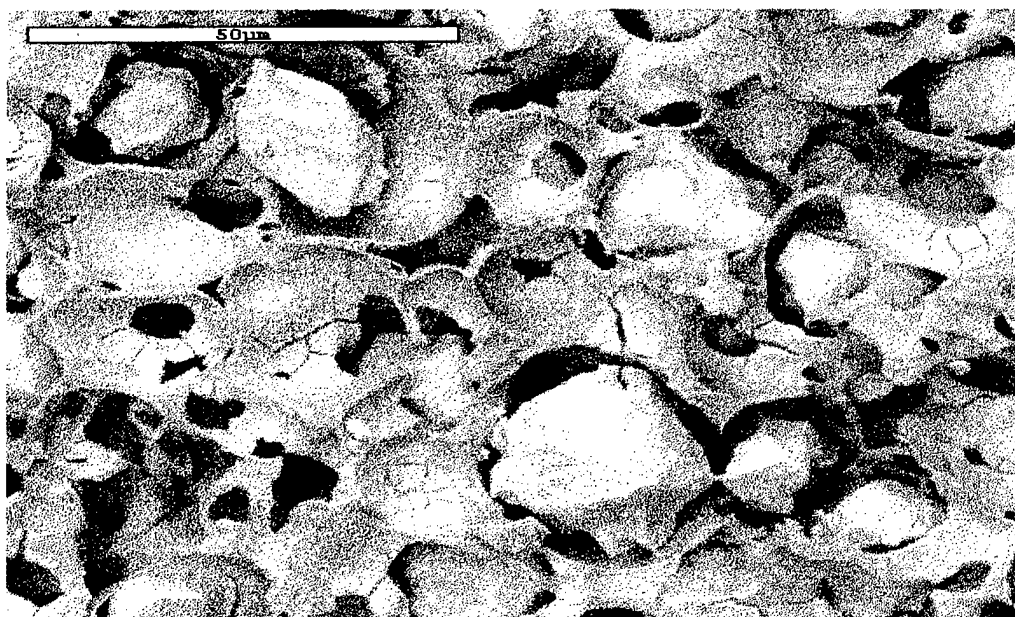
Figure 3.27. SEM photomicrograph of alloy sample HD-17-13.9364. Note tungsten grains leached out. This sample came directly from an immersion test and is not a "pillbox" sample.
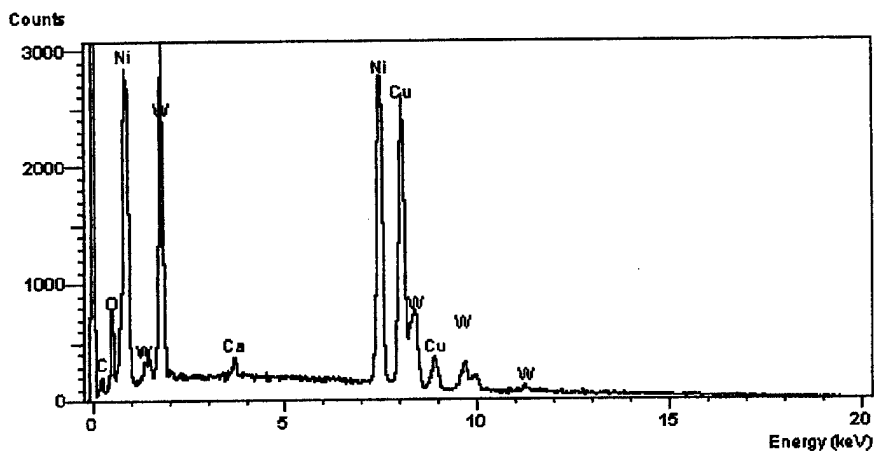
Figure 3.28. EDX analysis of sample HD-17-13.9364 binder. Note small oxygen peak compared to Ni and Cu peaks.
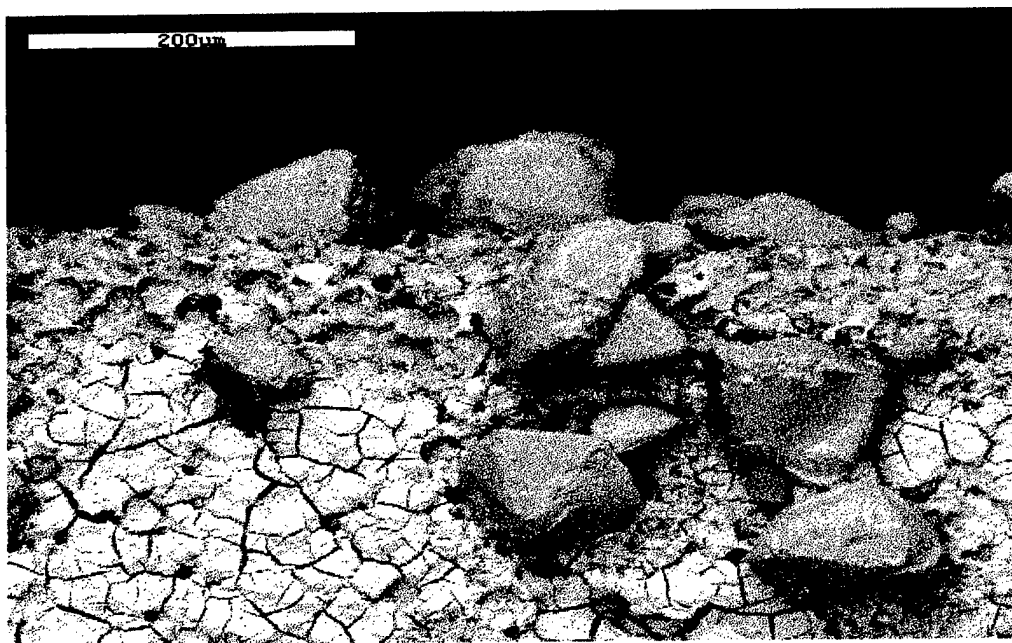
Figure 3.29. SEM photomicrograph of sample HD-17-14.2243 from a pillbox. Cu crystals precipitated on the alloy surface with tungsten grains leached out.

It is significant that in order to maintain constant pH in the HD-17 immersion solutions, base (i.e., NaOH) had to be added instead of acid. Because tungsten dissolution tends to decrease the pH of the solution (see reaction 3.4), the pH data is consistent with the observation that tungsten is preferentially leached relative to nickel and copper. The fact that the binder phase was cathodic in the ground water experiments was most likely due to the presence of copper in the binder. Elemental copper is stable to higher oxidation-reduction potentials than is pure tungsten metal (Figure 3.30; Poubaix et al., 1974). Apparently, its presence in the binder allows the binder to be cathodic while the pure tungsten grains behave as anodes.

The fact that the nickel versus time curves for this alloy in ground water show negative slopes (e.g., Figure 3.26) suggests that some precipitation reaction(s) controlled nickel concentrations during the immersion experiments. One possibility is a cathodic reaction of the type:

$$1/2 \; O_2 + Ni^{2+} + H_2O + 2e^- \Leftrightarrow Ni(OH)_2 \tag{3.7}$$

Other possibilities are the following precipitation reactions:

$$Ni^{2+} + 2 \; OH^- \Leftrightarrow Ni(OH)_2 \tag{3.8}$$

$$Ni^{2+} + WO_4^{2-} \Leftrightarrow NiWO_4 \tag{3.9}$$
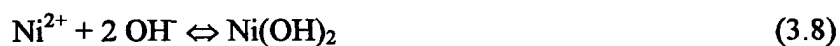
The corrosion behavior of alloy HD-17 in artificial surface water is of particular interest because this is the water type most likely to contact the alloy at the Eglin test sites. The experiments with this water composition resulted in a variety of trends in nickel mass versus time including maxima and negative slopes (Figure 3.31). Both of these features are consistent with precipitation of a compound that incorporates nickel and with corrosion reactions in which the binder phase is cathodic. Only the immersion experiment in which the pH was allowed to drift to its natural level (ambient) showed linear trends suggestive of an absence of precipitation.
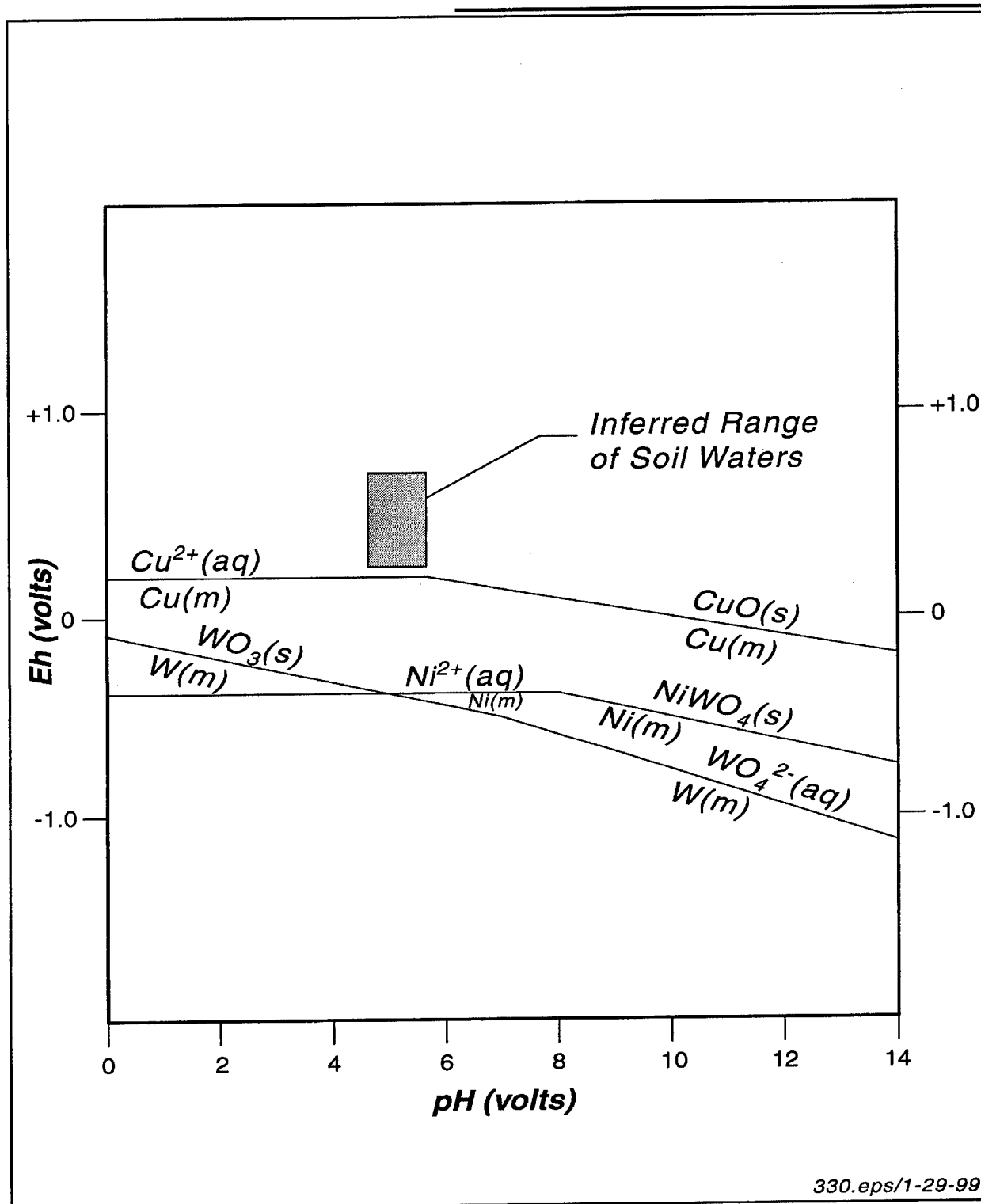
Figure 3.30. Eh-pH diagram for stability of metals, ions in solutions, and compounds of metals. (aq) represents aqueous species, (m) represents a metal phase and (s) represents a solid phase.
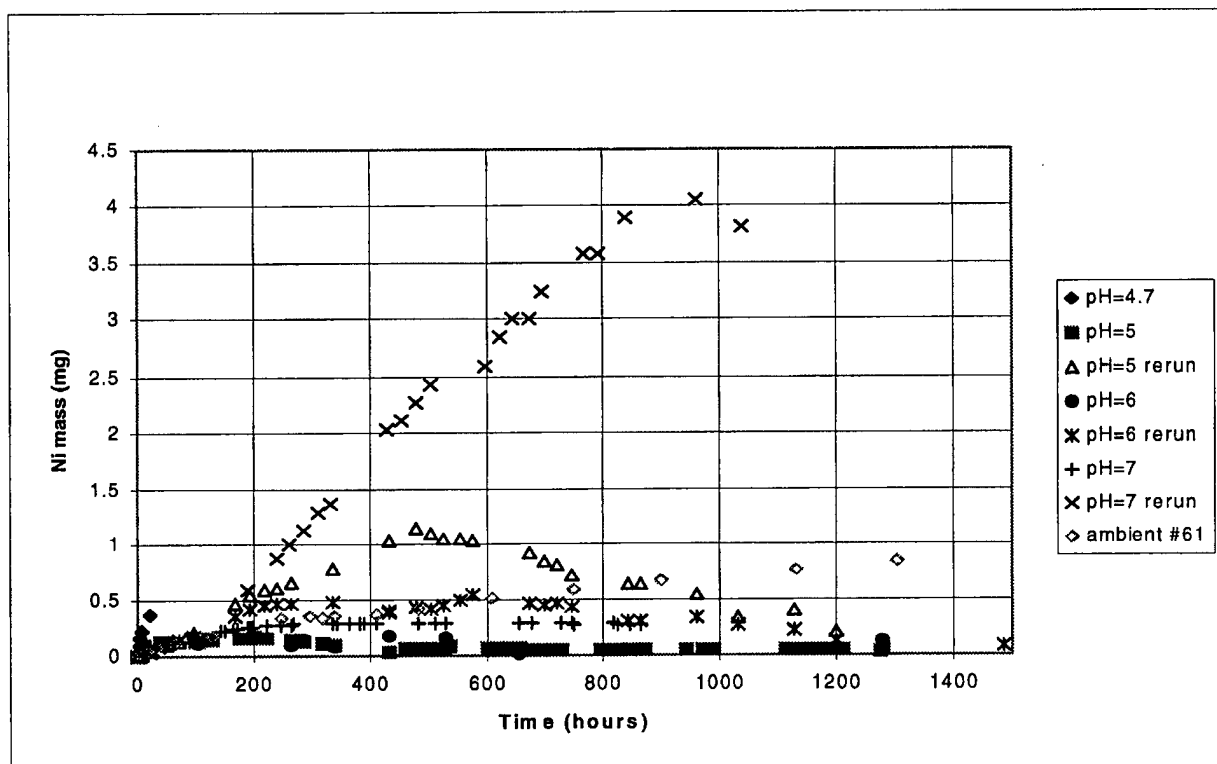
Figure 3.31. Cumulative Ni mass vs. time for immersion experiments with alloy HD-17 in artificial surface water at various pH values. The data points plotted for "Ambient #61" represent an experiment in which the pH was allowed to drift.

The fact that initial experiments with alloy HD-17 in surface water resulted in very low Ni leach rates was considered suspect. The experiments were rerun at three different pH values with somewhat different results (Figure 3.31). The new experiments generally resulted in high masses of leached Ni to solution. However, the mass vs. time trends for these experiments also exhibited maxima consistent with precipitation reactions as in the earlier experiments (Figure 3.31).

Overall, the range in maximum nickel masses (0.02-4.0 mg) observed in these experiments was similar to the range observed in the ground water experiments and much lower than the concentration observed in the artificial seawater experiments. Further, similar amounts of base (NaOH) were used to maintain constant pH in the surface and ground water experiments (Appendix B). These observations suggest similar corrosion mechanisms for experiments with HD-17 in ground and surface waters. As discussed above, a likely mechanism is one in which tungsten grains are dissolved preferentially to the binder phase causing the tungsten concentration in solution to substantially increase but limiting the nickel and copper masses to low levels (up to several mg).

In many of the "pillboxes" containing HD-17 disks in artificial surface water crystals of a yellow phase were formed with time. These crystals showed a variety of forms as depicted in Figures 3.32 through 3.35. An EDAX analysis of one of the crystals shown in Figure 3.33 is shown in Figure 3.36. This analysis suggests the crystal is tungstite (WO_3).

Summary of Nickel Leach Rates

The data discussed in the previous section and additional data presented in Appendix B can be used to calculate both long-term and short-term leach rates for the three alloys of interest. The procedures for calculation of the leach rates are presented in the introduction to Appendix B.

Time-averaged "long-term" nickel leach rates (i.e., at 500 hours) for the different alloys in artificial seawater are plotted in Figure 3.37 as a function of pH. The data suggest that (1) the nickel leach rates for each alloy are similar in artificial seawater and (2) the leach rates increase with decreasing pH. A similar plot for leach rates in artificial ground water is shown in Figure 3.38. In this case, the leach rates are different for the three alloys. The leach rates for WL-1 and NS are similar although those for NS are on average slightly smaller. The increase in leach rate with decreasing pH is evident among the data for WL-1 and NS. The leach rates for HD-17 are substantially smaller than those for the other two alloys. In artificial surface water, the leach rates for WL-1 are substantially higher than rates for both NS and HD-17 as shown in Figure 3.39.
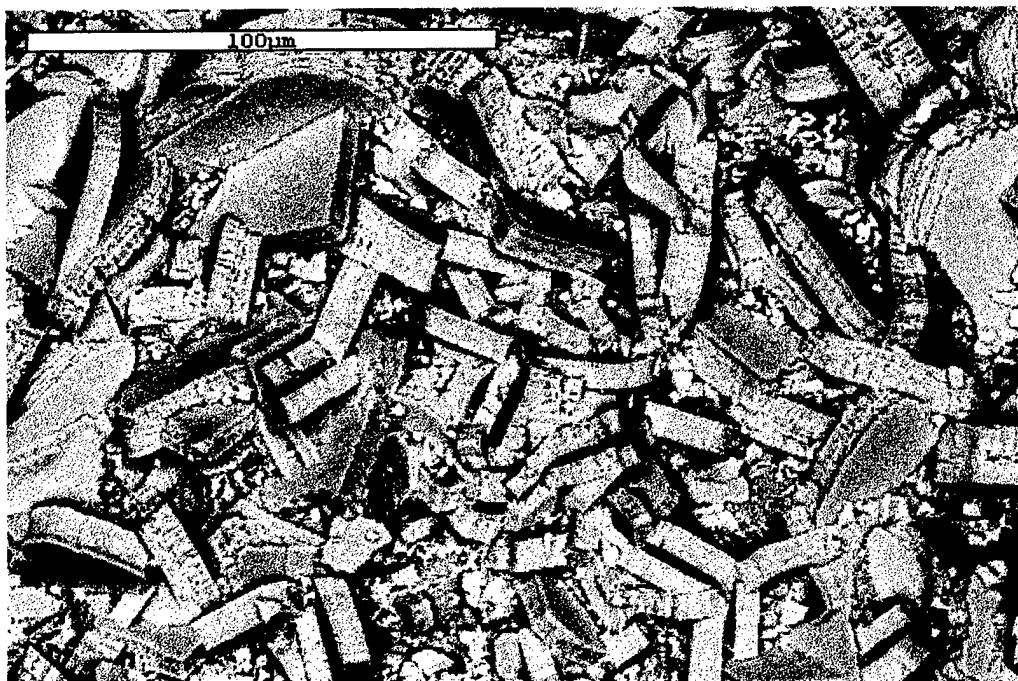
Figure 3.32. SEM photograph of sample HD-17-13.7315. Tungsten oxide crystals formed in a pillbox with artificial surface water.
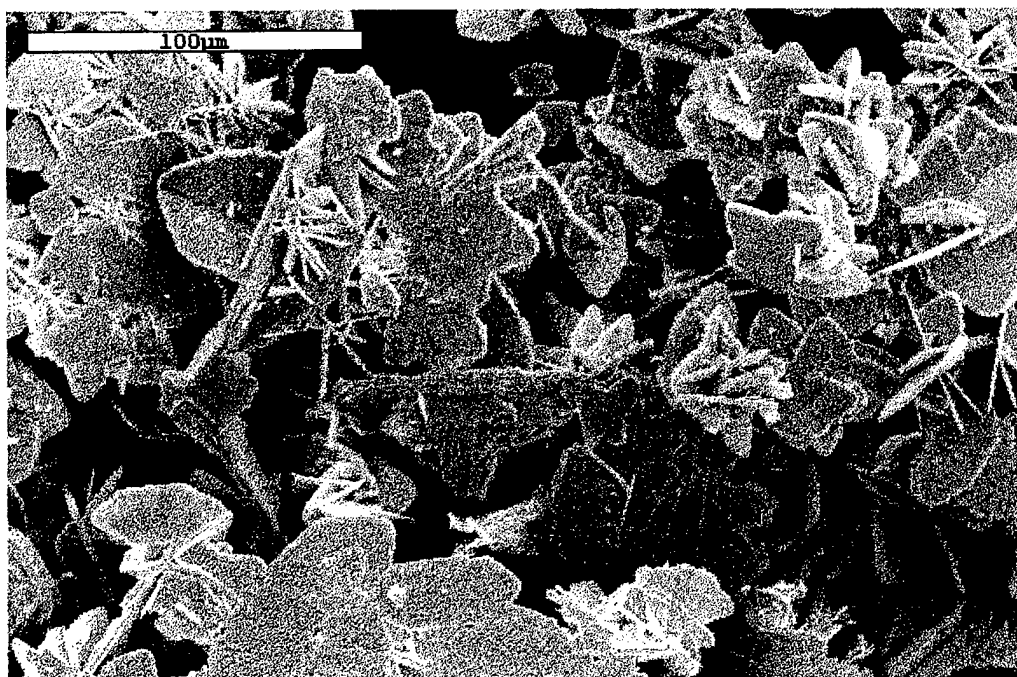
Figure 3.33. SEM photograph of sample HD-17-13.7315. Tungsten oxide crystals formed in a pillbox with artificial surface water.
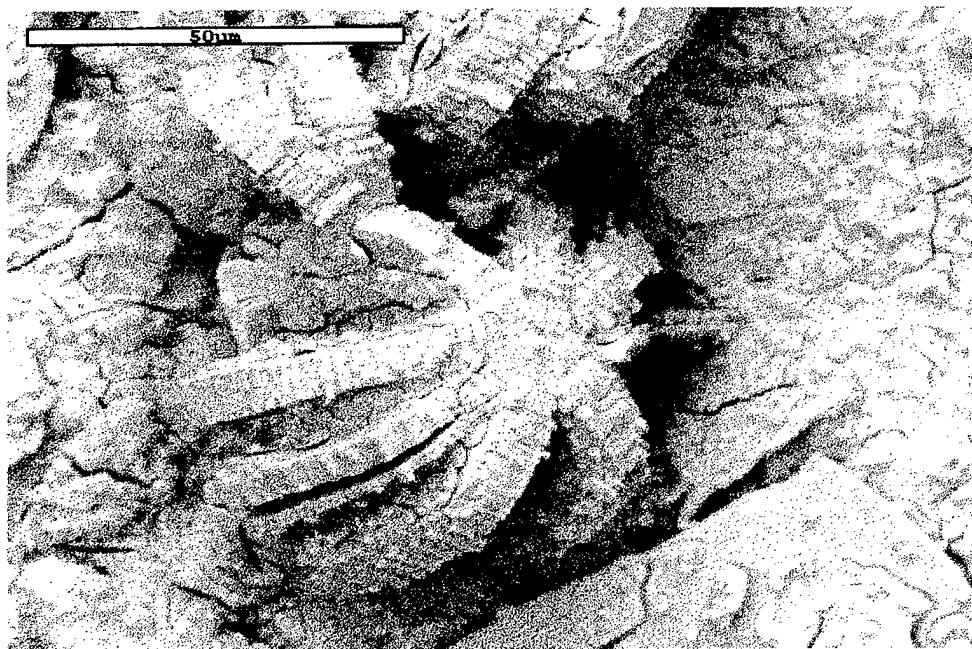
Figure 3.34. SEM photograph of sample HD-17-13.9005. Tungsten oxide crystals formed in pillbox with artificial surface water.

Figure 3.35. SEM photograph of sample HD-17-13.5250. Tungsten oxide crystals formed in a pillbox with artificial surface water.
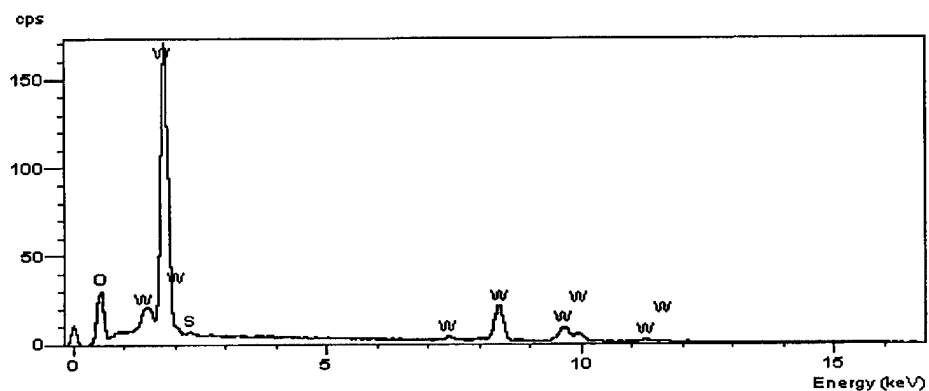
Figure 3.36. EDX analysis of sample HD-17-13.7315. Analysis of tablets in Figure 3.33.
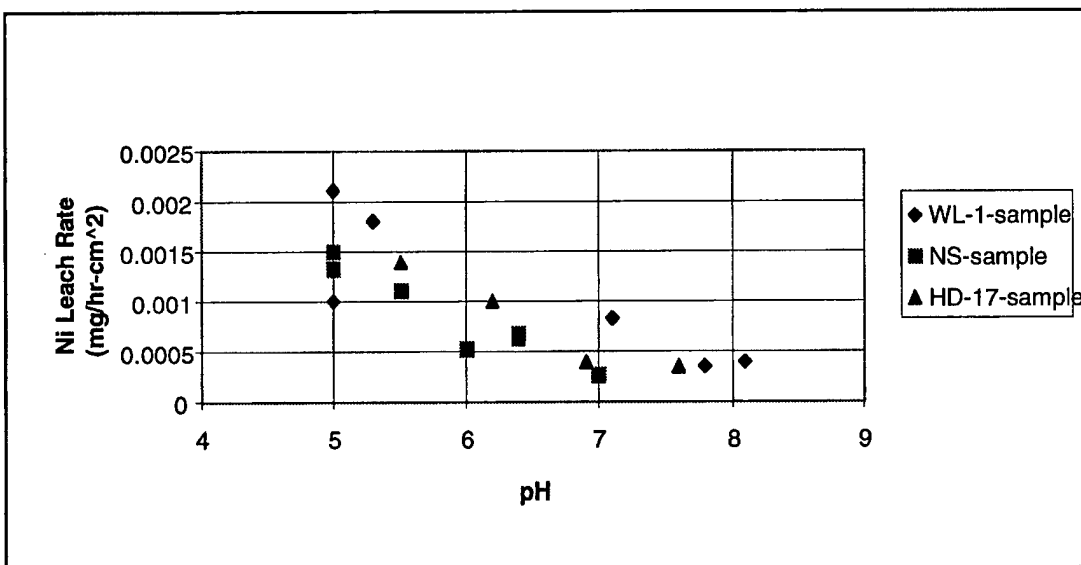
Figure 3.37. Calculated Ni leach rate vs. pH at 500 hours for three different alloys in artificial sea water.
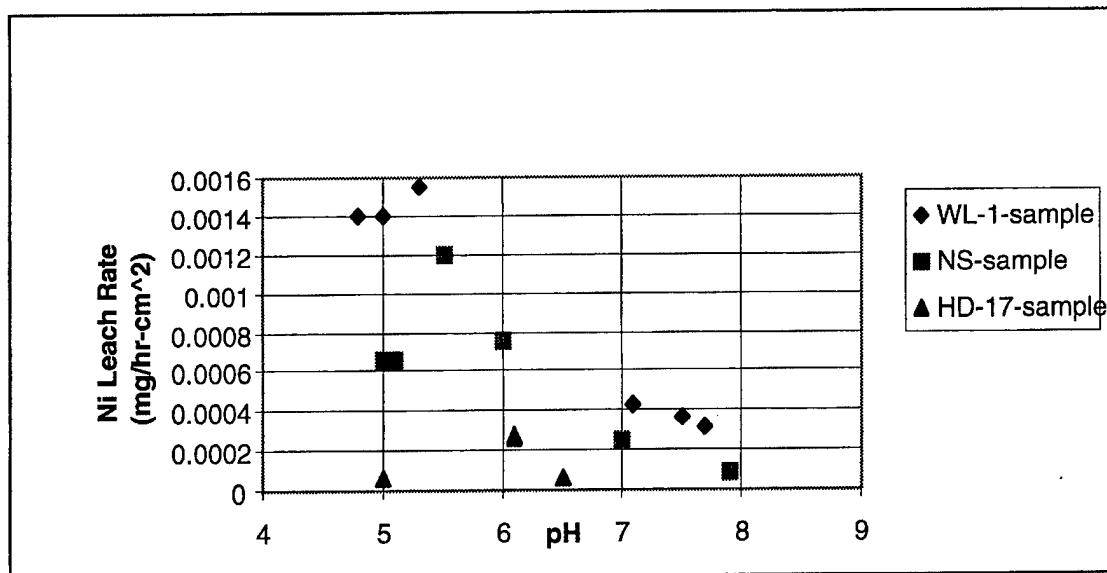
Figure 3.38. Calculated Ni leach rate vs. pH at 500 hours for three different alloys in artificial groundwater.
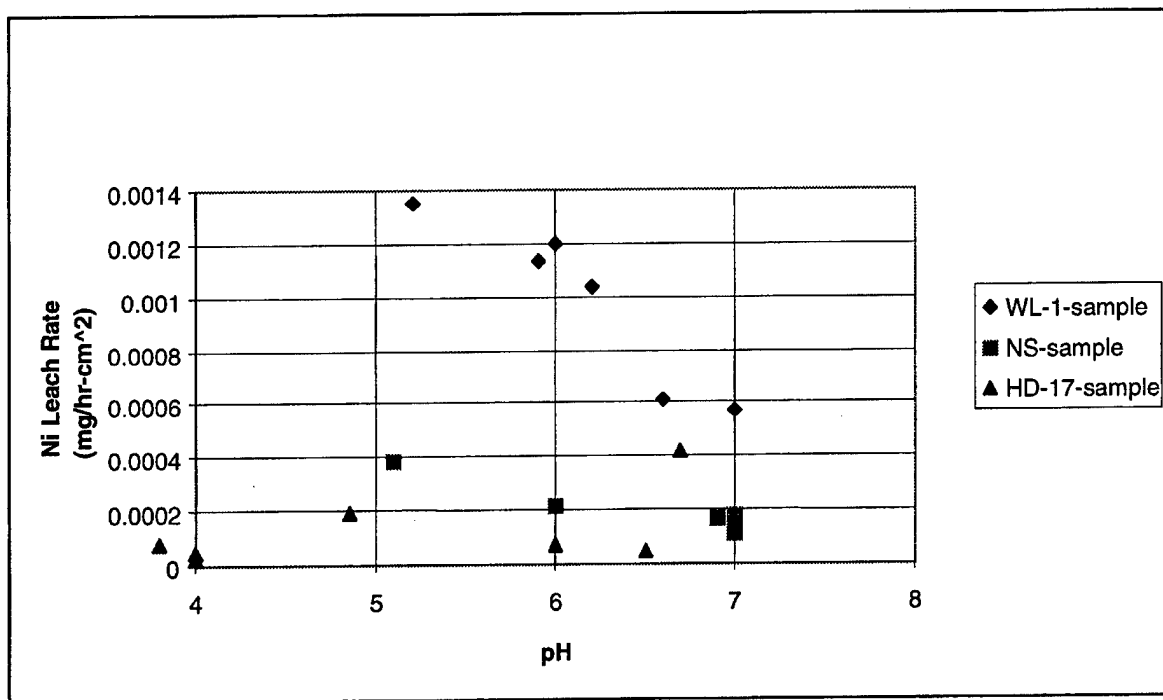
Figure 3.39. Calculated Ni leach rate vs. pH at 500 hours for three alloys in artificial surface water.

Plots in which nickel leach rates for a given alloy are compared in different water compositions are shown in Figures 3.40 to 3.42. The nickel leach rates for alloy WL-1 are not much different in the three artificial waters as shown in Figure 3.40. For the NS alloy, the nickel leach rates in artificial seawater and ground water are similar except at the lowest pH value (Figure 3.41). The leach rate in surface water is approximately 30% of the leach rates in the other waters. In artificial surface water, the leach rates for NS and HD-17 are much lower than the rates for WL-1. Because the water most likely to contact the alloy fragments dispersed on a test range is surface water, the data plotted in Figure 3.42 suggest that the NS and HD-17 alloys will be leached more slowly than the WL-1 alloy.

Although time-averaged "long-term" leach rates are of interest in gaining an understanding of the leaching behavior of the alloys of interest, as noted above, it is the short-term rates that will determine the amounts of metal leached during a typical rainfall event at Test Area C-64A. Short-term nickel leach rates can be calculated from a number of the immersion experiments. Only the short-term leach rates for surface water are discussed here because surface water is the most likely of the waters to have short-term contact with the alloys on Eglin test sites. Short-term leach rates for the other water compositions were calculated from the data in Appendix B.

Leach rates based on 6 hour immersion data are plotted in Figure 3.43. The data indicate that the WL-1 and NS alloys have similar short-term leach rates while the HD-17 alloy has much lower short-term leach rates. Note that the short-term and long-term leach rates for WL-1 are similar (compare data in Figures 3.43 and 3.40) suggesting its leaching behavior does not change with time. The short-term rate for NS is 4-5 times higher than the time-averaged "long-term" rate plotted in Figure 3.41. This is consistent with the precipitation of a nickel compound in the long-term experiments. For alloy HD-17, the short-term rates are 2-5 times higher than the "long-term" rates. Most likely, this also reflects the precipitation of a nickel compound.
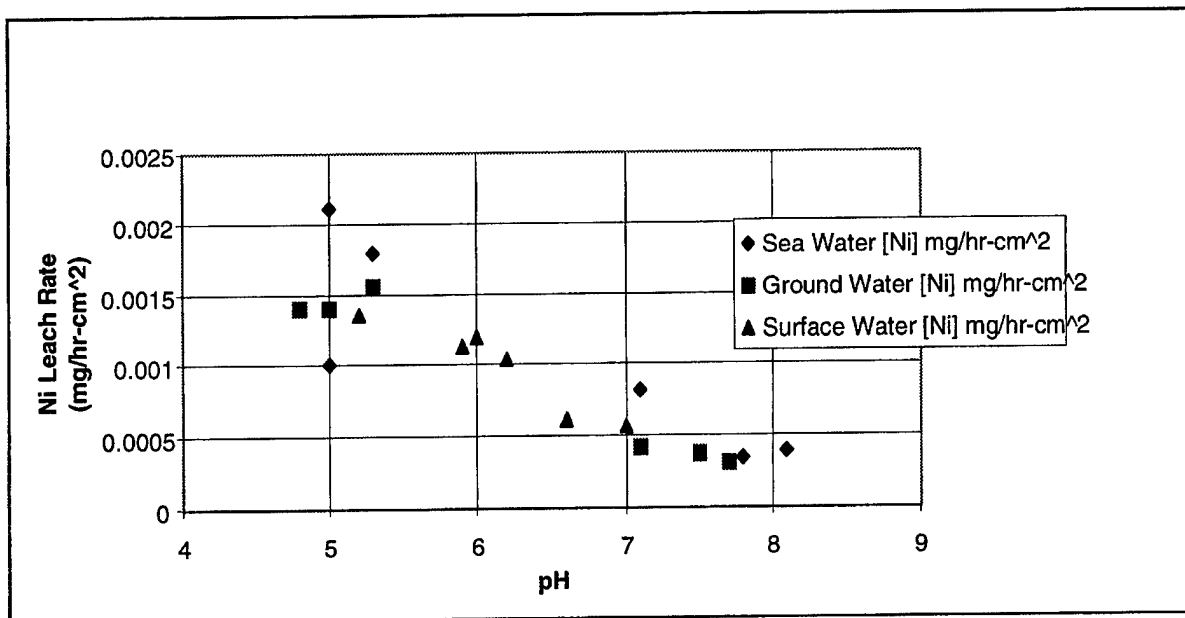
Figure 3.40. Calculated Ni leach rate vs. pH at 500 hours for WL-1 alloy in three artificial water types.
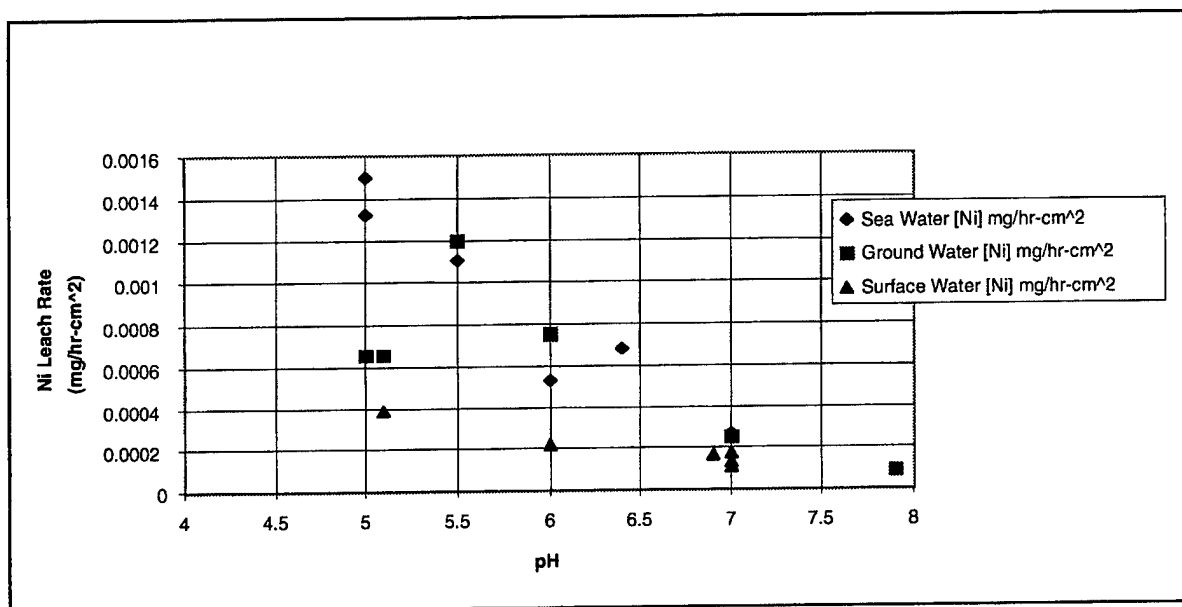
Figure 3.41. Calculated Ni leach rate vs. pH at 500 hours for NS alloy in three artificial water types.
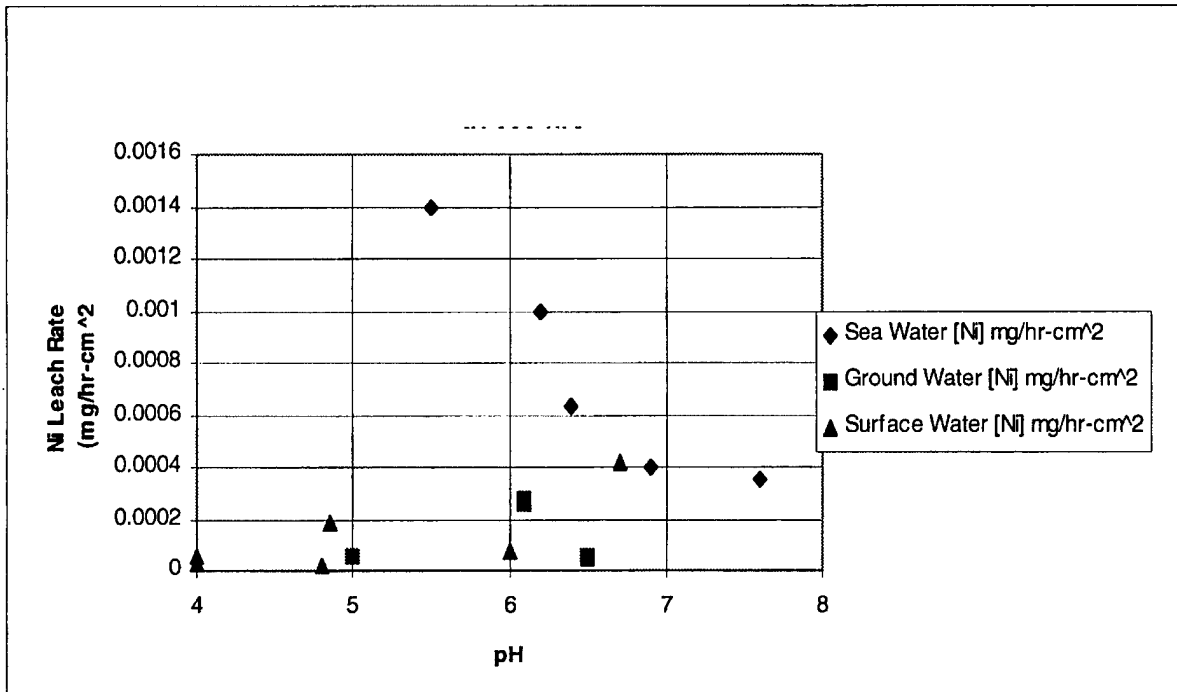
Figure 3.42. Calculated Ni leach rate vs. pH at 500 hours for HD-17 alloy in three artificial water types.
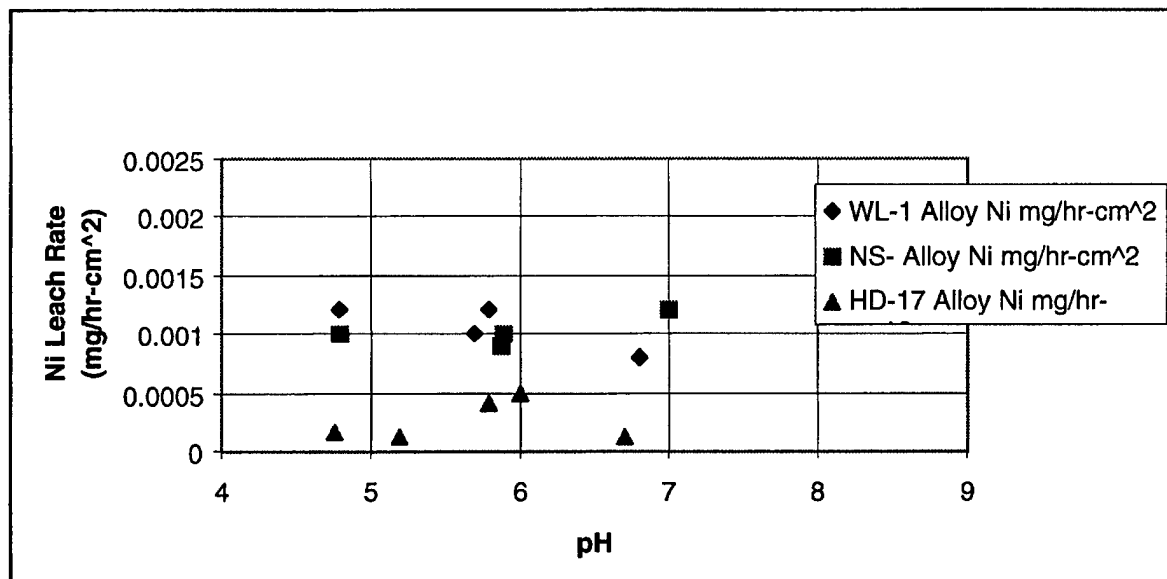
Figure 3.43. Six hour immersion Ni leach rates of tungsten alloys in surface water vs. pH.

To investigate why alloy HD-17 appears to have lower "short-term" and "long-term" leach rates than the other alloys and why the alloy NS appears to have higher "short-term" leach rates relative to the "long-term" rates, chemical equilibrium calculations were carried out. These calculations were carried out with the EQ3/6 chemical modeling code developed by Lawrence Livermore National Laboratory (Wolery, 1990). Inputs to the code are the detailed water compositions including concentrations of the metals measured in the immersion experiments. Using an extensive database of thermodynamic constants for liquid, gas and solid phases, the code calculates saturation indices for compounds in the database that are saturated in the input water composition. A saturation index value greater than zero indicates the solution is saturated with the compound of interest. A saturation index greater than one is normally taken to reflect supersaturation. A negative value for the index reflects undersaturation.

On the basis of these types of calculations (Appendix E), it is clear that the solubilities of compounds such as $NiWO_4$ and $CoWO_4$ are actually quite low (0-1 mg/L of WO_4^{2-} and Ni or Co) in the artificial surface and ground waters used in the immersion experiments. Most of the surface and ground water solutions had higher nickel and tungstate concentrations than this at the end of the immersion experiments suggesting that these solutions were saturated with nickel and/or cobalt tungstate compounds. This is consistent with the SEM observations. Surprisingly, the very low nickel concentrations measured in some of the HD-17 experiments (0.1 mg/L) also reflect conditions of supersaturation with nickel tungstate. In this case, it was due to the high tungstate concentrations present in these experiments (See Appendix E for calculations).

These observation lead to the question of why many of the nickel concentration trends in the experiments with the WL-1 and NS alloys in surface and ground waters did not show clear evidence of precipitation even though the solutions were highly supersaturated with nickel tungstate according to the EQ 3/6 calculations. The most reasonable answer to this question is that the nucleation and crystallization kinetics of nickel tungstate are slow in experiments with these alloys. In experiments with the alloy HD-17, the nucleation and crystallization kinetics of this phase are apparently faster and may be catalyzed by the presence of copper in the alloy.

In experiments with alloy HD-17 in surface and ground water, copper concentrations were generally below saturation with known copper compounds based on the equilibrium calculations. This observation reinforces the idea that cathodic behavior is inhibiting the leaching of copper in these solutions. Nonetheless, the high tungsten concentrations in these experiments (Appendix B) caused supersaturation with tungstite at low pH (≤ 5.0).

Leach Rates for the Other Metals

In a previous section, it was possible to plot Ni leach rates versus time because Ni concentrations were measured during the course of the various experiments (Appendix B). For the other metals contained in the alloys, only the final concentrations at the end of each immersion experiment were measured. This was done because the analyses of all the metals required relatively large sample volumes as previously discussed.

To obtain leach rates for the other metals, the final solution concentrations obtained by ICP-MS were multiplied by the ending solution volumes to obtain the mass of each metal in the solution. This mass is the minimum metal mass leached from each alloy. This mass is considered a minimum value because small amounts of metal were lost with each solution aliquot removed from a given experimental container for purposes of pH measurement, etc. The minimum mass was divided by the duration of the experiment in hours and by the nominal surface area of the disc to obtain a minimum leach rate with units of mg/hr-cm^2.

The impact of the "lost mass" can be estimated by comparing the nickel leach rates calculated on the basis of ICP-MS analyses ("laboratory results"-Appendix B) with the leach rates calculated on the basis of real-time nickel analyses (see "corrected" nickel masses in Appendix B). Comparison of the nickel results obtained by these two different techniques suggests that the leach rates calculated on the basis of the ICP-MS data are at most 30 percent lower than the rates calculated using the other data set. In most cases, the difference is much less. This difference is considered in the input data for the MEPAS code as described more fully below.

Plots showing the long-term leach rate data for tungsten versus pH in the various experiments involving each alloy and water composition are shown in Figures 3.44 through 3.46. In artificial seawater, tungsten leach rates are similar in the WL-1 and NS alloys but generally higher in the HD-17 alloy experiments. In artificial ground water, the HD-17 sample shows much higher leach rates than the other two tungsten alloys with the NS alloy showing the lowest leach rates (Figure 3.45). Similar behavior is observed in artificial surface water (Figure 3.46). As discussed above, the high tungsten leach rates associated with the HD-17 sample probably result from the anodic behavior of tungsten grains in experiments with this alloy. The eventual result of this behavior is the precipitation of tungsten oxide phases such as tungstite.

Leach rates for the other metals also increase with decreasing pH, particularly at pH values less than 5.5. In experiments with the NS alloy, the leach rates for cobalt closely tracked the leach rates for nickel in essentially all the experiments (Figure 3.47). However, the actual leach rates for cobalt are lower than the nickel leach rates by approximately a factor of three. This most likely reflects the fact that the concentration of cobalt in the NS alloy is approximately one third of the nickel concentration.

The leach rates for iron are given in Appendix B but are not discussed in detail here because iron is a common coating on grains of sand from the Eglin soils. The relatively small amounts of iron added to the soils as a result of munitions testing should not be of environmental concern.

The metal manganese was also analyzed for by ICP-MS in all the immersion test solutions. The concentrations reported were all below the limit of detection. Assuming manganese was present in the WL-1 alloy, the data indicate the leach rates for this metal must be sufficiently small so as to be insignificant.

Unlike cobalt, the leach rates for copper in experiments with the HD-17 alloy do not track the nickel leach rates very closely (Figure 3.48). Further, the copper leach rates are on the order of ten times lower than the leach rates for nickel even though the concentration of copper in the HD-17 alloy is only 30% lower than the concentration of nickel. This implies the leaching
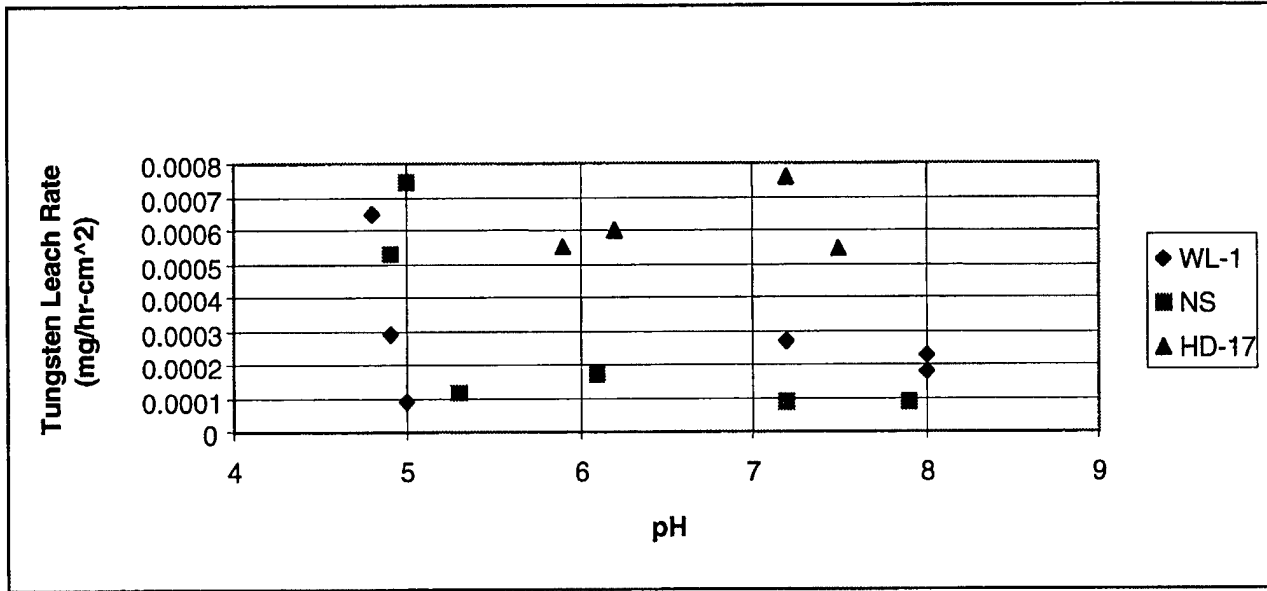
Figure 3.44. Scatter plot of W leach rate vs. pH for tungsten alloy samples in artificial sea water.
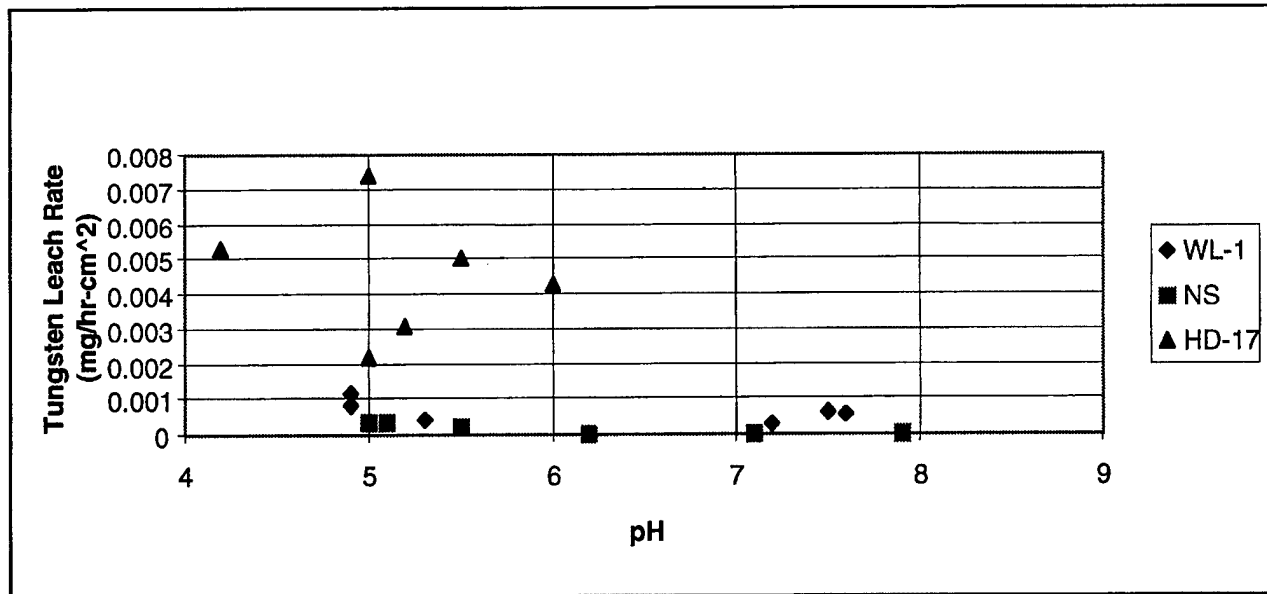
Figure 3.45. Scatter Plot of W leach rate vs. pH of tungsten samples in artificial groundwater.
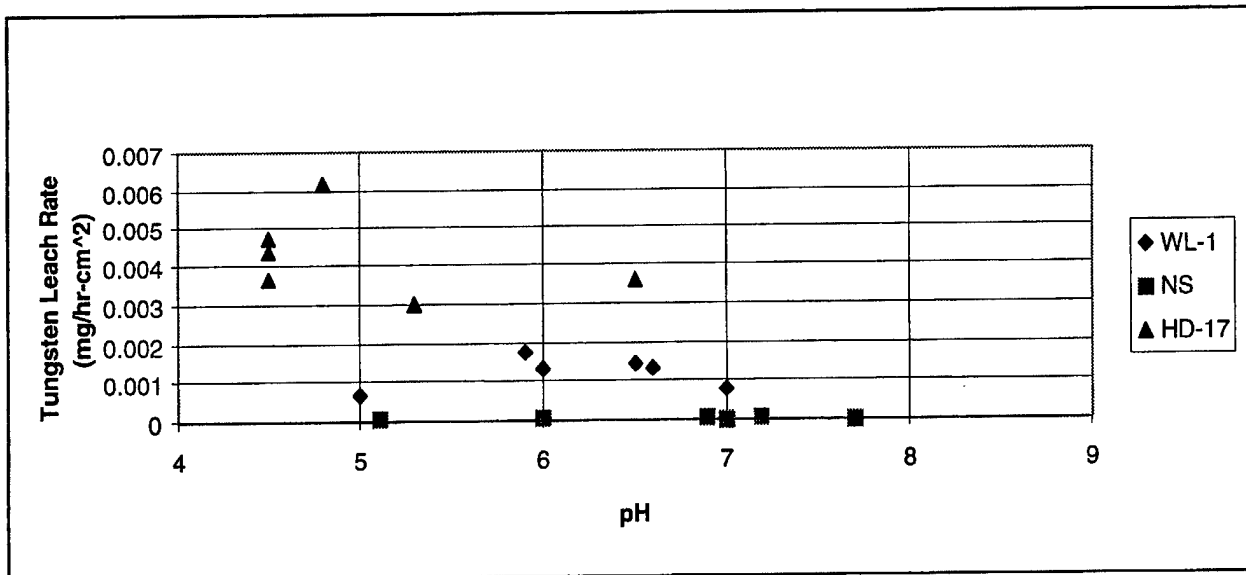
Figure 3.46. Scatter Plot of W leach rate vs. pH of tungsten alloy samples in artificial surface water.
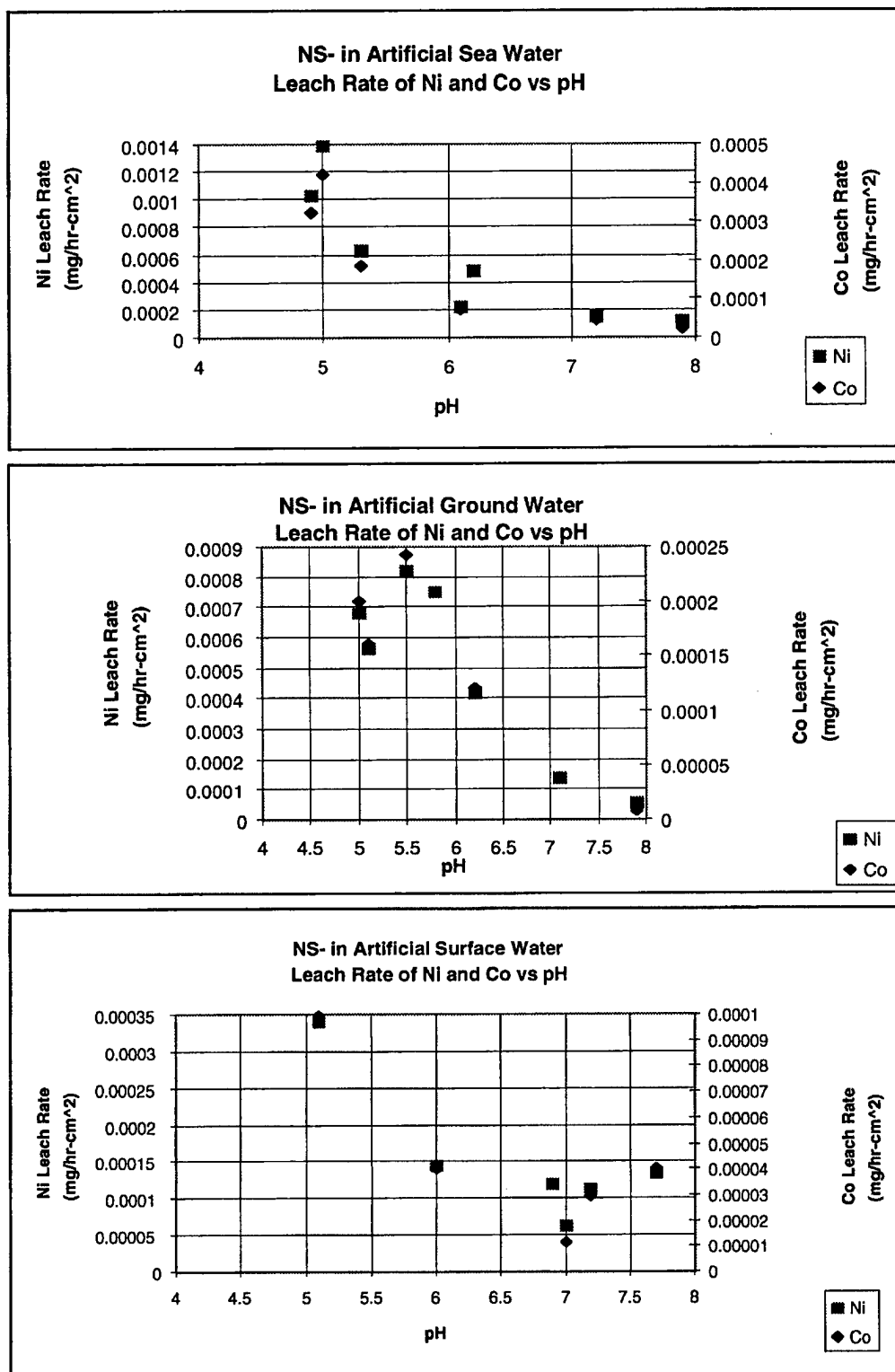
Figure 3.47. Ni and Co leach rate vs. pH plots for NS alloy in artificial sea, ground and surface water.
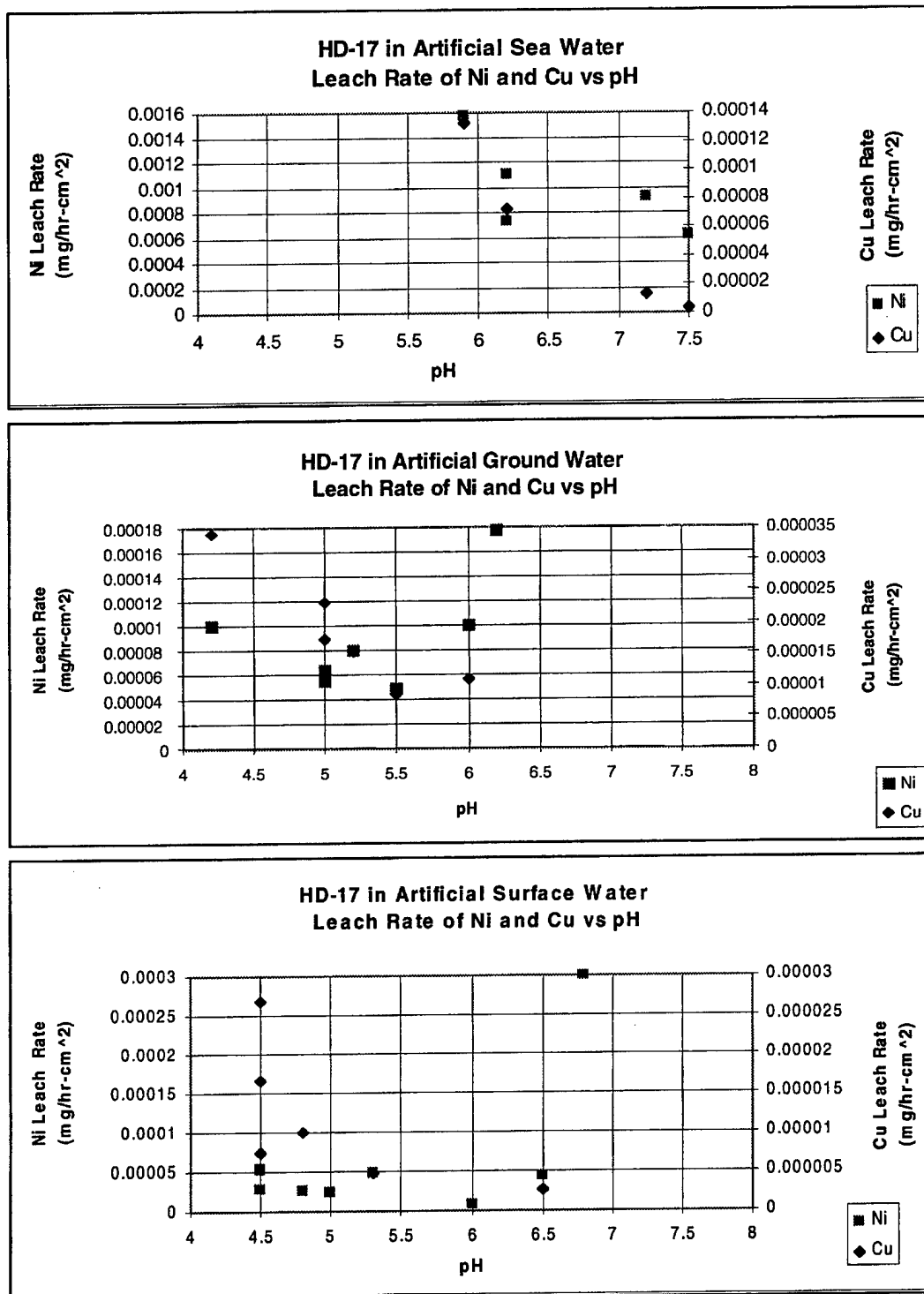
Figure 3.48. Ni and Cu leach rate vs. pH for HD-17 alloy samples in artificial sea, ground, and surface water.

reactions for copper differ from the leaching reactions for nickel. The more noble (i.e., cathodic) character of copper is likely the cause of this difference.

The immersion experiments with tantalum metal showed that this metal is not leached in the water types and pH ranges addressed by this study. All the ICP-MS analyses of tantalum showed concentrations at or below the limit of detection (Appendix B). This is true even for experiments that lasted 2500 hours. Solubility experiments in which a radioactive isotope of tantalum was added to the various waters of interest were carried out to provide upper limits to the solubility of tantalum. These experiments provide upper limits because tartaric acid had to be used to solubilize tantalum into a stock solution (see Appendix C). When the waters of interest were spiked with the stock solution, tartaric acid was also added to the waters. With this qualification, the solubility values obtained on the waters of interest are given in Table 3.4.

Table 3.4. Tantalum concentrations in saturated solutions with tartaric acid.

Water Type	pH	Tantalum (μg/l)
Artificial Seawater	3.8	4.15 ± 0.72
Artificial Ground Water	8.1	2.6 ± 0.47
Artificial Surface Water	7.8	2.46 ± 0.46
Distilled Water	5.9	1.48 ± 0.31

These solubility data indicate that tantalum metal will not be leached in significant amounts in the soil environments at Eglin AFB. This conclusion is consistent with other data on the corrosion of tantalum in dilute water as reported in the literature (Johnson, 1969; Schussler, 1985). According to Schussler (1985):

"The outstanding corrosion resistance and inertness of tantalum are attributed to a very thin, impervious, protective oxide film that forms upon exposure of the metal to slightly anodic or oxidizing conditions (Chelius, 1957). Although tantalum pentoxide (Ta_2O_5) is the usual oxide form, suboxides may also exist in transition between the base metal and the outer film (Flanders, 1979). It is only when these

oxide films react with or are penetrated by a chemical reagent that attack occurs on the underlying metal substrate."

3.3.2 Drip Tests

The drip test was developed to more directly simulate the corrosion environment that penetrator fragments could encounter in the soil zones of the Eglin test ranges. The general experimental design is shown in Figure 3.49. In this design, an alloy disk was put into a small funnel and water was dripped into the funnel at a rate and a total volume representative of average rainfall events at Eglin sites. The water percolating out of the bottom of the funnel was collected and analyzed for the metals of interest. In most tests, the total solution volume eluted from the funnel was required to analyze for one or two of the metals of interest. In some tests, the elution rate was increased by approximately a factor of 2 over that representative of the average rainfall rate at the site. This allowed the collection of a greater volume of water in the approximately 6 hour intervals over which the tests were carried out. This interval represents the estimated average duration of rainfall events at the site. The larger volumes of water collected in these tests allowed the analysis of several aliquots of water for one or two of the metals of interest. In order to maintain a humidity level appropriate to the Eglin sites, a plastic bag was put around the sample holder and the sample collection vessel.

The experimental matrix for the drip tests was oriented specifically to conditions at Eglin Test Area C-64A.

Two different types of drip experiments were carried out with the design shown in Figure 3.49. In one type, an alloy disk was placed in the funnel and water was dripped into the disk. This could represent the situation in which alloy materials were exposed on the surface at the test area. In the other type, the alloy disk was submerged in soil and water was dripped onto the surface of the soil. This could represent the situation in which alloy materials were buried in surface soils of the test area. In this type of experiment, any interaction between the soil and the alloy (e.g., capillary action, pitting corrosion) resulting from contact of sand grains with the alloy, would be reflected in the analytical results.
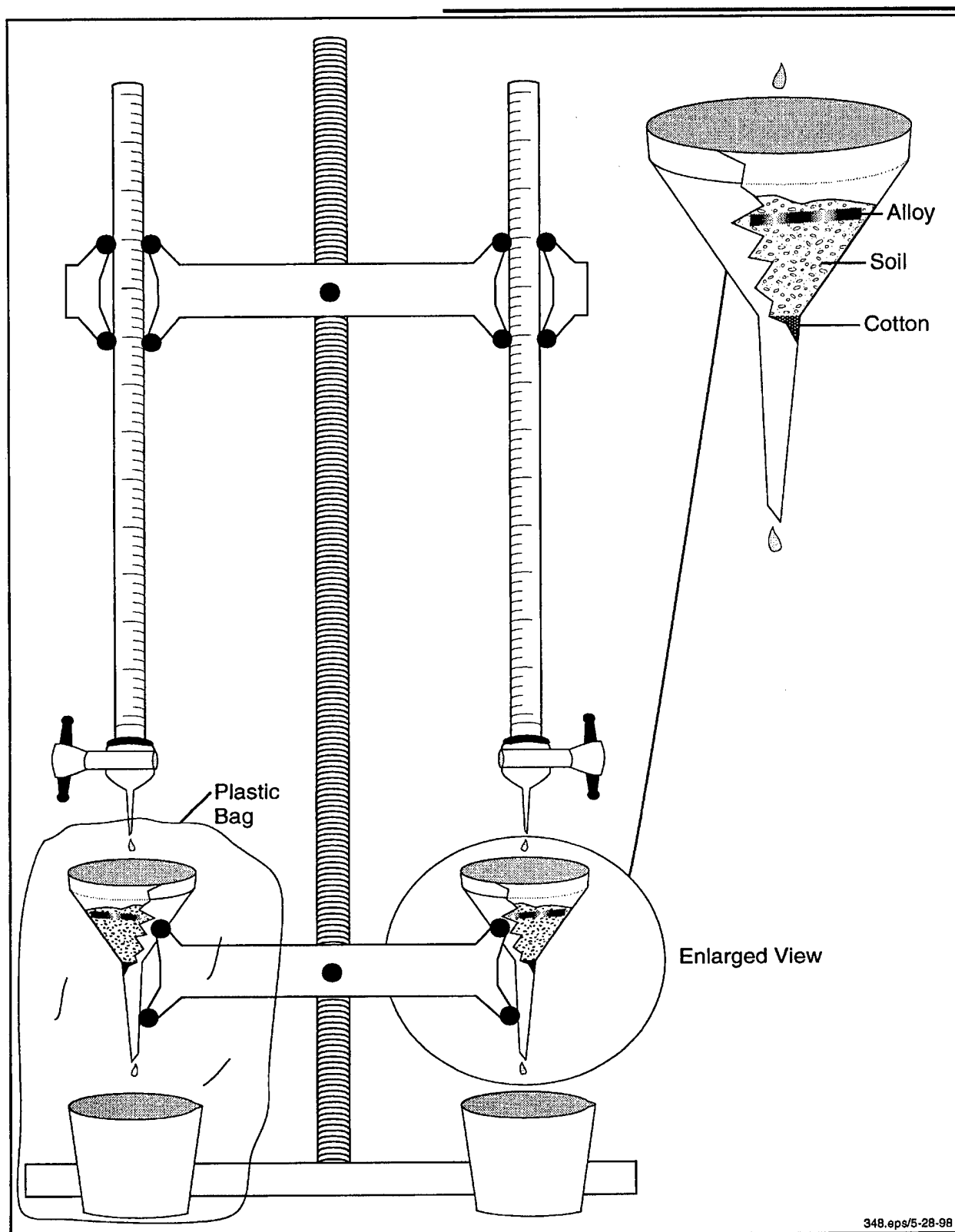
Figure 3.49. Drip corrosion test experiment setup.

As shown in Figure 3.49, in the experiments containing soil, the alloy disk was put into a funnel containing enough soil so that the edge of the disk nearly touched the inside of the funnel. This restricted to a minimum the amount of incoming water that bypassed the disk without reacting with the disk. The amount of soil in the funnel was kept at a minimum so that the sorption capacity of the sand would not be the dominant factor influencing the concentration of metals in the effluent solutions in the initial aliquots recovered from a given experiment. As discussed further below, the results suggest this may not always have been the case. The experiments were carried out at ambient temperature and pressure.

The rates and total volumes of water dripped into the funnel in a given experiment were selected to represent typical rainfall events at Eglin. An average rainfall event at Eglin is 1.43 cm (0.56 inches) and lasts 6 hours (Section 2.2). This equates to 7.6 to 11.9 ml of rainwater per drip experiment given the different face areas of the alloy disks. The total water volumes used in the individual experiments varied from as little as 3 ml up to 30 ml. This equates to precipitation (i.e., rainfall) rates of 0.6 to 5.6 centimeters (0.2 to 2.2 inches) per storm. The duration of these storms would vary from 1.5 to 24 hours given the average precipitation rate. However, the duration of the majority of the experiments was 6 hours.

Not all the water dripped into the funnel in each experiment was recovered. This was due to the fact that the dry soils retained on the order of 4-5 ml of water at field capacity. In any case, the water volumes recovered from these drip tests were generally small (1-15 ml) and allowed only limited metals analysis. For example, the aliquots obtained from the tests were too small to allow for the analysis of a full suite of metals by a commercial laboratory using ICP-MS. Therefore, only one or two metals were analyzed for each of the aliquots recovered from the drip tests. Nickel was the primary metal analyzed in the eluant solutions although a limited number of copper and tungsten analyses were also carried out.

Water Composition

An important aspect of the drip corrosion experiments was the chemical make-up of the water used in the experiments. To duplicate precipitation specific to Test Area C-64A, the

following parameters were evaluated: chemical composition and pH of rain, rates of precipitation, yearly total precipitation, number of precipitation events per year, and average duration of precipitation events (i.e., storms). The average chemical composition for rain at Eglin was obtained from data on precipitation samples collected at Quincy, Florida by the National Atmospheric Deposition Program/National Trends Network (NADP). This average composition is listed in Table 2.7. Because the average rainwater composition is very similar to the composition of surface water from Bull Creek (Table 27), the surface water composition was used in the drip tests. A recipe for the preparation of this water is given in Appendix A. To best duplicate the leaching behavior of natural rainwater at the Eglin test sites, the pH of this artificial surface water was adjusted to a value of 4.7 to equal the average pH value measured in precipitation samples from the Quincy, Florida site. It was assumed that the pH of precipitation at the Eglin test sites would be similar to the rainfall sampled at the Quincy site.

Drip-Test Results

The results of nickel analyses of drip test solution with "bare alloy" are shown in Table 3.5 for each alloy. The average leach rates calculated for these tests are lowest for the NS alloy, intermediate for the WL-1 alloy and highest for the HD-17 alloy. The average nickel leach rates obtained in drip tests in which the alloys were submersed in soil are listed in Table 3-6. As with the bare-alloy tests, the calculated average leach rates are lowest for the NS alloy and highest for the HD-17 alloy.

Table 3.5. Data for bare alloy drip leach tests.

Alloy	Average Nickel Concentration (mg/L)	Average Nickel Leach Rate (mg/hr-cm^2)
NS	5.4	0.001
WL-1	17.0	0.003
HD-17	33.7	0.012

Table 3.6. Data for drip leach tests with soil.

Alloy	Average Nickel Concentration (mg/L)	Average Nickel Leach Rate (mg/hr-cm^2)
NS	4.5	0.0004
WL-1	12.8	0.002
HD-17	247	0.03

In detail, the drip test data show some interesting trends. Figures 3.50 and 3.51 show the nickel concentrations and leach rates for "bare-alloy" drip tests with alloy HD-17 plotted as a function of the cumulative volume of water dripped onto the sample in a single experiment lasting no more than one day. Note that for samples with only one concentration value reported, the sample represents the integrated effluent from the experiment. In experiments with more than one sample reported, the concentration values represent individual aliquots of effluent collected during the experiment. The data do not show evidence of a consistent increasing or decreasing trend with cumulative precipitation volume. A decreasing trend might be expected, for example, if corrosion reactions continued during the time the alloy sample was not used in experiments. The metal concentrations in the initial aliquots of a drip experiment following such a period of nonuse might be expected to preferentially dissolve the corrosion products formed during the days in between experiments and thereby have higher than usual concentrations.

A set of "bare-alloy" data for alloy WL-1 is shown in Figure 3.52 and 3.53. These data are somewhat more variable than the HD-17 data. There is a general decreasing trend of nickel concentration with cumulative precipitation volume although the 4/8/98 sample is clearly an exception to this trend. The leach rate data are less consistent. Interestingly, there does not appear to be any enhancement of the leach rate in the first aliquots taken on a given day. This suggests the alloy samples do not corrode readily when exposed to the atmosphere even if they are initially wet. The average value calculated for these data is listed in Table 3.6.
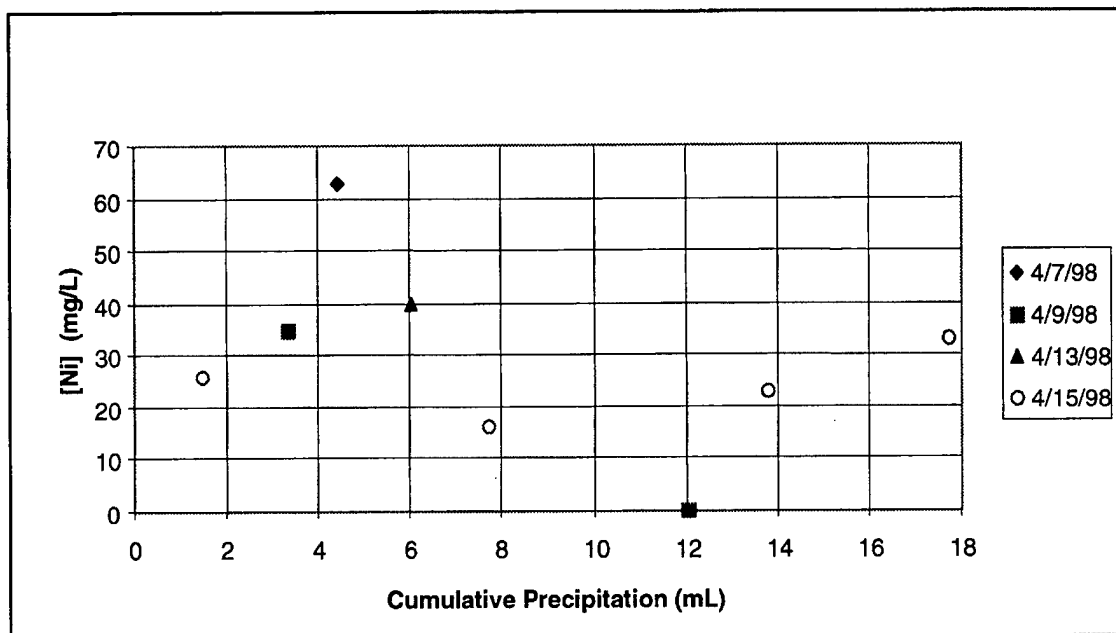
Figure 3.50. Ni concentrations as a function of cumulative water volume dripped onto "bare alloy" sample HD-17-13.7803.
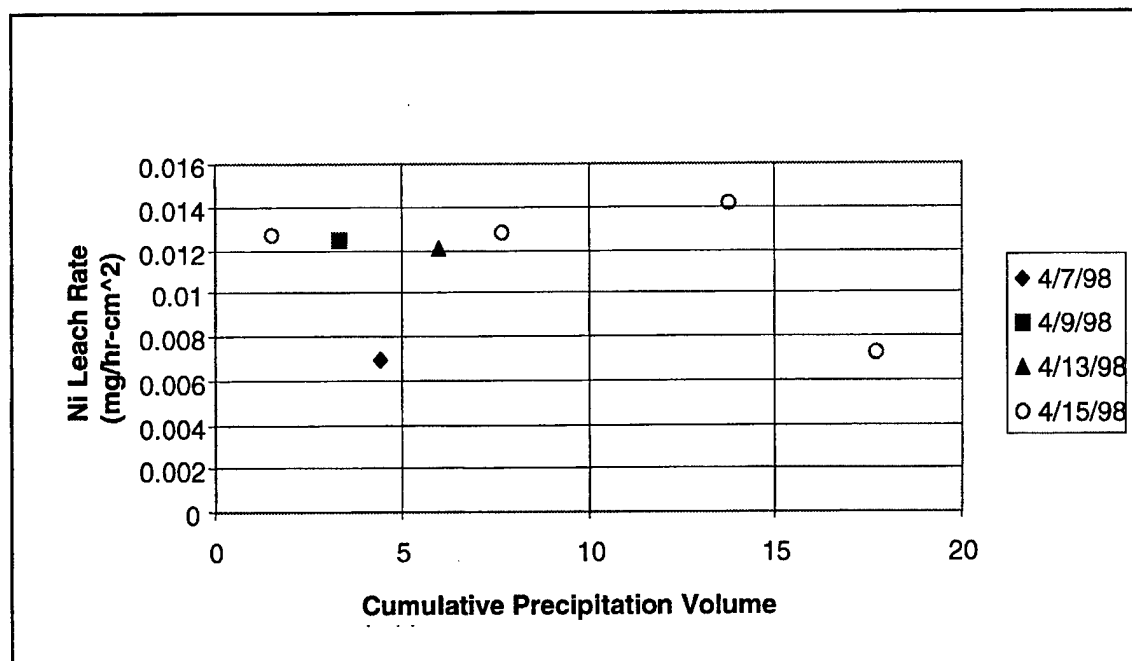
Figure 3.51. Ni leach rates as a function of cumulative water volume dripped onto "bare alloy" sample HD-17-13.7803.
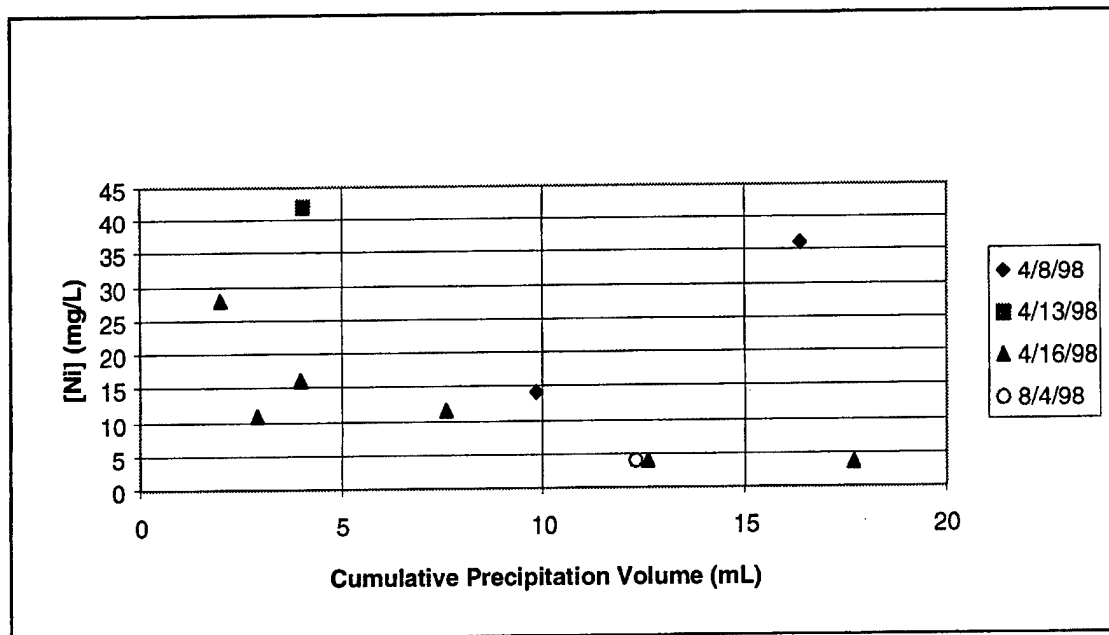
Figure 3.52. Ni concentrations as a function of cumulative water volume dripped onto "bare alloy" sample WL-1-18.4573.
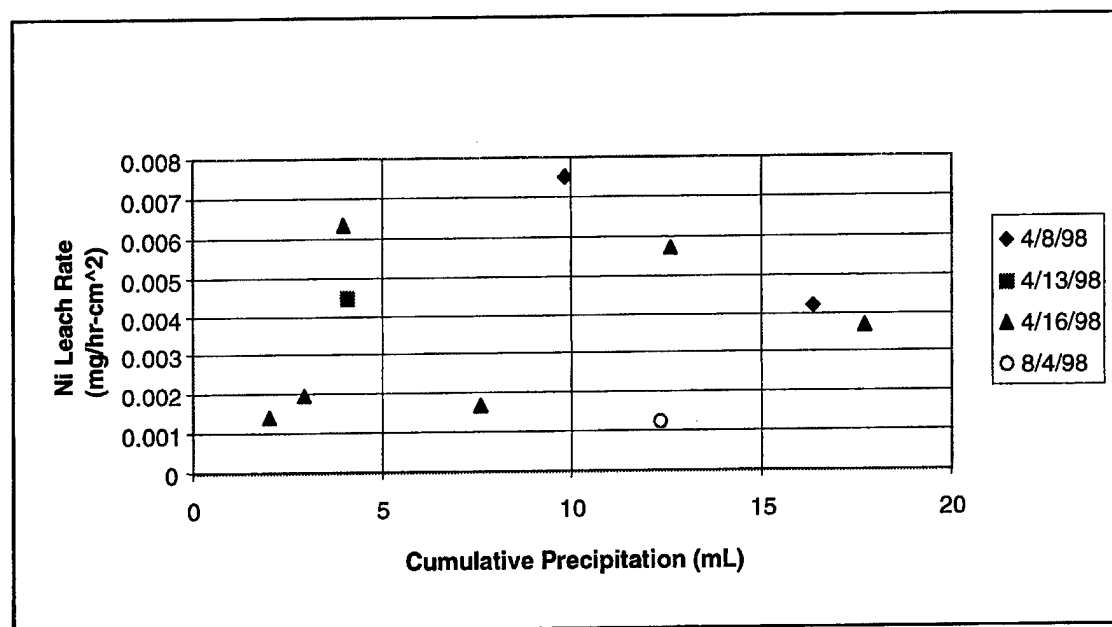
Figure 3.53. Ni leach rates as a function of cumulative water volume dripped onto "bare alloy" sample WL-1-18.4573.

The "bare-alloy" drip test data set for alloy NS is shown in Figures 3.54 and 3.55. Again, the data do not show consistent increasing or decreasing trends. Note that the nickel concentrations and leach rates are generally lower for this alloy compared to those observed in tests on HD-17 and WL-1.

The nickel concentration and leach rate data obtained in drip experiments with soil show more consistent trends. Figures 3.56 and 3.57 show the nickel concentration and leach rate data for alloy sample HD-17. The nickel concentrations show a definite decrease with increasing cumulative precipitation volume. The steep decrease observed below approximately 7 ml cumulative precipitation volume likely reflects nickel that was corroded from the disk during the time the disks were not in use but still in contact with wet soil in the funnel. The water dripped onto the soil early in following experiment would tend to preferentially leach these corrosion products.

As shown in Figure 3.57, the leach rates calculated for these drip experiments also show a decreasing trend with increasing cumulative precipitation volume although this trend is less well defined. Comparison of the data plotted in Figure 3.57 with the data plotted in Figure 3.51 indicates that the nickel leach rates in soil are higher on average than the leach rates for "bare alloy." Given that the average precipitation volume per storm at the Eglin sites for an area the size of the HD-17 disks is approximately 7.6 ml, the nickel leach rate derived from the trend of the data in Figure 3.57 would be approximately 0.02 mg/hr-cm^2. Note that the higher leach rates observed early in a given experiment must be included in the average because they reflect corrosion reactions that could also occur at the Eglin test site.

Drip test data for alloy sample WL-1 with soil are shown in Figures 3.58 and 3.59. As with sample HD-17, the nickel concentrations show a decreasing trend with increasing cumulative precipitation although much less pronounced than the trend observed in the HD-17 dataset (Figure 3.56). Unlike the HD-17 dataset, the nickel leach rates calculated for alloy WL-1 show no consistently increasing or decreasing trend. This suggests corrosion reactions that
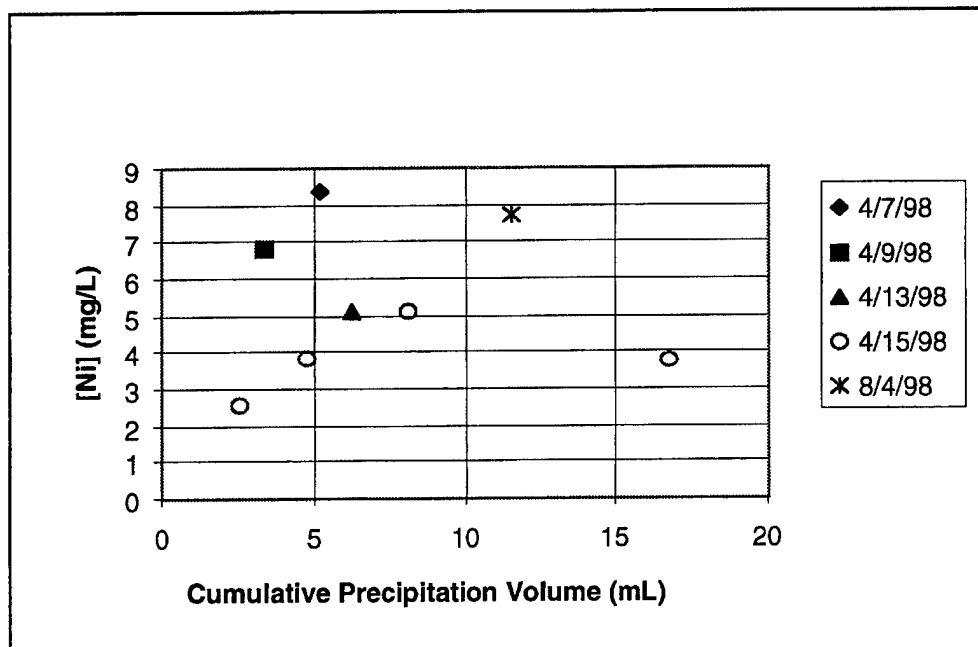
Figure 3.54. Ni concentrations as a function of cumulative water volume dripped onto "bare alloy" sample NS-22.6361.
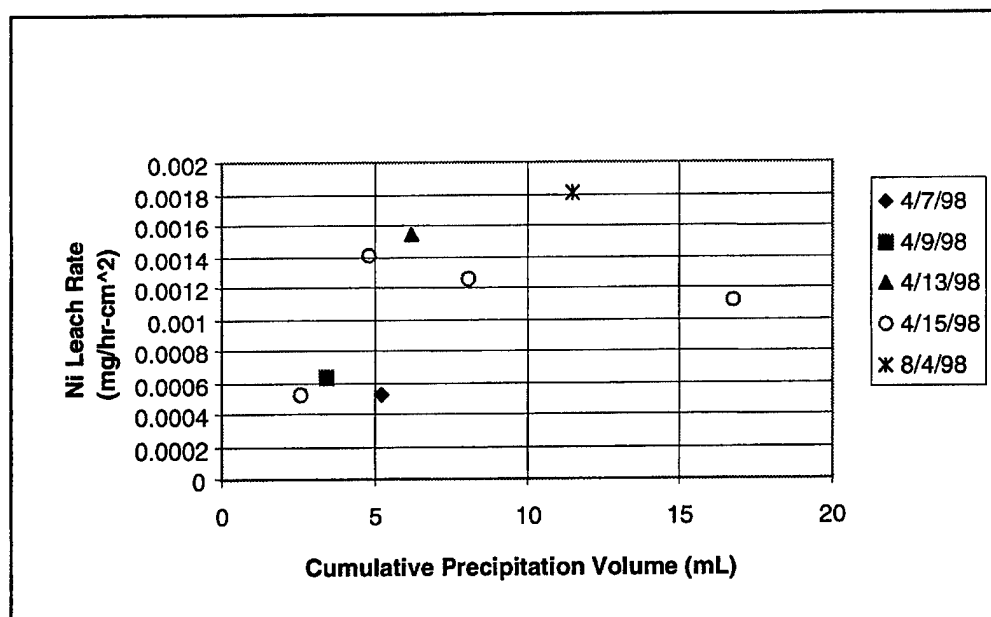
Figure 3.55. Ni leach rates as a function of cumulative water volume dripped onto "bare alloy" sample NS-22.6361.
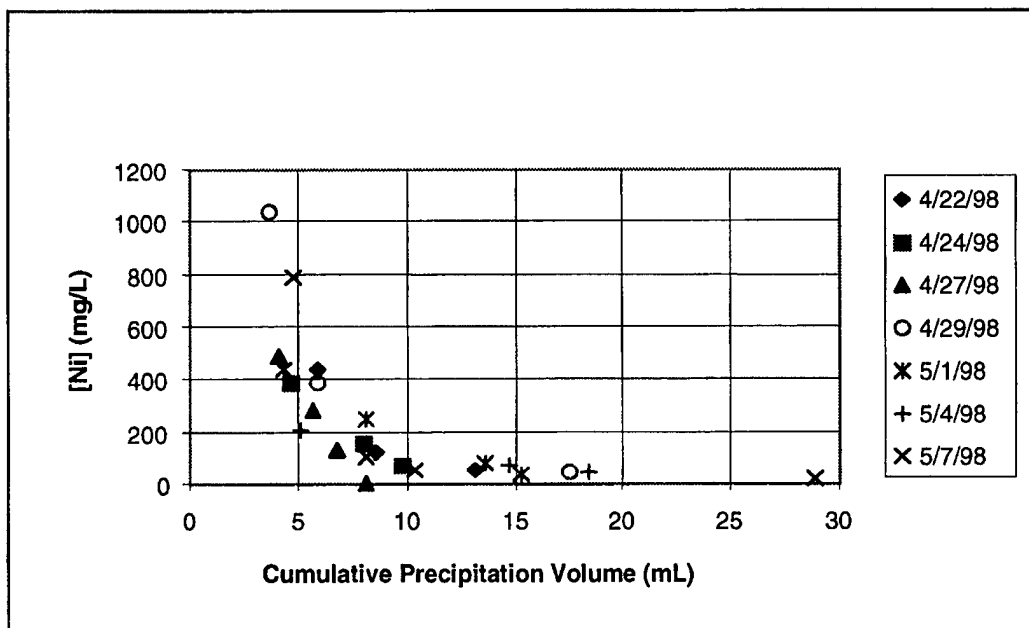
Figure 3.56. Ni concentrations as a function of cumulative volume of water dripped onto sample HD-17-13.7803 in soil.
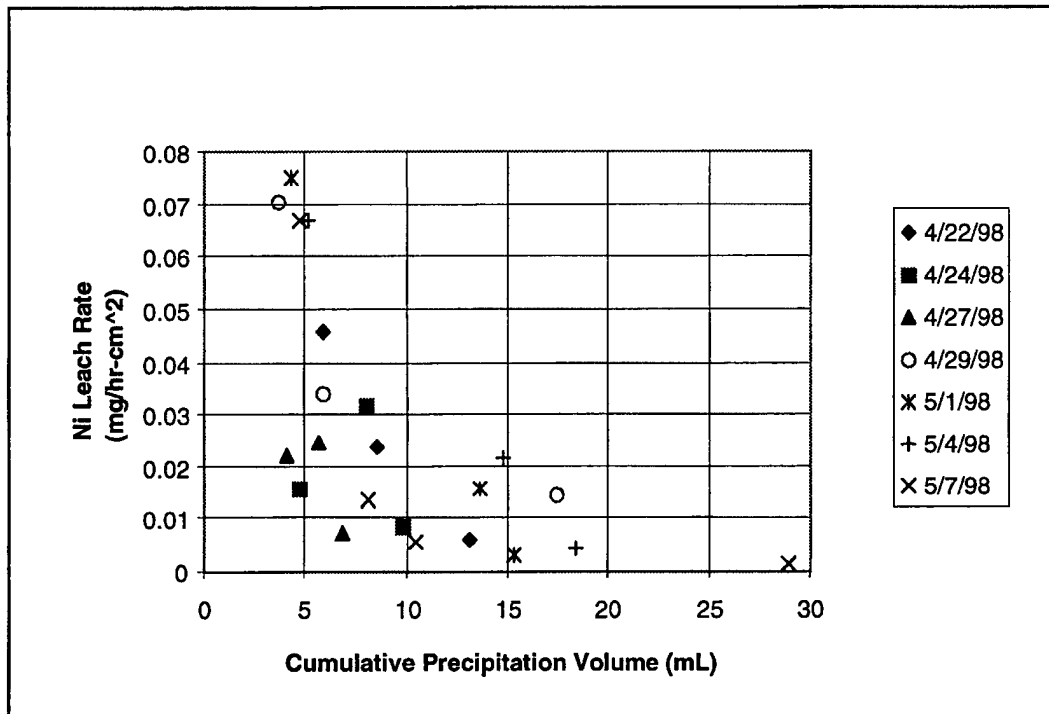
Figure 3.57. Ni leach rates as a function of cumulative volume of water dripped onto sample HD-17-13.7803 in soil.
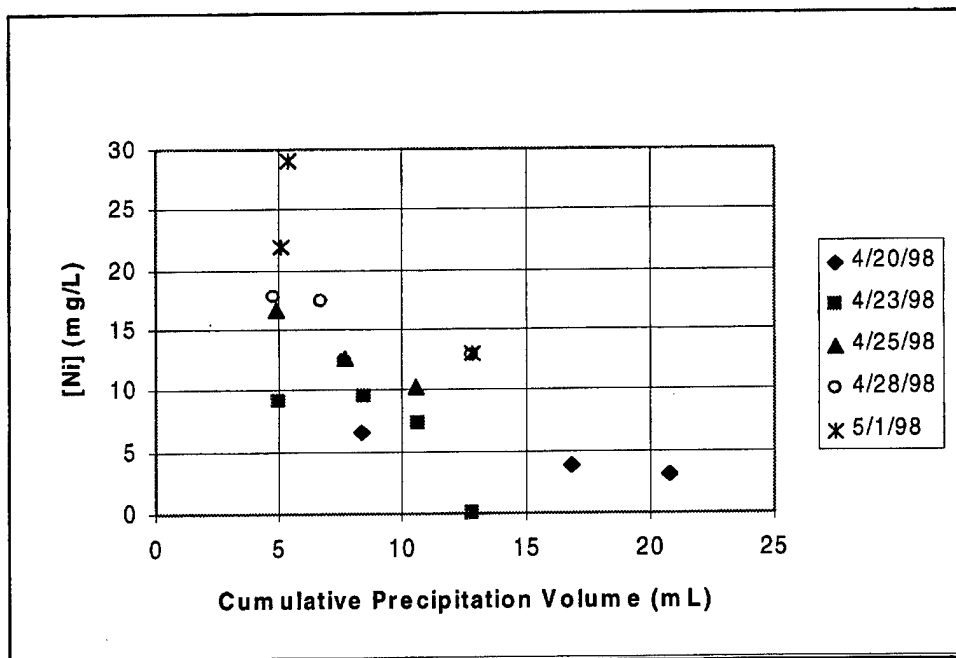
Figure 3.58. Ni concentrations as a function of cumulative volume of water dripped onto sample WL-1-18.4573 in soil.
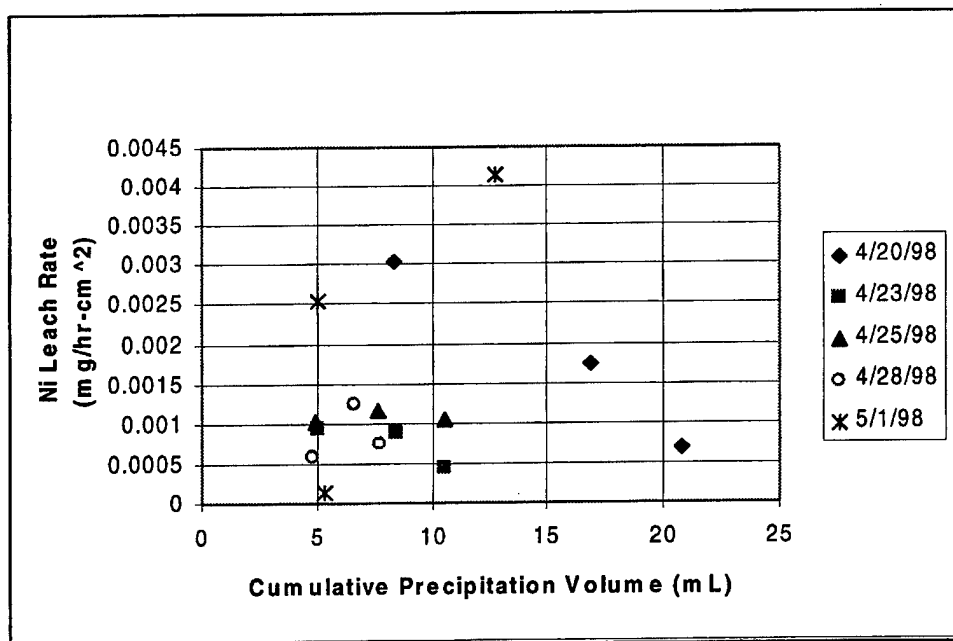
Figure 3.59. Ni leach rates as a function of cumulative volume of water dripped onto sample WL-1-18.4573 in soil.

might occur during the time the sample is not in use but still in soil, are somehow self-limiting and do not impact leach rates in subsequent drip tests with this alloy.

The drip test data for alloy NS with soil are shown in Figures 3.60 and 3.61. The nickel concentration data plotted in Figure 3.60 show more variability than indicated for the HD-17 and WL-1 alloy samples. However, the nickel concentrations measured in the NS experiments are lower than those observed in the other experiments. Some of the variability in the concentration data might be thought to be due to sorption of nickel onto the soil in the experiment. However, the fact that nickel concentrations reported for the "bare-alloy" experiments (Figure 3.54) are in the range of the experiments with soil (Figure 3.60) suggests this is not a problem. The nickel leach rate data for the NS alloy plotted in Figure 3.61 are the lowest rates for any of the alloys. They are also somewhat lower than the rates observed for the bare-alloy experiments (Figure 3.55). This indicates the presence of soil does not enhance the leach rate for this metal in this alloy.

The enhancement of nickel leach rates for alloy sample HD-17 in experiments with soil relative to "bare-alloy" and "static" immersion tests (i.e., no bubbled air) is of interest and its cause was investigated further. One possible cause involves limitations on the access of oxygen to the alloy surface during the immersion tests. Although sporadic measurements of dissolved oxygen suggested the bulk water in the "static" immersion experiments was near saturation with atmospheric oxygen (Appendix B), oxygen may have become depleted close to the alloy surface by rapid oxidation reactions. To test this possibility, immersion tests were carried out in which air was vigorously bubbled through the water surrounding the alloy disk (Figure 3.2). The resulting concentration and nickel leach rate data are compared with "static" immersion tests in Table 3.7. Vigorous aeration of the water in the immersion experiments with HD-17 appears to increase the measured leach rates relative to "static" experiments by approximately a factor of one hundred. This suggests oxygen depletion at the water/alloy interface could have been a significant factor in the determination of leach rates for this alloy. This may reflect the fact that tungsten grains are anodic in this sample and that the alloy is composed largely of tungsten grains.
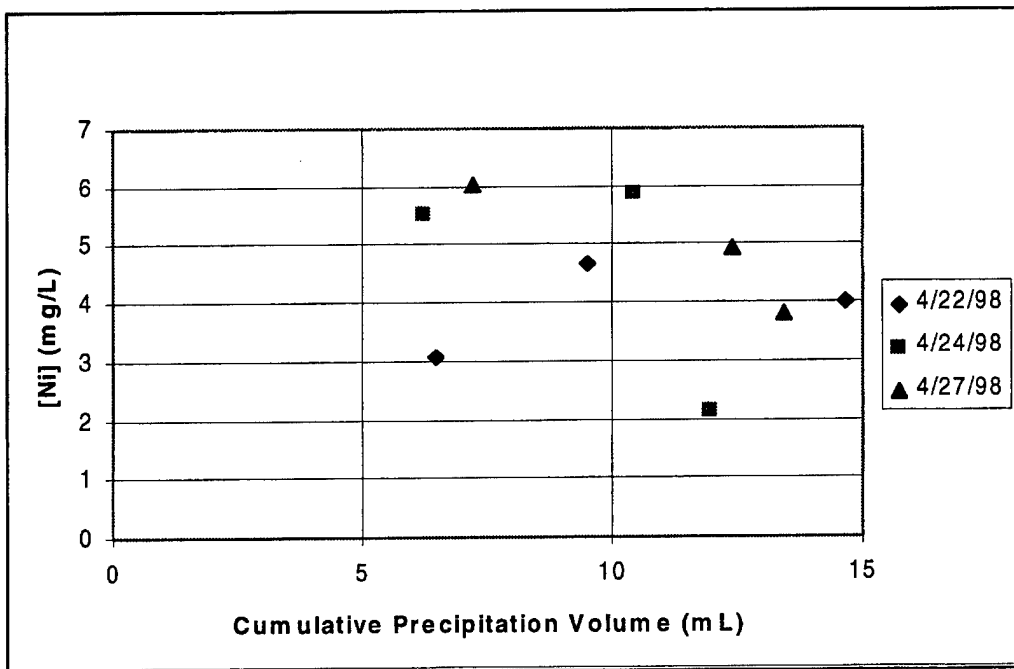
Figure 3.60. Ni concentrations as a function of cumulative volume of water dripped onto sample NS-22.6361 in soil.
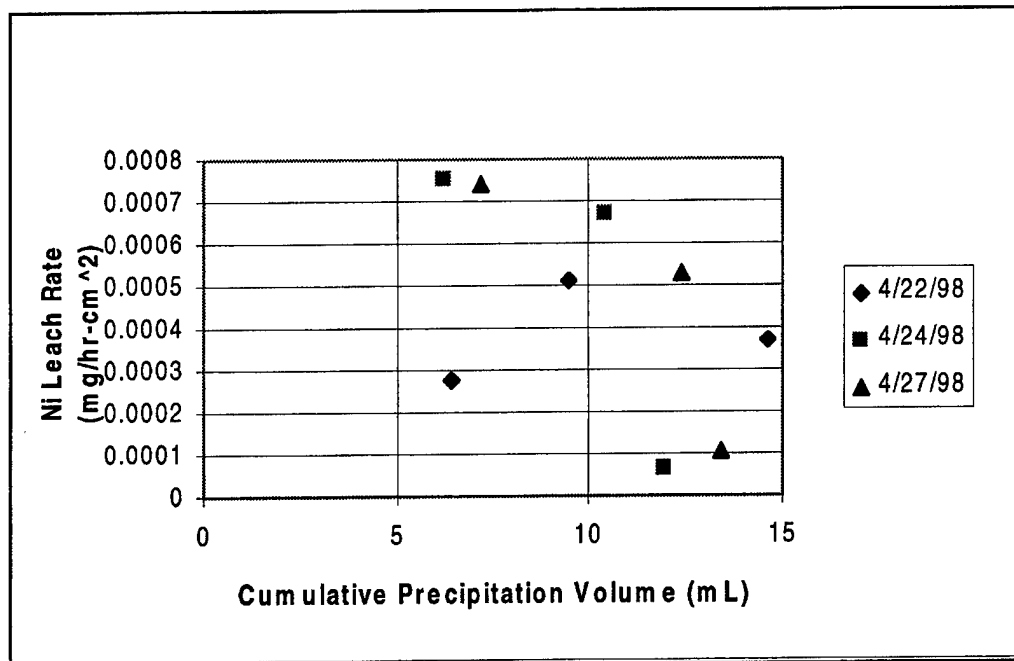
Figure 3.61. Ni leach rates as a function of cumulative volume of water dripped onto sample NS-22.6361 in soil.

Table 3.7. Comparison of leach rates from different tests.

	Average Nickel Concentration after 6 hours (mg/L)				Average Nickel Leach Rate during a 6 hour event (mg/hr-cm^2)			
Alloy	"Bare Alloy" Drip Test	Drip Test in Soil	"Static" Immersion Test	"Aerated" Immersion Test	"Bare Alloy Drip Test	Drip Test in Soil	"Static" Immersion Test	"Aerated" Immersion Test
NS	5.4	4.5	0.07	2.2	0.001	0.0004	0.001	0.009
WL-1	17	13	0.06	1.3	0.003	0.0016	0.001	0.007
HD-17	34	247	0.01	2.5	0.01	0.03	0.0002	0.02

The leach rate observed in the aerated immersion experiment involving alloy HD-17 are in between the leach rates observed in the drip experiments with this alloy in soil and the "bare alloy" test (Table 3-7). This suggests that the disks in the experiments containing soil have ready access to atmospheric oxygen. Interestingly, the "bare-alloy" drip experiments reported in Table 3.7 show lower leach rates than the drip experiments with soil. Apparently, the rate of oxygen consumption at the disk surface is high enough so that even in the water dripped onto the alloy disks in the "bare-alloy" experiments, oxygen becomes depleted at the alloy-water interface. Note that the water dripped onto the "bare alloy" disks forms tends to accumulate in a bubble held to the top of the disk by capillary forces. This bubble eventually breaks and the water runs down through the funnel. The time for a bubble to form is on the order of 30-60 minutes which is apparently enough time to cause the oxygen depletion.

Vigorous aeration increased the immersion leach rates for the other two alloys by at most a factor of ten relative to the "static" test as shown in Table 3.7. For these alloys, the soil-containing drip experiments resulted in lower calculated leach rates than the vigorously aerated immersion experiments. Further, the results indicate that the "static" immersion experiments and the drip experiments with and without soil all resulted in leach rates that varied by approximately a factor of 2-3. This suggests the presence or absence of soil is not a major factor in determination of the leaching behavior of these alloys. It also suggests that the vigorous aeration experiments involving these samples produced excessive leach rates. Vigorous aeration is

known to cause erosion corrosion effects (Trethewey and Chamberlain, 1988) that could unrealistically enhance the leach rates for these alloys by a factor of 2-3.

The difference observed between the leach rates for nickel in drip tests and "static" immersion test (Table 3.7) suggest that leach rates for the other metals in the alloys would also be different in the drip tests. One could normalize the immersion test long-term leach rates for the other metals using the difference in Ni leach rates in drip and immersion tests. For example, for W this would involve multiplying the drip test Ni leach rate for a given alloy by the ratio of long-term Ni to W leach rates from immersion tests. When this normalization is applied to data for the HD-17 alloy, the leach rate calculated for W implies the entire disk would dissolve in less than six months. Because HD-17 disks remained in tact at more than one-half their original mass after 12 months, this normalization procedure must be flawed. In order to more accurately predict tungsten mass flux values for the three tungsten alloy samples, an additional set of drip tests were carried out using "bare-alloy" disks without soil. Because tungsten is strongly sorbed to soil particles at low pH (see following section), drip tests with soil would produce eluants that did not accurately reflect the tungsten leach rates particularly for alloys NS and WL-1.

The solutions collected in these drip tests were analyzed for tungsten at Los Alamos National Laboratory using an inductively coupled plasma emission spectrometer. Results from these analyses are presented in Table 3.8. The W leach rates are 9-18 times the leach rates calculated for Ni in the "bare-alloy" leach tests (Table 3.7). This is similar to the range in the ratio of the concentration of W to Ni in alloys (13-19) suggesting leaching in drip tests is largely a congruent reaction (i.e., all parts of the alloy dissolve at the same rate).

Table 3.8. Bare alloy drip tests tungsten concentrations and leach rates.

Drip Test	BARE ALLOY	BARE ALLOY
	W concentration	W Leach Rate
Sample	mg/L	mg/hr-cm^2
NS	8.9	0.017
WL-1	12.6	0.027
HD-17	98.1	0.18

3.4 Source Term

The MEPAS code requires as input values for the fluxes of various metals that would enter the soil zone at Test Area C-64A after testing. These fluxes can be calculated using the leach rate data discussed in the previous sections and assumptions about the mass and surface areas of alloy fragments deposited on the soil surface as a result of munitions testing. According to AFRL/MN personnel, testing may result in the dispersal of as much as 500 lbs (226.8 kg) of alloy per year onto the C-64A site and the testing may go on for a period of ten years. Particles of greater than 1 cm in size will be recovered (i.e., removed from the test site for recycling). Based on observations of previous detonations of penetrator munitions, it is assumed that the particles that remain on the site will be predominantly between 0.001 and 1.0 cm in size. Three size ranges are considered: 0.001-0.01 cm, 0.01-0.1cm and 0.1-1.0 cm. Further, it was specified by the Air Force personnel that an equal number of particles will exist in each of these size ranges. These assumptions allow the calculation of the total surface area of alloy particles dispersed onto the site.

The number of particles in each size range, the total mass of the particles in each size range and the total surface area of particles in each size range have been calculated using the median sized particle to represent each size range (i.e., 0.005, 0.05 and 0.5 cm) and assuming the particles are cubes. As shown in Table 3.9, the largest particle size (0.5 cm) dominates both the total mass and the total surface area dispersed on the test sites each year.

Table 3.9. Data for alloy particles.

Average Particle Size (cm)	Number of Particles/yr	Total Particle Surface Area/yr (cm^2)	Total Particle Mass/yr (g)
0.005	9.4×10^4	1.4×10^1	2.26×10^{-1}
0.05	9.4×10^4	1.4×10^3	2.26×10^2
0.5	9.4×10^4	1.4×10^5	2.26×10^5
Totals	2.8×10^5	1.4×10^5	2.26×10^5

To calculate the flux of metal leached from alloys each year requires data for (1) the leach rate of the metal from the alloy in the soil zone, (2) the total surface area of the alloy fragments exposed in the soil zone over time and (3) the number of hours of rain per year. The leach rates used for the various metals in the different tungsten alloys are the drip test values given in Tables 3.7 and 3.8. The total surface area of the alloy fragments is the sum of the alloy fragments dispersed on the test range over the testing period. AFRL/MN personnel have indicated that penetrator munitions testing would continue for 10 years. Therefore, the total surface area of the fragments dispersed on Test Area C-64A after ten years would be 1.4×10^5 $cm^2/yr \times 10$ years $= 1.4 \times 10^6 \ cm^2$ assuming all the 0.5 cm alloy fragments are intact at the end of the 10 yr testing period. Based on the data presented in Section 2.1, there are an average of 108 rainfall events of 0.24 cm/hr lasting an average of 6 hours each. Therefore, there are 648 hours of rain per year. A sample calculation for the flux of Ni from alloy WL-1 follows:

$$0.0016 \ mg \ Ni/hr\text{-}cm^2 \times 1g/1000mg \times 648 \ hr \ rain/yr \times 1.4 \times 10^6 \ cm^2 = 1,497 \ g \ Ni/yr.$$

The fluxes for all the metals in each of the tungsten alloys are listed in Table 3.10. The fluxes calculated for Ni, Cu and W are based directly on drip test data. The fluxes for Fe, Mn and Co are based on normalized leach rates calculated from immersion data as explained above. These fluxes are less reliable than those calculated on the basis of drip tests. However, the fluxes of iron and manganese are not an issue because these metals are normally present in the environment at concentrations well above the concentrations resulting from the testing operations. As discussed in Section 4, iron and manganese are not associated with significant human and ecologic risks at the concentrations expected on the test sites after the cessation of testing. The chemical behavior of cobalt is similar to the behavior of nickel in surface environments. Therefore, the cobalt flux rates calculated on the basis of immersion tests are believed to be reliable.

Also listed in Table 3.10 are the number of the years required to totally leach a given metal from an alloy. These values are based on the total mass of alloy dispersed on the test ranges and the percentage of each metal in each alloy (Table 3.11).

Table 3.10. Mass flux and dissolution time.

Sample	Ni Mass Flux g/Yr	Dis. Time (Ni) Yrs.	W Mass Flux g/Yr	Dis. Time (W) Yrs.	CF (Ni-Fe)	Fe Mass Flux g/Yr	Dis. Time (Fe) Yrs.	CF (Ni-Cu)	Cu Mass Flux g/Yr	Dis. Time (Cu) Yrs.	CF (Ni-Co)	Co Mass Flux g/Yr	Dis. Time (Co) Yrs.	CF (Ni-Mn)	Mn Mass Flux g/Yr	Dis. Time (Mn) Yrs.	Sample
WL-1 (High MF)	1496				0.28	417	233							0.00	1.20	28392	WL-1 (High MF) (1E)
WL-1 (Low MF)	1496				0.06	95	1020							0.00	0.11	299814	WL-1 (Low MF) (1E)
WL-1 (Ave MF)	1496	100	1622	1224	0.18	270	360							0.00	0.52	64896	WL-1 (Ave MF) (1E)
WL-1 Measured*	1496	100	1622	1224													
NS (High MF)	327				0.35	113	290				0.30	98	346				NS (High MF)
NS (Low MF)	327				0.04	12	2660				0.18	58	577				NS (Low MF)
NS (Ave MF)	327	342	857	2437	0.15	49	662				0.26	86	392				NS (Ave MF)
NS Measured*	328	342	857	2437													
HD-17 Measured*	19232	18	13332	152					3456	27							HD-1 (Ave MF) (E)

* "Measured" values calculated from drip test leach rates calculated from measured metal concentrations.

NOTE:: HD-17 shown mass flux Ni represents maximum flux possible, flux is limited by the total mass available each year, 13,608g Ni/yr are available.

Table 3.11. Calculated metal mass after ten years of testing.

Alloy	metal % W	Metal Mass W (kg/10yr)	metal % Ni	Metal Mass Ni (kg/10yr)	metal % Fe	Metal Mass Fe (kg/10yr)	metal % Cu	Metal Mass Cu (kg/10yr)	metal % Co	Metal Mass Co (kg/10yr)	metal % Mn	Metal Mass Mn (kg/10yr)
HD-17	89.80%	2036.664	6.00%	136.08	0.00%		4.20%	95.256	0.00%		0.00%	
WL-1	87.60%	1986.768	6.60%	149.688	4.30%	97.524	0.00%		0.00%		1.50%	34.02
NS-	92.10%	2088.828	4.95%	112.266	1.45%	32.886	0.00%		1.50%	34.02	0.00%	

The penetrator munitions are assumed to be tested in a portion of Test Area C-64A that is 500 ft X 500 ft (152.4 m X 152.4 m) in area (see Figure 2.3). Assuming the alloy fragments are homogeneously distributed over this area, the initial concentrations of metals in the soils can be calculated if the depth of mixing is known. For the residential farmer scenario discussed in Section 5, the depth to which alloy fragments and metals are presumed to be mixed into the soil is taken as 8 inches (20.3 cm). This is a typical depth of soil tillage for agricultural purposes. With this soil depth, the average concentrations of the metals in the soil can be calculated for the period after the cessation of testing. The results of these calculations are presented in Table 3.12.

Table 3.12. Metal concentrations in soil at Test Site C-64A after ten years of testing.

Constituent	Maximum Concentrations	
	1.0 cm Soil mg/kg (ppm)	20 cm Soil mg/kg (ppm)
Cobalt	90	4.5
Copper	250	12.5
Iron	250	12.5
Manganese	90	4.5
Nickel	360	18
Tantalum	5500	275
Tungsten	5500	275

For ecologic purposes, the risk is maximized if no agricultural activity occurs at the site. Without agricultural activity at the site, the alloys and metals will tend to remain in the uppermost portion of the soil profile. A conservative value of 1.0 cm of penetration of the alloys and the metals is assumed for ecologic risk calculations. This results in the second set of soil concentrations listed in Table 3.12.

3.5 Sorption Experiments

Sorption experiments were carried out to determine the affinity of the metals which compose the alloys for the soils at the C-64A test site at Eglin AFB. A metal with high affinity for the soil will be greatly retarded in its transport through the soil profile. The metals investigated are W, Ni, Cu, Co, Mn, and Ta. Iron was not included even though it is found in several of the alloys because the soil at the site contains a significant amount of iron naturally.

The partitioning of the metals between the soil and solution is quantified by the sorption coefficient, or K_d. The K_d is calculated as the concentration of metal adsorbed to the soil divided by the concentration of metal in solution: $K_d = [Me]_{soil} / [Me]_{solution}$. The data collected were used as input parameters for the MEPAS model which was used to assess the environmental impact of testing tungsten penetrator munitions at site C-64A.

3.5.1 Experimental Design

The sorption experiments were performed by contacting soils from Eglin AFB with artificial waters containing several dissolved metals. A detailed procedure for these experiments is presented in Appendix A. The samples were periodically agitated to ensure equilibration of metals with soil. After a contact time of three weeks, the water was separated from the soils, filtered, and prepared for metal analysis. Concentrations of metals in solution were analyzed by ICP-MS (Inductively Coupled Plasma Mass Spectrometry) at a commercial laboratory. The laboratory data are presented in Appendix B. The experiments were carried out under ambient temperature (25°C) and pressure conditions (900mm/5000 feet altitude). Since Ta metal is very sparingly soluble, a different method, described in Appendix C, was used to determine sorption coefficients for this metal. To ensure that conditions under which the experiments were

performed replicate environmental conditions at the site as well as cover a range of other conditions, an experimental matrix was designed to incorporate various water types, pH values, and soil types which could be encountered by the dissolved metals. This matrix is presented in Table 3.13.

Table 3.13. Soil sorption matrix.

SURFACE WATER

METALS	SOIL TYPE: SAND pH 4.5	SOIL TYPE: SAND pH 6.5	SOIL TYPE: SAND pH 8.5	SOIL TYPE: CLAY pH 4.5	SOIL TYPE: CLAY pH 6.5	SOIL TYPE: CLAY pH 8.5
NiWCu : (low)*	X	X		X	X	
NiWCu : (high)*	X		X	X		X
NiWMn : (low)*	X			X		
NiWMn : (high)*	X	X		X	X	
NiWCo : (low)*	X		X	X		X
NiWCo : (high)*	X			X		
Ta : (low)*	X			X		
Ta : (high)*	X			X		

GROUND WATER

METALS	SOIL TYPE: SAND pH 4.5	SOIL TYPE: SAND pH 6.5	SOIL TYPE: SAND pH 8.5	SOIL TYPE: CLAY pH 4.5	SOIL TYPE: CLAY pH 6.5	SOIL TYPE: CLAY pH 8.5
NiWCu : (low)*	X	X		X	X	
NiWCu : (high)*		X			X	
NiWMn : (low)*		X	X		X	X
NiWMn : (high)*	X	X		X	X	
NiWCo : (low)*		X	X		X	X
NiWCo : (high)*		X			X	
Ta : (low)*		X			X	
Ta : (high)*		X			X	

SEA WATER

METALS	SOIL TYPE: SAND pH 4.5	SOIL TYPE: SAND pH 6.5	SOIL TYPE: SAND pH 8.5	SOIL TYPE: CLAY pH 4.5	SOIL TYPE: CLAY pH 6.5	SOIL TYPE: CLAY pH 8.5
NiWCu : (low)*	X		X	X		X
NiWCu : (high)*			X			X
NiWMn : (low)*		X	X		X	X
NiWMn : (high)*	X		X	X		X
NiWCo : (low)*		X	X		X	X

NiWCo : (high)*			x			x
Ta : (low)*			x			x
Ta : (high)*			x			x

* Low and high refer to the upper and lower starting concentrations used in the experiments.

Water Types and pH values

Three types of artificial waters were used in the experiments: surface water, ground water, and sea water. As described in previous sections, these solutions were intended to mimic the waters found at Eglin AFB. The composition and procedure for their preparation is found in Appendix A. Artificial surface water at pH 4.5 was selected to represent surface waters at site C-64A. Shallow ground water sampled from wells at Eglin AFB has an average pH ranging from 6.0-6.5 (Trapp et al., 1974). The target pH level selected for ground water experiments was 6.5. Sea water in the Gulf of Mexico is represented by artificial sea water at pH 8.5. Target pH levels prevalent to each water type were emphasized in the matrix but experiments with all three pH levels were conducted with each water type to evaluate the effect of pH on the sorption coefficients.

Soil Types

Soils used in the sorption experiments were collected from Eglin AFB. The two soil types used were designated as "sand" and "clay". The "sand" sample was collected from the upper layer (A-horizon) of the Lakeland series soil. The "clay" soil sample was collected from the sandy clay loam sub surface layer (Bt-horizon) of the Lucy series. The collection locality for the sand sample is shown on Figure 3.1. The Lakeland series "sand" soil represents 90%-99% of the soil type found at the C-64A site. It is generally light tan in color. Zero to five percent of the soil at C-64A are represented by the Lucy series sample. Quartz grains of sand size are the main component of the Lakeland series sample. These grains are sparingly coated by clays. The sample also contains approximately 1% organic fragments. The Lucy series soil is also dominated by quartz grains but these grains have more extensive clay coatings colored red by iron oxides.

<u>Metal concentrations</u>

Each metal was tested at two different initial solution concentrations. This was done to evaluate the effect of metal concentrations in solution on the K_d. Higher initial solution concentrations can result in lower measured K_d values. This effect is evident in Figure 3.62 in which the concentration of metals on the solid is plotted versus the concentration of metal in solution. The "curve" in Figure 3.62 is called a sorption isotherm. A sorption isotherm can be linear or non-linear over a given concentration range. The linear part of the "curve" depicted in Figure 3.62 represents a constant K_d value. To investigate the shape of the isotherm relating to the metals and soils of interest to the project, sorption experiments were conducted at two different initial solution concentrations (nominally 1 and 5 mg/L) for each metal of interest.
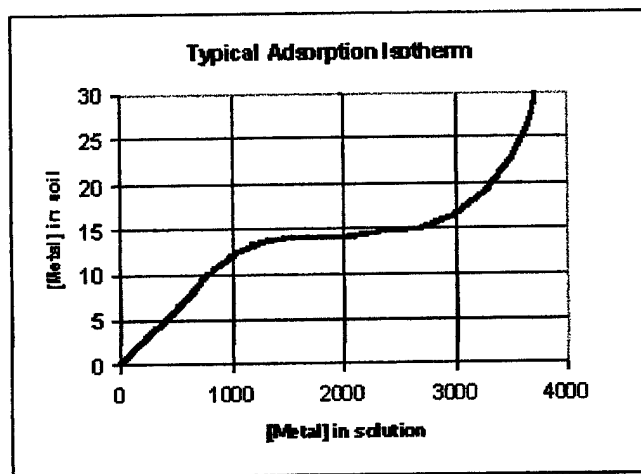
Figure 3.62. A typical adsorption isotherm.

Another reason for using two different metal concentrations is to investigate potential competitive effects between different metals on soil sorption sites. The metals tested (Ni, Cu, Co, Mn, W) can be divided into two groups, cations and anions, based on the form they most commonly take in solution. W is the only metal tested that is predominantly anionic in solution (negatively charged). Ni, Cu, Co, and Mn are typically found as cations in solution (positively charged). As shown in the experimental matrix, the higher concentrations of cations were

combined with the lower concentrations of the anionic metal and visa-versa to reduce the risk of saturating the solution with compounds of the metals.

3.5.2 Experimental Results

The metals investigated exhibit some definite trends in their sorption behavior as a function of several factors. These factors include: ionic charge on the metal, pH, soil type, water type, and initial metal concentration. Scatter plots of K_d versus pH are used to evaluate the characteristic trends of each metal in different environments.

The Effect of Ionic Charge and pH on K_d

The ionic charge of the metals in solution (i.e. whether they are cationic or anionic) has a clear effect on their sorption behavior. For each of the metal cations, the K_d increases with increasing pH regardless of the water or soil type. Figures 3.63 through 3.66 illustrate this trend for nickel, cobalt, manganese, and copper. The log (K_d) is plotted against the pH. As shown in Figures 3.63 to 3.65, the trend appears approximately linear for Ni, Co, and Mn. For Cu, the K_d increases from pH 4.5 to 6.5 and levels off at higher pH values (see Figure 3.66). In contrast to the cations, the K_d for W increases with decreasing pH (Figure 3.67).

The contrasting sorption behavior of tungsten versus the cations as the pH changes is due to changes in the surface charge of the soil as the contact solution becomes more acidic or alkaline. The surfaces of the soil particles carry two "spheres" of charge, an inner-sphere and an outer-sphere layer (Stumm, *1992*). The outer-sphere charge occurs as a result of the net inner-sphere charge. All soils contain metal oxides consisting of positively charged metal atoms and negatively charged oxygen atoms. Metal and hydrogen ions exchange on the surface of these oxides. In an acidic solution, the abundance of protons displaces metal ions from the negatively charged oxide surface. This results in the formation of an inner-sphere having a net positive charge. To balance the positive charge, anions are drawn to the inner-sphere. This explains the increasing K_d values for W as the pH decreases. If the contact solution is alkaline, the inner sphere becomes negatively charged because of the low relative abundance of protons.
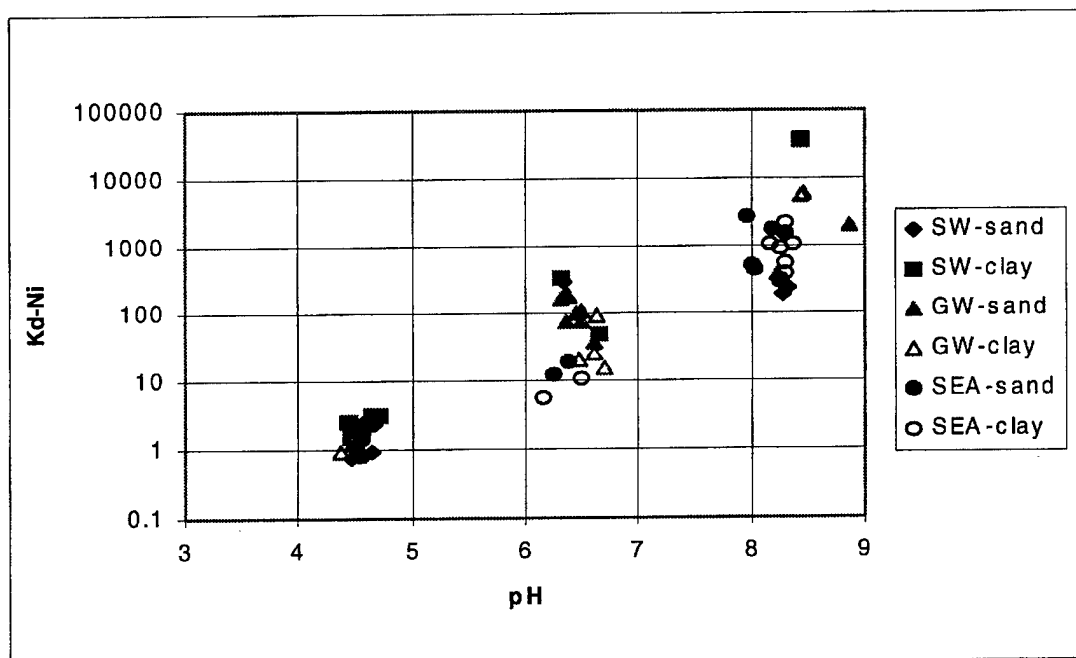
Figure 3.63. K_d-Ni vs. pH for sand and clay in artificial sea water, groundwater and surface water.
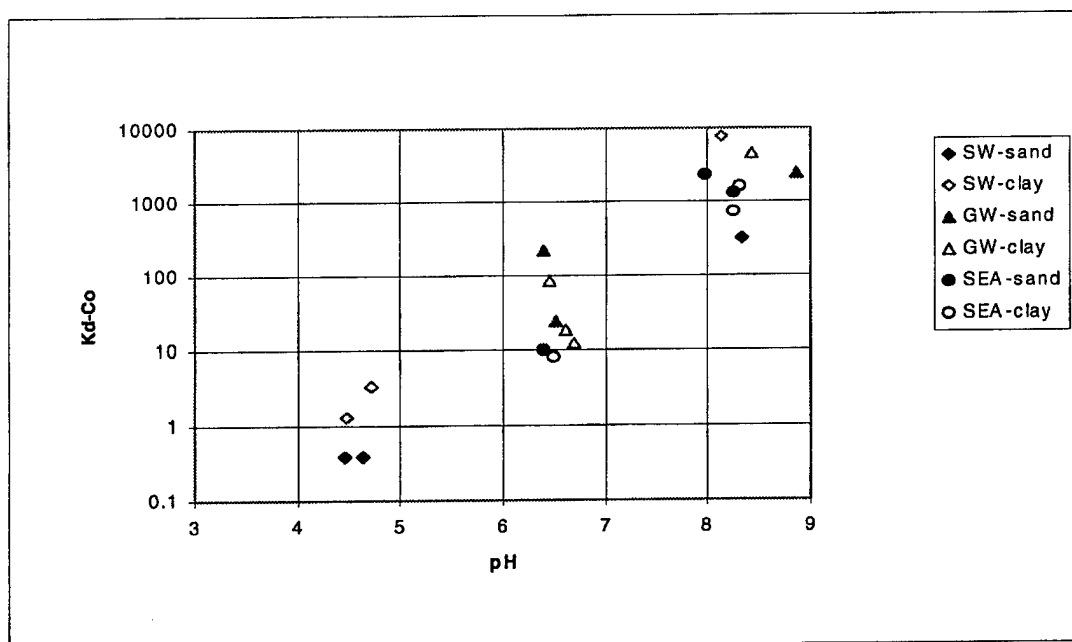
Figure 3.64. K_d-Co vs. pH for sand and clay in artificial sea water, groundwater and surface water.
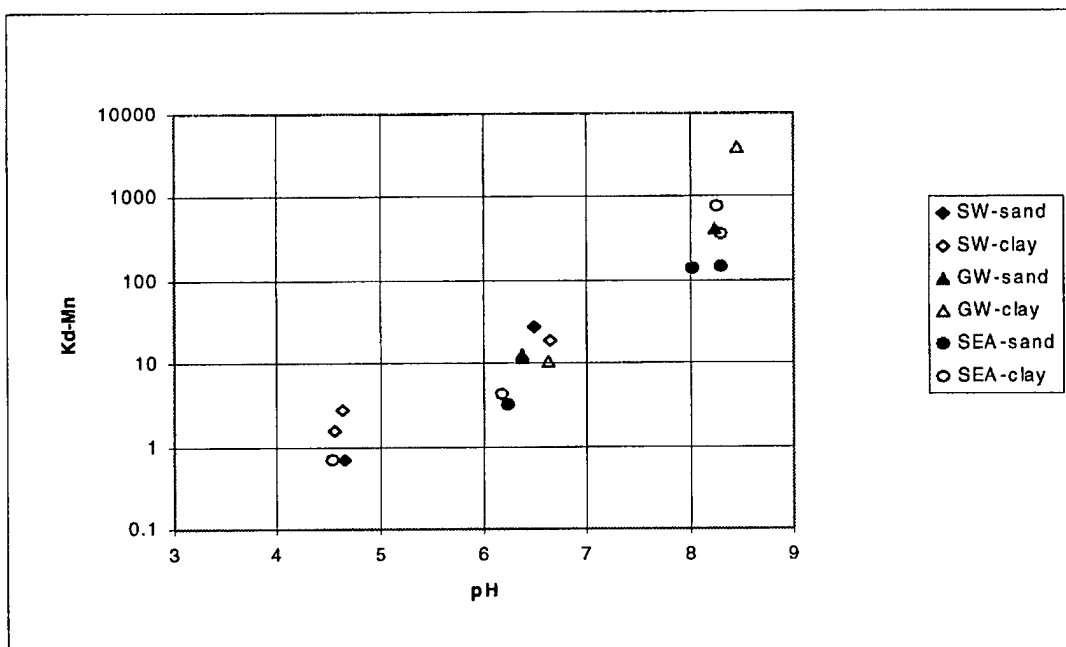
Figure 3.65. K$_d$-Mn vs. pH for sand and clay in artificial sea water, groundwater and surface water.
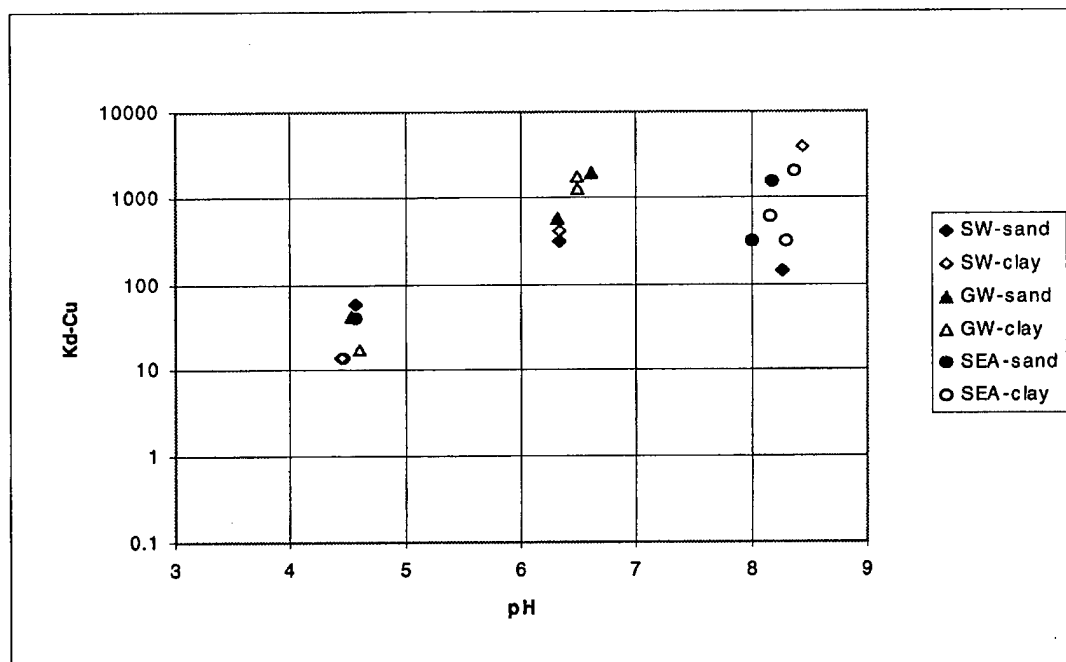
Figure 3.66. K$_d$-Cu vs. pH for sand and clay in artificial sea water, ground water and surface water.
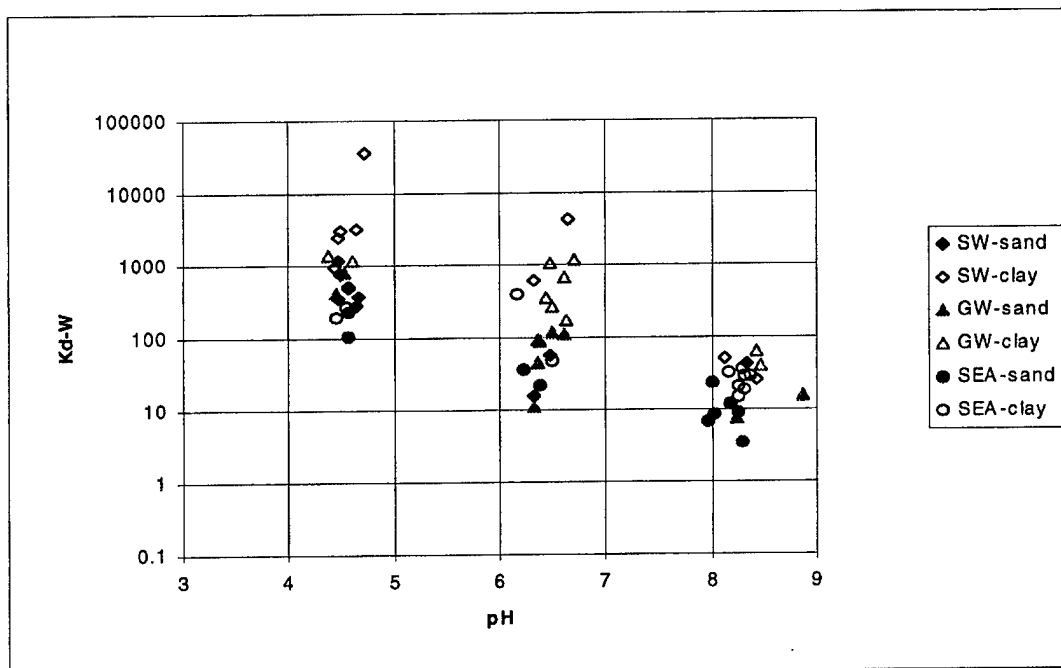
Figure 3.67. K$_d$-W vs. pH for sand and clay in artificial sea water, ground water and surface water.

The net negative charge attracts positive cations to the inner sphere. Therefore, the sorption coefficients of Ni, Cu, Co, and Mn increase as the pH increases.

The influence of water type on K$_d$

In examining Figures 3.63 to 3.67, trends regarding the effect of water type on the K$_d$ value at different pH values become evident. In general, K$_d$(surface water) > K$_d$(ground water) > K$_d$(sea water) at every pH value tested. This trend breaks down for Ni, Co, and Cu contacted with sand at pH 8.5 where K$_d$ values are large and the trend in the K$_d$ values is K$_d$(sea water) > K$_d$(ground water) > K$_d$(surface water) (Figures 3.63-66). Some other exceptions are seen in Figures 3.63 to 3.67. At K$_d$ values greater than 100, the differences in values are significantly affected by the error in the analysis of the very small concentrations of metals remaining in solution.

The effect of soil type on the K_d

In general, Figures 3.63 to 3.67 show that the K_d of the metals is higher in solutions contacted with clay than with sand. This trend is evident for all metals at pH 8.5, for Mn and W at pH 6.5 (Figures 3.65 and 3.67), and for Co, Mn, and W at pH 4.5 (Figures 3.64, 3.65, and 3.67). There is no clear difference between sand and clay for Ni at pH 4.5 and Cu at pH 6.5 as shown in Figures 3.63 and 3.66. The trend is reversed for Co at pH 6.5 and Cu at pH 4.5 where K_d(sand) > K_d(clay) (Figures 3.64 and 3.66). The reversals in these results are attributed to analytical error and possibly the details of the sorption reactions.

The Effect of Initial Solution Metal Concentration on K_d

There is no clear relationship between the initial metal concentration and the sorption coefficient over the concentration ranges tested. This is shown in Figures 3.68 to 3.82 in plots of K_d against initial concentration of metal in solution. For example, in Figure 3.68, the plot of K_d versus initial tungsten concentration at pH 4.5 shows little variation in the K_d values calculated at different initial metal concentrations. Most of the other figures are consistent with this observation. This indicates that the range of initial metal concentrations tested falls on the linear part of the adsorption isotherm (Figure 3.62) and that the K_d values calculated are applicable for all metal concentrations in the range.

3.5.3 MEPAS Data

The MEPAS model, which is used in this report to calculate the risks associated with the testing of tantalum and tungsten penetrator munitions at test site C-64A, requires sorption coefficient data specific to the test site. To supply the most specific information for the MEPAS code, the soil profile was broken into three sections. The first layer, surface soil zone, is the upper-most layer. This layer is the zone containing plant roots and contains water which is available to plant roots. Below the roots is the vadose zone. The vadose zone is the unsaturated layer between the surface soil zone and saturated zone. A saturated layer containing the ground water is the third layer. For each of the three layers a pH value, water type and soil type was assigned which best approximated the properties.
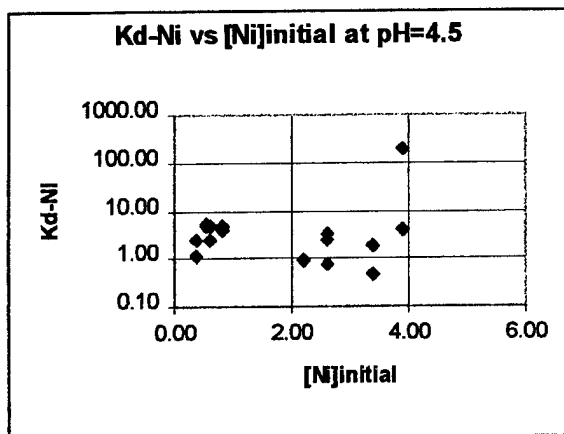
Figure 3.68.
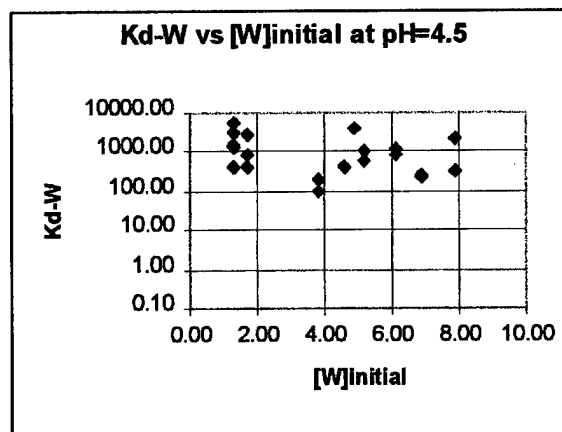
Figure 3.69.
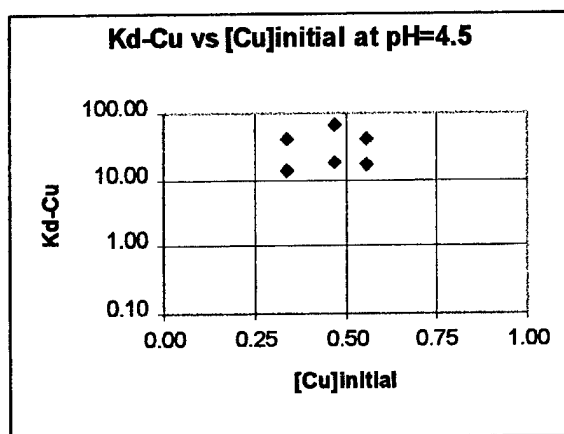
Figure 3.70.
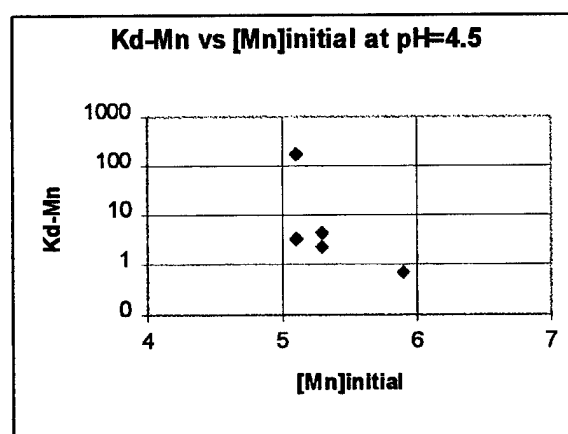
Figure 3.71.
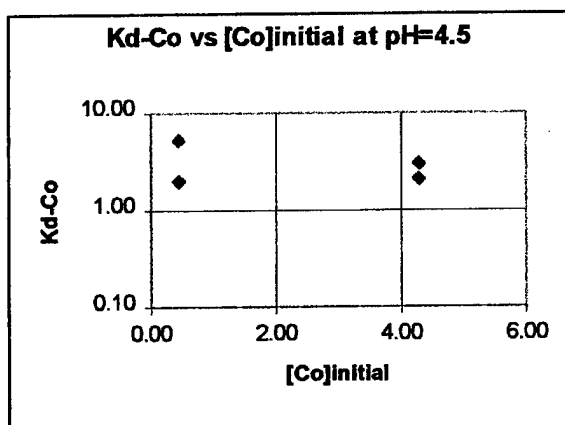
Figure 3.72.
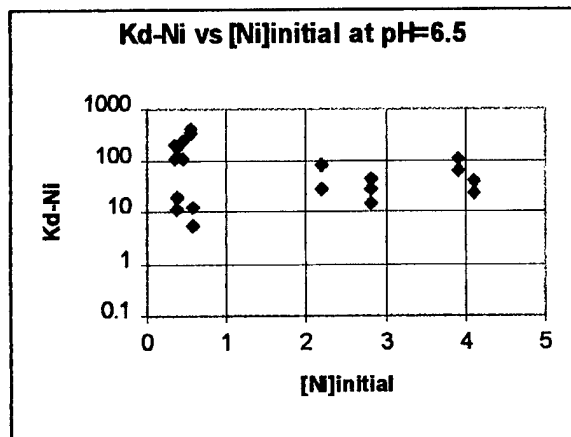
Figure 3.73.
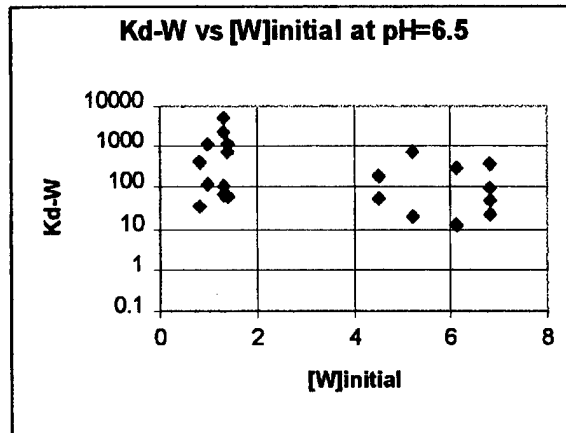
Figure 3.74.
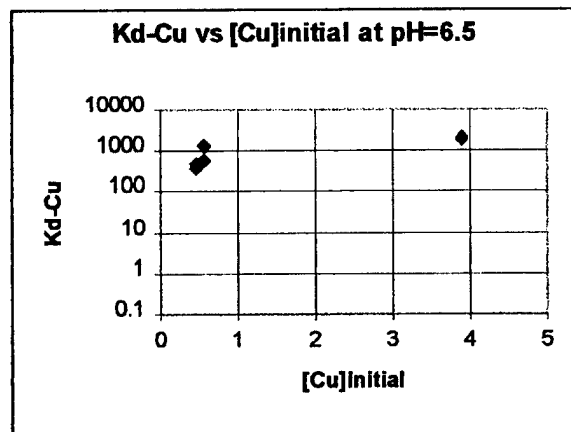
Figure 3.75.

Figure 3.76.

Figure 3.77.

Kd-Ni vs [Ni]initial at pH=8.5

Figure 3.78.

Kd-W vs [W]initial at pH=8.5

Figure 3.79.

Kd-Cu vs [Cu]initial at pH=8.5

Figure 3.80.

Kd-Mn vs [Mn]initial at pH=8.5

Figure 3.81.

Kd-Co vs [Co]initial at pH=8.5
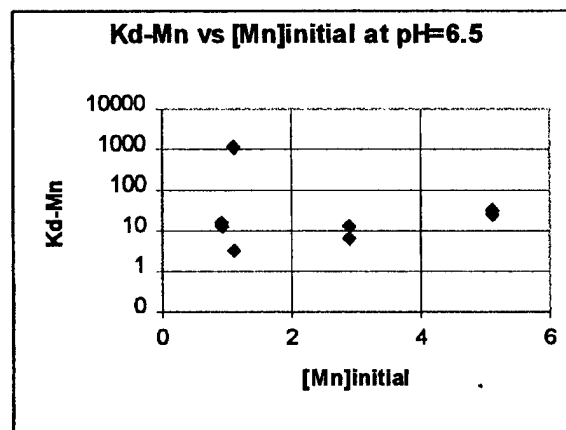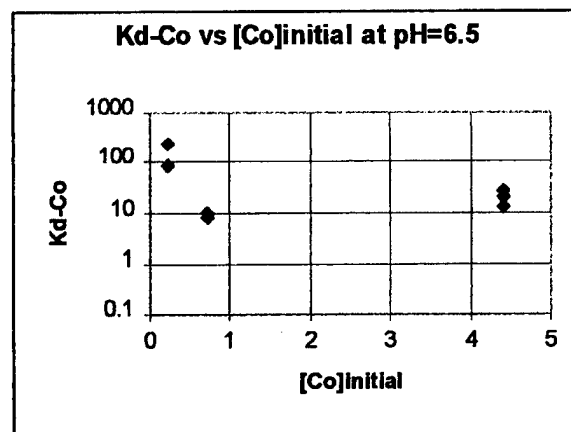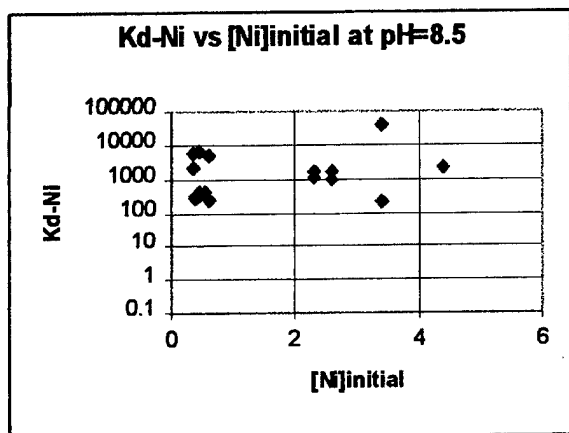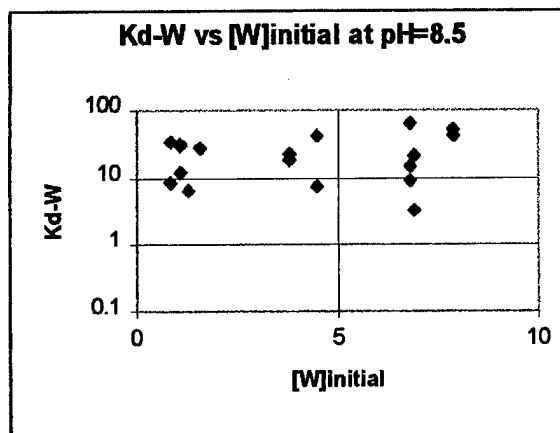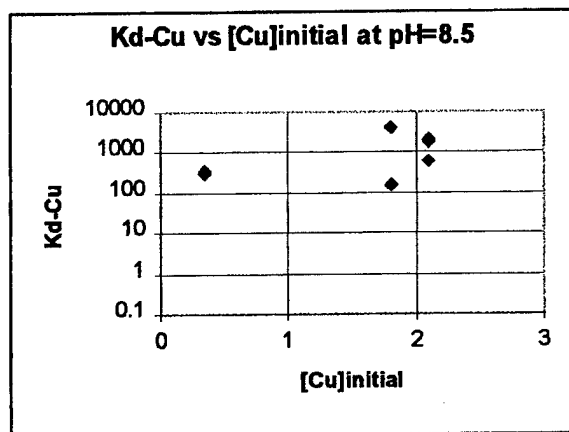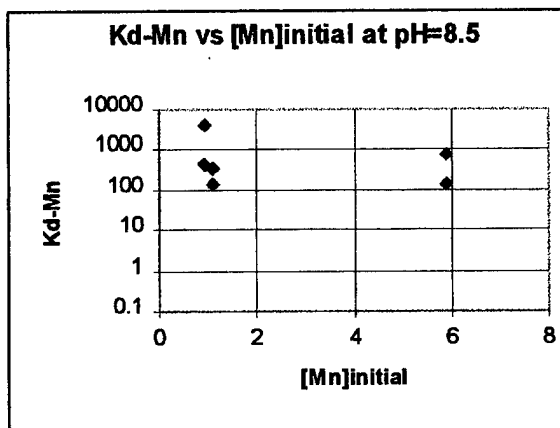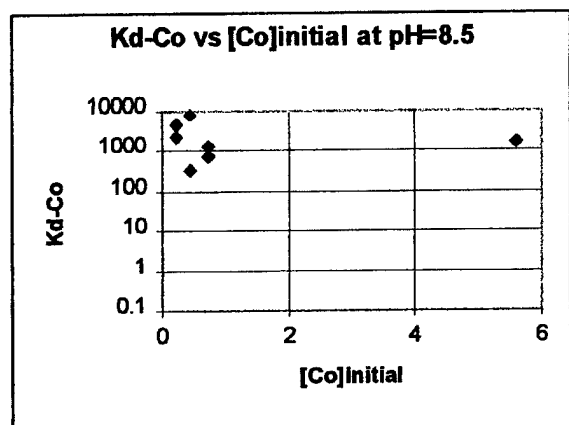
Figure 3.82.

Average pH values were assigned to each soil zone based on measurements reported in the literature and interpretations of hydrochemistry (see section 2.6). The following pH values were assigned to each zone: surface soil zone pH = 5.0, vadose zone pH = 5.5, saturated soil zone pH =6.0. In the surface soil zone, the effect of the soil on the pH is minimal because it is thin, composed predominantly of quartz and is highly permeable so that water passes through in a short period of time. Therefore, the pH of the water in the surface soil zone is largely determined by the pH of precipitation. The surface soil zone was assigned a nominal pH value of 5.0 because the average pH of precipitation at Eglin AFB is most likely near 5.0 (see section 2.6). The sandy units of the vadose zone have a greater effect on the pH of the water as it passes through the pore spaces as thin films. The thickness of the highly permeable units of the vadose zone results in longer contact times for percolating waters leading to slight pH increases. The assigned pH value for waters in this zone is 5.5. The waters of the saturated zone have still longer contact times and therefore higher pH values. Well-water taken from the shallow sand and gravel aquifer near the test site have a pH near 6.0. This is the value chosen to represent the saturated zone waters.

The water composition of each soil layer was also taken into account when determining sorption coefficients for MEPAS. The water composition of each zone is related to its residence time in that zone. Soil zone water is influenced very little by contact with soil. Therefore, the water flowing through this layer largely retains the chemistry of precipitation. Water samples from streams near the site show that the water of the vadose zone also has a composition similar to precipitation (see section 2.6). Artificial surface water was used to approximate both the surface soil water and vadose zone water. The artificial ground water composition was used to approximate the water found in the saturated zone. Because the Lakeland sand is the dominant composition at C-64A test site, the sorption data in MEPAS emphasizes the sorption coefficients obtained for sand.

Sorption coefficients were provided to the MEPAS model at the pH values noted above. The values for these coefficients were interpolated from the plots of K_d versus pH shown in Figures 3.83 to 3.92. All the K_d values for the surface soil zone were interpolated to pH = 5.0

from experiments conducted with sand in artificial surface water (see Figures 3.83 to 3.87).
Vadose zone K_d values were interpolated to pH = 5.5 from the same plots. Graphs from
experiments with sand and artificial ground water at pH = 6.0 were used to interpolate sorption
coefficients for the saturated zone. The data used to provide sorption coefficients for tantalum
are found in Appendix C. The K_d values used as input to the MEPAS model are provided in
Table 3.14.

Table 3.14. K_d (ml/g) values used as input to MEPAS model.

	Surface Soil Zone pH = 5.0	Vadose Zone pH = 5.5	Saturated Zone pH = 6.0
Nickel	7	20	30
Tungsten	200	100	100
Copper	100	200	200
Cobalt	4	10	10
Manganese	4	10	8
Tantalum	16890	16890	4395

K_d vs pH of Nickel in Artificial Surface Water contacted with Sand

Figure 3.83.

K_d vs pH of Cobalt in Artificial Surface Water contacted with Sand

Figure 3.84.

K_d vs pH of Manganese in Artificial Surface Water contacted with Sand

Figure 3.85.

K_d vs pH of Copper in Artificial Surface Water contacted with Sand

Figure 3.86.

K_d vs pH of Tungsten in Artificial Surface Water contacted with Sand

Figure 3.87.

K_d vs pH of Ni in Artificial Ground Water contacted with Sand

Figure 3.88.

K_d vs pH of Cobalt in Artificial Ground Water contacted with Sand

Figure 3.89.

K_d vs pH of Manganese in Artificial Ground Water contacted with Sand

Figure 3.90.

K_d vs pH of Copper in Artificial Ground Water contacted with Sand

Figure 3.91.

K_d vs pH of Tungsten in Artificial Ground Water contacted with Sand

Figure 3.92.

4.0 REVIEW OF METALS TOXICOLOGY IN TERMS OF HUMAN ENVIRONMENT

Information in the scientific literature regarding the toxicology of the metals contained in the alloys has been reviewed. Toxicologic data for the alloys of interest are not available. The following discussion will focus on information available on the toxicology of the individual metals. If an exposure pathway involves the original alloy (e.g., dust inhaled after detonation), a dose could be calculated for the alloy metal with the greatest toxicity assuming the presence of the toxic metal in an alloy does not increase its toxicity. If an exposure pathway involves metal generated as a result of dissolution of the alloy (e.g., metal ions in soil or ground water), a dose based on the toxicity of the pure metal could be calculated directly.

For tungsten, no carcinogenic, mutagenic, teratogenic or reproductive effects in humans have been reported (Sittig, 1985). Based on occupational exposures, it appears inhalation of tungsten powder may cause transient or permanent lung damage depending on dose. Unfortunately, occupational exposure to tungsten powder generally also involves exposure to other metals. For example, exposure to tungsten carbide powder in the "hard metal" industries usually also involves contemporaneous exposure to metals such as cobalt and nickel. This makes it difficult to ascribe observed toxicologic effects solely to tungsten. Nonetheless, the ACGIH (American Conference of Government Industrial Hygienists) has set a maximum exposure level for insoluble tungsten of 5 mg/m^3 of air determined as the Time Weighted Average (TWA) concentration for up to a 10-hour shift in a 40 hour workweek. A Short-Term Exposure Limit (STEL) value of 10 mg/m^3 was also set by the ACGIH.

The most soluble form of tungsten (i.e., Na_2WO_4) is moderately toxic by ingestion according to results obtained in animal studies. The main target organ is the central nervous system although chronic elevated exposure in rats also causes reduction in weight, reduction of albumin and γ-globulin as well as uric acid in blood, and changes in the motility of spermatozoa. At large overdoses, acute signs of toxicity include central nervous system disturbances, diarrhea, respiratory failure and death (Seiler and Sigel, 1988). Lifetime administration of 5 mg/l Na_2WO_4

in drinking water to rats showed no impact on tumor induction, body weight or longevity. Human exposure data are much more limited. Chemists working with WO_4^{2-} solutions showed higher uric acid blood levels associated with the development of gout. In fish, tungsten was shown to be the least toxic element of the components in coal (Birge, 1978). Tungsten is accumulated by certain species of plants (Seiler and Sigel, 1988) but no data on plant toxicity were identified for this report.

The exposure limits for soluble tungsten compounds are lower than those for insoluble tungsten compounds. The ACGIH has set a maximum exposure level for soluble tungsten of 1 mg/m^3 of air determined as the TWA concentration for up to a 10-hour shift in a 40 hour workweek. An STEL value of 3 mg/m^3 was also set by the ACGIH for soluble tungsten. No drinking water limit has been set in the United States although a limit of 0.1 mg/l was set for drinking water in the former U.S.S.R. (Seiler and Sigel, 1988). The State of Florida has set a 24-hour exposure limit of 0.012 mg per m^3 for ambient air (Sittig, 1994).

Toxicologic data for iron were not evaluated because background concentrations of iron in most surface environments exceed the concentrations expected to result from corrosion of dispersed alloy fragments.

Toxicologic data for cobalt were reviewed by Smith and Carson (1981). The following discussion is based on their review. Cobalt is an essential element in man and is a fundamental constituent of vitamin B_{12}. Nonetheless, cobalt is associated with various health effects in man and other animals. Chronic inhalation of cobalt-bearing dusts can lead to upper respiratory tract irritation, exertional dyspnea (shortness of breath), coughing, weight loss, extrinsic asthma, diffuse interstitial pneumonitis, fibrosis and pneumoconiosis. In addition, data on occupational exposure to cobalt suggest it can lead to decreased sense of smell, nausea, decreased hemoglobin and red blood cell counts, and dermatitis. Cobalt has not been shown to cause significant carcinogenic, teratogenic or reproductive effects in humans. Nonetheless, cobalt is classified as a suspected carcinogen (EPA, 1988).

Animal studies generally lead to similar conclusions as those stated above except in those studies where high doses were administered. On the other hand, doses of approximately 1 mg/l can have significant impact on the mortality of aquatic organisms such as shrimp, stickleback fish and freshwater zooplankton. Further, cobalt has a greater impact (2-3X) when it is added to softwater, than when it is added to hard water. The effect of cobalt on plants is variable depending on dose. At low dosages, cobalt appears to stimulate growth in some plants. However, at 1 mg/l, various nonleguminous plants showed negative growth effects. Interestingly, leguminous plants showed negative effects at dosages as low as 0.05 mg/l. The recommended OSHA inhalation exposure limit for cobalt is 0.1 mg/m^3 of air for a 7-8 hr workday. The ACGIH TLV is 0.05 mg/m^3 of air and the STEL is 0.1 mg/m^3 of air. The State of Florida has set a 24-hour exposure limit of .00012 mg per m^3 for ambient air (Sittig, 1994). No limits have been set for cobalt concentrations in drinking water.

Copper is an essential element in man and is found in over a dozen copper specific proteins. In humans, copper can cause irritation, allergic effects and gastroentreric distress at high doses. No human carcinogenic, teratogenic, mutagenic or reproductive effects due to ingestion or inhalation of environmental concentrations of copper were identified in the literature (Prager, 1995). For industrial inhalation exposure, a TWA of 1.0 mg/m^3 has been set by the ACGIH and NIOSH. A 24-hour short-term exposure limit of 2.4 $\mu g/m^3$ has been proposed by the State of Florida for ambient air. A recommended concentration limit of 1.0 mg/l has been proposed for domestic and drinking water in the State of Florida (Sittig, 1994).

Copper is known to be ecotoxic at relatively low concentrations. For abalone, the LC_{50} (lethal concentration; 50% kill) is 0.05 mg/l/95-hr in natural seawater at 14 °C. Copper sulfate concentrations of 0.009-0.17 mg/l stopped growth in juvenile brook trout. Further, copper is associated with bioconcentration factors of 200-700 for fish and up to 1,500 for marine invertebrates. No concentration limits have been set for fresh or marine fishery waters in the United States. Copper is an essential element in plants and no toxic effects have been noted at natural concentrations (NAS, 1977).

Manganese is classed as an essential element in man and animals (NAS, 1973). It is among the trace elements least toxic to mammals and is more often a problem because of deficiency than toxicity. However, toxic effects have been identified in association with high doses by both inhalation and ingestion pathways. The disease manganism has been associated with high inhalation doses in industrial settings. In Japan, an encephalitis-like disease was reported to result from high ingestion doses from drinking water (NAS, 1973). A TWA of 0.2 mg/m^3 has been set by the ACGIH. The State of Florida has set a short-term (24 hr) exposure limit for ambient air of 12 $\mu g/m3$ and a domestic/drinking water limit of 0.05 mg/l.

Manganese toxicity in plants is highly variable. For cotton, wheat, tobacco, sugarbeets, alfalfa and many other crops, manganese concentrations must be over 1,000 ppm (dry wt.) to show toxic effects. In soybeans, concentrations of several hundred ppm appear to be toxic (NAS, 1973).

Of the four metals in the tungsten alloys (Table 3.1), nickel appears to cause the most serious health effects. Nickel is classified as a Class A human carcinogen (EPA, 1988). Nickel oxides, nickel subsulfide and nickel sulfate are considered the most hazardous in terms of carcinogenic potential. These compounds are strongly implicated in lung and nasal cancers in nickel refinery workers. The exposure pathway in this case is primarily in the inhalation of nickel-containing dusts. Nickel is also associated with genetic, reproductive, developmental and immunologic effects as reported by the U. S. Department of Health and Human Services (1993). Nickel poses serious risks to aquatic life. Nickel concentrations of 0.1 mg/liter produce acute toxicity in a variety of aquatic organisms.

The Federal standard for nickel metal and its soluble compounds is 1 mg/m^3 of air. NIOSH recommends adherence to an exposure limit of 15 micrograms of nickel per cubic meter of air as a TWA for up to a 10 hr workday, 40-hour workweek. The ACGIH has set 1 mg/m^3 of air as a TWA for nickel metal and 0.1mg/m^3 of air for soluble nickel compounds. An STEL of 0.3 mg/m^3 of air was set for soluble nickel compounds. The EPA has set a drinking water standard for nickel of 0.1 mg/liter.

Tantalum is not an essential metal for mammals (Seiler et al., 1988). The toxicity of Ta is low probably due to its low solubility. No adverse effects have been reported as a result of industrial exposure. A few animal exposures have suggested that after inhalation, tantalum may produce benign and nonfibrotic pulmonary effects (Seiler et al., 1988). No effects concerning ecotoxicity have been reported according to Seiler et al. (1988). A TWA of 5.0 mg/m^3 has been set by the ACGIH. The State of Florida has set a 24-hour exposure limit of 0.12 mg per m^3 for ambient air (Sittig, 1994).

5.0   HUMAN AND ECOLOGICAL RISK ANALYSIS

This section presents the methodology and results of the baseline human and ecological risk assessments which were conducted to evaluate potential environmental impacts that could result from the testing and eventual breakdown of high-density tungsten alloy penetrator munitions at Test Area C-64A on Eglin AFB, in Okaloosa County, Florida.

Metal transport, exposure, and human health risk were quantified using the Multimedia Environmental Pollutant Assessment System (MEPAS) developed by Pacific Northwest Laboratory and the U.S. Department of Energy (Whelan et al., 1992) along with guidance on conducting preliminary human health risk evaluations presented in "Risk Assessment Guidance for Superfund, Volume 1, Human Health Evaluations Manual" USEPA (1989). Ecologic risk was quantified using transport results derived from MEPAS and methodologies outlined in USEPA's "Framework for Ecological Risk Assessment" (USEPA 1992; 1998). The risk assessments were conducted using geochemical and toxicological data presented in previous sections of this report.

MEPAS is a physically-based risk computation code which integrates source-term, transport, and exposure models with toxicological data on individual constituents of interest to calculate risk values in the case of chemical and radioactive carcinogens, and hazard quotients for noncarcinogens (Whelan et al., 1992). With MEPAS, constituent source-to-receptor analyses can be conducted through multiple transport and exposure pathways as illustrated in Figure 5.1. Constituents can undergo complex processes of transport, degradation/decay, transformation, biological accumulation and concentration, and intermedia transfer among atmospheric, overland, subsurface, and surface-water pathways. The waterborne transport pathways are linked through temporally varying contaminant-flux boundary conditions, while the linkage between waterborne pathways and exposure routes is made through temporally varying water constituent concentrations at receptor locations. The linkage between the atmospheric and surface exposure pathways is based on air concentrations and ground-deposition factors which provide the spatial variation of ground and air constituent concentrations surrounding the site.
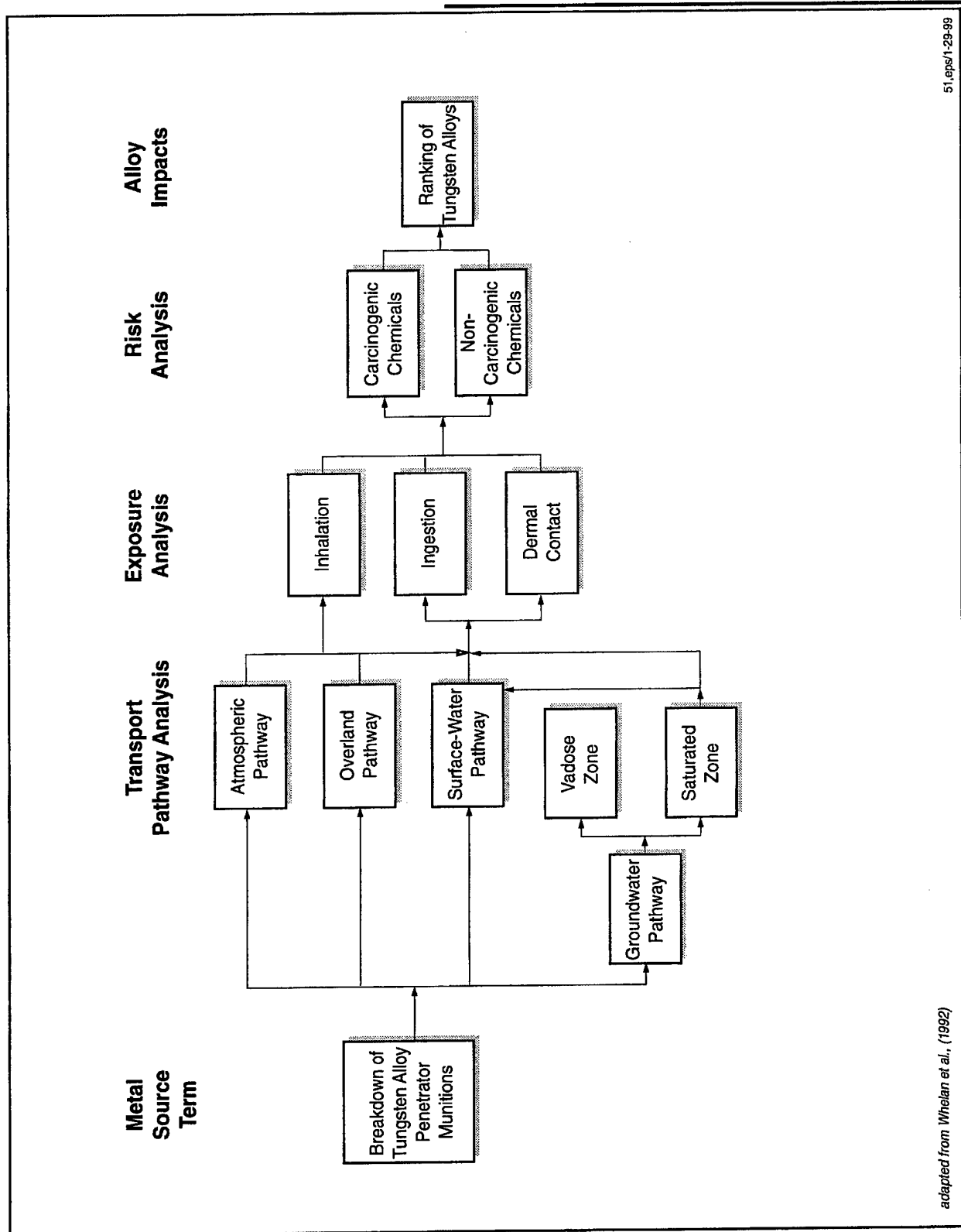
Figure 5.1. Flow diagram of risk assessment methodology.

Presentation of the preliminary risk assessment is divided into three sections, following the structure depicted in Figure 5.1. Section 5.1 presents hypothetical source terms for metals resulting from the leaching and breakdown of tungsten alloy penetrator munitions at Test Area C-64A. These are developed as input to the transport analysis. Note that Ta and W are not considered in the groundwater and surface water models because these metals remain in the soil and vadose zones. Section 5.2 presents the transport analysis, which consists of air, groundwater, and surface water transport pathway models and results. Transport pathway model results consist of estimated concentrations of metal contaminants at different receptor locations along air, groundwater, and surface water pathways. Section 5.3 presents exposure and risk analyses which comprise the human and ecologic risk assessments. These analyses start with exposure point concentrations for metals at different receptor locations in different environmental media calculated as part of the transport pathway analysis in Section 5.2. Different exposure pathways models are then developed, which integrate transport pathways and exposure routes. Exposure pathway models, along with metal and pathway specific human and ecologic exposure parameters are used to estimate average daily dose to human and biotic receptors. Toxicological data are then combined with estimates of average daily dose to calculate risk to human and biotic organisms and populations. Baseline risk is characterized both qualitatively and quantitatively in order to rank the relative environmental impact of tantalum and different tungsten alloys that may be used in penetrator munitions testing at Eglin, AFB.

5.1 Test Area Source Term

The source term describes the mechanism and rate of metal release from alloys that may be dispersed at Test Area C-64A penetrator munitions test area. The source term provides the boundary conditions for transport models used to estimate migration of metals present in test area soils as a result of the leaching breakdown of munitions fragments left over from penetrator weapons testing. The following sections describe the derivation of the source term for metals transported away from the site via wind or groundwater.

5.1.1 Air Pathway Source Term

The air transport pathway model in MEPAS requires input of soil emission rates from the C-64A test area in order to estimate transport and dispersion of metal-bearing soils. There are several different ways that this emission rate is determined in MEPAS. The most straightforward is the special case in which the site is completely covered with vegetation or a thick crust (or a wet, saturated soil) and no mechanical disturbances occur at the site. In this case, the emission rate can be considered to be zero. This situation does not apply at Test Area C-64A. Although there is a thin grass cover over most of the area and a concrete slab over another part, there is some potential for soil emission from the site. Two other ways in which the soil emission rate is determined in MEPAS is by direct input and by calculations based on site characteristics. Because soil emission rates from Test Area C-64A site have not been independently determined, the latter method is used here.

The suspension of metal-bearing soil particles from test area surface soils may occur as a result of wind action or other physical action on the surface such as vehicular traffic and walking. Site specific data on local climate, wind, and surface soil characteristics were entered into MEPAS to calculate a soil particle emission rate for C-64A test area soils. MEPAS calculates the suspension of respirable particles (particles with diameters less than 10 μm) using empirical relationships based on studies of wind erosion and surface disruption (Droppo and Buck, 1996). The source-term release methodology for computing suspension rates in MEPAS is an adaptation of the methodology proposed by Cowherd et al. (1985) for rapid computation of potential long-term impacts from spills of hazardous materials. This methodology, which includes formulations for contaminant suspension by winds, vehicular traffic, and other physical disturbances of the surface, is similar to, but not identical to, the U.S. Environmental Protection Agency's (EPA) AP-42 revision of the Cowherd et al. (1985) model for industrial wind erosion (EPA 1988, 1995).

MEPAS uses the soil particle size distribution, apparent roughness of the site, vegetation cover, presence of a crust on the soil, and presence of nonerodible elements (e.g., large stones) to

define the potential for suspension of soil particles. A site is characterized as having: 1) unlimited erosion potential, 2) limited erosion potential, or 3) no erosion potential.

As noted above, Teat Area C-64A has some erosion potential. Therefore, it must be characterized either as having limited or unlimited erosion potential. These two erosion potentials are calculated using different methodologies as described in Cowherd et al. (1985). In MEPAS, the results of the two separate calculations are summed which was not the case in the original methodology described by Cowherd et al. (1985)

The potential for wind erosion is quantified in terms of a threshold friction velocity. The greater the value of the threshold friction velocity for a site, the lower the potential for particle suspension. The threshold friction velocity for the test area is determined from the mode of the aggregate particulate size distribution based on site specific soil composition data according to the following equation:

$$U_f = \frac{f_{ne} \exp\left[0.412 \ln(A_{dist}) + 4.17\right]}{100} \qquad (5.1)$$

where U_f = threshold friction velocity (m s^{-1})

f_{ne} = nonerodible elements correction factor (unitless)

A_{dist} = soil aggregate size distribution (mm).

Soil aggregate size distribution is estimated using:

$$A_{dist} = 0.0106 P_{sand} + 0.05 \qquad (5.2)$$

where P_{sand} is the percent sand in the soil (unitless). This relationship provides relatively realistic estimates for soils with greater than 75% sand content. For other soils, the relationship provides relatively conservative estimates that are more typical of disturbed soils than undisturbed soils (Droppo and Buck, 1996).

The correction factor, f_{ne}, in Equation 5.1 allows for the effects of any nonerodible elements in the source area. As the silhouette area of nonerodible elements increases, so does the threshold friction velocity. If the threshold friction velocity is less than 0.75 m s^{-1}, the area has unlimited erosion potential; otherwise, the area has only limited erosion potential.

In order to calculate the soil emission rates using the limited erosion potential and unlimited erosion potential methodologies, the critical wind speed must first be determined. The critical wind speed is calculated using the equation:

$$U_c = \frac{1}{c_{vk}} U_f \ln\left(\frac{h_{ref}}{L_r}\right) \tag{5.3}$$

where U_c =   critical wind speed at the reference height above the soil surface (m s^{-1})

   c_{vk} =   von Karman constant (unitless)

   h_{ref} =   reference height above the soil surface (m)

   L_r =   surface roughness length (m).

The critical wind speed is used to define the erosion potential. The recommended value of h_{ref} is 7 m. The surface roughness length of the test area, L_r, is related to the size and spacing of the roughness elements in the area. The von Karman constant is equal to 0.4. (Droppo and Buck, 1996)

5.1.1.1   *Limited Erosion Calculation*

For a source area having limited wind-erosion potential, the following equation is used to predict potential emissions:

$$E_{lim} = \left(8.76 \times 10^{-4} \, A\right)(0.83) \left[\frac{f_d \, E_{pot} \, (1 - f_v)}{\left(\dfrac{f_{PE}}{50}\right)^2} \right] f_{cr} \qquad (5.4)$$

where f_d =   frequency of mechanical disturbances to the soil (month^{-1})

      E_{pot} =   erosion potential of the soil (g m^{-2})

      f_v =   vegetation coverage on the surface (unitless)

      f_{PE} =   Thornthwaite's Presciipitation-Evaporation (PE) Index (unitless)

      f_{cr} =   fraction of soil surface that is crusted (unitless)

      A   =   area.

In Equation 5.4, the factor $(8.76 \times 10^{-4} A)$ is used to convert E_{lim} from the units used in Cowherd et al. (1985) (mg m^{-2} hr^{-1}) to those used in MEPAS (g yr^{-1}). The frequency of disturbances per month, f_d, is defined as the number of actions that could expose fresh surface material. A disturbance could be vehicular traffic, plowing or turning of the soil, or construction. The erosion potential, E_{pot}, depends on the maximum wind speed, U_{max}, so that

$$E_{pot} = \begin{cases} 6.7 \, (U_{max} - U_c) & \text{if } U_{max} \geq U_c \\ 0 & \text{if } U_{max} < U_c \end{cases} \qquad (5.5)$$

where U_{max} is the maximum wind speed at a reference height above the soil surface (m s^{-1}). The vegetation fraction, f_v, varies from 0 for bare ground to 1 for total coverage. The Thornthwaite's PE Index, f_{PE}, is used as a moisture-correction parameter for wind-generated emissions and is provided in Buck et al., (1995).

5.1.1.2   Unlimited Erosion Calculation

For unlimited erosion potential, the relationship for the surface emission rate is:

$$E_{unlim} = (0.876\,A)(0.036)(1-f_v)\left(\frac{\overline{U}_y}{U_c}\right)^3 F(U_c,\overline{U}_y)(1-f_{cr}) \qquad (5.6)$$

where $\overline{U}_y$ is the mean annual wind speed (m s^{-1}) and $F(U_c, \overline{U}_y)$ is a function defined below. In Equation 5.6, the factor (0.876 A) is a units conversion factor.

The vertical flux of particles smaller than 10 μm in diameter is assumed to be proportional to the cube of the horizontal wind speed. The function, $F(U_c, \overline{U}_y)$, comes from the cubic relationship of the vertical transport of particles and the wind speed. It is defined in MEPAS as:

$$F(U_c,\overline{U}_y)=\begin{cases} 0.0 & \text{if } x<0.0 \\ 1.91 & \text{if } 0.0\le x<0.5 \\ 1.9-(x-0.5)0.6 & \text{if } 0.5\le x<1.0 \\ 1.6-(x-1.0)1.3 & \text{if } 1.0\le x<2.0 \\ 0.18\,x\,(8x^2+12)\,e^{-x^2} & \text{if } 2.0\le x \end{cases} \qquad (5.7)$$

where $x = 0.886(U_c/\overline{U}_y)$.

5.1.1.3 Emission Rate Computation

The soil particulate emission rate for the source area surface is computed as the sum of the unlimited and limited erosion emissions:

$$E_{wind} = E_{lim} + E_{unlim} \qquad (5.8)$$

where E_{lim} = annual average limited emission rate per unit surface area (g yr^{-1})

E_{unlim} = annual average unlimited emission rate per unit surface area (g yr^{-1})

E_{wind} = total emission rate for wind erosion (g yr^{-1})

The wind suspension rate is calculated from the emission rate for respirable particulates.

$$S = \frac{E_{wind}}{\beta_s \bullet A} \qquad (5.9)$$

where S   =   volumetric wind suspension rate (cm yr^{-1})

   B$_s$ =   dry bulk density of surface soil (g cm^{-3})

   A   =   area of the source area (cm^2).

Both the wind suspension rate, S, and the total emission rate, E$_{wind}$, are used as input to the atmospheric dispersion, transport, and deposition model. The atmospheric pathway model, then computes airborne soil particle concentrations, which when multiplied by source area soil metal concentrations gives airborne metal concentrations.

5.1.1.4   Source Area Soil Metal Concentration

In order to calculate emission of metals from source area soils, the soil particulate source term emission rate estimated by MEPAS must be multiplied by source area soil metal concentrations. Table 5.1 presents source area soil metal concentrations utilized in air transport pathway calculations for both current and future conditions. These soil metal concentrations were derived based on experimental data as presented in Section 3.4. When calculating source area soil metal concentrations under current conditions, metals derived from the breakdown of penetrator munition alloys were assumed to be distributed evenly across the entire source area to a depth of 1 cm. The depth of 1 cm is was chosen conservatively, assuming the site will not be disturbed and so metals which accumulate in surface soils will not migrate downward rapidly.

If the site is developed in the future for agricultural, residential, or commercial use, the physical characteristics of the test site and surrounding areas may change, as well as the disturbance regime experienced by surface soils. Because the extent and type of future changes at the site are unknown, it was assumed that the site will be used for agriculture and eventually developed into a residential community in the future. When calculating source area soil metal concentrations under future conditions, metals derived from the leaching/breakdown of

penetrator munition alloys were assumed to be distributed evenly across the entire source area to a depth of approximately 20 cm. The depth of 20 cm represents an average plow depth and was choosen to simulate disturbance and mixing of metals in surface soils from agriculture use or from grading during residential development.

Table 5.1. Source term concentrations for source area soil metals for air transport pathway.

Metal	Metal Concentration in Source Area Soils (mg-C/g-soil)	
	Current Conditions	Future Conditions
W and Ta	5.5	0.275
Ni	0.36	0.018
Cu and Fe	0.25	0.0125
Co and Mn	0.09	0.0045

5.1.2 Groundwater Pathway Source Term

For metals transported in groundwater via infiltrating precipitation, test site data on local climate, precipitation, surface soil, and vegetation were entered into MEPAS to calculate a vertical flux rate for water leaving the surface soil zone beneath the source area and entering the groundwater flow system. Annual flux of metals released from munitions fragments were calculated independently for each alloy based on data presented in Section 3.4 and are summarized in Table 5.2. Note that Ta and W are not listed in Table 5.2. These metals remain in the soil zone because they have large sorption coefficients and, in the case of Ta, are also extremely insoluble. The two fluxes (fluid and metal) were combined in MEPAS to obtain the concentration of various metal species in water leaving the soil zone and entering groundwater.

Table 5.2. Contaminant source terms for groundwater and surface water transport pathways.

Alloy	Contaminant Name	Flux Rate g/yr	Release Time yrs
WL-1	Nickel	1497	100
	Manganese	1.2	999[a]
NS	Nickel	327	343
	Cobalt	98	347
HD-17	Nickel	19232	7
	Copper	3456	28

a) Minimum value

MEPAS computes the annual vertical flux of water through the source area based on the concept of water balance. The method involves a monthly water-balance calculation using meteorologic and site information, including monthly estimates of precipitation, potential evapotranspiration, snowmelt, temperature, and runoff. These are summed to obtain an average annual infiltration of water from source area soils to groundwater.

The water balance is a mass balance of the flow and storage of water in surface soil on a per unit area basis, using the hydrologic equation: Inflow – Outflow = Change in Storage. The inflow is precipitation less overland runoff, the outflows are actual evapotranspiration (AET), deep-drainage percolation, and water stored as soil moisture. The wet season is that portion of the year where precipitation exceeds potential evapotranspiration (PET), while in the dry season, PET exceeds precipitation. The specific calculations in the monthly water balance are summarized in the following nine steps:

- Adjusted Average Temperature – The temperature obtained from the local weather station represents the average monthly temperature at the station location. Using adiabatic lapse rates, this temperature is adjusted for any elevation difference that may exist between the source area site and the local weather station.

- Potential Evapotranspiration (PET) – MEPAS estimates PET based on average air temperature, minimum relative humidity, ratio of actual to maximum possible sunshine

hours, and average wind speed. Because the soil moisture storage calculations are based on PET rate, the computation of PET rate has a significant influence on the amount of water that percolates through source area soils.

- Adjusted Precipitation – Monthly precipitation is obtained from the local weather station. Precipitation occurring in months with an adjusted temperature below freezing is assumed to be in the form of snowfall, and it is also assumed that the snow is stored on the ground during the months when the adjusted average monthly temperature is below freezing. During the spring melt, a portion of the snowmelt is combined with the precipitation and this adjusted precipitation is used to calculate percolation. Required parameters include average temperature, average wind speed, site elevation, mean sky cover (i.e., degree of cloudiness), and monthly precipitation as rainfall.

- Overland Runoff – The Soil Conservation Service (SCS) curve number technique forms the basis of estimating the net monthly overland runoff.

- Maximum and Potential Percolation – Maximum percolation represents the difference between adjusted precipitation and monthly overland runoff. Potential percolation represents the difference between the maximum percolation and the PET. For months with an adjusted temperature below freezing, both the maximum and potential percolation are zero.

- Accumulated Potential Water Loss – This step represents the potential soil moisture water loss during a year. It is computed using the potential percolation and the soil moisture retention tables from Thornthwaite and Mather (1957).

- Soil Moisture Storage – This step computes the moisture contained in the surface soil at the end of each month. In dry months (i.e., months where PET is greater than adjusted precipitation), soil moisture storage is computed using the accumulated potential water loss and the soil moisture retention tables provided by Thornthwaite and Mather (1957). In wet months (i.e., months where adjusted precipitation is greater than PET), the soil moisture storage is computed using the potential percolation and the previous month's soil moisture.

- Actual Evapotranspiration (AET) – Actual evapotranspiration equals PET, if the maximum percolation (i.e., adjusted precipitation less overland runoff) is greater than or equal to PET. If maximum percolation is less than PET, then there is not enough new moisture to entirely satisfy PET. Thus, AET will equal the sum of maximum percolation and the amount by which soil moisture storage is reduced (i.e., maximum percolation minus the change in soil moisture storage between the current and previous months).

- Deep-Drainage Percolation – The leachate generated from a soil column is zero if the adjusted temperature is below zero. If the temperature is above zero, the leachate generated equals the maximum percolation minus AET and change in soil moisture storage.

The leachate generated in any month is the amount of maximum percolation in excess of AET and soil moisture recharge. The model then calculates an annual infiltration rate (i.e., darcy flux density) by summing the monthly values of leaching. Total annual infiltration through the C-64A source area is obtained by multiplying the annual infiltration rate by the areal dimensions of the source area. The penetrator munitions source area at C-64A was assumed to have dimensions of 500 feet (152.4 m) by 500 feet (152.4 m), encompassing an area of 250,000 square feet (23,226 square meters) as specified by the AFRL/MN (memo from Tom Brantley to GCX, Inc.).

5.2 Transport Pathway Analysis

Analysis of potential transport pathways by which metals released from munitions fragments could migrate away from the Test Area C-64A over time indicates three principle pathways of concern as depicted in Figure 5.2. Metals could be suspended and transported in air due to wind; they could infiltrate down through the vadose zone and be transported via groundwater beneath the site; and they could be discharged with groundwater and transported into local surface-water streams such as Ramer Creek. Overland transport is not considered a potentially significant transport pathway due to the highly permeable soils at the test site which results in rapid infiltration of precipitation (see Section 2.3-Soils). Significant overland runoff is rarely observed
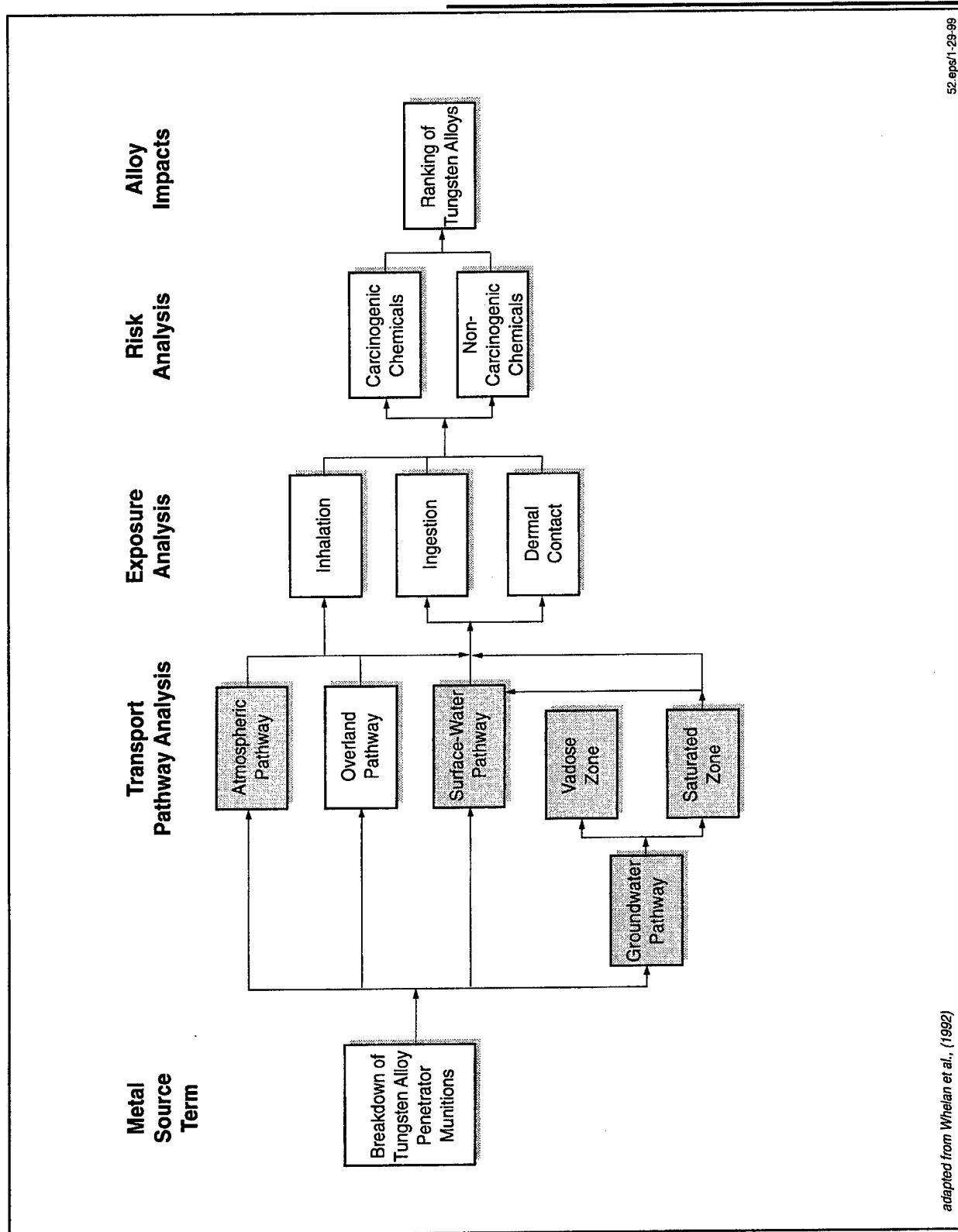
Figure 5.2. Transport pathways modeled using MEPAS.

at the test site. Becker (1994) observed that it generally takes successive days of precipitation to generate runoff.

Transport modeling was performed to estimate the rate of transport of metals and provide estimates of metal exposure concentrations in various environmental media at points remote from Test Area C-64A over time. Transport models contained in MEPAS were used to model transport of metals released from munitions fragments along air, groundwater, and surface water pathways. Although MEPAS contains an overland transport component, overland transport was not modeled as indicated above.

Transport models were used to estimate maximum metal concentrations and changes in metal concentrations over time at select locations down gradient from Test Area C-64A. Metal concentrations resulting from the transport of metals along the air pathway under current conditions were evaluated at radial distances of 100, 200, 500, and 1000 meters from the center of the source area based on predictions of the air transport model. Concentrations of metals transported along the groundwater pathway were evaluated based on predictions of the groundwater transport model at a hypothetical future well (local well) located approximately 550 feet down gradient of the center of the source area. The groundwater model was used to estimate maximum metal concentrations and changes in metal concentrations over time at this location. The local well was assumed to be located along the centerline of the groundwater flowpath being simulated, and metal concentrations predicted by the groundwater model were evaluated at the water table. Metals migrating in groundwater past the local well were simulated until they were discharged into Ramer Creek. Groundwater and metals discharging to Ramer Creek were assumed to do so at right angles to the direction of streamflow. Metal concentration resulting from the transport of metals along the surface water pathway were evaluated at a point approximately 1.0 foot (0.3 m) downstream from where groundwater discharged into Ramer Creek.

The following subsections describe the models in MEPAS used to model metal transport, document the various assumptions and transport parameters used to construct the models, and

present transport model results for each metal/penetrator alloy combination. Source terms used in the transport models were calculated as discussed in Section 5.1.

5.2.1 Air Pathway Model

5.2.1.1 Model Description

The fate of metals released to the atmosphere as a result of penetrator munitions testing depends on a number of complex processes. These include release mechanisms and characteristics, dilution and transport, chemical reactions, washout by cloud droplets and precipitation, and deposition onto the underlying surface cover. The atmospheric pathway model in MEPAS was used to compute metal air concentrations needed for evaluating inhalation exposure to individuals living within 80 km of the site under current conditions. Inhalation exposure to individuals living at Test Area C-64A under hypothetical future conditions are calculated separately.

The atmospheric pathway has several components including estimation of source area soil suspension/emission rates, atmospheric transport and dispersion calculations, and wet and dry deposition. The relationship of these atmospheric components in the MEPAS model is shown in Figure 5.3. Source area soil suspension/emission rates were derived in Section 5.1. This section focuses on the atmospheric transport and dispersion model used to compute downwind air concentrations under current conditions. As the plume travels away from a site, airborne metal concentrations are reduced both by dispersion and wet and dry deposition processes. Input data requirements include site-specific climatologic information, such as wind speed and direction, atmospheric stability, precipitation, and site and metal characteristics for computing emission rates. Output from the model consists of average air and surface metal concentrations by 16 directions and 10 distances (to 80.0 km). The following sections present an abbreviated description of the air transport model in MEPAS. For further information concerning the model, consult Droppo and Buck (1996).

adapted from Droppo and Buck (1996)

53.eps/1-29-99
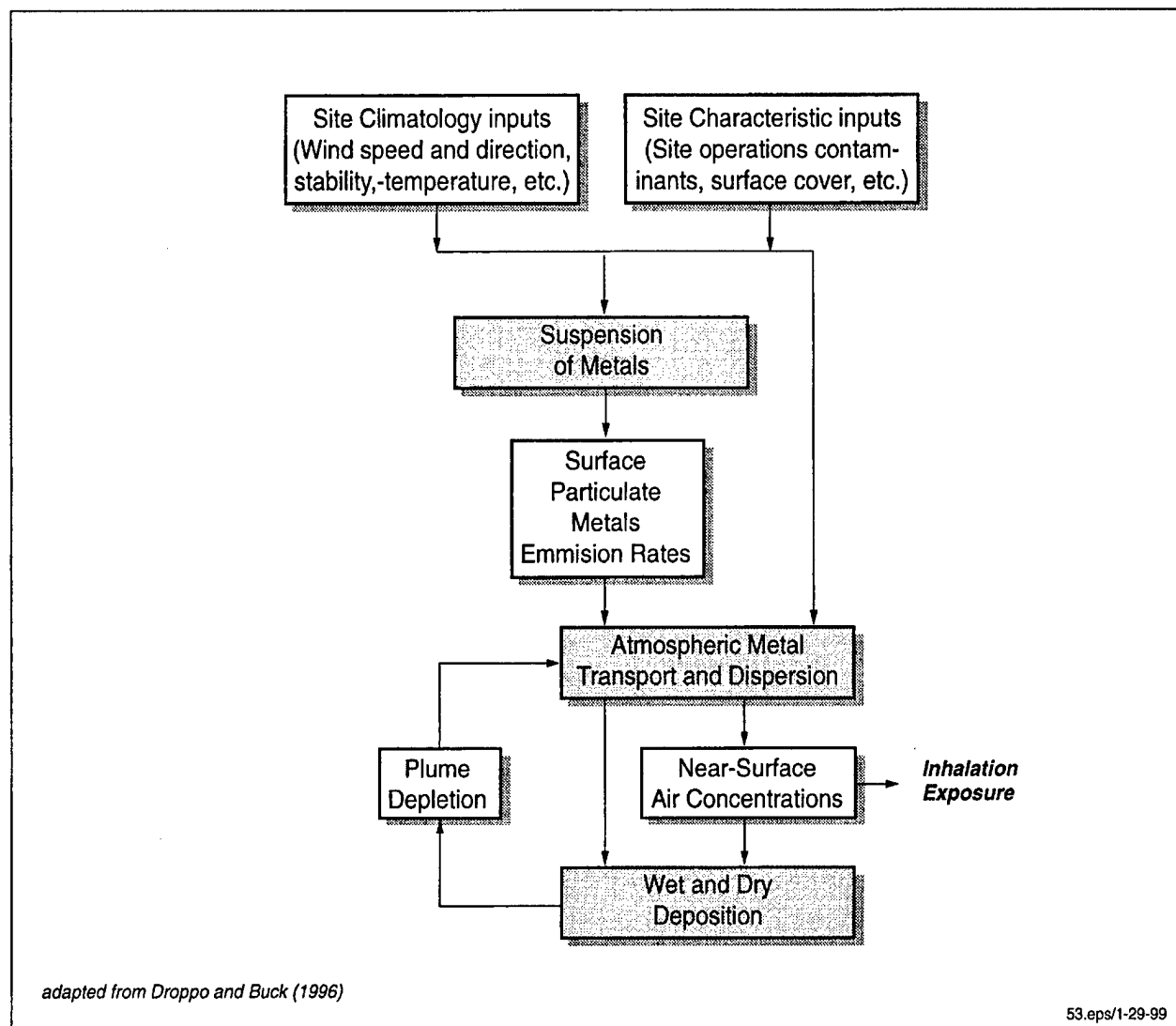
Figure 5.3. Atmospheric pathway model methodology.

Atmospheric Transport Dispersion and Deposition

Transport and dispersion of metals emitted from the source area are computed in terms of a sector-averaged Gaussian dispersion model. This provides sector average metal concentrations, $C(x, z)$, for a downwind distance x and a height z in a plume from a continuous source release as:

$$C(x,z) = \sum_{i=j}^{n} \sum_{j=1}^{m} \sum_{k=1}^{p} [f_{ij} \, Q_K \, R_{,}(x) \, (\frac{1}{2\pi})^{1/2} * \frac{1}{u_i \sigma_{z_j} \, 2\pi \, x/n} \, F(z,h,\sigma_{z_j})] \qquad (5.10)$$

where   i   =   wind speed class

         n   =   total number of wind speed classes (dimensionless)

         j   =   stability category (dimensionless)

         m   =   total number of stability classes (dimensionless)

         k   =   metal-bearing particle size class

         p   =   total number of metals (dimensionless)

         f_{ij} =   climatological fractional frequency of occurrence of the wind speed and stability class conditions within the specified direction (dimensionless)

         Q_k =   emission rate of metal-bearing particle size class (g/s)

         $R_k(x)$ =   deposition and/or decay plume source depletion fraction, which varies as a function of the position of the plume for each size class (dimensionless)

         u_i =   wind speed central value for the i wind speed class interval (m/s)

         σ_{zj} =   standard deviation of concentration in vertical dimension for stability class (m)

         $2\pi x/n$ =   sector width (dimensionless)

$F(z, h, \sigma_{zj})$ = functional relationship for the vertical variation of the plume concentrations (dimensionless) where h is the plume height (m).

Deposition is computed as the sum of outputs from empirical wet and dry deposition algorithms (see Droppo and Buck, 1996). The indexed variables are defined in terms of central values for each atmospheric frequency class (i.e., a set of wind speed, wind direction, and stability conditions). The removal of the metal from the atmospheric plume, by various depletion process, is computed according to:

$$R(x) = r \, c \, d \, w \qquad\qquad (5.11)$$

where fractional losses are defined as

r = radioactive decay term (dimensionless)

c = chemical decay term (dimensionless)

d = dry deposition term (dimensionless)

w = wet-deposition term (dimensionless).

For metals derived from penetrator alloy munitions, r and c are not relevant and are set to 1.0 in the model.

The central wind speed, u_i, in a wind-speed category is not necessarily applicable to the movement of an atmospheric plume in a region of interest. The wind speed needs to be adjusted for differences in height and local surface roughness. Local surface roughness is characterized by a surface roughness length. Table 5.3 shows examples of the magnitude of this parameter for various surface covers. The surface roughness lengths in the region surrounding the release are used to account directly for local influences in both dispersion and dry-deposition computations.

The atmospheric component of MEPAS computes an equivalent central wind speed at plume height for each wind speed category. For neutral atmospheric conditions, the following expression is used to calculate the wind variation with height:

$$\overline{u} = \frac{u_*}{0.4} \ln \left(\frac{z}{z_0} \right) \tag{5.12}$$

Table 5.3. Typical surface roughness lengths.

Surfaces	Roughness Length (cm)
Snow, sea, desert	0.005 – 0.03
Lawn	0.1
Grass (5 cm)	1 - 2
Grass (tall)	4 - 9
Mature root crops	14
Low forest	50
High forest	100
Urban area	>100

Adapted from Droppos and Buck (1996)

For unstable atmospheric conditions, the following expressions is used to calculate the wind variation with height:

$$\overline{u} = \frac{u_*}{0.4} \left(\ln \left(\frac{z}{z_0} \right) - 2\ln \left[\frac{1}{2} \left(1 + \frac{1}{\phi} \right) \right] - \ln \left[\frac{1}{2} \left(1 + \frac{1}{x}{\phi_m} \right) \right] \right) \tag{5.13}$$

$$+ 2 \tan \left(\frac{1}{\phi_m} \right) - \frac{\pi}{2} \Bigg)$$

where $\bar{u}$ = average wind speed (m/s)

u_* = friction velocity (m/s)

z = height over land/water surface (m)

z_0 = roughness length of surface (m)

ϕ_m = wind-gradient parameter (dimensionless).

MEPAS uses a literature-derived central value of 0.458 to approximate the sum of the last three terms in equation 5.13.

For stable conditions, the following expression is used to calculate the wind variation with height:

$$\bar{u} = \frac{u_*}{0.4} \left[\ln\left(\frac{z}{z_0}\right) + 5\frac{z}{L} \right] \tag{5.14}$$

where L is the Monin-Obukhov length (m), a scaling length of atmospheric turbulence. To use Equations 5.12 and 5.13 for determining the wind variation with height, the roughness length, friction velocity, and Monin-Obukhov length must be known or calculated.

Empirical relationships are used in the MEPAS atmospheric model to estimate the friction velocity (u_*) over water surfaces. These friction velocity relationships were taken from drag coefficient relationships by substituting for friction velocity using $C_D = u_*^2/u_s$:

$$u_* = 0.0346\ u_x \qquad\qquad \text{for } 4 \le u_x < 11 \text{ m/s}$$

$$\tag{5.15}$$

$$u_* = 0.0316\ u_x\,(0.49\ +\ 0.065\ u_x)^{1/2} \qquad \text{for } 11 < u_x \le 25 \text{ m/s}$$

where u_x = wind speed at the 10-m height.

The roughness length is an input parameter for overland surfaces. For overwater surfaces MEPAS calculates roughness length (z_o) according to:

$$z_o = \frac{m\, u_*^2}{g} \qquad (5.16)$$

where g = acceleration of gravity (m/s^2)

m = coefficient (= 0.0144).

The Monin-Obukhov length is a function of atmospheric stability.

Using the approach of computing appropriate wind speeds for the underlying surface allows the wind speeds to vary as a function of distance downwind of the release. The plume speed is computed at a height of the approximate vertical center of mass of the plume at each downwind distance. This speed is used to compute a travel time for each computation interval. The total travel time divided by the distance traveled defines an average plume speed for use in Equation 5.10.

Total Deposition

Deposition of metals from the atmosphere to surfaces can occur as the result of both wet- or dry-removal processes. Wet removal is caused by the scavenging and deposition of metal-bearing particles by precipitation or cloud droplets. Dry deposition is the direct deposition of the airborne metal-bearing particle onto a surface by processes such as impaction, sorption, and gravitational settling. The total deposition at a specified location is computed as the sum of the wet- and dry-deposition fluxes to the surface:

$$T(x,z) = \sum_{i=j}^{n} \sum_{j=1}^{m} \sum_{k=1}^{p} \left[f_{ij} \, D_{ijk} \, (x,z) + g' \, W_{ijk} \, (x,z) \right] \qquad (5.17)$$

where $T(x,z)$ = total surface concentration (g/m^2)

$D_{ijk}(x,z)$ = dry-deposition flux (g/m^2)

$W_{ijk}(x,z)$ = wet-deposition flux (g/m^2) for wind speed (i), stability class (j), and metal (k)

g = climatologic fractional frequency of occurrence of the indexed precipitation conditions within the specific direction (dimensionless).

Deposition contributes to depletion from the plume. The formulation of the dry and wet deposition models are discussed further in Droppo and Buck (1996).

Dispersion Coefficients

The MEPAS atmospheric pathway model uses six classes of atmospheric stability to characterize dispersion rates. The atmospheric stability classes are designated by the letters A to F and are commonly referred to as the Pasquill Stability Categories. The classes A, B, and C stand for very unstable, unstable, and slightly unstable conditions, respectively; D stands for a neutral condition; and E and F stand for stable and very stable conditions, respectively. Dispersion varies from being fastest for very unstable conditions to being slowest for very stable conditions.

The Pasquill dispersion curves used in the atmospheric pathway model are computed as a function of elapsed plume travel time. The conversion from the distance dependence to the time dependence is based on equivalent wind speeds. The Pasquill curves are applied as a function of time for the conditions for which the curves were originally developed. Equations 5.12 through 5.14 are used to compute wind speeds. The plume travel time is computed as the sum of travel

times over various surfaces, thus allowing for local wind shear effects in the dispersion computation.

In terms of the computed dilution rate in the air, the influence of roughness on dispersion rates and wind speed tend to cancel each other. As a result of surface-induced mechanical mixing, the local surface roughness influences local dispersion rates and the wind speed profile. At a given distance from the source, a site with a smoother surface will have smaller dispersion rates and larger near-surface wind speeds than a site with a rougher surface. The equation for computing sector-average air concentrations (Equation 5.10) contains the product of the vertical dispersion rate and the wind speed. All other factors being equal, these two local surface influences almost exactly cancel each other. The result is that the computed dilution at a potential receptor location does not vary with the surface roughness.

Eventhough the dilution does not vary with surface roughness, the computed metal concentrations and deposition rates will vary with surface roughness. The roughness-induced changes in dispersion rate and wind speed, directly change the estimated deposition rates. Deposition rates indirectly change computed air concentrations through the plume depletion rate.

Calm and Missing Wind Conditions

In the characterization of frequency of winds in each of the six atmospheric stability classes, often some fraction of the reported cases are for calm or zero wind speed conditions. Since the atmospheric pathway model requires a non-zero wind speed, calm conditions are modeled with a wind speed of 0.5 m/s. This procedure is appropriate because calm conditions are more correctly defined as conditions when the winds are less than the starting speed of the anemometer—the atmosphere is very seldom really calm with no air movements.

The occurrences of calm conditions in each stability class are distributed in a special wind speed class. The relative frequencies of occurrence of winds in the lowest wind speed class are used to distribute calms as a function of direction. If the lowest wind speed class has no entries, then the calms are distributed equally over the 16 direction sectors.

The input table of dispersion conditions is normalized to represent all conditions. That is, missing conditions are distributed according to the input frequencies of occurrence.

Deposition Classes

A mass budget approach is used to compute the deposition of net Gaussian plume source depletion fractions as a function of distance from the release. The implementation of removal rates is accomplished in MEPAS using six deposition classes which represent the constituent properties shown in Table 5.4. The air concentration and deposition patterns are computed for each of these classes based on a unit emission rate. Depending on the properties of a constituent, each constituent is assigned to a deposition class. Then the air concentration and deposition patterns for each constituent are computed using the appropriate normalized concentration patterns and the constituent emission rate.

Class 1 is most appropriate for area releases of suspended soil materials, as in the current study, while Class 2 is most appropriate for point releases. If the material is released in a gaseous form, then the constituent database contains the most appropriate value from Classes 3, 4, 5, and 6.

Table 5.4. Definition of deposition classes.

Deposition Class	Class of Constituent
1	particles with average radius = 7.5 μ
2	particles with average radius = 0.3 μ
3	gas with moderate surface resistance (s/cm)
4	nondepositing gas
5	gas emission that deposits as a Class 3 particle
6	gas with fast deposition rate (zero surface resistance)

Airborne Metal Concentration

Airborne metal concentrations resulting from the suspension of a specific metal-bearing surface particles, θ, are computed based on airborne soil particle concentrations provided by the atmospheric pathway model using the following equation:

$$C_\theta = \alpha \, C_s \tag{5.18}$$

where C_θ = airborne metal concentration (g/m^3)

C_s = airborne soil concentration (g/m^3)

α = mass fraction of metal in the suspended surface soil (g/g).

Future Airborne Metal Concentrations at Test Area C-64A

The soil particulate source term emission rate estimated by MEPAS as described in Section 5.1 and input to the atmospheric transport pathway model is determined based on current conditions at the site. If the site is developed in the future for agricultural, residential, or commercial use, the physical characteristics of the test site and surrounding areas may change. In the event of such changes, the emission rate for source area soils may also change. Because the extent and type of future changes at the site are unknown, a conservative approach was taken to estimate future air metal concentrations at the site. Metal concentrations in soil particulate matter in air near the test area under these future conditions were estimated using a simple mass loading approach from MEPAS (Strenge and Chamberlain, 1995). The following equation was used:

$$C_a = 10^3 \, C_s \, ML \tag{5.19}$$

where C_a = average concentration of metals in air $(mg\text{-}C/m^3\text{-}air)$

C_s = average concentration of metals in source area soils (mg-C/g-soil)

ML = mass loading factor for airborne particulate matter $(kg\text{-}soil/m^3\text{-}air)$

10^3 = conversion factor (g/kg).

Source area soil metal concentrations under future conditions provided in Table 5.1 were input in the above equation, along with an airborne soil mass loading factor (ML) of 1E-07 kg/m^3 soil in air obtained from MEPAS (Strenge and Chamberlain, 1995).

5.2.1.2   Model Climatic Parameters

Table 5.5 presents climatological data used as input to the air transport model. These data were derived from climatic data collected at Eglin Air Force Base main weather station. Wind joint frequency data consisting of the relative frequency of occurrence of wind speed and direction for six wind speed categories, sixteen wind directions, and six atmospheric stability categories (Pasquill stability classes) were input to the model along with frequency of calm conditions. Wind joint frequency data can be found in Appendix E.

Table 5.5. Air transport model parameters.

Input Parameters		
Current Conditions	Morning Mixing Height	700 m
	Afternoon Mixing Height	1200 m
	Number Precipitation Days	57 /yr
	Num of Thundst	71 /yr
	Total Annual Precipitation	61 inches/yr
	Wind Sensor Height	4.6 m
	Roughness Length	5 cm
	Mean Wind Speed	4 m/s
	Fastest Wind Speed	67 m/s
	Percent Sand in Soil	92 %
	Precipitation-Evaporation Index	110
	Roughness Length	1.5 cm
	Vegetation Cover	0.5
	Disturbances/month	0
	Fraction of Soil Crusted	0
Future Conditions	Soil Mass Loading Factor	$1E - 0.7\, \dfrac{\text{kg-soil}}{\text{m}^3\text{-air}}$

5.2.1.3 Air Transport Pathway Model Results

The air transport model in MEPAS was used to predict both soil particulate and source area metal emissions from Test Area C-64A source area soils. Results of the air dispersion component of the model, when combined with metal specific source area emission rates, predict concentrations of metals in air for sixteen directions and several radial distances from the source area. The model predicts both acute short-term one-hour average air concentrations and chronic long-term seventy year average air concentrations. Table 5.6 presents initial source area soil concentrations and air transport model results for tungsten, tantalum, nickel, copper, iron, cobalt, and manganese. Because model predicted metal air concentrations were quite low using current site conditions, only results predicted for 100 m radial distance from the source area are presented. Complete air model results can be found in Appendix E.

Air transport model results indicated a soil particulate emission rate of 6.9E-06 g soil/sec (0.6 g soil/day) from Test Area C-64A soils for soil particles with a radius of 7.5 μm. Metal specific source area emission rates ranged from 3.7E-05 mg/sec for tungsten and tantalum, to 6.1E-07 mg/sec for cobalt and manganese.

Maximum acute metal air concentrations given current site conditions occurred 100 m northwest of the source area and the ranged from 8.0E-07 mg/m^3 for tungsten and tantalum, to 1.3E-08 mg/ m^3 for cobalt and manganese. Ninety-five percent of the time, acute contaminant air concentrations 100 m from the source area ranged between 1.7E-08 mg/ m^3 for tungsten and tantalum, and 2.7E-10 mg/m^3 for cobalt and manganese.

Maximum long-term chronic metal air concentrations occurred 100 m south of the source area and range from 1.0E-08 mg/ m^3 for tungsten and tantalum, to 1.7E-10 mg/ m^3 for cobalt and manganese. Long-term chronic metal air concentrations at 100 m averaged over all directions range between 3.5E-09 mg/ m^3 for tungsten and tantalum, to 5.7E-11 mg/ m^3 for cobalt and manganese.

Table 5.6. Air pathway model results.

Metal	Source Area Soil Concentration (mg-C/kg- soil)	Source Area Soil Particulate Emission Rate (g Soil/sec)	Source Area Soil Metal Emission Rate (mg C/sec)	Air Concentration at 100 m (mg-C/m³-Air) Under Current Conditions*				Air Concentration (mg-c/m3-air) Under Future Conditions
				Acute Short-Term (1 hr) Average Concentration		Chronic Long Term (70 yr) Average Concentration		
				Maximum (NW Sector)	95ᵗʰ Percentile	Maximum (S Sector)	Mean (16 Sectors)	
Tungsten/Tantalum	5.5	6.9E-06	3.7E-05	8.0E-07	1.7E-08	1.0E-08	3.5E-09	5.5E-04
Nickel	0.36	6.9E-06	2.4E-06	5.2E-08	1.1E-09	6.7E-10	2.3E-10	3.6E-05
Copper/Iron	0.25	6.9E-06	1.7E-06	3.6E-08	7.6E-10	4.6E-10	1.6E-10	2.5E-08
Cobalt/Manganese	0.09	6.9E-06	6.1E-07	1.3E-08	2.7E-10	1.7E-10	5.7E-11	9.0E-09

* Concentration at ground level 100m from center of source area.

Air metal concentrations near the test site under future conditions, which were estimated as discussed in Section 5.2.1.1, are also presented in Table 5.6. Air metal concentrations under future conditions ranged from 5.5E-04 mg/m^3 for tungsten and tantalum, to 9.0E-08 mg/m^3 for cobalt and manganese. These air metal concentrations ranged from one to five orders of magnitude above maximum acute short-term average air concentrations predicted by MEPAS using the air transport pathway model with current site conditions. The reason for the differences in the predicted air concentrations are the different conceptual models used in the calculations. In any case, even the higher concentrations do not result in significant risk as discussed further below.

Table 5.7 contains Time Weighted Average (TWA) and ambient air 24-hour exposure limit for soluble cobalt, copper, manganese, nickel, tantalum, and tungsten in air that were presented in Section 4.0. Comparison of these exposure concentrations with results from the air transport pathway model indicates that both maximum acute and long-term chronic air concentrations predicted by the air transport model are far below recommended maximum exposure levels for soluble cobalt, nickel, and tungsten in air. The non-volatile behavior of metals derived from the leaching/breakdown of penetrator munition alloys, as well as the presence of ground cover, and minimal disturbance on the site, are the principle cause of low metal concentrations from airborne dust derived from source area soils. Even under future conditions in which site specific characteristics such as ground cover and disturbance may be altered, air concentrations are still far below recommended maximum exposure levels for soluble cobalt, nickel, and tungsten in air.

Table 5.7. Maximum exposure levels for soluble contaminants in air.

Metal	TWA (mg/m3-air)	AAEL* (mg/m3-air)
Cobalt	0.05	0.00012
Nickel	0.1	0.00012
Tungsten	1.0	0.012
Copper	1.0	0.0024
Manganese	0.2	0.012
Tantalum	5.0	0.012

* Ambient Air 24-hour Limit (Sittig, 1994).

5.2.2 Groundwater Pathway Model

5.2.2.1 Model Description

The groundwater transport pathway model in MEPAS models metal transport from the source area through the groundwater environment both partially saturated (i.e., vadose) and saturated zones. This provides estimates of groundwater metal fluxes at various transport medium interfaces (e.g., water table or aquifer/river interface) and metal concentrations at receptor locations such as withdrawal wells. A schematic diagram illustrating the groundwater transport pathway is presented in Figure 5.4. The following sections present an abbreviated description of the groundwater transport model in MEPAS. Additional information concerning the model, can be obtained in Whelan et al., (1996).

The groundwater pathway model in MEPAS accounts for the major mechanisms of constituent mobility (i.e., adsorption/desorption), persistence (i.e., degradation or decay), advection, and hydrodynamic dispersion. Mobility is described by an equilibrium sorption coefficient that assumes instantaneous adsorption/desporption between the soil matrix and the pore water. Persistence is described by a first-order degradation/decay coefficient. Advection is described by constant, unidirectional flow in the vertical direction in the partially saturated (vadose) zone and in the longitudinal direction in the saturated zone. Hydrodynamic dispersion is described in one dimension for the partially saturated zone and three dimensions for the saturated zone.

Other assumptions associated with the groundwater model in MEPAS include the following:

- The groundwater environment is initially free of contamination.

- All transport media properties are homogeneous and isotropic.

- Flow in both the partially saturated and saturated zones is uniform.
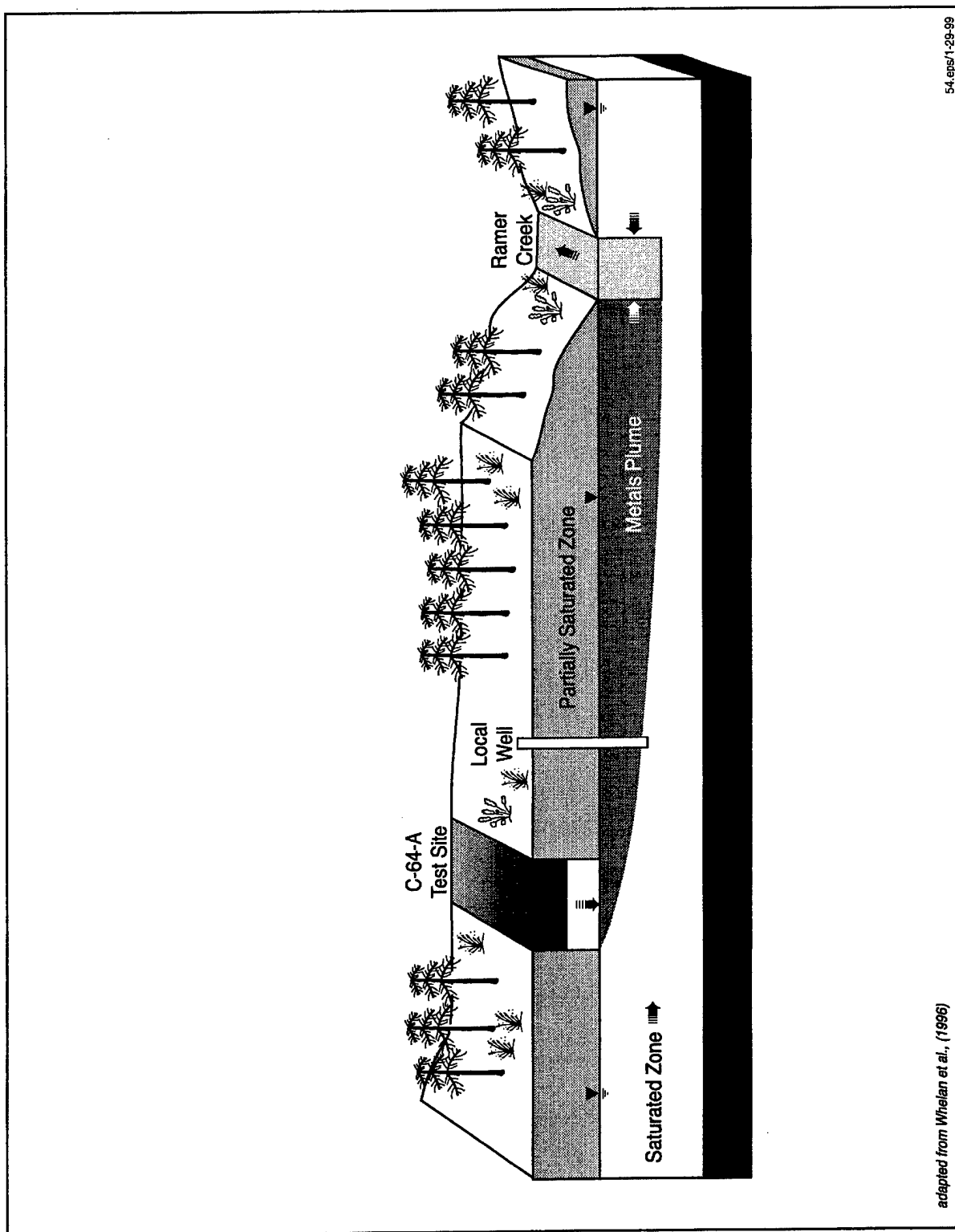
Figure 5.4. Schematic diagram illustrating the groundwater environment for the groundwater to a well and groundwater to a river transport scenarios.

- The saturated zone is of finite, constant thickness, and infinite lateral extent.

- The flow system is at steady state. Drawdown effects of withdrawal wells and other transient stresses on the aquifer are not considered by the semianalytical solutions. Flow velocities are provided by the user.

- Density differences between a metal-bearing plume and the natural groundwater are negligible.

In MEPAS, the following one-dimensional advective, three-dimensional dispersive equation for solute movement through a porous medium with a unidirectional, constant flow velocity and degradation/decay forms the basis of the groundwater transport model:

$$\frac{\partial C}{\partial t} = (\frac{u}{R_f})(\frac{\partial C}{\partial x}) = (\frac{D_x}{R_f})(\frac{\partial^2 C}{\partial x^2}) + (\frac{D_y}{R_f})(\frac{\partial^2 C}{\partial y^2}) + (\frac{D_z}{R_f})(\frac{\partial^2 C}{\partial z^2}) + \lambda c \qquad (5.20)$$

in which
$$R_f = 1 + \beta\, K_d\, /\, n_e \qquad \text{(saturated zone)} \qquad (5.21)$$

$$R_f = 1 + \beta\, K_d\, /\, \theta \qquad \text{(vadose zone)} \qquad (5.22)$$

$$\theta = n\, [K(\theta)\, /\, K_s]^b \qquad \text{(vadose zone)} \qquad (5.23)$$

where C = dissolved concentration (g/mL)

u = pore-water velocity (cm/s)

R_f = retardation factor (dimensionless)

D_x, D_y, D_z = dispersion coefficients in the x, y, and z directions, respectively (cm^2/s)

λ = degradation/decay rate (1/s)

β = bulk density (g/cm^3)

K_d = distribution coefficient (mL/g)

n_e, n = effective and total porosities, respectively (fraction)

θ $\quad=\quad$ moisture content (fraction)

$K(\theta)$ $\quad=\quad$ hydraulic conductivity (cm/s) at moisture content θ

K_s $\quad=\quad$ saturated hydraulic conductivity (cm/s)

b $\quad=\quad$ empirically based parameter that is a function of soil properties.

For vadose zone modeling, Equation 5.20 is reduced to one-dimensional (z-direction) solutions of the advective-dispersive equation. Saturated-zone modeling is based on two-dimensional (x and y directions), vertically averaged solutions to Equation 5.20. By solving Equation 5.20 with appropriate initial and boundary conditions, a set of semi-analytical expressions are obtained that characterize contaminant transport through the vadose and saturated zones. These functions are based on Green's functions and are described further in Whelan et al. (1996).

Equation 5.20 is applied to the partially saturated zone by assuming that the total and effective porosities are equal to the soil moisture content. One-dimensional, unidirectional flow and dispersion are assumed only in the vertical (z) direction in the partially saturated zone. The coordinate system is rotated such that the x-axis corresponds to the z-direction with dispersion considered only in the flow direction (i.e., D_y and D_z equal zero). Under these assumptions, Equation 5.22 defines the retardation factor for the partially saturated zone.

The partially saturated soil beneath the waste site is assumed at a unit hydraulic gradient, and the moisture content is assumed to fluctuate between field capacity and saturation. If the rate of water infiltration from waste site (i.e. leach rate) is less than the maximum soil transmission rate (unit gradient * saturated hydraulic conductivity [K_s]), then K is equal to infiltration rate and soil moisture content is computed from Equation 5.23. Otherwise, the infiltration rate is equal to the maximum transmission rate. Metal fluxes are computed to indicate transfer of contaminants between successive media. Models assume a unidirectional flow field with flux calculations based on metals crossing a plane perpendicular to the axis of flow.

In the saturated zone, the vertically averaged depth is defined as the vertical distance over which the metal is considered fully mixed. MEPAS calculates the fully mixed region based on

hydrodynamic (e.g., dispersion coefficient) and geometric (e.g., aquifer depth) considerations using a Gaussian-distribution analysis. Groundwater-metal transport between vadose-zone layers or vadose and saturated zones is linked through metal-flux boundary conditions. The groundwater transport pathway model allows for degradation and decay at the source of metals, in the environment following release from the source, or both at the source and in the environment.

Mixing Length Equations

When a metal travels from a waste site to a receptor of concern (e.g., well or river), the metal is temporally and spatially redistributed – longitudinally, vertically, and laterally – by the transporting medium. At any given distance downgradient from a waste site releasing metals to an aquifer of constant thickness, metals near the water table can be considered to be fully mixed over some distance in both the lateral and vertical directions. As the metal moves downgradient from the point of release, the mixed region increases in vertical and lateral extent while the aquifer geometry becomes more of an influence on the spatial distribution of the metal, especially in the vertical direction. MEPAS calculates vertical mixing lengths in order to estimate metal concentrations in a well, and lateral mixing lengths when estimating metal concentrations in groundwater discharging to a surface water body such as a stream.

Vertical Mixing Length

Both vertical and lateral mixing lengths are estimated in MEPAS by employing the advective-dispersive equation and its associated Gaussian distribution solution. The one-dimensional, advective-dispersive equation in the vertical direction is written as

$$\frac{\partial C}{\partial t} = \frac{D_z}{R_f} \frac{\partial^2 C}{\partial z^2} \tag{5.24}$$

The unit area solution to Equation 2.24 in an aquifer of infinite vertical extent is described by

$$C = \frac{M}{\sigma_v (2\pi)^{1/2}} \exp\left(-\frac{z^2}{2\sigma_v^2}\right)$$ (5.25)

in which

$$\sigma_v = \left(2\frac{D_z}{R_f} t_t\right)^{1/2}$$ (5.26)

where M = metal mass per unit area (g/cm^2)

σ_v = standard deviation in the vertical direction (cm)

t_t = representative metal travel time (see Equation 5.29) (s).

MEPAS assumes that no metal diffusion occurs through the water table once the metal has entered the saturated aquifer. The vertical mixing depth for the fully mixed condition is assumed as the dispersive distance associated with one-half the standard deviation:

$$h_m = \frac{1}{2}\sigma_v = \left(\frac{D_2 t_t}{R_f 2}\right)$$ (5.27)

where h_m = vertical distance over which the metal is assumed to be uniformly distributed (equivalent to one-half the standard deviation) (cm).

Equation 5.27 is used to describe the vertical mixing length in the groundwater environment.

Lateral Mixing Length

The lateral distance over which the groundwater pathway intercepts and supplies metal-bearing water to the surface water pathway is estimated by computing the lateral mixing length at the point where groundwater discharges to surface water. This is then used as the line source

term for the surface-water pathway model computations. The lateral mixing length for a conservative substance identifies the extent over which metal-bearing water at the groundwater/surface-water interface is considered fully mixed in the lateral direction. The metal concentration is assumed to be uniformly distributed over this lateral region and is used in computing the boundary conditions for modeling the surface-water environment. MEPAS estimates the lateral mixing length according to Equations 5.24 through 5.26 substituting the y dimension for the z dimension.

The lateral mixing distance for the fully mixed condition, approximately adjusted for a source term of width b, is assumed equal to the dispersion distance associated with one standard deviation:

$$l_m = \sigma_t + b = (2 \frac{D_y}{R_f} t_t)^{1/2} + b \qquad (5.28)$$

where l_m = lateral distance over which the metal is assumed to be uniformly mixed (cm).

Travel Time and Time to Peak Equations

To define a vertical or lateral mixing length, MEPAS estimates the representative travel time (t_t) of a metal in a groundwater system by dividing the distance the metal travels by the flow velocity, adjusted for retardation:

$$t_t = \frac{x}{u^*} \qquad (5.29)$$

where t_t = representative metal travel time (s)

    x = longitudinal distance traveled (cm)

    u^* = u/R_f.

MEPAS estimates the time to the peak concentration by assuming a point source and its accompanying analytical Green's function solution in the direction of flow for an instantaneous release, and solving its derivative with respect to time when its equal to zero, as described in Whelan et. al., (1996).

A given modeling scenario can be considered near-field or far-field depending on several criteria. When a receptor well is located far from a source, the physical dimensions of the source have a negligible effect on receptor concentrations. Under these conditions, a scenario is said to be spatially far-field, and the equations for an area source-release reduce to those of a point source release. A scenario in which the physical dimensions of the source have a significant effect on receptor concentrations is a spatially near-field scenario.

A modeling scenario can also be considered temporally far-field. This occurs when the duration of release from the source is small relative to the time required for the metal to travel from the source to the receptor. In this case, numerically integrated solutions reduce to the analytical solutions for an instantaneous release. A scenario in which the duration of release has a noticeable effect on receptor concentrations is a temporally near-field scenario.

For each groundwater medium (i.e., partially saturated and saturated zones), the ratio of representative travel time to the duration of time over which a metal is released to that medium is used to determine if metal migration through the medium is temporally far-field:

$$T_{ratio(i)} = \frac{t_{t(i)}}{t_{r(i)}} \qquad (5.30)$$

where $T_{ratio(i)}$ = ratio of representative metal travel time to the duration of time over which metal is released to the i-th medium (dimensionless)

$t_{t(i)}$ = representative travel time for a metal in the i-th medium (s) (see Equation 2.59)

$t_{r(i)}$ = duration of time over which a metal is released to the i-th medium (s).

If $T_{ratio(i)}$ is greater than or equal to 30, metal migration through that medium is considered to be temporally far-field, and the analytical equations for an instantaneous release are used. Otherwise, numerical integration is performed.

In the groundwater pathway model, metal-bearing water from a site leaches from the source through the vadose zone to the water table. The metal-bearing leachate then mixes with the saturated zone water while migrating to the receptor. MEPAS assumes that the amount of water entering from the vadose zone at the receptor is relatively insignificant compared to the flux of metal-bearing water. This is true as long as the distance of the receptor from the waste site is sufficiently large. However, for receptor locations (i.e., wells) near the source, the volume of uncontaminated water percolating from the vadose zone may be significant relative to the flux of metal-bearing water. In these cases, MEPAS can over predict concentrations for receptors near the waste site. In an attempt to account for this flux of water from the partially saturated zone, MEPAS uses a near-field dilution ratio:

$$W_{ratio} = \frac{Q_{sz}}{Q_{sz} + Q_{psz}} \qquad (5.31)$$

where W_{ratio} = ratio of saturated zone water flux to total water flux at the receptor well (dimensionless)

Q_{sz} = saturated zone water flux (cm^3/s)

Q_{psz} = partially saturated zone water flux beneath the source (cm^3/s)

Concentrations at a receptor well are multiplied by W_{ratio} for releases from an area source to the partially saturated zone:

$$C_f = C \cdot W_{ratio} \qquad (5.32)$$

where C = computed concentration (g/mL)

C_f = final reported solute concentration (g/mL).

Under near-field conditions, $W_{ratio} < 1$, which accounts for metal-free water entering from the partially saturated zone. Under far-field conditions, the saturated zone water flux is much larger than the partially saturated zone water flux, and W_{ratio} approaches unity.

5.2.2.2   Model Flow and Transport Parameters

Metals released from munitions fragments deposited at the source area will be transported through the unsaturated and saturated zone with the flow of groundwater. Their movement is affected by hydrodynamic dispersion, and is slowed by sorption to the sediment matrix. The following describes site specific hydrogeologic and transport parameters used to construct the groundwater transport pathway models in MEPAS. These data were derived from information on the geology and hydrogeology of Test Area C-64A presented in Sections 2.3 and 2.4, and sorption experiments presented in Section 3.5. A detailed list of all inputs to the MEPAS code can be found in Appendix E.

Sediment Layer Parameters

Sediment parameters are those parameters which are specific to the sediment porous matrix through which groundwater migrates. Table 5.8 presents sediment porous matrix properties required as input to the groundwater transport pathway model in MEPAS. Based on results of field studies presented in Section 2.3 (soils and geology), which indicated that soils and sediments beneath the test area site derive from essentially the same unconsolidated sedimentary units, sediment particle size, total and effective porosity, field capacity, bulk density, and sediment hydraulic conductivity were specified identically for the soil, unsaturated, and saturated zone model layers.

Sediment particle size was specified as 93 percent sand, 4 percent silt, and 3 percent clay. Total porosity was set at 0.40, effective porosity at 0.25, field capacity at 0.10, bulk density at 1.60 g/cm^3, and hydraulic conductivity at 150 ft/fday based on literature values and site specific information. The highest estimated groundwater darcy velocity was specified at 0.45 feet/day. Organic matter content was set at 1.0 percent for soil, and 0.05 percent for unsaturated and

saturated zone sediments. Unsaturated zone thickness beneath the test area was estimated at approximately 80 feet based on the difference between ground surface elevation at the C-64A test area (210 feet) and groundwater table elevation measured beneath nearby Test Area C-64C (130 feet). The saturated zone thickness was estimated at 60 feet based on the difference between the estimated thickness of the Sand and Gravel aquifer beneath Test Area C-64A (150 ft) and the approximate thickness of the unsaturated zone (80 ft).

Table 5.8. Groundwater transport pathway sediment layer input parameters.

Sediment Layer Parameter	MEPAS Input Parameter
Total Porosity	0.40
Effective Porosity	0.25
Field Capacity	0.10
Bulk Density	1.60 g/cm^3
Hydraulic Conductivity	150 ft/day
Darcy Velocity	0.45 ft/day
Unsaturated Layer Thickness	80 feet
Saturated Layer Thickness	70 feet

Dispersivity

Dispersion refers to the spreading of the metal-bearing plume in groundwater caused by the fact that not all of the metals actually move at the same speed as the average linear velocity of groundwater. Deviations from the average linear groundwater velocity are caused by local sediment heterogeneities.

Quantification of dispersion is complicated by the scale effect, where the effective dispersivity increases as the plume moves downgradient. In the absence of site-specific data for the dispersivity at the site, equations presented in Buck et al., (1995), were used to approximate dispersivities based on the travel distance between the source area and the two downgradient receptors at the local well (550 ft) and Ramer Creek (1520 ft), as follows:

$$D_l = 0.1 \ (T_r) \qquad\qquad (5.33)$$

$$D_t = 0.33 \ (D_l) \qquad\qquad (5.34)$$

$$D_v = 0.0025 \ (D_l) \qquad\qquad (5.35)$$

where D_l = longitudinal dispersivity in feet.

D_t = transverse dispersivity in feet.

D_v = vertical dispersivity in feet.

T_r = metal travel distance in feet.

MEPAS then calculates the dispersion coefficient internally according to:

$$D_h = \alpha \, v \qquad\qquad (5.36)$$

where: α = dispersivity (ft)

v = average linear groundwater velocity (ft/day)

Table 5.9 presents travel distances and estimated dispersivities input to MEPAS as part of the groundwater pathway simuations.

Table 5.9. Groundwater transport model dispersivities.

Downgradient Receptor	Travel Distance (D_t) In feet	Longitudinal Dispersivity[1] (D_l) in feet	Transverse Dispersivity (D_t) in feet	Vertical Dispersivity (D_v) in feet
Water Table[1]	80	8	Not Modeled	Not Modeled
Local Well	550	55	18.2	0.14
Ramer Creek	1520	152	50.2	0.38

1) Water table receptor represents point where source area metals leave the unsaturated zone and enter the saturated zone. In this instance, the longitudinal dispersivity represents a vertical dispersivity since the principle axis of flow is downward.

Distribution and Retardation Coefficients

Adsorption of metals to the aquifer matrix retards their rates of migration. For a given mass of dissolved chemical, the fraction available for advective transport is influenced by the adsorptive properties of the soil matrix. Metals partition between the aqueous and sorbed phases, as defined by the distribution coefficient, K_d:

$$K_d = \frac{C_s}{C_{aq}} \qquad (5.37)$$

where: C_s = mass of metal on the solid phase per unit mass of solid phase

C_{aq} = concentration of metal in aqueous solution

Distribution coefficients used in the groundwater transport model were derived experimentally and varied with pH as discussed in Section 3.5. These were used along with bulk density and effective porosity to calculate retardation factors (R_f) for each metal species simulated. Retardation coefficients are used to define the migration of dissolved metals relative to advective transport in MEPAS, and are calculated according to Equations 5.21 and 5.22 presented previously. Table 5.10 presents distribution coefficients (K_d) input to MEPAS, and calculated retardation coefficients (R_f) for each metal simulated. Retardation coefficents were calculated internally by MEPAS. Note that Ta and W transport was not simulated because sorption coefficients for these metals were sufficiently large (Appendices B and C) to preclude significant migration.

Table 5.10. Groundwater transport adsorption parameters.

	pH	Distribution Coefficient K_d (mL/g)				Retardation Coefficient (R_f)			
Metal		Co	Cu	Ni	Mn	Co	Cu	Ni	Mn
Unsaturated Zone	5.5	10	200	20	10	105	2086	209	105
Saturated Zone	6.0	10	200	30	8	65	1281	193	52

NOTES: K_d from sorption experiments at indicated pH (Section 3.5).
Retardation coefficients calculated according to Equations 5.20 or 5.21 assuming
ρ_b = 1.60 g/cm^3 and n_e = 0.25, or moisture content θ.

Metal Degradation and Decay

Because metals are not subject to degradation by physical, chemical, or biological processes, MEPAS uses an extremely high degradation half-life (1E+20 days) which effectively eliminates degradation impacts in MEPAS transport simulations.

5.2.2.3   Groundwater Pathway Model Results

Groundwater transport model results for the unsaturated zone indicated an average steady state vertical infiltration rate of approximately 16 inches per year and a vertical pore water velocity of approximately 64 inches/year. The model calculated a moisture content under these conditions of 15.4 % which represents a saturation of approximately 38 percent relative to the total assumed porosity of 0.40. The vertical infiltration rate calculated by MEPAS is within the range of estimates reported for nearby watersheds. Data on groundwater recharge reported by Vecchioli et al., (1990) indicated infiltration rates ranging from 15 to 50 inches per year for Okaloosa County while precipitation in excess of potential evapotranspiration reported by Fernald et al., (1992) for northwest Florida indicate yearly infiltration ranges between 15 and 20 inches per year. A groundwater pore velocity of 1.8 ft/day was used by MEPAS for modeling the groundwater pathway and was calculated based on the darcy velocity of 0.45 ft/day and effective porosity of 0.25 initially input to the model.

The groundwater transport model was used to predict metal concentrations resulting from leaching/breakdown of penetrator munitions fragments in groundwater down gradient of Test Area C-64A. The groundwater model was used to estimate maximum metal concentrations and changes in metal concentrations over time in a hypothetical local well located approximately 550 feet down gradient of the center of the source area. Figures 5.5 to 5.9 present model predicted concentration versus time curves in the local well for each of the metals released by the three different penetrator alloys. Table 5.11 summarizes maximum peak concentrations and time to peak concentration for each of the metal/alloy combinations.
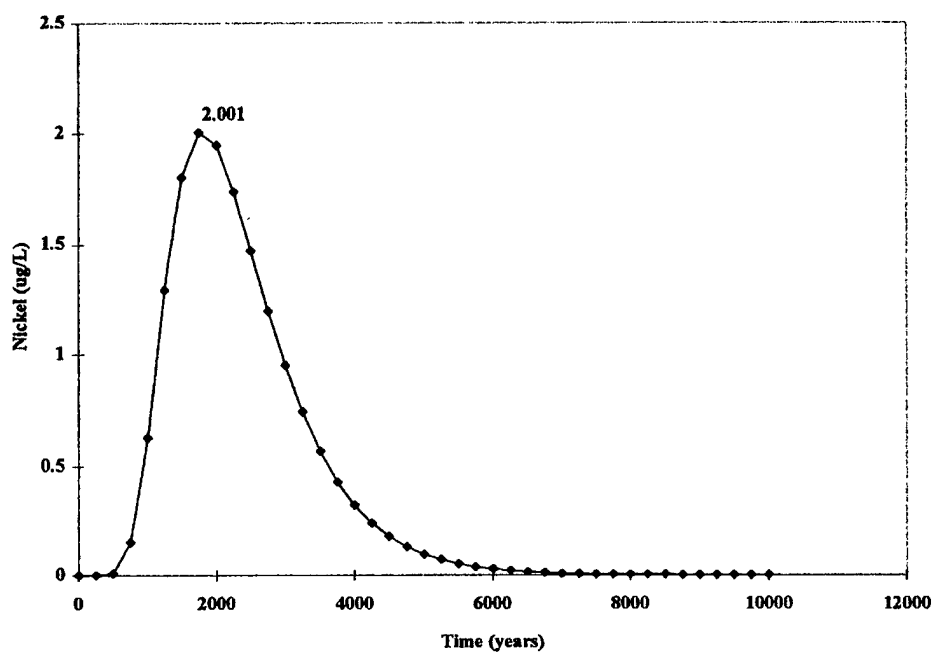
Figure 5.5. Alloy WL-1 Ni in local well.
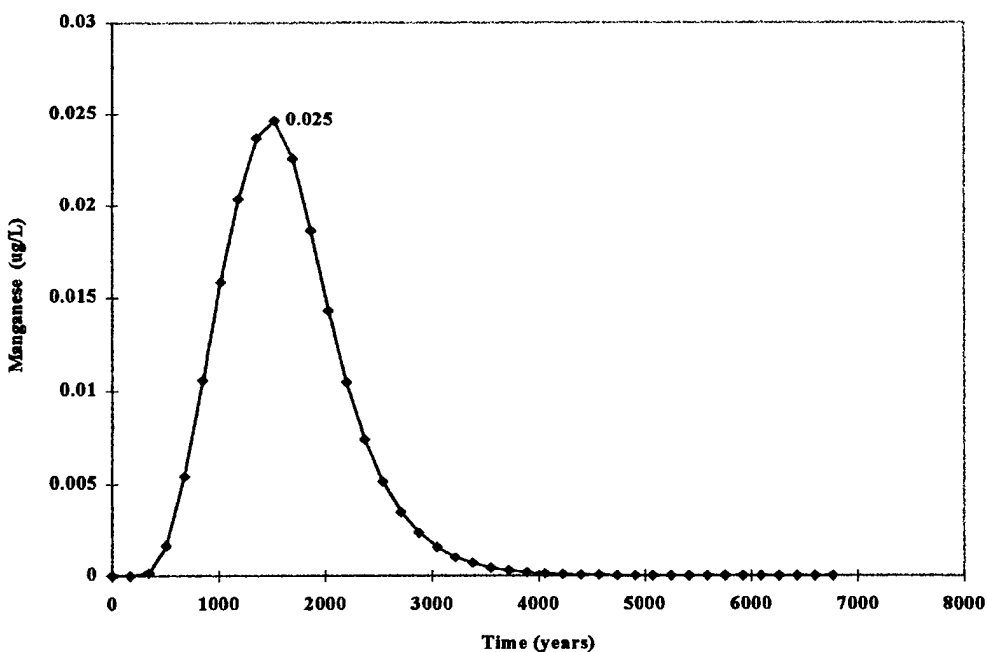
Figure 5.6. Alloy WL-1 Mn in local well.
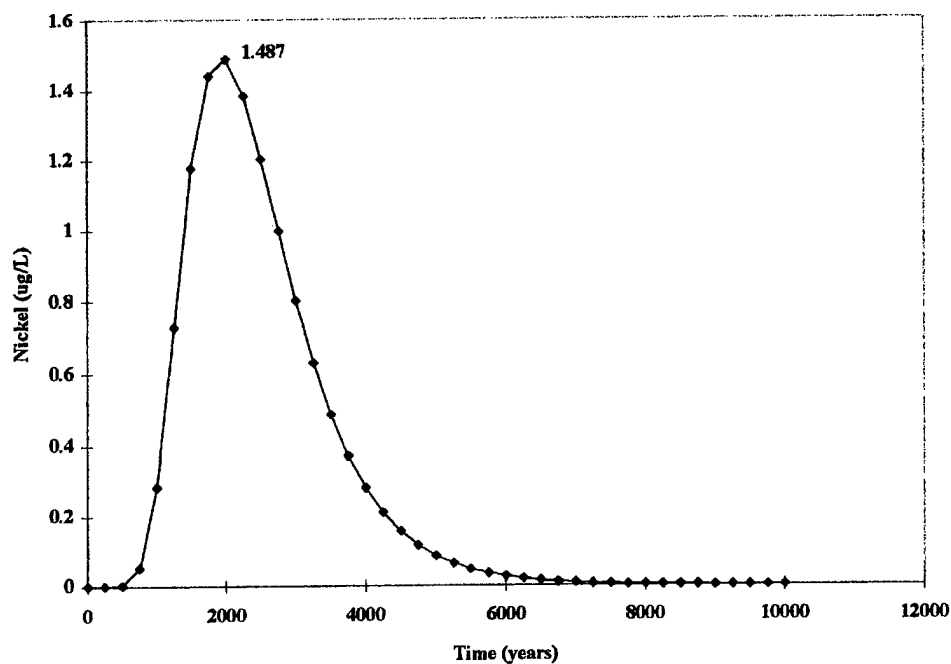
Figure 5.7. Alloy NS Ni in local well.
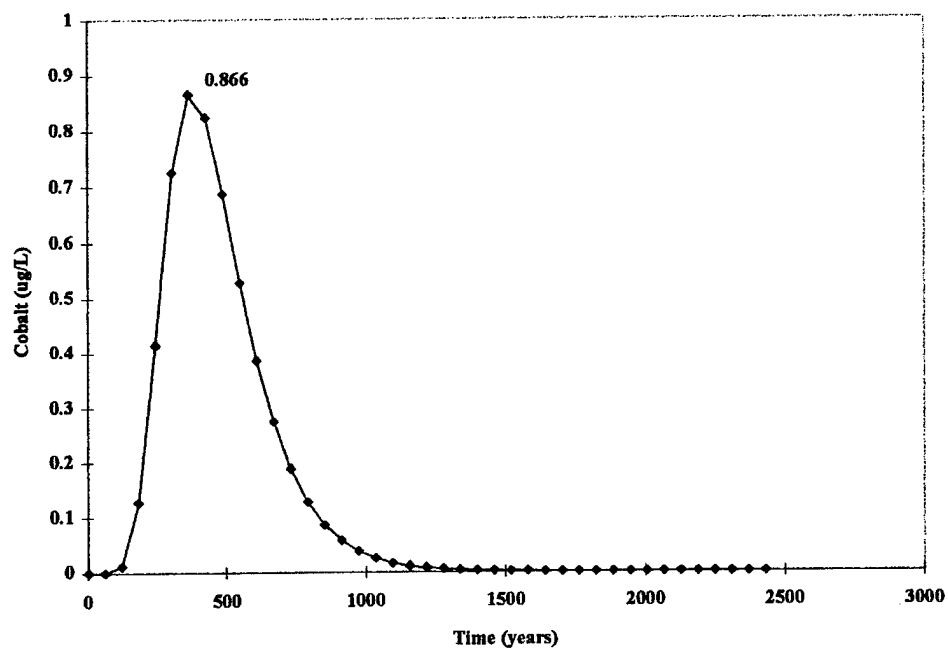
Figure 5.8. Alloy NS Co in local well.
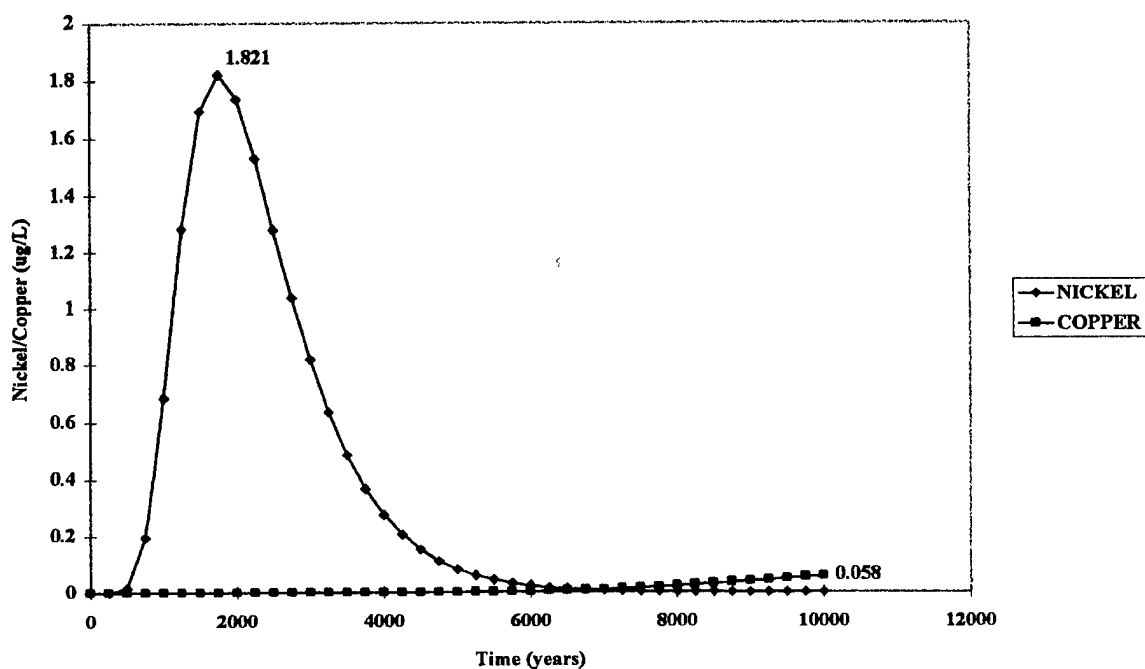
Figure 5.9. Alloy HD-17 Ni and Cu in local well.

Table 5.11. Groundwater pathway transport results for local well.

| Metal | Alloy WL1 | | Alloy NS | | Alloy HD-17 | | EPA[1] |
	Peak Concentration ug/L	Peak Time Years	Peak Concentration ug/L	Peak Time Years	Peak Concentration ug/L	Peak Time Years	Drinking Water MCL ug/L
Nickel	2.001	1750	1.487	2000	1.821	1750	100
Manganese	0.025	1519					
Cobalt			0.886	1014			
Copper					0.058	10001	

[1] Federal Register, July 25, 1990, pages 30370-30448.

Model results indicate metal concentrations in groundwater ranged between a low of 0.025 ug/L for manganese and a high of 2.0 ug/L for nickel. Nickel results are considerably lower than drinking water maximum concentrations established by EPA as indicated in Table 5.11. Model results indicate travel times to peak concentration generally well in excess of 1000

years. All other factors being equal, both peak concentrations and time to peak concentrations are controlled by the distribution/retardation coefficient. Retardation coefficients for groundwater conditions are quite high, indicating reduced potential for these metals to migrate in the groundwater environment.

5.2.3 Surface Water Pathway Model

5.2.3.1 Model Description

The surface-water pathway model in MEPAS was used to provide estimates of metal concentrations in Ramer Creek downstream from where metal-bearing groundwater would discharge into the creek. The migration and fate of metals along the surface water pathway are described by the steady-state, two-dimensional advective-dispersive equation for solute transport. The surface-water equation accounts for the major mechanisms of constituent persistence (i.e., degradation/decay), advection, and hydrodynamic dispersion. Persistence is described by a first-order degradation/decay coefficient. Advection is described by constant unidirectional flow in the longitudinal direction. Hydrodynamic dispersion is accounted for in the lateral direction. The processes associated with adsorption/desorption between the water column and suspended and bed sediments are not addressed. This represents a conservative assumption with regard to water column contaminant concentrations. The following sections present an abbreviated description of the surface water transport model in MEPAS. Additional information concerning the model is available in Whelan and McDonald (1996).

Assumptions associated with the surface water transport model in MEPAS include the following:

- Flow is steady and uniform in the longitudinal direction.

- The effects of metal adsorption to or desorption from sediment particles suspended in the water column or in the river bed are negligible; therefore, all metals travel at the same speed as the river flow.

- Metal releases to the riverine pathway are assumed to be long term relative to the travel time in the river. Therefore, a steady-state solution to the advective-dispersive equation is applicable for describing metal transport.

- The river geometry can be represented by a rectangular cross-section.

- A line source along the stream bank can be approximated as a point source located at the center of the line source; therefore, only the point source equation is used in MEPAS.

- Advection dominates dispersion in the longitudinal direction, and the metals plume is assumed to be fully mixed over the depth of the river; therefore, dispersion is only considered in the lateral direction.

- An appropriate lateral dispersion coefficient can be estimated based on the flow velocity and depth of the river.

- The single concentration value specified by the user for the measured concentrations option is assumed to be temporally constant.

The steady-state, vertically-integrated, mass-balance equation for transport in a river (where longitudinal advection dominates longitudinal dispersion) is as follows:

$$u \frac{\partial C}{\partial x} = D_y \frac{\partial^2 C}{\partial y^2} - \lambda C \tag{5.38}$$

in which

$$\frac{\partial C}{\partial y} = 0 \tag{5.39}$$

at $y = 0$ and $y = B$

where C = dissolved instream metal concentration (g mL^{-1})

u = average instream velocity (cm s^{-1})

D_y = dispersion coefficients in the y- direction (cm^2 s^{-1})

λ = degradation/decay constant [= (ln 2)/(half-life)] (s^{-1})

B = width of stream channel (cm).

When Equation 5.38 is solved with the appropriate boundary conditions (i.e., Equation 5.39), the riverine pathway is described by an analytical expression that characterizes the transport of metals through a river. For a point-source metal release from the bank of a stream having a rectangular cross-section, the solution to Equation 5.38 employing the boundary conditions defined by Equation 5.39 is:

$$ C = \left(\frac{Q_c}{uBh}\right) \exp\left(-\frac{\lambda x}{u}\right) \left\{1 + 2\sum_{n=1}^{\infty}\left[\exp\left(-\frac{n^2\pi^2 D_y\, x}{uB^2}\right)\left(\cos\frac{n\pi y}{B}\right)\right]\right\} \qquad (5.40) $$

where Q_c = metal Flux at the source (g s^{-1})

h = depth of stream (cm)

x = downstream distance to receptor (cm)

y = lateral distance from river banks to receptor (cm).

MEPAS computes surface water metal concentrations at y = 0.

$$ C = \left(\frac{Q_c}{uBh}\right) \exp\left(-\frac{\lambda x}{u}\right) \left\{1 = 2\sum_{n=1}^{\infty}\left[\exp\left(-\frac{n^2\pi^2 D_y\, x}{uB^2}\right)\right]\right\} \qquad (5.41) $$

Because of lateral mixing in groundwater, metals entering a surface water body, such as a stream, will do so along a finite length of the stream bank. A line source along the edge of the stream can be represented as a series of point sources along the length of the line source. As the downstream receptor location is moved farther away, the line source resembles a point source located at the center of the line source (Receptor A in Figure 5.10). As the receptor location is moved closer to the center of the line source, only that portion of the source term upstream of the receptor has an opportunity to influence metal concentrations at the receptor. Under these circumstances, MEPAS approximates the line source as a point source that is located at one-half the distance between the receptor location and the upstream end of the line source (Receptor B in Figure 5.10), and the reduced strength of the source is accounted for by multiplying Equation 5.41 by the fraction of the source term upstream of the receptor:

$$f = \frac{l_{ur}}{l_s} \qquad (5.42)$$

where f = fraction of the source term upstream of the receptor (dimensionless)

l_{ur} = length of the source term upstream of the receptor (cm)

l_s = total length of the source term (cm).

Discharge in a river channel varies along the length of the river, generally increasing in downstream direction due to inflowing tributary streams and groundwater. The surface water pathway model accounts for an increase in discharge between the source location and the receptor location by using a dilution ratio:

510.eps/1-29-99
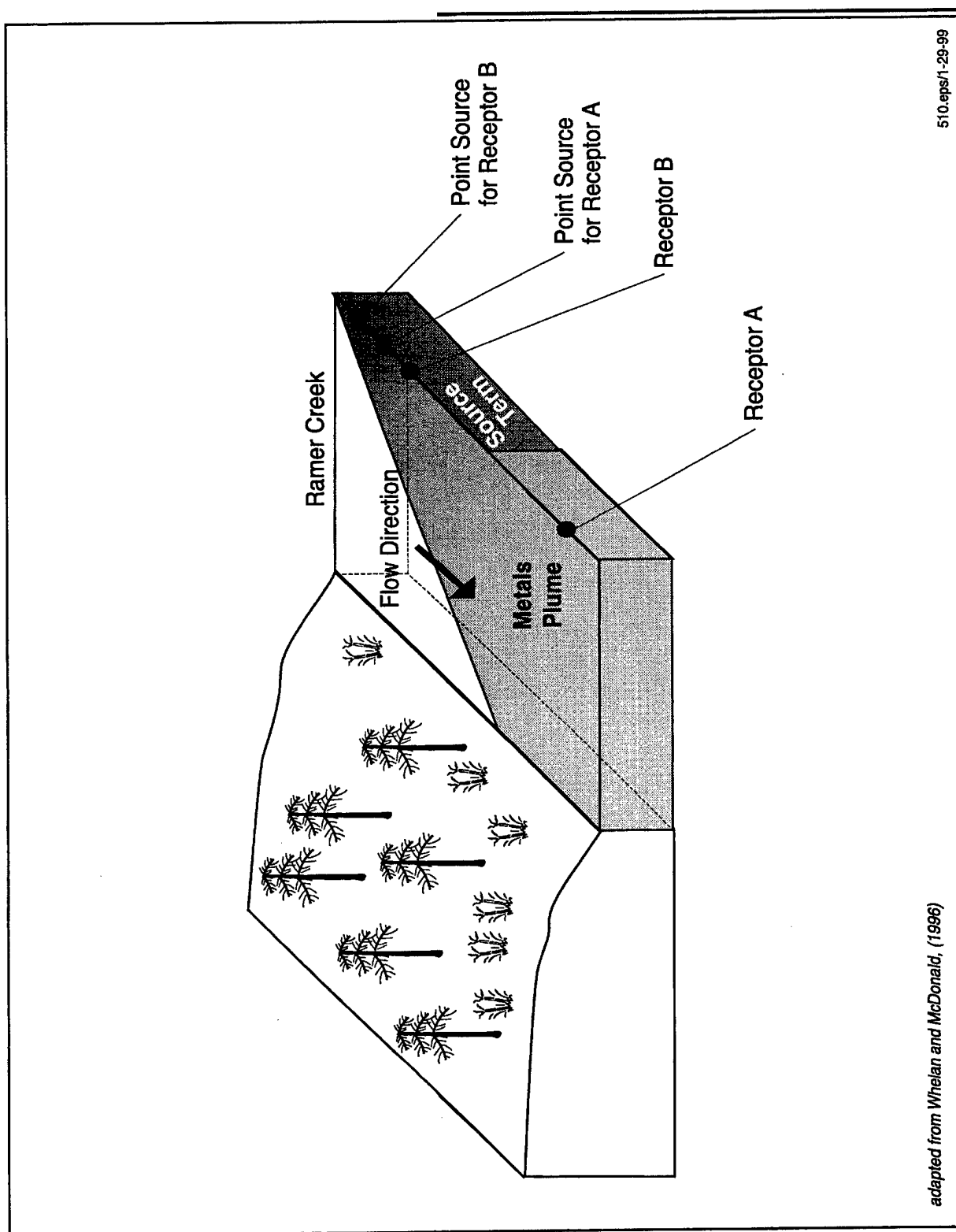
Figure 5.10. Schematic diagram illustrating the Ramer Creek surfacewater transport pathway.

adapted from Whelan and McDonald, (1996)

$$Q_{ratio} = \frac{Q_r}{Q_s} \qquad (5.43)$$

where Q_{ratio} = dilution ratio (dimensionless)

$\quad Q_r$ = river discharge at the receptor location ($cm^3 s^{-1}$)

$\quad Q_s$ = river discharge at the source location ($cm^3 s^{-1}$).

Incorporating Equations 5.42 and 5.43 into Equation 5.41 gives the final form of the steady-state equation used to simulate concentrations in the surface water pathway model of MEPAS:

$$C = Q_{ratio} \ f \left(\frac{Q_c}{uBh} \right) \exp \left(-\frac{\lambda x}{u} \right) \left\{ 1 + 2 \sum_{n=1}^{\infty} \left[\exp \left(-\frac{n^2 \pi^2 D_y \, x}{uB^2} \right) \right] \right\} \qquad (5.44)$$

5.2.3.2   Surface Water Pathway Parameters

Metals transported in groundwater beneath the test area will eventually discharge to Ramer Creek. The surface water transport model was used to predict maximum metal concentrations and changes in metal concentrations over time immediately down stream of where groundwater is expected to discharge to Ramer Creek.

Site specific surface water parameter inputs used to construct the surface water transport pathway model in MEPAS are summarized in Table 5.12, and were derived from information presented in Section 2.5. A detailed list of all inputs to the MEPAS code can be found in Appendix E. Baseflow discharge estimates for the Ramer Creek watershed were used as input to the surface water transport model because these conditions are the most common, and because they represent the most conservative approach for the transport and risk calculations.

Table 5.12. Stream transport model parameters.

Model Parameters	Parameter Value
Flow Velocity at Groundwater Discharge Point	0.5 ft/sec
Depth of Flow at Groundwater Discharge Point	1.0 ft
Width of Flow at Groundwater Discharge Point	4.6 ft
Downstream Discharge at Receptor	2.6 cfs
Distance to downstream receptor from Discharge Point	1.0 ft

Baseflow discharge from the Ramer Creek watershed was estimated at 5.6 cfs based on the area of the Ramer Creek watershed (2.8 mi^2) and discharge-watershed area relationship for Yellow River basin watersheds presented in Figure 2.13 in Section 2.5. This estimated discharge was then divided by the total length of Ramer Creek (1.7 mi) to obtain a ratio of Ramer Creek discharge/mile of stream length. The Ramer Creek receptor location where groundwater is estimated to discharge into Ramer Creek is located approximately 1 mile upstream from the mouth of the watershed. Multiplying the Ramer Creek discharge ratio (3.3 cfs/mile) by one and subtracting the result from 5.6 cfs gives an estimate of discharge at the Ramer Creek receptor location of approximately 2.3 cfs. A discharge velocity of 0.5 ft/sec was assumed for the receptor location, giving a stream cross-sectional area of 4.6 ft^2. An average discharge velocity of 0.7 ft/sec was measured at the receptor location in February, 1998 under high flow runoff conditions caused by recent high rainfall. The slightly lower discharge velocity used for estimating baseflow conditions is probably closer to the average discharge velocity that would be encountered during baseflow conditions at the site. A stream depth of 1.0 feet was used to estimate the stream width at the receptor location of 4.6 feet.

5.2.3.3 Surface Water Pathway Model Results

The surface water transport model was used to predict maximum metal concentrations and changes in metal concentrations over time where metal-bearing groundwater discharges to Ramer Creek. Results of the groundwater transport model indicate that the width of metal plumes discharging along Ramer Creek is approximately 890 feet, most likely due to the slow

rate of plume movement, which enhances lateral dispersion of the groundwater metal plume. Figures 5.11 to 5.15 present model predicted concentration versus time curves in Ramer Creek for each of the metals released by the three different tungsten alloys. Table 5.13 summarizes maximum peak concentrations and time to peak concentration for each of the metal/alloy combinations. Model results indicate that metal concentrations in Ramer Creek ranged between a low of 0.0002 ug/L for copper and manganese and a high of 0.017 ug/L for nickel. Model results indicate travel times to peak concentration generally lag peak concentrations in local well groundwater by as little as 17 years in the case of manganese, to as high as 500 years for nickel. These differences are largely due to differences in retardation, and secondarily to source term characteristics such as metal flux rate and duration of metal release from the source area.

Table 5.13. Surface water pathway transport results for Ramer Creek.

Metal	Alloy WL-1		Alloy NS		Alloy HD-17	
	Peak Concentration ug/L	Peak Time years	Peak Concentration ug/L	Peak Time years	Peak Concentration ug/L	Peak Time years
Nickel	0.017	2250	0.013	2250	0.015	2250
Manganese	0.0002	1536				
Cobalt			0.008	1200		
Copper					0.0002	10001
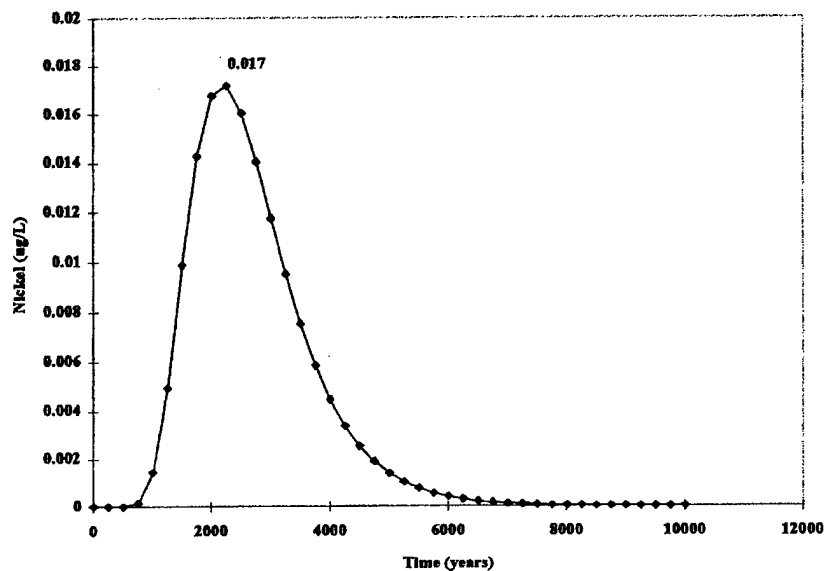
Figure 5.11. Alloy WL-1 Ni in Ramer Creek.
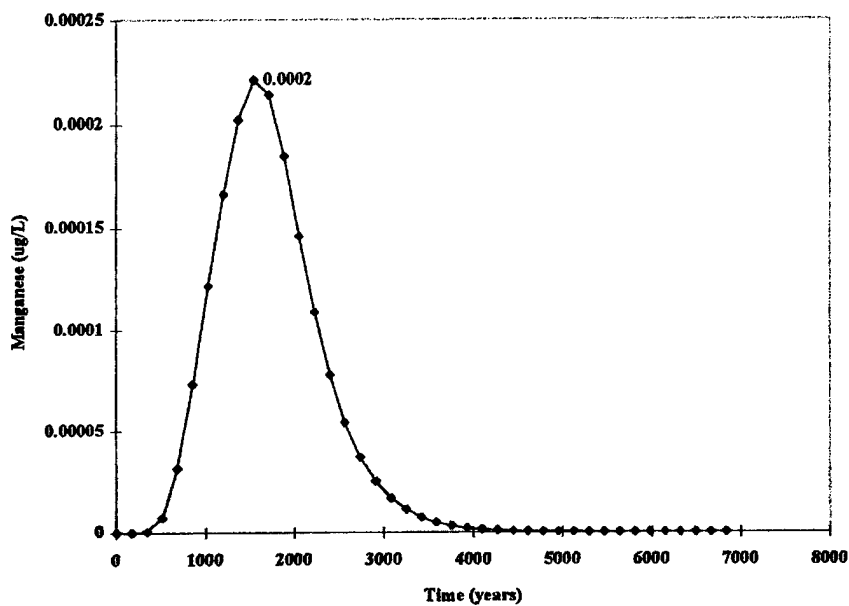
Figure 5.12. Alloy WL-1 Mn in Ramer Creek.
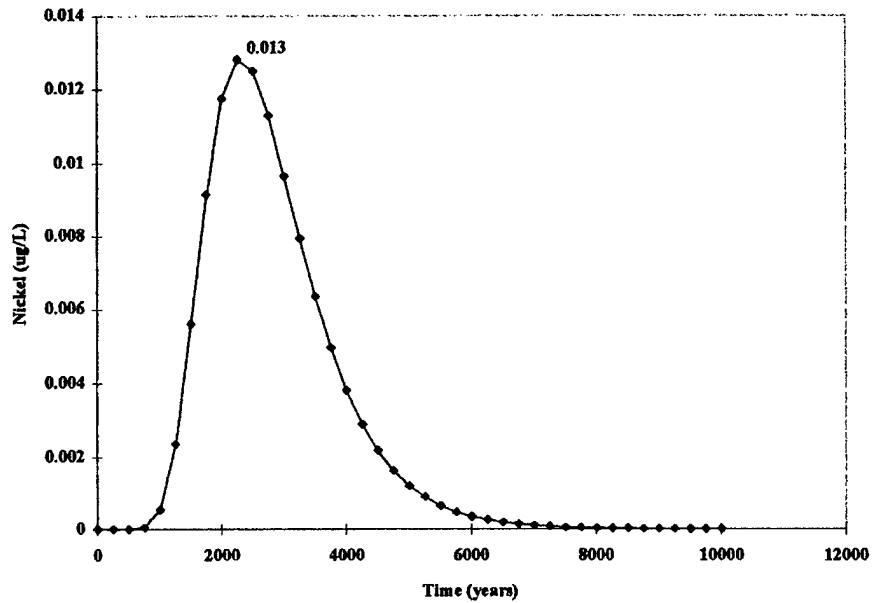
Figure 5.13. Alloy NS Ni in Ramer Creek.
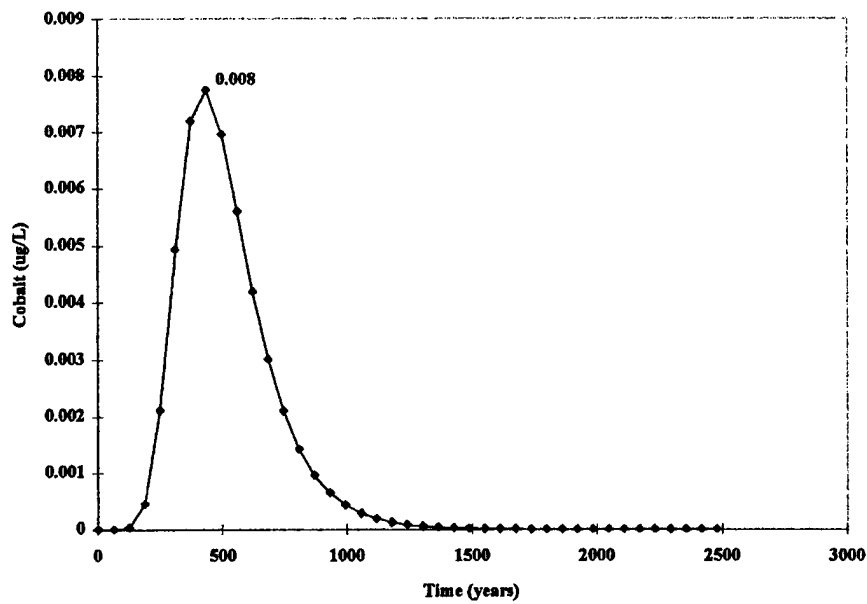
Figure 5.14. Alloy NS Co in Ramer Creek.
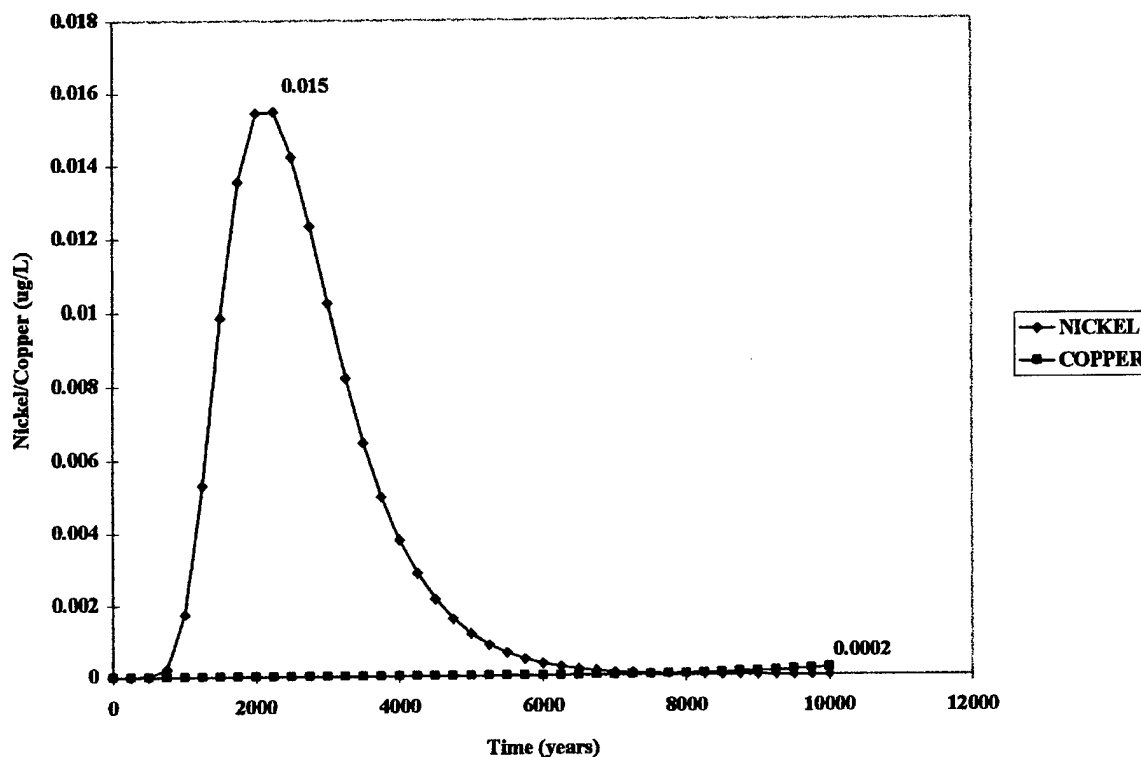
Figure 5.15. Alloy HD-17 Ni and Cu in Ramer Creek.

5.3 Exposure and Risk Analysis

5.3.1 Human Exposure Analysis

The objective of the exposure analysis is to estimate the type and magnitude of human exposures to alloy-derived metals that may occur in the future at the C-64A Test Area as a result of the leaching/breakdown of penetrator munition alloys. This information is then integrated with toxicity information to characterize the potential risks associated with human exposure to those metals. Elements that make up the exposure assessment include: 1) characterization of the exposure setting; 2) identification of potentially exposed populations surrounding the test area; 3) delineation of exposure pathways; and 4) calculation of average daily dose for individuals

potentially exposed to metals using exposure pathway models (EPA, 1989). The average daily dose is used to assess risk in Section 5.3.2.

5.3.1.1 Characterization of Exposure Setting

Information characterizing the physical setting of Test Area C-64A was presented in Section 2. The principle exposure routes along which human exposure to alloy-derived metals could occur include ingestion, dermal contact, and inhalation, as depicted in Figure 5.16.

5.3.1.2 Surrounding Populations

Low population densities are characteristic of Test Area C-64A for a distance of five miles to the north, and over ten miles to the west, south, and east. The test site and surrounding areas are located within the Eglin reservation and are not open to the public. The only people present in the area are those that work at the test area, which includes both military and civilian personnel. According to Eglin AFB, average population densities on the reservation are less than or equal to 3 individuals per square mile, although no one lives on the reservation in or around the test areas. Beyond the reservation boundaries, population in the surrounding area is predominantly rural, with population densities that range between 3 and 39 individuals per square mile. To the south of the reservation, the population is more urban, with area towns and cities having population densities greater than 39 individuals per square mile. The total population within 50 miles of the test area was 408,161 in 1990. Table 5.14 lists total population as a function of radial distance in miles from the test site according to the 1990 U.S. Census (Ciesin-Sedac, 1998). Table 5.15 lists principal nearby cities and towns, their distance from the test area site and their populations according to the 1990 U.S. Census (Ciesin-Sedac, 1998).
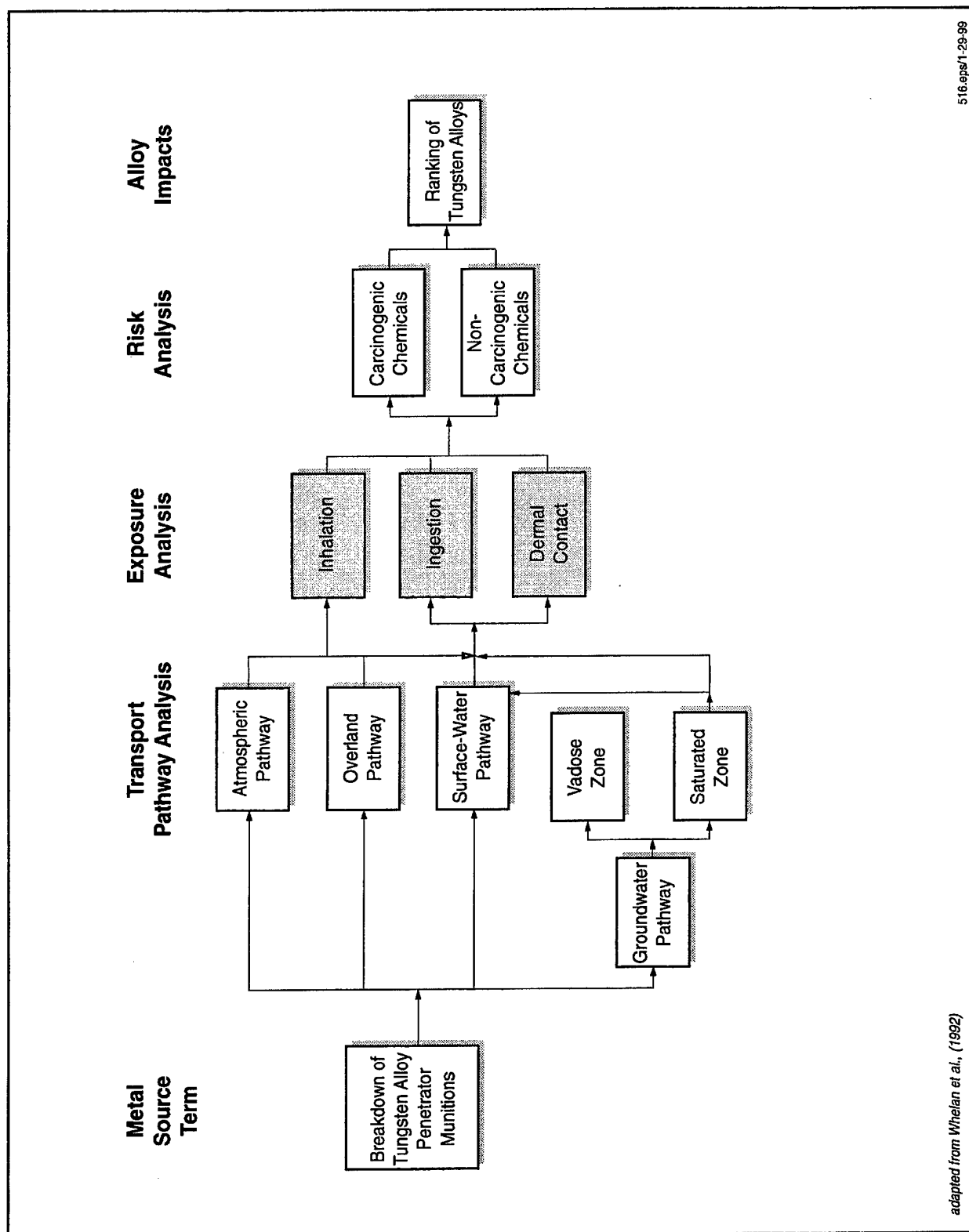
Figure 5.16. Exposure pathway figure with emphasis on exposure route.

Table 5.14. Total population with radial distance from Test Area C-64A.

Radial Distance (miles)	Population (1990 Census)[1]
1	0
5	0
10	7653
20	122830
30	179438
40	232109
50	408161

[1] Population from CIESIN-SEDAC (1998)

Table 5.15. Population centers relative to Test Area C-64A.

City	Distance (miles)	Direction	Population (1990 Census)[1]
Crestview	12	NW	9886
Niceville/Valparaiso	12	SSW	15179
De Funiak Springs	18	ENE	5120
Fort Walton Beach/Ocean City	20	SW	26893
Pensacola	50	WSW	58165

[1] Population from CIESIN-SEDAC (1998)

5.3.1.3 Exposure Pathways

Delineation of exposure pathways involves identification of metal sources and release mechanisms, definition of environmental transport media, identification of exposure points for the transfer of metals from the transport media to individuals, and definition of exposure routes by which contact can occur for the individual receiving the metal. This information is integrated using exposure pathway models to evaluate exposure to individuals for the risk analysis.

Test Area soils receiving alloy fragments from penetrator munitions tests are the principal source media from which metals could potentially be transported and dispersed to other media where human exposure may occur. Potential exposure to metals in the soil can occur through several exposure routes and transport mechanisms. Direct human contact with test area soil could result in incidental ingestion and dermal exposure. Metals may be transported from the soil to the air in particulate form (dust) through wind erosion. People located near the site or downwind from the site could potentially be exposed through the inhalation of the metal-bearing dust.

Metals in test area soils could also be transported through the unsaturated zone to groundwater via precipitation infiltrating through the soil zone. Once in the groundwater, metals could be ingested by people directly in drinking water, or incidentally during showering or bathing. People may also be exposed through dermal contact with the water during showering, bathing, and other domestic or commercial water use activities. Groundwater used as an irrigation source may reintroduce metals to the soil. Metals could also be transported in groundwater to livestock if groundwater is used as a livestock water source.

Hayes and Barr (1983) indicate that wells screened in the Sand and Gravel aquifer in southern Okaloosa County typically yield between 200 and 400 gallons per minute (gpm). Thus, groundwater beneath the test site could potentially be developed as a source for drinking and irrigation water. Assuming the maximum well yield of 400 gpm, neglecting aquifer storage considerations, and assuming a daily water requirement of 150 gallons per day per person (Buck et al., 1995), as many as 3800 people could potentially be sustained by a drinking water well installed near the source area. Assuming irrigation at a rate of 85 liters/m^2/month (Bruce Ward, 1998, personal communication), a groundwater well pumping at 400 gpm could potentially irrigate an area approximately 190 acres in size.

Alloy metals from test area soils that have migrated to groundwater may also be transported to surface water. Groundwater flowing under the test area enters Ramer Creek which could potentially be used as a water source for drinking and irrigation, or for recreational

activities such as hiking, swimming, or fishing. In addition, metals could bind onto sediments where contact during recreational use may occur.

Exposure to contaminated surface water through drinking water and food crop irrigation pathways was eliminated from consideration because surface water is not used as source of drinking or irrigation water anywhere in Okaloosa County (Tom Pratt, 1998 personal communication). The principal source of water for domestic and agricultural use is the Floridan aquifer. In southern Okaloosa County, in the Fort Walton Beach area, the Sand and Gravel aquifer is used as a source for drinking and irrigation water, but this is too far downgradient from the test site to be impacted by test site activities addressed in this report.

Although fishing activities could potentially expose humans to metals derived from test area soils, exposure to contaminated fish and shellfish was eliminated from consideration due to the small watershed area and corresponding low discharge associated with Ramer Creek. Sampling of fish populations in Ramer Creek in 1976 found relatively low species diversity indices compared to other nearby streams, such as Bull Creek. Fish species found were mostly minnow-sized fish. Only one potential game species was found, the redfin pickerel (AFAL, 1976). As a result of these considerations, Ramer Creek was ruled out as a significant potential source of fish or shell fish for human consumption for the purposes of this study.

Uptake of alloy-derived metals from source area soils by agricultural crops and livestock could result in the transport of metals from soil to humans. For example, domestic animals, while grazing, can ingest soil containing alloy metals. This would be in addition to ingesting plants that may have taken up metals directly from soil or from the deposition of metals on plants due to application of metal-bearing irrigation water. Crops or garden produce grown in soils containing metals or irrigated with metal-bearing groundwater are another source of potential exposure for humans.

Table 5.16 presents exposure pathways considered in the present analysis of potential impacts from penetrator munitions testing at Test Area C64A. Although the test area is currently undeveloped and inaccessible to the public, conditions may change in the future as a result of base closing. If turned over to civilian use, the site could be used for agriculture, or developed for residential or commercial use. Ramer Creek could see increased use for recreational purposes such as hiking, and swimming.

Because future use is uncertain, exposure pathways presented in Table 5.16 could apply to a number of different future scenarios. Exposure pathways associated with exposure to source area soils could apply if the site is used for agricultural production or for residential development or both. They are also applicable to the current use of the site, in that Air Force and civilian personnel could potentially come into contact with metal-bearing source area soils in the course of their daily work activities.

The same is true for exposure pathways associated with use of groundwater from a local well installed downgradient of the source area. These exposure pathways could apply if the site is developed for agricultural or residential use or both. Because surface-water in Okaloosa County is not used as a source of drinking water or irrigation, exposure pathways associated with the use of surface water from Ramer Creek are restricted to recreational use scenarios, both now, and in the future.

Air inhalation exposure pathways apply for both current conditions, and future scenarios involving agricultural or residential development of the site. Because of the small, restricted nature of the source area and its current undeveloped soil and vegetation characteristics, exposure to resuspended contaminated soils is expected to be local and not significant under current conditions. If the site is developed, however, then local exposure could change to the degree that development disturbs current site characteristics.

Table 5.16. Transport and exposure pathway summary.

Transport Pathway	Contaminated Medium and Exposure Setting	Exposure Route	Exposure Pathways
Source Area Soils	Soil near residences	Ingestion Dermal Inhalation External	Soil Soil contact Soil suspension Soil
	Soil used for gardening or agricultural production	Ingestion Ingestion Ingestion Ingestion	Leafy vegetables Other vegetables Meat Milk
Groundwater	Local well water used for residential waste supply	Ingestion Ingestion Dermal	Drinking water Water while showering Shower water contact
	Local well water used for irrigation for agricultural or livestock production	Ingestion Ingestion Ingestion Ingestion	Leafy vegetable Other vegetables Meat Milk
	Local well water irrigating soil at location of agricultural production	Ingestion Ingestion Ingestion Ingestion	Leafy vegetable Other vegetables Meat Milk
Surface Water	Ramer Creek water at recreational use location	Ingestion Ingestion Dermal Dermal	Water while swimming Sediment from shoreline Swimming water contact Shoreline sediment contact
Atmosphere	Air near test area	Inhalation	Air

5.3.1.4 Exposure Pathway Models

Experimental data on the leaching/breakdown of penetrator munitions fragments presented in Section 3.0 and transport pathway modeling results presented in Section 5.2 were used to provide exposure point concentrations in soil, groundwater, and surface water media for metals derived from penetrator fragments dispersed during penetrator weapons testing at Test Area C-64A. These exposure point concentrations were then used in exposure pathway models to estimate average daily dose to exposed individuals from contact with the transport medium or a secondary medium contaminated by the transport medium. The average daily dose is used to estimate a measure of health impact appropriate to the type of metal considered. MEPAS was used to calculate both exposure and risk for the exposure pathways in Table 5.16. This section presents general and pathway specific equations for exposure pathway models as outlined by EPA (EPA, 1989). Special factors which modify these general exposure model equations are provided in the MEPAS program (see Strenge and Chamberlain, 1995) and have been included in the following equations.

The basic equation for calculating average daily dose via ingestion (soil, water, or biota) or inhalation is:

$$ADD_i = \frac{C \times IR \times EF \times ED \times CF}{BW \times AT} \tag{5.45}$$

where:

C = Concentration of metal in the medium

IR = Contact or intake rate

EF = Exposure frequency (d/yr)

ED = Exposure duration (yr)

CF = Conversion factor (as appropriate)

BW = Body weight (kg)

AT = Averaging time (yr x 365 d/yr)

$$\text{ADD}_i = \text{Metal-specific average daily dose from ingestion or inhalation (mg/kg-d).}$$

Typical concentration units are mg/kg, ml/L, mg/m^3 for soil, water, or air, respectively.

Equation 5.45 is modified to provide an equation for calculating the averaging daily dose resulting from dermal exposure to metal-bearing water as follows:

$$\text{ADD}_w = \frac{C_w \times SA \times Kp \times ET \times EF \times ED \times CF}{BW \times AT \times GF} \qquad (5.46)$$

where:

C_w	=	Concentration of metal in water (mg/L)
SA	=	Skin surface area available for contact (cm^2)
Kp	=	Metal-specific permeability coefficient (cm/hr)
ET	=	Contact event time (hr/d)
EF	=	Exposure frequency (d/yr)
ED	=	Exposure duration (yr)
CF	=	Conversion factor (1 L/1000 cm^3)
BW	=	Body weight (kg)
AT	=	Averaging time (yr x 365 d/yr)
GF	=	Metal-specific gastrointestinal tract absorption coefficient (unitless)
ADD_w	=	Metal-specific average daily dose from dermal exposure to metal-bearing water (mg/kg-d).

Similarly, equation 5.45 is modified to provide the average daily dose equation for dermal exposures to metal-bearing soil or sediment:

$$\text{ADD}_s = \frac{C_s \times SA \times AF \times ABS \times FE \times EF \times ED \times CF}{BW \times AT \times GF} \qquad (5.47)$$

where:

C_s = Concentration of metal in soil (mg/kg)

SA = Skin surface area available for contact (cm^2)

AF = Soil-to-skin adherence factor (mg/cm^2/event)

ABS = Metal-specific absorption factor (unitless)

FE = Contact event frequency (events/d)

EF = Exposure frequency (d/yr)

ED = Exposure duration (yr)

CF = Conversion factor (1E-06 kg/mg)

BW = Body weight (kg)

AT = Averaging time (yr x 365 d/yr)

GF = Metal-specific gastrointestinal tract absorption coefficient (unitless)

ADD_s = Metal-specific average daily dose from dermal exposure to test site soil (mg/kg-d).

In MEPAS, dermal exposures to metals from contact with water or soil are treated as ingestion intakes with correction for the fraction of the metal absorbed in passing through the gastrointestinal tract. This is accomplished using a metal specific gastrointestinal tract absorption fraction coefficient (GF) found in Equations 5.46 and 5.47.

Table 5.17 presents exposure factors utilized for calculating average daily dose for each of the exposure pathways in Table 5.16 according to Equations 5.45, 5.46, and 5.47. For each exposure pathway, exposure duration (ED), body weight (BW) and averaging time (AT) were set at 70 years, 70 kg, and 70 yrs x 365.25 d/yr, respectively, for both carcinogens and noncarcinogens. An exposure frequency (EF) of 365.25 days/year was used in all exposure calculations. These represent default values used in MEPAS, and they were not modified so that estimated exposures would be conservative. Exposures calculated according to these parameters are greater than would be the case if the exposure parameter assumptions were selected according to the concept of reasonable maximum exposure proposed by EPA (EPA, 1989).

Table 5.17. Exposure pathway parameters.

Media	Route	Daily Intake/Contact Rate	Conversion Factors	Other Factors
Pathway			**Exposure Parameters**	
Soil	Ingestion	0.1 g/d	1E-03 kg/g, 365.25 d/yr	None
	Dermal	1 mg/cm²/d[a]	1E-06 m³/cm³, 365.25 d/yr	SA = 5800 cm², ABS[i], and GF[i]
	Inhalation	2E-06 kg-soil/d[b]	365.25 d/yr	ML = 1E-07 kg/m³
Groundwater	Drinking-Ingestion	2 L/d	None	None
	Shower-Ingestion	0.001 L/d[c]	None	None
	Shower-Dermal	0.167 hr/d[d]	1E-03 L/cm³	SA = 20,000 cm², Kp[i] (cm/hr), GF[i]
Surface Water	Swimming Ingestion	0.0083 L/d[e]	None	None
	Swimming-Dermal	0.033 hr/d[f]	1E-03 L/cm³	SA = 20,000 cm², Kp[i] (cm/hr), GF[i]
	Shoreline-Ingestion	0.0033 g/d[g]	1E-03 kg/g	None
	Shoreline-Dermal	0.066 mg/cm²/d[h]	1E-06 kg/mg	SA = 5800 cm², ABS[i], and GF[i]
Food	Leafy Vegetables	21 g/d	1E-03 kg/g	None[j]
	Other Vegetables	130 g/d	1E-03 kg/g	None[j]
	Meat	65 g/d	1E-03 kg/g	None[j]
	Milk	75 g/d	1E-03 kg/g	None[j]

Notes:

[a] 1 mg-soil adheres per cm² skin (AF) per contact event X 1 contact event per day (FE)

[b] 20 m³-air inhaled per day X 1E-07 kg-suspended soil per m³-air

[c] 0.06 L water ingested per hour duration of shower X 0.0167 hour duration per shower X 1 shower per day

[d] 0.167 hour water contact per shower X 1 shower per day

[e] 0.1 L water ingested per hour duration swimming X 0.5 hour duration per swim X 0.066 swims per day

[f] 0.5 hour water contact per swim X 0.066 swims per day

[g] 0.1 g-soil ingested per hour contact duration X 0.5 hour contact duration per contact event X 0.066 contact events per day

[h] 1 mg-soil adheres per cm² skin (AF) per contact event X 0.066 contact events per day (FE)

[i] See Table 5.18 for contaminant specific transfer factors

[j] See Table 5.19 for plant-animal contaminant transfer parameters

MEPAS implements these general equations, but includes additional factors, such as water treatment, contaminant decay, and time delay factors when calculating exposure. The following discussion presents these special factors and other considerations employed by MEPAS in calculating intake rates for exposure pathways listed in Table 5.16. Because metals analyzed as part of this study are nonvolatile, loss rate and decay constants for these metals, denoted by (λ) in the following equations, are set by MEPAS at extremely low values (1.87E-10 d^{-1}), corresponding to extremely long decay half-lives (3.79E+09 days). As a result, exposure point concentrations and average daily dose calculated by MEPAS are not effected by consideration of decay and loss

Drinking Water Ingestion.

Drinking water may result in exposure if metal-bearing groundwater is used as a source of drinking water. In this case, groundwater used for drinking is assumed to come from the local well installed down gradient of the penetrator munitions test area.

For the drinking water ingestion pathway, average daily dose is calculated according to Equation 5.45 utilizing an intake rate (IR) of 2.0 liters per day. The drinking water ingestion pathway in MEPAS incorporates special factors into the general equation for ingestion (5.45) which account for reductions of metal concentrations during processing in the water supply treatment plant (if present) and in transport through the water distribution system to the exposed individuals. For the current analysis, water treatment was conservatively presumed not to occur while loss and decay for metal contaminants rates are too low to significantly effect calculation of average daily doses.

Shower Water Ingestion and Dermal Exposure Pathways

Water used for showering may result in exposure if metal-bearing groundwater is used as a source of water for domestic use. In this case, metal-bearing groundwater used for showering is assumed to come from a local well installed down gradient of the penetrator munitions test area.

For the shower water ingestion pathway, average daily dose was calculated according to Equation 5.45. An intake rate (U) of 0.001 liters per day was used assuming inadvertent ingestion of shower water occurs at a rate of 0.06 liters per hour, each shower has a total duration time of 0.167 hour, and that each individual takes one shower per day.

For the shower water dermal exposure pathway, average dose was calculated according to Equation 5.46. A shower water contact event time (ET) of 0.167 hours per day was used assuming each shower lasts 0.167 hours and each individual takes one shower per day. Area of skin exposed to water while showering (SA) was set at 20,000 cm^2. Metal-specific transfer factors (Kp, GF) are listed in Table 5.18.

Table 5.18. Metal-specific transfer factors.

Contaminant	ABS	GF	K_p (cm/hr)
Cobalt	0.001	0.30	0.0004
Copper	0.001	0.50	0.001
Nickel	0.001	0.10	0.003
Manganese	0.001	0.05	0.0004

Like the drinking ingestion pathway, both the shower water ingestion and dermal exposure pathways in MEPAS can incorporate special factors, which account for reductions of metal concentrations during processing in the water supply treatment plant (if present) and in transport through the water distribution system to the exposed individual. The shower water ingestion and dermal exposure pathways utilized the same special factor assumptions as presented previously for the drinking water ingestion pathway.

Soil Ingestion, Dermal Exposure and Resuspended Soil Inhalation Pathways

Individuals may encounter test area soils directly if the test area is later developed for residential or agricultural use. MEPAS evaluates exposure to source area soils directly as residential exposures without special processes applied to soil concentrations except for losses due to decay. Three exposure pathways are evaluated; exposure to source area soils via ingestion, exposure to source area soils via dermal contact, and exposure to source area soils via inhalation of resuspended soil particles. Equations for determining average daily dose from direct exposure to source area soils are provided below because they differ from general Equations 5.45 5.46, and 5.47 for exposure via ingestion and dermal contact.

Average daily dose for source area soil ingestion pathway is calculated in MEPAS according to:

$$ADD_i = 10^{-3}\ IR\ SMF_i\ EF \left[\frac{1 - e^{-\lambda_i\ ED\ 365.25}}{\lambda_i\ AT\ BW\ 365.25} \right] \qquad (5.48)$$

where: ADD_i = average daily dose for metal i from ingestion of source area soil (mg/kg/d)

   IR = ingestion rate for soil (g/d)

   10^{-3} = units conversion factor (kg/g)

   SMF_i = average soil concentration for metal i (mg/kg)

   365.25 = units conversion factor (d/yr)

   λ_i = environmental loss rate constant for surface soil for metal i (d^{-1})

other factors as described previously.

For the soil ingestion pathway, an inadvertent sediment intake rate (IR) of 0.1 grams soil per day was used.

Average daily dose for dermal contact with source area soil is calculated in MEPAS according to:

$$ADD_i = 10^{-6}\ SMF_i \left[\frac{EF\ FE\ AF\ SA\ ABS_i}{GF_i} \right] \left[\frac{1 - e^{-\lambda_i\ ED\ 365.25}}{\lambda_i\ AT\ BW\ 365.25} \right] \qquad (5.49)$$

where: ADD_i = average daily dose for metal i from dermal contact with source area soil (mg/kg/d)

   10^{-6} = units conversion factor (m^3/cm^3)

   SMF_i = average soil concentration for metal i (mg/kg)

and other variables as previously described.

For the residential soil dermal exposure pathway, a sediment contact rate of 1.0 mg soil per cm^2 skin surface area per day was used assuming that sediment adheres to the body during residential activities at a rate of 1mg soil per cm^2 of exposed skin per event (AF) and that individuals come into contact with soil in a residential setting at a rate of one event per day (FE). Area of skin exposed to residential soil (SA) was set at 5,800 cm^2. Metal-specific transfer factors (ABS_i, GF_i) are listed in Table 5.18.

Average daily dose from inhalation of resuspended source area soil is calculated in MEPAS according to:

$$ADD_i = SMF_i\ ML\ U\ EF \left[\frac{1 - e^{-\lambda_i\ ED\ 365.25}}{\lambda_i\ AT\ BW\ 365.25} \right] \qquad (5.50)$$

where: ADD_i = average daily dose for metal i from inhalation of resuspended source area soil (mg/kg/d)

   SMF_i = average soil concentration of metal i (mg/kg)

ML = mass loading factor for airborne particulate material (kg/m^3)

U = inhalation rate of air for soil resuspension pathway (m^3/d)

other variables as described earlier.

For inhalation of resuspended source area soil, an intake rate (IR) of 2E-06 kg resuspended soil per day was used assuming that individuals inhale 20 m^3 of air containing resuspended soil per day (U) and that the air contains 1E-07 kg of resuspended soil per m^3 of air (ML). Each of the above equations for direct exposure to source area soils incorporates an environmental loss rate constant for metals in soil. Because inorganic contaminants do not degrade, this parameter does not effect calculated average daily dose for metals in source area soils.

Food (Vegetable /Meat/Milk) Ingestion Exposure Pathways

Food consumed by humans include various agricultural crops as well as meat and milk products. Agricultural crops and animals may be exposed to metals when crops are grown directly in source area soil, or groundwater is used as a source of irrigation water. Animals fed feed crops grown in the source area soils and metal-bearing water will produce meat and dairy products enriched in metals. Animals and animal products can also be exposed to metals via inadvertant ingestion of source area soil while feeding. Crops for human and animal consumption are assumed to have been grown in penetrator munitions test area soils. Water used for crop irrigation and raising livestock is assumed to come from a local well installed down gradient of the penetrator munitions test area. The paths by which metals in transport media may reach crops and farm animals is depicted in Figure 5.17. MEPAS simulates transfer of metals via these various routes in order to estimate metal exposure concentrations in plant and animal foods consumed by humans.

MEPAS estimates average daily dose due to consumption of metal-enriched foods for two categories of agricultural crops (leafy vegetables and other vegetables) and two categories of animal products (meat and milk). Leafy vegetables include items such as lettuce, spinach, broccolli, and fruits which are exposed directly to metal-bearing irrigation water. Other

Plant and Animal Transfer Processes

Irrigation Water from Local Well → *irrigation* → Source Area Agricultural Soil

irrigation

root uptake

Edible Plant Parts Consumed by Humans

Feed Plant Parts Consumed by Animals

animal feed ingestion

harvest and distribution delay

Edible Animal Products

harvest and distribution delay

Human Exposure

Crop and Animal Product Ingestion

adapted from Strenge and Chamberlain, (1995)

517.eps/1-29-99

Figure 5.17. Pollutant transfer to edible crops and animal products.

vegetables includes items such as grains, root crops, fruits that must be peeled, and other crops for which the consumed food is generally not exposed directly to deposition of metal-bearing irrigation water. Meat can come from a variety of sources, but for the current study, was assumed to consist entirely of beef products. Milk is assumed to derive from dairy cattle.

Estimation of Contaminant Concentration in Plant Foods and Animal Feed Crops

The application of irrigation water to croplands results in deposition of metals to soils and plants at a constant average rate over the period of irrigation. The deposition rate is given as follows:

$$DP_i = \frac{C_{ir} \; IR}{30} \tag{5.51}$$

where: DP_i = rate of deposition of metal i in irrigation water to cropland soil and plants $(mg/m^2/d)$

C_{ir} = metal i concentration in irrigation water (mg/L)

IR = irrigation water application rate during irrigation periods $(L/m^2/mo)$

30 = units conversion factor (d/mo).

Note that the irrigation water metal (C_{ir}) concentration is taken from the groundwater transport pathway analysis.

The accumulation of metals in soil over a multiple-year period (multiple growing periods) due to irrigation is accounted for by a soil accumulation factor (SAF). This factor accounts for previous years' deposition and accumulation to evaluate an average soil metal concentration over the exposure duration defined for the current usage location. The factor is evaluated as a time integral of soil metal concentration over the exposure period. The soil accumulation factor is evaluated as the time integral of the solution to the deposition and decay differential equation, normalized to unit deposition and averaged over the deposition period. This process is represented by the following two equations:

$$\frac{d\,C_i}{dt} = UD_i - C_i\,\lambda_i \tag{5.52}$$

and

$$SAF_i = \frac{\int_0^{ED\ 365.25} C_i\ dt}{UD_i\ ED\ 365.25} \tag{5.53}$$

where: C_i =   soil concentration of metal i from irrigation water deposition as a function of time (mg/m^2)

UD$_i$ =   unit deposition rate of metal i to soil via irrigation water deposition (mg/m^2/d)

SAF$_i$ =   soil accumulation factor for an exposure duration of ED years for metal i (d)

other variables are as described earlier.

The division by UD$_i$ normalizes the SAF values to unit deposition rate. The above equations are used for the agricultural exposure pathways from groundwater irrigation deposition.

Enrichment of plants in metals from irrigation deposition onto edible parts of vegetable and animal crops will result in a metal level at harvest that is estimated as follows:

$$CWD_i = DP_i\ TV\ r\ \frac{\left[1 - e^{-\lambda_{ei} TC_{lv}}\right]}{\lambda_{ei}\ Y} \tag{5.54}$$

where: CWD$_i$ =   metal i concentration in vegetables or animal crops at time of harvest from irrigation water deposition onto plants (mg/kg)

TV = translocation factor from plant surfaces to edible parts of the plant for vegetables or animal crops (dimensionless)

r = fraction of deposition retained on plant surfaces

λ_{ei} = effective weathering and decay constant for metal i ($= \lambda_{di} + \lambda_w$ d^{-1})

TC = duration of the growing period for vegetables or animal crops (d)

λ_w = weathering decay constant for losses from plant surfaces (d^{-1})

Y = yield of vegetables or animal crops (kg/m^2)

and other terms are as previously defined.

Metal-enrichment of vegetables and animal crops at the time of harvest due to uptake from source area soil via roots is estimated as follows:

$$CWR_i = \frac{FI \; SAF_i \; B_i \; DP_i}{P} \qquad (5.55)$$

where: CWR_i = metal i concentration in edible parts of vegetables or animal crops at time of harvest from root uptake (mg/kg)

FI = fraction of year that irrigation occurs for vegetable or animal crops (dimensionless)

B_i = soil-to plant transfer factor for metal i (kg dry soil/kg wet weight plant)

P = area soil density of farmland (kg dry soil/m^2 farmland)

and other terms are as previously defined.

The total concentration of a metal in vegetables or animal crops is evaluated as the sum of concentrations from the two uptake routes: deposition onto plants and root uptake from soil.

$$C_i = (CWD_i + CWR_i) \; e^{-\lambda_i \; TH} \qquad (5.56)$$

where: C_i = vegetable or animal crop metal i plant concentration at time of consumption (mg/kg)

λ_i = loss and decay rate constant for metal i in closed water systems (d^{-1})

TH = holdup time between harvest of vegetables or animal crops and consumption by humans or animals (d)

and other terms are as previously defined. The loss rate constant for closed water systems is used to simulate loss from food products between harvest and consumption as a conservative representation for food handling and packaging. This representation is considered appropriate for frozen and canned foods and conservative for fresh foods.

In addition to metal-enrichment of vegetables and animal crops due to deposition of metal-bearing irrigation water on plants and soils, vegetables and animal crops may also be metal-enriched if grown directly in test area soils. For the source area soil pathway, exposure to metals in vegetables and animal crops is evaluated based on initial direct estimates of soil metal concentrations, with loss and decay during the exposure period.

The change in soil concentration over the exposure period affects the total amounts of metals ingested by the exposed individuals or animals. The average concentration of a metal in soil is evaluated as the time integral of the concentration of the metal in the soil divided by the exposure duration, as follows:

$$SMF_i = \frac{\int_0^{ED\,365.25} C_{si}\ dt}{ED\ 365.25} \tag{5.57}$$

where: SMF_i = average soil concentration for metal i over the exposure duration (mg/kg dry soil)

C_{si} = measured concentration of metal i in soil (mg/kg dry soil)

and other terms are as previously defined.

The concentration of metals in edible parts of vegetable or animal crops due to root uptake from source area soils is evaluated as follows:

$$C_i = SMF_i \; B_i \qquad (5.58)$$

where terms are as previously defined.

For source area soils, the average daily dose from ingestion of metals in vegetables and animal crops is evaluated using the plant metal concentration from Equation (5.58) and intake Equation (5.45).

Estimation of Metals in Meat and Milk

Animals may be exposed to metals due to consumption of metal-bearing drinking water, consumption of feed crops that have been irrigated with metal-bearing water, consumption of crops grown in soils irrigated by metal-bearing water, or from being grown directly in source area soils. Equations 5.54 and 5.55 are used to estimate metal concentrations in animal feed crops grown using metal-bearing irrigation water. In addition, animals may be exposed to metals by ingestion of soil along with the forage or feed. The concentration of metals in soil ingested with feed is evaluated as an average value over the exposure duration using the same soil accumulation factor as for the plant root uptake pathway. This factor is evaluated using Equations 5.52 and 5.53. The soil concentration is evaluated as follows:

$$CWS_i = \frac{FI \; SAF_i \; DP_i}{P} \qquad (5.59)$$

where: CWS_i =   average soil concentration for metal i in soil eaten by meat and milk animals along with feed (mg/kg dry soil)

and other terms are as previously defined.

The concentration of metals in meat or milk products at the time of consumption by humans includes animal intake of metal-bearing feed, water, and soil, as follows:

$$C_{mi} = FM_i \{ FC_f [(CWD_i + CWR_i) Q_f + (CWS_i Q_s)]$$
$$+ C_{ir} FC_w Q_w \} e^{-\lambda_i \, TH} \tag{5.60}$$

where: C_{mi} = concentration of metal i in meat or milk at time of consumption by humans (mg/kg or mg/L)

FM_i = transfer factor for uptake of metal i by animals to meat or milk (d/kg or d/L)

FC_f = fraction of meat or milk animal feed that contains alloy-derived metals (dimensionless)

Q_f = meat or milk animal ingestion rate of feed (kg/d)

Q_s = meat or milk animal intake rate of soil (kg/d)

C_{ir} = average concentration of metal i in irrigation water (mg/L)

FC_w = fraction of meat or milk animal drinking water that contains alloy-derived metals (dimensionless)

Q_w = meat or milk animal ingestion rate of water (L/d)

λ_i = rate constant for decay and loss in confined waster system, used to simulate loss during storage and distribution of meat or milk (d^{-1})

TH = holdup time between harvest (slaughter) and consumption of animal meat or milk by humans (d)

and other terms are as previously defined.

In addition to exposure of vegetables and animal crops due to deposition of metal-bearing irrigation water on plants and soils, vegetables and animal crops may also be exposed to metals if grown directly in test area soils. For the source area soil concentration pathway, exposure is

evaluated based on initial direct estimates of soil metal concentrations, with loss and decay during the exposure period.

The evaluation of the concentration of metals in feed plants eaten by meat and milk animals is performed similarly to the evaluation of vegetable plant concentrations described previously. The average soil metal concentration is evaluated using Equation (5.57), and the plant metal concentration is evaluated using Equation (5.58). The animal may also ingest soil. The soil concentration ingested by the meat or milk animal is equal to the average soil concentration given by Equation (5.57). The concentration in the animal product is evaluated according to:

$$C_{mi} = FM_i \ FC_f \ [\ C_{fi} \ Q_f + SMF_i \ Q_s \ ] e^{-\lambda_i \ TH} \qquad (5.61)$$

where: C_{fi} = concentration in meat or milk animal feed for metal i (mg/kg wet weight feed)

and other terms are as previously defined.

Estimates of metal concentrations in plant and animal foods consumed by humans were calculated according to the equations presented above, and plant-animal metal transfer parameters presented in Table 5.19. Once estimates of metal concentrations in plant and animal foods consumed by humans were calculated as indicated above, average daily doses for these metals via ingestion of such food products was calculated according to Equation 5.45 assuming typical daily intake rates (IR) for vegetables, meat and milk products.

Table 5.19. Plant-animal metal transfer parameters.

Metal Transfer Parameter	Parameter Variable	Parameter Value	
		Leafy Vegetables	Other Vegetables
Vegetable Yield (kg/m^2)	Y	1.26	0.7
Vegetable delay time to ingestion (d)	TH	2	60
Vegetable translocation factor	TV	1	0.1
GW vegetable growing period (d)	TC	60	60
Retention fraction on plants	r	0.25	0.25
		Meat	Milk
Animal feed yield (kg/m^2)	Y	0.37	0.37
Delay time to ingestion (d)	TH	20	4
Animal feed intake (kg/d)	Q_f	68	55
Animal water intake (L/d)	Q_w	50	60
Animal feed translocation factor	TV	0.1	1.0
Animal soil intake rate (kg/d)	Q_s	0.5	0.5
Agricultural areal soil density (kg/m^2)	P	240	240
GW irrigation rate (L/m^2/mo)	IR	85	85

Agricultural yields of foods for human consumption and animal feeds in Okaloosa and Santa Rosa Counties, Florida, reported in Shor et al., (1982) were used to estimate yields for leafy vegetables, other vegetables, and animal feed required by MEPAS. Shor et al., (1982) reports no agricultural production of leafy vegetables in Okaloosa County, Florida, but leafy vegetable yields of 1.26 kg/m^2 are reported for neighboring Santa Rosa County, Florida. Projected produce and grain for food yields in Okaloosa County are reported as 0.5 and 0.18 kg/m^2 (Shor et al., 1982). Areal yields of hay in Okaloosa County are reported as 0.41 kg/m^2, while feed grain and silage yields of 0.19 and 0.51 kg/m^2 are reported for Santa Rosa County, but not for Okaloosa County. Leafy vegetable yields of 1.26 kg/m^2 reported for Santa Rosa County were used to represent leafy vegetable yield required by MEPAS for Okaloosa County. A

separate vegetable yield of 0.7 kg/m² for Okaloosa County was estimated by combining protected produce (0.5 kg/m²) and grain for food yields (0.18 kg/m²) reported for Okaloosa County in Shor et al., (1982). Animal feed yield for Okaloosa County was set by taking the average of hay areal yield for Okaloosa County (0.41 kg/m²), and feed grain (0.19kg/m²) and silage yields (0.51 kg/m²) reported for Santa Rosa County in Shor et al., (1982).

For the leafy vegetable ingestion pathway, an intake rate (IR) of 21 grams per day was used. For other vegetable ingestion pathway, an intake rate (IR) of 130 grams per day was used. Meat and milk ingestion pathway intake rates were set at 65 and 75 grams/day, respectively.

Food ingestion pathway models in MEPAS incorporate special factors which account for reductions of metal concentrations during processing in the water supply treatment plant (if present), in transport through the water distribution system, and in storage of food products prior to consumption. Food ingestion pathways utilized the same special factor assumptions with regard to water treatment and environmental loss rate constants as presented previously for the drinking water ingestion pathway.

Swimming Water Ingestion and Dermal Exposure Pathways

The metal concentrations in surface water used for swimming may increase when metal-bearing groundwater discharges to the surface water body. In this case, surface water in Ramer Creek is derived in part from metal-bearing groundwater originating beneath the penetrator munitions test area.

For the swimming water ingestion pathway, average daily dose is calculated according to Equation 5.45. An intake rate (IR) of 0.0083 liters per day was used assuming inadvertent ingestion of surface water occurs while swimming at a rate of 0.1 liters per hour, each swimming event lasts for a total duration time of 0.5 hours, and that each individual swims at a rate of 0.066 swimming events per day (once every 15 days).

For the swimming water dermal exposure pathway, average daily dose is calculated according to Equation 5.46. A swimming water contact event time (ET) of 0.033 hours per day

was used assuming each swimming event lasts for a total duration time of 0.5 hours, and that each individual swims at a rate of 0.066 swimming events per day (once every 15 days). Area of skin exposed to metal-bearing water while swimming (SA) was set at 20,000 cm^2. Metal specific transfer factors (K_p, GF) are listed in Table 5.16.

The swimming water ingestion and dermal exposure pathways in MEPAS incorporate special factors into the general equation for ingestion (5.45) which account for reductions of metal concentrations due to volatilization during transport between the entry point to surface water and the downstream location where swimming occurs. This is not a significant issue in the current analysis because dissolved metals derived from leaching/breakdown of penetrator munitions fragments are not volatile and the downstream transport distance between the entry point of metals into Ramer Creek and the downstream exposure point is very short (1 foot).

Shoreline Sediment Ingestion and Dermal Exposure

Metals transported in surface water are deposited on stream shoreline sediments which may be inadvertently ingested or contacted dermally during recreational activities. In this case, shoreline sediments are exposed by contact with metal-bearing surface water in Ramer Creek, which, in turn, was derived from metal-bearing groundwater originating beneath the penetrator munitions test area.

MEPAS estimates a sediment surface metal concentrations derived from metal-bearing surface water according to the following equation:

$$CS_i = 100 \ln (2) \ C_{wi} \ \frac{1 - e^{-\lambda_i \frac{TE \ 365.25}{2}}}{\lambda_i} \qquad (5.62)$$

where:
CS_i = surface concentration of metal i in shoreline sediment (mg/m^2)

100 = empirical constant for transfer of metals from water to sediment (L/m^2/d)

C_{wi} = concentration of metal i in surface water at the location of the shoreline (mg/L)

λ_i = loss or decay rate constant for metal i in surface waters (d^{-1})

TE = period over which shoreline sediment has accumulated (yr).

Surface sediment concentrations are converted to sediment mass concentration assuming sediment density of 1.5 g/cm^3 and shoreline sediment thickness of 1 cm according to:

$$C_{si} = \frac{CS_i \, 10^{-6} \, 10^3}{t\rho}$$

(5.63)

where: C_{si} = shoreline sediment concentration for metal i at the location of recreational shoreline use (mg/kg)

10^{-6} = units conversion factor (m^3/cm^3)

10^3 = units conversion factor (g/kg)

t = thickness of shoreline sediments (m)

ρ = density of shoreline sediments (g/cm^3)

and CS$_i$ is as previously defined.

For the shoreline sediment ingestion pathway, average daily dose is calculated according to Equation 5.45. An inadvertent sediment intake rate (IR) of 0.0033 grams soil per day was used assuming inadvertent ingestion of shoreline sediment occurs during recreational activities at a rate of 0.1 grams soil per hour, that each period of recreational activity occurs for a total period of 0.5 hours, and that recreational activities are engaged in at a rate of 0.066 events per day (once every 15 days).

For the shoreline sediment dermal exposure pathway, average daily dose is calculated according to Equation 5.47. A sediment contact rate of 0.066 mg soil per cm^2 of skin surface area per day was used assuming that sediment adheres to the body during recreational activities at a rate of 1mg soil per cm^2 of exposed skin per event (AF), and that each individual engages in

shoreline recreational activities at a rate of 0.066 events per day (FE, once every 15 days). Area of skin exposed during recreational activities (SA) was set at 5,800 cm². Metal specific transfer factors (ABS, GF) are listed in Table 5.18.

The shoreline dermal exposure and sediment ingestion pathways in MEPAS incorporate special factors into the general equation for dermal exposure (5.47) which account for reductions of metal concentrations due to volatilization during transport between the entry point to surface water and the downstream location where swimming occurs. This is not a significant issue in the current analysis because dissolved metals derived from leaching/breakdown of penetrator munitions fragments are not volatile and the downstream transport distance between the entry point of metals into Ramer Creek and the downstream exposure location is very short (1 foot).

5.3.2 Human Risk Assessment

This human risk analysis provides quantitative and qualitative descriptions of the results of risk-based calculations performed by the MEPAS code. Estimates of average daily dose calculated according to methods presented in the previous section as part of the human exposure analysis are integrated with information provided in the toxicity assessment presented in Section 4.0 to form the basis for the characterization of risk and human health hazard presented here. Potential hazards are quantified as risk estimates for carcinogenic chemicals, and as hazard quotients for noncarcinogenic chemicals, according to equations presented below.

For carcinogens, risks are estimated as the likelihood of an individual developing cancer over a lifetime as a result of exposure to a potential carcinogen (incremental or excess individual lifetime cancer risk). The lifetime risk of cancer incidence is estimated using USEPA slope factors for chemical carcinogens for inhalation and ingestion exposure pathways (Table 5.20). Dermal exposures are evaluated as equivalent ingestion intakes as described in the sections on dermal absorption pathways. The USEPA slope factors give the lifetime cancer incidence risk per average daily dose. For inhalation and ingestion exposures, the lifetime cancer incidence risk is evaluated as follows:

$$R_{pi} = ADD_{pi} \ SF_i \qquad\qquad (5.64)$$

where: R_{pi} = risk of developing cancer from the lifetime exposure for pathway p and metal i (risk/lifetime)

ADD_{pi} = average daily dose for exposure pathway p for metal i (mg/kg/d)

SF_i = slope factor for cancer incidence risk for metal i (risk per mg/kg/d dose).

Table 5.20. Reference dose[1] and slope factors by metal and exposure route for evaluating human health risk.

Contaminant ------------------- Exposure Route	Non-Carcinogen Reference Dose (R_fD) (mg/kg/d)		Carcinogen Slope Factor (risk per mg/kg/d)	
	Inhalation	Ingestion	Inhalation	Ingestion
Cobalt	3.5E-04	8.1E-03	NC	NC
Copper	1.0E-02	3.7E-02	NC	NC
Manganese	1.43E-03[1]	7.0E-02	NC	NC
Nickel	C	2.0E-02[2]	8.4E-01[2]	NC

C   = Carcinogen
NC = Non-Carcinogen
1   = Default value in MEPAS database unless otherwise noted
2   = IRIS approved R_fD or Slope Factor

When the risk value estimated using Equation (5.64) is greater than 0.01, the value is revised using the following equation, which mathematically limits the maximum risk value to 1.0:

$$R_{pi} = 1 - e^{-ADD_{pi} \ SF_i} \qquad\qquad (5.65)$$

where terms are as previous defined.

In the present study, any metal-derived from penetrator munition alloys whose pathway-specific risk or total risk exceeds 1.0E-06 is considered a contaminant of potential concern with regard to evaluating potential human health impacts of penetrator munitions testing at Test Area C-64A.

Potential human health hazards associated with exposure to noncarcinogenic substances are expressed as a hazard quotient. The average daily dose over a specified time interval (lifetime or shorter) is compared to a reference dose (R_fD), and the ratio of the average daily dose to the reference dose is defined as the hazard quotient:

$$HQ_{pi} = ADD_{pi}/R_fD_{pi} \tag{5.66}$$

where HQ_{pi} = hazard quotient for the ingestion or inhalation pathway p and non-carcinogenic metal i.

ADD_{pi} = average daily dose along the ingestion or inhalation pathway p for non-carcinogenic metal i.

R_fD_{pi} = reference dose for the ingestion or inhalation pathway p and non-carcinogenic metal i.

Dermal exposures are treated as equivalent ingestion exposures prior to calculating a dermal exposure hazard quotient.

MEPAS uses reference doses established in the IRIS database by the EPA (USEPA, 1993) and from other sources for calculating hazard quotients based on modeled exposures (Table 5.20). Reference doses represent a level that is believed to be safe for members of the general population. Exposure at this level will result in hazard quotient of 1.0. If the hazard quotient exceeds unity, the possibility exists for systemic toxic effects. The hazard quotient is not a mathematical prediction of the severity or incidence of the effects, but rather is an indication that effects may occur. Hazard quotient values can also be added across exposure pathways or contaminants. The sum of hazard quotients is referred to as a hazard index (HI). Note that only individual hazard quotients and indices are presented when evaluating noncarcinogenic chemical hazard.

In the present study, any metal derived from penetrator munition alloys whose pathway specific HQ_{pi} or total HI exceeds 1.0 is considered a contaminant of potential concern with regard to evaluating potential human health impacts of penetrator munitions testing at Test Area C-64A.

5.3.2.1   Noncarcinogenic Hazard

Risk analysis HQ and HI results for exposure pathways identified in Section 5.3.1.3 are presented in Tables 5.21 through 5.24, for each metal and penetrator munition alloy tested in the current study. Hazard quotients and hazard indices reported in the tables are one or more orders of magnitude below 1.0, indicating that, in general, toxic effects from human exposure to metal contamination from different penetrator alloys are not expected at exposure levels estimated in this study.

Table 5.21. Hazard quotients for alloy WL-1 by exposure pathway.

Source Area Soil Exposure Pathways	Nickel	Manganese
Soil Ingestion	1.3E-03	9.2E-05
Soil Dermal Contact	1.5E-03	5.3E-05
Resuspended Soil Inhalation	CR	9.0E-05
Leafy Vegetables Ingestion	4.1E-03	7.2E-04
Other Vegetables Ingestion	2.5E-02	4.5E-03
Meat Ingestion	7.6E-03	7.3E-05
Milk Ingestion	1.3E-03	6.2E-05
Local Well Groundwater Exposure Pathways	**Nickel**	**Manganese**
Drinking Water Ingestion	2.9E-03	1.5E-05
Showering Dermal	9.5E-06	1.7E-07
Showering Ingestion	1.4E-05	5.0E-08
Leafy Vegetables Ingestion	3.8E-04	1.7E-06
Other Vegetables Ingestion	7.5E-04	4.8E-06
Meat Ingestion	2.6E-04	9.0E-08
Milk Ingestion	2.0E-04	2.7E-07

Ramer Creek Exposure Pathways	Nickel	Manganese
Swimming Water Ingestion	4.0E-08	1.5E-10
Swimming Water Dermal Contact	1.6E-08	3.0E-10
Shoreline Sediment Dermal Contact	6.1E-07	1.1E-09
Shoreline Sediment Ingestion	1.0E-07	3.8E-10

CR = Carcinogenic Risk for this contaminant and exposure pathway

Table 5.22. Hazard quotients for Alloy NS by exposure pathway.

Source Area Soil Exposure Pathways	Nickel	Cobalt
Soil Ingestion	1.3E-03	7.9E-04
Soil Dermal Contact	1.5E-03	1.5E-04
Resuspended Soil Inhalation	CR	3.7E-04
Leafy Vegetables Ingestion	4.1E-03	1.6E-03
Other Vegetables Ingestion	2.5E-02	9.7E-03
Meat Ingestion	7.6E-03	5.9E-04
Milk Ingestion	1.3E-03	3.0E-04
Local Well Groundwater Exposure Pathways	**Nickel**	**Cobalt**
Drinking Water Ingestion	2.1E-03	3.3E-03
Showering Dermal	7.1E-06	6.7E-06
Showering Ingestion	1.1E-05	1.5E-05
Leafy Vegetables Ingestion	2.8E-04	3.7E-04
Other Vegetables Ingestion	5.6E-04	6.4E-04
Meat Ingestion	1.9E-04	4.0E-05
Milk Ingestion	1.5E-04	1.0E-04
Ramer Creek Exposure Pathways	**Nickel**	**Cobalt**
Swimming Water Ingestion	3.0E-08	4.4E-08
Swimming Water Dermal Contact	1.2E-08	1.2E-08
Shoreline Sediment Dermal Contact	4.6E-07	1.1E-07
Shoreline Sediment Ingestion	7.8E-08	1.1E-07

CR = Carcinogenic Risk for this contaminant and exposure pathway

Table 5.23. Hazard quotients for Alloy HD-17 by exposure pathway.

Source Area Soil Exposure Pathways	Nickel	Copper
Soil Ingestion	1.3E-03	5.0E-04
Soil Dermal Contact	1.5E-03	5.8E-05
Resuspended Soil Inhalation	CR	3.6E-05
Leafy Vegetables Ingestion	4.1E-03	6.5E-03
Other Vegetables Ingestion	2.5E-02	4.0E-02
Meat Ingestion	7.6E-03	1.5E-02
Milk Ingestion	1.3E-03	2.2E-03
Local Well Groundwater Exposure Pathways	**Nickel**	**Copper**
Drinking Water Ingestion	2.6E-03	4.5E-05
Showering Dermal	8.6E-06	1.5E-07
Showering Ingestion	1.3E-05	2.3E-07
Leafy Vegetables Ingestion	3.4E-04	1.0E-05
Other Vegetables Ingestion	6.8E-04	3.3E-05
Meat Ingestion	2.4E-04	1.4E-05
Milk Ingestion	1.8E-04	5.8E-06
Ramer Creek Exposure Pathways	**Nickel**	**Copper**
Swimming Water Ingestion	3.7E-08	2.8E-10
Swimming Water Dermal Contact	1.5E-08	1.1E-10
Shoreline Sediment Dermal Contact	5.5E-07	4.2E-10
Shoreline Sediment Ingestion	9.4E-08	7.1E-10

CR = Carcinogenic Risk for this contaminant and exposure pathway

Table 5.24. Summary hazard indices for alloys.

EXPOSURE PATHWAYS	ALLOY					
	WL-1		NS		HD-17	
	Nickel	Manganese	Nickel	Cobalt	Nickel	Copper
Source Area Soil Exposure Pathways	4.1E-02	5.6E-03	4.1E-02	1.4E-02	4.1E-02	6.4E-02
Local Well Groundwater Exposure Pathways	4.5E-03	2.2E-05	3.3E-03	4.5E-03	4.1E-03	1.1E-04
Ramer Creek Surface Water Exposure Pathways	7.7E-07	1.9E-09	5.8E-07	2.8E-07	7.0E-07	1.8E-09
Total Metal - All Exposure Pathways	4.5E-02	5.6E-03	4.4E-02	1.9E-02	4.5E-02	6.4E-20
Total Alloy - All Exposure Pathways	5.1E-02		6.2E-02		1.1E-01	

Source area soil exposure pathway hazard quotients were generally the highest for any of the pathways and ranged from a low of 5.3E-05 for soil dermal contact with manganese in alloy WL-1 to a high of 4.0E-02 for ingestion of other vegetables containing copper from alloys HD-17. No alloy metals exhibited hazard quotients exceeding 1.0 for any of the source area soil exposure pathways.

5.3.2.2 Carcinogenic Risk

Of the metals contained in alloys evaluated as part of this study, only nickel is potentially carcinogenic when inhaled along with resuspended source area soils. Excess individual lifetime cancer risk for the resuspended source area soil exposure pathway was 4.3E-07 for inhalation of nickel from all alloy sources.

5.3.3 Ecologic Risk Assessment

This section presents the results of an ecological risk assessment, which evaluates the potential for adverse effects to non-domesticated flora and fauna in ecological habitats associated with Test Area C-64A of Eglin Air Force Base in Okaloosa County, Florida. Ecological risk assessment, as defined by the USEPA's *Framework for Ecological Risk Assessment*, is a process that evaluates the likelihood that adverse ecological effects may occur or are occurring because of exposure to one or more stressors (USEPA, 1992; 1998). The potential stressors identified in association with these test areas are metals released to environmental media on or adjacent to the sites as a result of the testing of tantalum and tungsten alloy penetrator munitions. Therefore, the purpose of this ecological risk assessment is to provide a qualitative and quantitative analysis of the likelihood of adverse effects to receptor ecosystems associated with these releases of alloy-derived metals to environmental media on or adjacent to the site.

Objectives

This ecological risk assessment has been conducted according to USEPA guidance (USEPA, 1992; 1998). The objectives of the ecological risk assessment are to:

- Qualitatively characterize the potential ecological receptors that have been observed or could be present in terrestrial or aquatic habitats on or adjacent to the site;

- Assess potential exposures of ecological receptors to constituents of interest in various environmental media within terrestrial or aquatic habitats under current conditions; and

- Characterize the risks associated with exposures of ecological receptors to constituents of interest in various environmental media under current conditions.

Overview

This ecological risk assessment uses the general framework outlined in USEPA (1992) and expanded upon in USEPA (1998). This framework is conceptually similar to the approach used for the human health risk assessment, but is distinctive in its emphasis in three areas:

- The ecological risk assessment considers effects beyond those on individuals of a single species and examines effects on populations, communities, or ecosystems;

- There is no single set of ecological values or resources to be protected that can be generally applied to every site; and

- If appropriate, the ecological risk assessment can consider nonchemical, as well as chemical, stressors.

Approach

As outlined in USEPA (1992, 1998), an ecological risk assessment consists of three main elements:

- **Problem Formulation**. This is a review of available physical and biological data for the site and on receptor habitats that may be affected by releases of constituents to environmental media to (1) identify potential ecological receptors (i.e., biological communities, populations, individuals, or habitats potentially at risk); (2) determine the constituents of interest and other stressors for ecological receptors; (3) identify potential exposure pathways; and (4) determine the appropriate assessment and measurement endpoints for the ecological risk assessment.

- **Analysis (Exposure and Effects Assessments)**. This is a concurrent estimation of the exposure of the ecological receptors to the constituents of interest and identification of exposure-response standards based on the concentrations of constituents of interest in various environmental media.

- **Risk Characterization**. This is a description of the nature and magnitude of potential environmental risks by comparing the exposure estimates for various media, the exposure-response standards for the ecological receptors, and the results of the site-specific surveys and bioassays.

This section is organized in a manner consistent with these elements of an ecological risk assessment. The results of these elements of the ecological risk assessment for Test Area C-64A of Eglin Air Force Base are described in the following subsections.

5.3.3.1 Problem Formulation

The objectives of the problem formulation phase are to identify potential ecological receptor species and habitats, to determine the constituents of interest and other stressors, to identify the likely exposure pathways, and to determine the assessment and measurement endpoints to be evaluated in the ecological risk assessment. The problem formulation is used to create a conceptual site model by describing the ecological receptors and exposure pathways to be evaluated during the analysis phase. As such, the problem formulation consists of the following steps:

- Identification of potential ecological receptors,

- Description of the conceptual site model,

- Selection of the constituents of interest, and

- Selection of appropriate assessment and measurement endpoints.

The potential ecologic receptors are identified in Section 2.7. The following subsections describe the results of the remaining steps.

Conceptual Site Model

A conceptual site model was developed for Test Area C-64A to focus the assessment on those ecological receptors and exposure pathways most relevant to current site conditions. The

conceptual site model identifies the likely transport and exposure pathways for constituents of interest in various environmental media to ecological receptors associated with the site.

Potential Exposure Pathways

Part of the rationale for selection of ecological receptor habitats and species is the presence of complete exposure pathways for the constituents of interest. A complete exposure pathway is one that meets the following four criteria (USEPA, 1989a):

- A source of constituents of interest must be present;

- Release and transport mechanisms and media must be available to move the constituents from the source to the ecological receptors;

- An opportunity must exist for the ecological receptors to contact the affected media; and

- A means must exist by which the constituent is taken up by ecological receptors, such as ingestion or direct contact.

Source, Release Mechanisms, Transport Media, and Exposure Media

The source of the constituents of interest for Test Area C-64A are alloy fragments remaining from munitions tests. The metallic residues are primarily small fragments (< 1 cm^3) of metal alloys containing tungsten (W), tantalum (Ta), nickel (Ni), cobalt (Co), iron (Fe), copper (Cu), and/or manganese (Mn). These chunks are exposed to the weather at the soil surface. In time, the metals in these chunks leach into the surface soils, and eventually may leach to groundwater. With groundwater, the metals may be transported to surface waters in Ramer Creek and then by surface flow to Titi Creek.

Potential Exposure Points

An exposure point is a location of contact between ecological receptors and metals of interest. Exposure points for terrestrial habitats would be surface soils or vegetation that may

have absorbed metals from surface soils. Surface water in Ramer Creek would be the exposure point in the aquatic habitats associated with the site.

Potential Exposure Routes

An exposure route is the mechanism by which a receptor species might take up a metal. For surface soils and terrestrial receptors, exposure to metal of interest may occur through three routes: (1) direct (including dermal) contact with soils, (2) inhalation, (3) ingestion of plants, animal prey, and soil (i.e., incidental ingestion of soil from feeding or grooming). In aquatic habitats, exposure of constituents of interest may occur through one primary route: (1) direct contact with surface water.

Surface Soils in Terrestrial Habitats

Direct Contact with Soils. This exposure route is important for uptake of the metals of interest by plants. Animals that forage in the terrestrial habitat associated with the test areas also have the potential to be exposed to metals of interest via dermal contact, but the dermal exposure pathway is not believed to be important for birds and mammals in these habitats because of the low dermal absorption potential of metals, the low concentration of organic compounds, the lack of exposed soils because of vegetation cover, and protection from dermal contact by fur and feathers. Any incidental surface contamination of the fur or feathers that is subsequently ingested is accounted for in the incidental soil ingestion pathway (USEPA, 1993),

Inhalation. Inhalation exposure is expected to be a minor contributor to metal uptake by terrestrial ecological receptors because the metals of interest are not VOCs. Also, metals in airborne dust from surface soils are likely to be minimal because of the vegetation cover, and dusts that may be deposited on plants are accounted for in the incidental soil ingestion pathway.

Ingestion of Plants and Soil. Herbivorous animals, such as the beach mouse and eastern meadowlark, may consume plants growing in terrestrial habitats associated with the test area. While foraging within these habitats, both herbivores may also incidentally ingest some surface soil with their food or during grooming.

Surface Water in Aquatic Habitats

Direct Contact with Surface Water. Aquatic invertebrates and fish are exposed directly to metals of interest in surface water.

Complete Exposure Pathways

Based on this evaluation, there are complete ecological exposure pathways for two types of environmental media associated with the site that may be potentially affected by releases of metals from the site: surface soil and surface water. The next section presents the potential metals of interest associated with these media.

Constituents of Interest

Based on analyses of the metallic residues, the following metals were identified as constituents of interest for both surface soil and surface water; tungsten (W), tantalum (Ta), nickel (Ni), cobalt (Co), iron (Fe), copper (Cu), and manganese (Mn)

Selection of Assessment and Measurement Endpoints

Two types of ecological endpoints are considered in this ecological risk assessment: assessment and measurement endpoints. Based on these endpoints, representative ecological receptors are selected for further analysis in the ecological risk assessment.

Assessment Endpoints

Assessment endpoints are explicit expressions of the environmental values or characteristics to be protected at a site (USEPA, 1992) and reflect societal and ecological values (USEPA, 1989b, 1992). Societal values address the need to protect species that are endangered, threatened, or of special interest, important as game or commercial species, or widely recognized as having aesthetic value. Ecological relevance refers to the importance of the species to the function of the ecosystem. Therefore, evaluation of the potential for adverse effects at the population level is used to infer the potential for adverse effects at higher levels of organization

such as communities and ecosystems. Based on the conceptual model for each ecological habitat, the following assessment endpoints are identified for the ecological risk assessment:

- Populations of terrestrial birds or mammals that could be reduced because of increased mortality or decreased reproduction because of releases of the metals of interest to surface soils.

- Populations of fish and aquatic invertebrates in Ramer Creek that may be reduced because of increased mortality or decreased reproduction because of releases of the metals of interest to surface water.

Measurement Endpoints

Measurement endpoints are measurable responses to stressors at a site that are related to the assessment endpoints and are intended to provide a basis for assessing the potential for risk with respect to the assessment point. They may be defined in terms of an unacceptable level of impact to ecological receptors, such as a certain relative percent decrease in survival or reproduction of ecological populations (Suter, 1993), but because the objective of this ecological risk assessment is to assess the potential for adverse effects to ecological receptors, the measurement endpoints for this ecological risk assessment are not defined in terms of specific threshold levels of ecological impact. As part of a weight-of-evidence approach, one or more measurement endpoints may be used for each assessment endpoint. The measurement endpoints for each ecological habitat in this ecological risk assessment are as follows.

- Whether the estimated concentrations of the metals of interest in surface soil of the test areas are likely to result in doses to terrestrial birds or mammals that are greater than those observed to result in increased mortality or decreased reproduction of these wildlife upon chronic exposure.

- Whether the estimated concentrations of the metals of interest in surface water of Ramer Creek are greater than those observed to result in increased mortality or decreased reproduction of fish and aquatic invertebrates upon chronic exposure.

Therefore, key components of this ecological risk assessment are:

- characterizations of the relationship between the amount of a metal of interest present surface water and a threshold for adverse effects,

- characterization of the relationship between the dose resulting from the amount of a metal of interest present in surface soil and a threshold dose for adverse effects,

Significant information for this ecological risk assessment is the threshold level or dose for adverse effects for each metal of interest and how exposures of ecological receptors compare with these values. For aquatic receptors, which are constantly in contact with surface water or sediments, this is a consideration of ambient metal concentrations and response. For wildlife receptors, which are intermittently exposed to metals in surface soil though ingestion, this is a consideration of ingested dose and response. This information is available in peer-reviewed literature rather than in the site-specific data. The measurement endpoints are related to the assessment endpoints in that the studies of adverse effects of metals of interest in the literature have been extrapolated to the conditions on Test Area C-64A.

Representative Ecological Receptors

Representative ecological receptor species are those that represent populations that might be exposed to metals of interest in different habitats on the test sites. To assess the potential for adverse ecological effects because of the metals of interest identified with various environmental media, several representative ecological receptor species were selected for detailed analysis. The selection of species or functional groups is based on residence in the receptor habitats, population dynamics, toxicological sensitivity to the metals of interest, ecological relevance, and other factors that may affect the perceived value of different species such as status as a game or commercial species or as a threatened or endangered species. For the purposes of this ecological risk assessment, the following representative species and functional groups were evaluated as potential ecological receptors:

- A terrestrial mammal that is common in the grassland on the test sites, the beach or old field mouse;

- A terrestrial bird that nests and forages in grassland habitats on the test sites, the eastern meadowlark; and

- Aquatic invertebrates and fish that inhabit Ramer Creek.

No specific fish or aquatic invertebrates were selected as a representative species, but bioassay data for the most sensitive species (based on the bioassay data), which is representative of the species expected in the aquatic habitats, will be used to determine the chronic effects values used in the risk characterization.

Because more specific exposure scenarios are required to assess the exposure of wildlife receptors, the beach mouse and eastern meadowlark will be assessed as representative wildlife species in this ecological risk assessment. These species were chosen because they are dominant species among those species of wildlife observed in the vicinity of the receptor habitats.

5.3.3.2   Analysis

The analysis phase of the ecological risk assessment is a parallel technical evaluation of data on the exposure of the ecological receptors to the identified stressors with data on the potential effects of the identified stressors based on the conceptual model. As such, this phase consists of two interactive steps that:

- characterize the exposure of ecological receptors to the metals of interest and

- characterize the potential effects on ecological receptors of the metals of interest.

Characterization of Exposure

Exposure is defined as contact between an ecological receptor and metals of interest in an environmental medium. For exposure to occur, a metal release must occur to an environmental medium, and an ecological receptor must have a point of potential contact with that medium. The first step in the characterization of exposure is the estimation of exposure point concentrations for the environmental media to which the receptors may be exposed. In ecological risk assessments where the level of protection is the population, the exposure point concentrations are the mean concentration of the metals of interest as estimated from the available constituent data.

Exposure is evaluated differently for receptors in continuous contact with an environmental medium (e.g., aquatic invertebrates) versus those with intermittent exposure (e.g., waterfowl). For aquatic invertebrates, effects are related to the exposure point concentrations in surface water or sediments, whereas an ingested dose is used for birds or mammals. Specific exposure pathways are generally not evaluated in aquatic invertebrate bioassays. The assumption for these receptors is that if the metals are present in the habitation medium (i.e., surface water or sediments), then exposure will occur.

For birds and mammals, the magnitude, duration, frequency, and route of exposure are factors that may affect exposure to the metals of interest. This is analogous to the exposure assessment for human receptors. Thus, a dose calculation is possible based on these specific exposure factors once an exposure point concentration is estimated.

Representative Concentrations of Constituents of interest

Computer transport-pathway models in MEPAS were used to predict the representative concentrations of the metals of interest in ground water and surface water. Surface soil concentrations were calculated according to methods described in section 3.6. These representative concentrations are presented in Table 5.25.

Table 5.25. Representative concentrations of metals of interest.

Metal	Maximum Concentration	
	Surface Soil (mg/kg)	Surface Water (µg/l)
Cobalt	90	0.008
Copper	250	0.0002
Iron	250	--[1]
Manganese	90	0.0002
Nickel	360	0.017
Tantalum	5500	--[1]
Tungsten	5500	--[1]

[1] Effective concentrations in surface water are zero.

Wildlife Exposure Estimates

The avian and mammalian wildlife evaluated as ecological receptors in the ecological risk assessment are the beach mouse and eastern meadowlark. For these ecological receptors, the magnitude, duration, frequency, and route of exposure are factors that will affect the degree of exposure to the metals of interest. Thus, doses can be calculated based on these specific exposure factors.

The primary exposure pathway for a terrestrial herbivore, such as the beach mouse, is the ingestion of plants that may have bioaccumulated metals of interest from surface soils. The primary exposure pathway for a terrestrial insectivore and herbivore, such as the eastern meadowlark, is the ingestion of plants or insects that have bioaccumulated metals of interest from surface soils. To a lesser degree, these animals may be exposed to metals of interest through incidental ingestion of surface soils during foraging and grooming of their feathers or fur. Other potential exposure pathways are negligible in their contribution to the total calculated dose for wildlife foraging on the test areas. The total daily dose because of exposure via these

pathways for terrestrial receptors is the sum of the doses for each pathway. Therefore, the total average daily dose (ADD_t) is calculated as:

$$ADD_t = ADD_f + ADD_s \qquad (5.68)$$

Where ADD_f is the average daily dose from ingestion of food and ADD_s is the average daily dose from incidental ingestion of surface soil.

The derivation of the specific exposure factors used in the calculation of a dose is described in the following subsections. Lacking species-specific data, conservative exposure assumptions were used.

Ingestion of Food - Beach mouse

The beach mouse is a herbivore that feeds primarily on vegetation. Table 5.26 presents the values used in the dose calculation for ingestion of plants by beach mouse. The derivation of these values are as follows.

Table 5.26. Values used in dose calculations for ingestion of food.

Symbol	Exposure Factor	Beach mouse	Eastern meadowlark
CS	Chemical concentration in Soil (mg DW/kg)	Chemical Specific	
UP_p	Uptake Factor for Plants (unitless)	Chemical Specific	
UP_a	Uptake Factor for Animals (unitless)		
IR_f	Ingestion Rate - Food (kg/day)	0.00107	0.0093
FF_p	Fraction of Food - Plants (unitless)	1.0	0.26
FF_a	Fraction of Food - Animals (unitless)		0.74
FS	Fraction of Food Derived from the Site (unitless)	1.0	0.77
AF	Gastric Absorption Factor (unitless)	1.0	1.0
BW	Body Weight (kg)	0.0128	0.0963

Equations:

$$ADD_p = CS \times UP_p \times IR_f \times FF_p \times FS \times AF \times 1/BW \qquad (5.69)$$

$$ADD_a = CS \times UP_a \times IR_f \times FF_a \times FS \times AF \times 1/BW \qquad (5.70)$$

Uptake Factor for Plants. Since no data were available on the concentrations of constituents of interest in plant tissues, soil-to-plant uptake factors were used to estimate these concentrations in plants. The uptake factor for plants (UP_{sp}) is the ratio of the concentration of each ecological metal of interest in plants to that in soil.

For metals, the UP_{sp} were derived from Baes et al. (1984) who estimated a soil-to-vegetation elemental transfer coefficient (B_v) based on an extensive literature review of measured soil and plant tissue concentrations. The uptake factors for each ecological metal of interest in surface soils are presented in Table 5.27.

Table 5.27. Derivation of plant and animal uptake factors for the metals of interest in surface soils.

Constituent	UP_{sp} [1]	UP_{si} [2]
Cobalt	0.020	0.40 [3]
Copper	0.40	0.52
Iron	0.0040	0.38
Manganese	0.25	0.40
Nickel	0.060	0.41
Tantalum	0.010	0.40 [3]
Tungsten	0.045	0.40 [3]

[1] From Baes et al. (1984).
[2] From Beyer & Stafford (1993).
[3] In the absence of a value from Beyer & Stafford (1993), a value of 0.40 was assumed.

Ingestion Rate. The food ingestion rate (IR_f) for the beach mouse is reported to be 0.00107 kg DW/day (Phelan and Baker, 1992).

Fraction of Food from Plants. The beach mouse is herbivorous and feeds primarily on the seeds of common herbaceous plants, such as *Aristida, Lespedeza, Diodia, Rumex,* and *Galactea* (Plelan and Baker, 1992). Therefore, the fraction of food obtained from plants for a beach mouse is 1.0.

Fraction of Food Derived from the Site. The home range of the beach mouse is similar to that of the deer mouse (*Peromyscus leucopus*), which has a home range of about 0.15 acres (USEPA, 1993). The area of the C-64A test area is about 5.74 acres. The mice use and forage in grassland areas and would use much of this area. It is a nonmigratory species that will spend the entire year near the site. Therefore, the fraction of food derived from the test areas by a resident mouse would be 1.0.

Gastric Absorption Factor. The gastric absorption factor is the ratio of gastric absorption of the constituent from the plants relative to the medium in which the metal is administered in bioassays. Since most bioassay data for mammals or birds are based on a dose in food, a gastric absorption factor of 1.0 was used.

Body Weight. For the beach mouse, average body weight is 0.0128 kg (Phelan and Baker, 1992).

Ingestion of Food - Eastern meadowlark

The diet of the eastern meadowlark includes both plants and animal prey. The animal prey of the eastern meadowlark is primarily insects. Therefore, the ADD_f for the eastern meadowlark is the sum of the average daily dose from plants (ADD_p) and that from animal prey (ADD_a):

$$ADD_f = ADD_p + ADD_a \qquad (5.71)$$

Table 5.26 presents the values used in the dose calculation for ingestion of plants and of animal prey by the eastern meadowlark. The derivation of these values are as follows. Specific data were selected for the subspecies, *S. magna argutata*, which is the subspecies of the eastern meadowlark that occurs in Florida.

Uptake Factors for Plants and Animals. No data were available on the concentrations of metals of interest in plant or invertebrate tissues. Therefore, soil-to-plant (Up_{sp}) and

soil-to-invertebrate uptake (UP_{si}) factors were used to estimate these concentrations in plants and invertebrate prey (Table 5.27).

The UP_{sp} estimates the uptake of each constituent of interest in plants. It is calculated as described for the terrestrial herbivores above.

For invertebrates, such as worms, the UP_{si} estimates bioaccumulation from soils. For metals, the concentration factor for earthworms from Beyer and Stafford (1993) was used as the Up_{si}.

Ingestion Rate. The mean food ingestion rate (dry weight - DW) for the eastern meadowlark may be estimated from body weight with the allometric equation for non-passerine birds from Nagy (1987):

$$IR\ (g\ DW) = 0.301\ BW(g)^{0.751} \qquad\qquad (5.73)$$

Based on a mean body weight of 0.0963 kg for the subspecies, *S. m. argutula* (Lanyon, 1995), the mean food ingestion rate would be 0.0093 kg DW/day.

Fraction of Food as Animals and Plants. The eastern meadowlark forages on a mixture of invertebrate prey and plant seeds. The relative proportions of invertebrates and plants seeds are 74% and 26%, respectively (Lanyon, 1995). Therefore, the fraction of food obtained from invertebrate prey is 0.74 and plants is 0.26.

Fraction of Food Derived from the Site. The eastern meadowlark is largely sedentary throughout most of its range. During the breeding season, the adults maintain a multipurpose territory within which they gather food, mate, and rear young. The average size of this territory is about 7.4 acres (3.0 ha) (Lanyon, 1995). Therefore, the fraction of food derived from the site by a resident pair would be 5.74/7.4 = 0.78.

Gastric Absorption Factor. The gastric absorption factor is the ratio of gastric absorption of the metal from food relative to the medium in which the metal is administered in

bioassays. Since most bioassay data for birds is based on a dose in food, a gastric absorption factor of 1.0 was used.

Body Weight. For *S. m. argutula*, the subspecies of the eastern meadowlark that occurs in Florida, average body weight is 0.0963 kg (USEPA, 1993).

Incidental Ingestion of Soil - Terrestrial Receptors

Table 5.28 presents the values used in the dose calculation for incidental ingestion of surface soil while grooming, preening, or foraging. Most of the values are the same as those used for ingestion of food for the beach mouse and eastern meadowlark, except the following.

Ingestion Rate - Soil. Although no species specific data for soil ingestion is available for the beach mouse and eastern meadowlark, Beyer et al. (1993) estimated soil ingestion for the white-footed mouse (*Peromyscus leucopus*) as 2.0% of food ingestion. Soil ingestion of 10.4% for the American woodcock (*Scolopax minor*) would be a conservative estimate for the eastern meadowlark. The resulting soil ingestion rates (IR_s) are 0.000021 kg/day for the beach mouse and 0.00097 kg/day for the eastern meadowlark.

Table 5.28. Values used in dose calculations for incidental ingestion of surface soil.

Symbol	Exposure Factor	Beach mouse	Eastern meadowlark
CS	Constituent Concentration in Soil (mg/kg)	Chemical Specific	
IR_s	Ingestion Rate - Soil (kg/day)	0.00021	0.00097
FS	Fraction of Soil from the Site (unitless)	1.0	1.0
AF_s	Gastric Absorption Factor - Soil (unitless)	1.0	1.0
BW	Body Weight (kg)	0.0128	0.0963

Equation:

$$ADD_s = CS \times IR_s \times FS \times AF_s \times 1/BW \qquad (5.72)$$

Gastric Absorption Factor. Many of the metals of interest in soils are bound to soil particles and are not readily bioavailable. However, without site-specific data, a conservative value of 1.0 was used in this risk assessment.

Exposure Estimates for Aquatic Receptors

Exposure is evaluated differently for receptors in continuous contact with an environmental medium (e.g., aquatic receptors) and those with intermittent exposure (e.g., birds, mammals, and humans). For aquatic receptors, effects are related to the concentration in the environmental medium, instead of an ingested dose. Specific exposure routes are not evaluated. The assumption is that if the metals are present in the habitation medium, then exposure will occur.

Surface Water

The toxicity of constituents in surface water to aquatic receptors is generally related to the ambient concentration. Therefore, exposures for aquatic receptors are assessed as the representative concentrations of the metals of interest in surface water (Table 5.24).

Characterization of Ecological Effects

The measurement endpoint for this ecological risk assessment is whether the observed concentrations of the metals of interest in an environmental medium and ecological habitat are greater than those associated with increased mortality or decreased reproduction of the ecological receptors with chronic exposure. Therefore, a key component of the ecological risk assessment is characterization of the relationship between the amount of a metal of interest present in each environmental medium and the potential for adverse effects. For birds and mammals, this is a consideration of ingested dose and response, while the ambient concentration and response are the relationship assessed in aquatic organisms, such as invertebrates and fish. The significant information for this ecological risk assessment is the threshold level for ecological effects for each metal of interest and how concentrations in environmental media compare with these values.

The toxicity values that are the most valuable for estimating the threshold for effects include the chronic ambient water quality criterion (AWQC), final chronic value (FCV), or no-observed-adverse-effects-level (NOAEL). These are values determined through chronic toxicity studies. Organisms exposed over a long period to levels of a metal of interest below a chronic AWQC, FCV, or NOAEL would not be expected to experience adverse effects.

When sufficient bioassay data are available, USEPA has used numerical methods to derive chronic criteria (Stephan et al., 1983), called ambient water quality criteria (AWQCs). The FCV is derived in the same manner as a chronic AWQC, but can be more site-specific, because only bioassay data for potential receptors at a site are used to derive the FCV.

The NOAEL is generally used if the bioassay data for a metal is limited. The NOAEL is the greatest concentration of a metal at which no adverse effects were observed in a toxicity study. In addition, the Lowest-Observed-Adverse-Effects-Level (LOAEL) is generally observed in toxicity studies. This is the lowest concentration of a metal at which adverse effects were discernible. If a NOAEL is not observed in a toxicity study, a NOAEL can be approximated from a LOAEL by incorporating uncertainty factors. If chronic toxicity data are not available for a metal of interest, acute toxicity data can be used to estimate chronic-effects-levels. If toxicity data are available for several potential receptor species, data for the most sensitive species are used. In the following sections, specific toxicity considerations for different types of receptors and environmental media are described.

Terrestrial Avian and Mammalian Receptors

Terrestrial birds and mammals are considered potential ecological receptors in terrestrial habitats associated with the test area; the beach mouse and eastern meadowlark were chosen as representative terrestrial receptors. These terrestrial receptors may be exposed to metals of interest in surface soils through incidental ingestion of surface soil with food or while grooming and by ingestion of plants or animal prey exposed to the surface soils. Bioassay data for terrestrial receptors are generally expressed in terms of the concentration of the metal of interest ingested by the organism.

Reference toxicity criteria were derived from studies of birds or mammals that ingested food containing the metals of interest in surface soils (Table 5.29). When data were available, studies of the representative terrestrial receptors were used. If such data were unavailable, data for the most sensitive species tested were used. If the endpoint of the bioassay was not a chronic NOAEL, the following factors were used to extrapolate the available data to a chronic NOAEL (Watkin and Stelljes, 1993):

- A LOAEL to a NOAEL   divide by 5

- A LD$_{50}$ to a NOAEL   divide by 6

- A subchronic study to a chronic study   divide by 5

- An acute study to a chronic study   divide by 10

For example, a subchronic LOAEL would be extrapolated to a chronic NOAEL by division with 25 (i.e., 5 * 5). If data for either birds or mammals were not available, a reference toxicity criterion for those receptors was not derived.

If data for the specific representative mammalian receptors were not available, a body size scaling factor (Sample et al., 1996) was used for extrapolation of the available data between species. The body size scaling factor is calculated as:

$$Body\ Size\ Scaling\ Factor = \sqrt[4]{BW_t/BW_r} \qquad (5.74)$$

Where BW$_t$ is the mean body weight of the test species and BW$_r$ is the mean body weight of the receptor species. Calculations for the body size scaling factors used in the mammalian ecological receptors are presented in Table 5.30. Recent research by Mineau et al. (1996)

Table 5.29. Derivation of reference toxicity dose of the constituents of interest in surface soils.

Metal	Test Organism	Effect	Endpoint	Daily Dose (mg/kg-day)	Reference	Total Uncertainty Factor[1]	Chronic NOAEL - Test Organism (mg/kg-day)
Cobalt	Rat	mortality	acute LD$_{50}$	6,171	RTECS (1998)	60	102
	--	--	--	--	--	--	--
Copper	Mink	reproduction	chronic NOAEL	11.7	Aulerich et al. (1982) Sample et al. (1996)	1	11.7
	Chicken (chicks)	growth	chronic NOAEL	47.0	Mehring et al. (1960) Sample et al. (1996)	1	47.0
Iron	Rat	mortality	acute LD$_{50}$	30,000	RTECS (1998)	60	500
	--	--	--	--	--	--	--
Manganese	Rat	reproduction	chronic NOAEL	284	Laskey et al. (1982) USEPA (1988a)	1	284
	Japanese quail	growth, aggressive behavior	chronic NOAEL	977	Laskey & Edens (1985) Sample et al. (1996)	1	977
Nickel	Rat	reproduction	chronic NOAEL	40.0	Ambrose et al. (1976) Sample et al. (1996)	1	40.0
	Mallard (ducklings)	mortality, growth, behavior	chronic NOAEL	77.4	Cain & Pafford (1981) Sample et al. (1996)	1	77.4
Tantalum	Rat	mortality	acute LOAEL	3,760	RTECS (1998)	50	75.2
	--	--	--	--	--	--	--
Tungsten	Rat	mortality	acute LD$_{50}$	5000	Venugopal & Luckey (1978)	50	100
	Mallard	mortality	chronic NOAEL	406	Ringelman et al. (1993)	1	406

[1] Uncertainty factors were used as described in this section.

-- = Not available

Table 5.30. Calculation of body size scaling factors for extrapolation of toxicological data for mammalians.

Test Species	Mean Body Weight (kg)	Reference	Receptor Species	Mean Body Weight (kg)	Reference	Scaling Factor
Rat	0.35	USEPA (1988)	Beach mouse	0.128	Phelan & Baker, 1992	2.29
Mink	1.0	USEPA (1993)	Beach mouse	0.128	Phelan & Baker, 1992	2.97

suggests that scaling factors as developed for mammals may not be appropriate for extrapolation between different species of birds (Sample et al., 1996). Mineau et al. (1996) calculated body size scaling factors for a number of pesticides and found that the scaling factors were generally not significantly different from one. Therefore, a body size scaling factor of one was used for birds. The derivation of the reference toxicity doses for the metals of interest detected in surface soils of the test area are presented Table 5.31 for the beach mouse and eastern meadowlark.

Aquatic Receptors

Aquatic receptors such as invertebrates or fish may be exposed to metals of interest in surface water or in sediments. Bioassay data for aquatic organisms are generally expressed in terms of the concentration of the metal in the environmental medium tested.

Surface Water

For surface water, reference toxicity criteria were derived directly from bioassay data for aquatic organisms in water (Table 5.32). In the cases of copper and nickel, the chronic AWQCs are variable and are related to water hardness (mg CaCO$_3$/L). AWQCs for these metals were calculated with the following equations based on a mean water hardness of 5.8 mg CaCO$_3$ measured for the site:

$$chronic\ AWQC_{total\ Cu} = e^{0.8545(ln(hardness)) - 1.465} \tag{5.75}$$

$$chronic\ AWQC_{total\ Ni} = e^{0.8460(ln(hardness)) + 1.1645} \tag{5.76}$$

The dissolved criterion is calculated by multiplying the total criterion by conversion factor of 0.960 or 0.997 for copper and nickel, respectively. In the cases of cobalt and manganese, Tier II values as described in Suter (1996) were available.

Table 5.31. Derivation of reference toxicity dose for the metals of interest in surface soils.

Metal	Test Species	Chronic NOAEL - Test Species (mg/kg-day)	Receptor Species	Body Weight Scaling Factor[2]	Reference Toxicity Dose (mg/kg-day)
Cobalt	Rat	102	Beach mouse	2.29	234
	--	--	Eastern meadowlark	1.0	--
Copper	Mink	11.7	Beach mouse	2.97	34.7
	Chicken (chicks)	47.0	Eastern meadowlark	1.0	47.0
Iron	Rat	500	Beach mouse	2.29	1150
	--	--	Eastern meadowlark	1.0	--
Manganese	Rat	284	Beach mouse	2.29	650
	Japanese quail	977	Eastern meadowlark	1.0	977
Nickel	Rat	40.0	Beach mouse	2.29	91.6
	Mallard (ducklings)	77.4	Eastern meadowlark	1.0	77.4
Tantalum	Rat	3,760	Beach mouse	2.29	8,610
	--	--	Eastern meadowlark	1.0	--
Tungsten	Rat	100	Beach mouse	2.29	229
	Mallard	406	Eastern meadowlark	1.0	406

[1] Uncertainty factors were used as described in this section.
[2] The reference toxicity dose for the beach mouse was estimated from the chronic NOAEL for the test species by multiplication with the body size scaling factor as described in Sample et al. (1996) and calculated in Table 5.27.

-- = Not available

Table 5.32. Derivation of reference toxicity values for metals of potential concern in surface water.

Metal	Receptor Species	Literature Value (μg/L)	Adverse Effect	Reference	Reference Toxicity Value[1] (μg/L)
Copper	--	chronic AWQC = 1.04 (hardness = 5.8 mg/L)	--	USEPA (1996)	AWQC = 1.04[2]
Cobalt	--	Tier II value = 3.06	--	Suter (1996)	Tier II value =3.06[3]
Manganese	--	Tier II value = 80.0	--	Suter (1996)	Tier II value = 80.0[3]
Nickel	--	chronic AWQC = 14.2 (Hardness = 5.8 mg/L)	--	USEPA (1996)	AWQC = 14.2[2]

[1] Methods for deriving Reference Toxicity Values is presented in this section.
[2] Based on freshwater acute or chronic ambient water quality criteria (AWQC, USEPA, 1996). For metals in which toxicity is related to hardness, mean hardness for water samples from the site is 5.8 mg/L.
[3] Based on Tier II value (Suter, 1996).

5.3.3.3 Risk Characterization

Risk characterization is the final step of an ecological risk assessment. It includes a description of the potential nature and magnitude of adverse effects that may occur to receptor species because of the presence of metals of interest in the identified ecological habitats on or adjacent to the site. In this step, the characterization of exposure and the characterization of ecological effects for each metal of interest are integrated into quantitative and qualitative estimates of the potential for adverse effects to ecological receptors.

Approach

The measurement endpoints of this ecological assessment are to determine whether the observed concentrations of the metals of interest in surface water or sediment are greater than those that are known or suspected to result in increased mortality or decreased reproduction of the ecological receptors following chronic exposure. Therefore, the estimated exposure concentrations of the metals of interest in surface water or sediments are compared with the metal-specific reference toxicity values. To quantify this comparison and characterize the potential ecological risk, ecological quotients were calculated. For aquatic receptors, the ecological quotient is calculated as:

$$\text{Ecological Quotient} = \frac{\text{Exposure point concentration}}{\text{Reference toxicity value}} \qquad (5.77)$$

For terrestrial and aquatic avian and mammalian receptors, the ecological quotient is calculated as:

$$\text{Ecological Quotien} = \frac{\text{Calculated exposure dose}}{\text{Reference toxicity dose}} \qquad (5.78)$$

In each case, the representative exposures are compared with the metal-specific reference toxicity values. A calculated ecological quotient that is greater than one indicates that a metal of interest may have an adverse effect on the ecological receptors.

Risk Characterization by Environmental Medium

The following sections characterize the potential for adverse effects to receptor species because of the presence of the metals of interest in each of the identified receptor habitats.

Surface Soils

Tables 5.33 and 5.34 present the calculations for the ecological hazard quotients to quantify the potential for adverse effects to the representative ecological receptors in the test areas because of exposure to the maximum estimated concentrations of the metals of interest in surface soils. All the ecological hazard quotients were less than one. Therefore, there is little potential for adverse effects to ecological receptors associated with the metals of interest in surface soils.

Table 5.33. Ecological quotient calculations of exposure of the beach mouse to metals of interest in surface soil.

Metal	Surface Soil Concentration[1] (mg/kg)	Average Daily Dose[2] (mg/kg-day)	Reference Toxicity Dose[3] (mg/kg-day)	Ecological Quotient
Cobalt	90.0	1.63	234	0.0070
Copper	250	12.5	34.7	0.36
Iron	250	4.19	1,150	0.0036
Manganese	90.0	3.36	650	0.0052
Nickel	360	7.71	91.6	0.084
Tantalum	5500	94.8	8,610	0.011
Tantalum	5500	111	229	0.27

[1] From Table 5.25.
[2] Calculated as outlined in this section (Table 5.26).
[3] From Table 5.31.

Table 5.34. Ecological quotient calculations of exposure of the eastern meadowlark to metals of interest in surface soil.

Metal	Surface Soil Concentration[1] (mg/kg)	Average Daily Dose[2] (mg/kg-day)	Reference Toxicity Dose[3] (mg/kg-day)	Ecological Quotient
Cobalt	90.0	0.832	--	--
Copper	250	9.38	47.0	0.41
Iron	250	2.01	--	--
Manganese	90.0	2.37	997	0.0052
Nickel	360	4.40	77.4	0.20
Tantalum	5500	46.7	--	--
Tungsten	5500	61.1	406	0.55

[1] From Table 5.25.
[2] From Table 5.28.
[3] From Table 5.31.

Surface Water

Table 5.35 presents the calculations for the ecological quotients to quantify the potential for adverse effects to aquatic receptors because of exposure to the estimated concentrations of the metals of interest in surface water. All the ecological hazard quotients were less than one. Therefore, there is little potential for adverse effects to ecological receptors associated with the metals of interest in surface water.

Table 5.35. Ecological quotient calculations for aquatic receptors and surface water.

Metal	Surface Water Concentration[1] (μg/L)	Reference Toxicity Value[2] (μg/L)	Ecological Quotient
Cobalt	0.008	1.04	0.008
Copper	0.0002	3.06	< 0.00007
Manganese	0.0002	80.0	0.000003
Nickel	0.017	14.2	0.001

[1] From Table 5.25.
[2] From Table 5.32.

Uncertainty Analysis

Uncertainties are inherent in every aspect of a quantitative ecological risk assessment. Site-specific factors, which this assessment has attempted to incorporate, decrease uncertainty, although uncertainty persists in even the most site-specific and accurate risk assessments. The major sources of uncertainty in this ecological risk assessment are identified below.

- Problem Formulation. Multiple uncertainties exist in the process of identifying potential hazards at a site. These include uncertainties associated with selection of constituents of interest selected for assessment in the ecological risk assessment. However, the procedures used in each of these parts of the problem formulation step are generally conservative and would result in exposure estimates that are greater than those that are likely to be experienced by the ecological receptors. Therefore, the risk of these constituents would generally be overestimated.

- Use of the No-Effect Concentration: A no-effect concentration or threshold (i.e., a NOAEL, an AWQC, and Tier II value) represents protection at the individual level and is more conservative than USEPA guidance, which recommends protection of ecological receptors at the population or community level (USEPA, 1989b). This approach is conservative such that if the observed concentrations of the constituents of interest are less than these thresholds, there is little potential for observable adverse effects on the species or habitats of concern. Also, this is more conservative than the suggestion of Suter et al. (1995) that a 20% effect level be treated as a conservative approximation of the threshold for regulatory concern. Therefore, the use of these reference toxicity values would overestimate the potential for significant adverse effects on species of concern and overestimate the potential for significant ecological risks.

- Lack of Avian RTVs for some Constituents of Interest: Avian toxicity data could not be found for cobalt, iron, and tantalum. Most research on avian toxicity has been concentrated on agricultural chemicals, because of the greater potential for exposure of avian ecological receptors in agroecosystems. As a result, toxicity data is not available for many industrial

constituents, such as the metals, which were the constituents of interest at this site. However, mammalian RTVs were available for these three constituents and the avian average daily dose for each of these constituents were less than the mammalian RTVs (Table 5.36).

Table 5.36. Comparison of average daily dose for the eastern meadowlark to the mammalian Rtvs.

Constituent	Average Daily Dose[1] (mg/kg-day)	Mammalian Reference Toxicity Dose[2] (mg/kg-day)
Cobalt	0.832	102
Iron	2.01	500
Tantalum	46.7	75.2

[1] See Table 5.26.
[2] From Table 5.29.

5.3.3.4 Conclusions

The following subsections describe the conclusions for each environmental medium.

Surface Soils

The results for surface soils indicate that the maximum estimated concentrations of the identified metals of interest were less than those that have been reported to have adverse effects on ecological receptors. These conclusions indicate that the testing of penetrator munitions at Test Area C-64A should not have adverse ecological effects.

Surface Water

The results for surface water indicate that the maximum estimated concentrations of the metals of interest were less than those reported to have adverse effects on ecological receptors. These conclusions indicate that the testing of penetrator munitions at Test Area C-64A should not have adverse ecological effects.

6.0 IMPACT ASSESSMENT

Overall, experimental, transport, and risk assessment results suggest that the use of tantalum or tungsten alloys WL-1 and NS in penetrator munitions tests at the C-64A test area on Eglin AFB will have minimal environmental impacts under testing regimes specified by the AFRL/MN.

The highest potential exposure point concentrations of metals released during the leaching/breakdown of penetrator munition alloys will be found in source area soils. In the case of tantalum, the leaching/breakdown rate is extremely slow with the result that munition fragments will not change much over a period of several thousand years. For tungsten, the sorption coefficient onto soil particles is very high, retarding its migration out of the soil zone. The same situation applies to copper. Nickel, cobalt, and manganese have the greatest potential for migration. However, the alloy that contains cobalt (NS) is leached rather slowly in the type of soil environment present at Test Area C-64A. Soil concentrations of cobalt will remain high for thousands of years. This leaves nickel and manganese as the metals with the greatest potential for migration to ground water and eventually to surface water.

Once metals are released due to leaching/breakdown of penetrator munition alloys, they may be transported from the C-64A test area in air, groundwater, and surface water. Results of transport simulations conducted using MEPAS indicate that metals suspended in air will tend to remain near the test area. Maximum simulated exposure concentrations in air within 100 m of Test Area C-64A will range between a maximum 70 year average of 1E-10 mg/m^3 in air for cobalt and manganese and 5.5E-04 mg/m^3 in air for tungsten and tantalum.

Metals dissolved in infiltrating precipitation will require from 1000 to over 10,000 years to be transported in groundwater to nearby Ramer Creek. For metals dissolved in groundwater, peak simulated exposure point concentrations approximately 550 feet downgradient of the test area generally occurred between 1000 and 2000 years and did not exceed approximately 2.0 ug/l. Peak simulated exposure point concentrations for metals dissolved in Ramer Creek surface water

also generally occurred between 1000 and 2000 years and were no greater than approximately 0.02 ug/l.

Under current conditions, the potential for human exposure at Test Area C-64A would be minimal both immediately after testing and in the future. Therefore, human risk from the testing of tantalum or tungsten alloy munitions would also be minimal. Based on calculations involving exposure to animals and plants, ecologic risk will also be minimal.

If humans take up residence at the site in the future, there are several potential pathways by which such residents could be exposed to metals resulting from the testing of penetrator munitions at the site. Using the MEPAS computer models, inhalation, ingestion, and or dermal contact with metals contained in source area soils, groundwater or nearby surface water were evaluated, along with potential exposure to metals contained in agricultural and animal products that could be produced using contaminated soil and groundwater.

Results of this analysis combined with toxicological data on the health impacts of exposure to these metals indicate that unacceptable non-carcinogenic risk is not expected from exposure to metals derived from the leaching/breakdown of tungsten and tantalum penetrator munition alloys. Hazard indices representing total non-carcinogenic risk from all exposure pathways evaluated in this study were 0.051 and 0.062 for alloys WL-1 and NS, while alloy HD-17 had a total hazard index of 0.11. The higher hazard index for alloy HD-17 is solely attributable to exposure to copper consumed in vegetable and animal products produced test area soils. It is important to state that the hazard indices cited here reflect rather conservative and in some cases even extreme assumptions regarding metal availability and toxicity. If more site-specific data were available, the calculated hazard indices would undoubtedly be smaller

In MEPAS, metals taken up by plants which are later consumed by humans and animals are estimated using a soil-to-plant transfer factor specific to each contaminant. Because such transfer is in all liklihood influenced by site-specific geochemical and physical characteristics, the adequacy of the factor used to estimate exposure to copper in this study is not well known. If the Air Force wishes to proceed with further testing of penetrator munitions using alloy HD-17,

the soil-to-plant transfer factor could be investigated more closely to determine the accuracy and reliability of risk estimates based upon it.

Of the metals contained in alloys evaluated as part of this study, only nickel is potentially carcinogenic when inhaled. Excess individual lifetime cancer risk due to inhalation exposure to source area soils containing nickel was 4.3E-07, and therefore does not pose significant individual cancer risk. Although not a risk to individuals, large populations might experience risk if nickel concentrations in air near the source area were widespread enough to expose large numbers of individuals to nickel at these concentrations. Because of the relatively small area of the test site, and the low potential for suspension of soil particles from the site, such exposure is not possible, and so population exposure to nickel inhaled from source area soils is not considered a significant risk.

7.0 RECOMMENDATIONS

Consideration of the risk factors derived in this study for the testing of four different penetrator munitions at Test Area C-64 A suggests that any of the alloys could be used under current conditions without imposing significant human or ecologic risks. The potential risks associated with such testing are lowest for tantalum metal and highest for alloy HD-17. Alloys WL-1 and NS pose intermediate but acceptable risks. Because tantalum is less attractive from an economic point of view, alloys WL-1 and NS are favored for use in testing penetrator munitions.

If there is human occupation of the site in the future, either in a farm or residential scenario, the recommendation would be the same. However, in this case the use of alloy HD-17 in testing could pose a higher risk to the residents on the site. Further, the potential risk associated with the use of alloy WL-1 although allowable under current standards is greater than that associated with the use of alloy NS. Therefore, alloy NS is recommended as the preferred alloy for use in penetrator munitions testing.

8.0 CONCLUSION

The objectives of this project were to obtain data and reach conclusions on the potential environmental impacts of the testing of tantalum or tungsten alloy penetrator munitions at Test Area C-64A on Eglin AFB. These objectives have been achieved. The required experimental data on the leaching/breakdown behavior of potential penetrator alloys under site conditions have been obtained using immersion and drip methodologies. Data on the migration potential (i.e., sorption coefficients) of the metals in the alloys were also obtained.

The potential human risks associated with the testing of the different penetrator alloys at Test Area C-64A were estimated using the MEPAS computer models with appropriate inputs of physical, chemical, demographic, agricultural, and climatic data. The calculated risk factors indicate that any of the four alloys could be used in munitions testing at Test Area C-64A without significant human or ecologic risk. If testing occurred at the rate assumed in this study, and if humans were to inhabit the site in the future, the calculations suggest the use of alloy HD-17 in testing would pose the highest risk. This risk would result primarily from copper in the alloy being taken up by agricultural products grown and consumed on the site. Of the other alloys, the use of tantalum in testing would pose the smallest future risk while use of alloys WL-1 and NS would pose intermediate risks that are acceptable under current standards. The potential future risk associated with the use of alloy WL-1 may be somewhat larger than the risk associated with alloy NS.

Analysis of potential ecologic risks indicates no unacceptable risks will result from testing of tantalum and/or tungsten alloy penetrator munitions at Test Area C-64A.

9.0 REFERENCES

Aiken, G. R., McKnight, D. M., Wershaw, R. L., Humic Substances in Soil, Sediment, and Water, John Wiley & Sons, Toronto (1985).

Air Force Armament Laboratory (AFAL), 1976. Species diversity indices of the fish populations of streams draining selected test areas on Eglin AFB Reservation, Florida. AFATL-TR-76-145. Pp. 44.

Ambrose, A.M., P.S. Larson, J.F. Borzelleca, and G.R. Hennigan, Jr. 1976. Long-term toxicologic assessment of nickel in rats and dogs. *Journal of Food Science Technology* 13: 181-187.

Aulerich, R.J., R.K. Ringer, M.R. Bleavins, et al. 1982. Effects of supplemental dietary copper on growth, reproductive performance and kit surival of standard dark mink and the acute toxicity of copper to mink. *Journal of Animal Science* 55: 337-343.

Baes, C.F., III, R.D. Scharp, A.L. Sjoreen, and R.W. Shor. 1984. *A review and analysis of parameters for assessing transport of environmentally released radionuclides through agriculture.* ORNL-5786. Oak Ridge National Laboratory, Oak Ridge, TN.

Barr, D.E., Hayes, L.R., and T. Kwader. 1985. Hydrology of the Southern parts of Okaloosa and Walton Counties, Northwest Florida, with Special Emphasis on the Upper Limestone of the Floridan Aquifer. US Geological Survey Water-Resources Investigations Report 84-4305, 66 p.

Barr, D.E., Maristany A.R., and T. Kwader. 1981. Water Resources of Southern Okaloosa and Walton Counties, Northwest Florida. Northwest Florida Water Management District Water Resources Assessment 81-1, 41 p.

Bautista R. G., Wong M. M., Rare Earths, John Wiley & Sons, Toronto (1968).

Beyer, W. N., E. Connor, and S. Gerould. 1993. Estimates of soil ingestion by wildlife. *Journal of Wildlife Management* 58: 375-382.

Beyer, W. N. and C. Stafford. 1993. Survey and evaluation of contaminants in earthworms and in soils derived from dredged material at confined disposal facilities in the Great Lakes region. *Environmental Monitoring and Assessment* 24: 151-165.

Birge,W.J., 1978 Department of Energy, Symp. Ser.1977, 48, p.219, (1978).

Buck, J.W., G. Whelan, J.G. Droppo, D.L. Strenge, K.J. Castleton, J.P. McDonald, C. Sato, and G.P. Streile. 1995. *Multimedia Environmental Pollutant Assessment System (MEPAS): Application Guidance.* PNL-10395/UC-630, Pacific Northwest National Laboratory, Richland, Washington.

Cain, B.W. and E.A. Pafford. 1981. Effects of dietary nickel on survival and growth of mallard ducklings. *Archives of Environmental Contamination and Toxicology* 10: 737-745.

Camp, T.R., R.L. Meserve, 1974. <u>Water and its Impurities</u>. Second Edition, Dowden, Hutchinson & Ross Inc., Stroudsburg, Pennsylvania.

Chelius, J. "Use of Refractory Metals in Corrosive Environment Service," Mater. Eng. Quart., Aug, 1957, p. 57-59.

Cowher, C., G.E. Muleski, P.J. Englehart, and D.A. Gillette. 1985. <u>Rapid Assessment of Exposure to Particulate Emissions from Surface Contamination Sites</u>. EPA /600/8-85/002, Prepared for US Environmental Protection Agency, Office of Research and Development, Washington, D.C.

Detome, E., N. DeZoubov, M. Pourbaix, 1959. *Tungsten* in <u>Atlas of Electrochemical Equilibria in Aqueous Solutions</u>, Pergamon Press & CEBELCOR.

Droppo, J.G., and J.W. Buck. In press. *Multimedia Environmental Pollutant Assessment System (MEPAS): Atmospheric Pathway Formulations.* PNNL-11080, Pacific Northwest National Laboratory, Richland, Washington.

Droppo, J.G., et. al., 1989. *MEPAS Application Guidance Volume 1 – Users Guide.* PNNL-7616, Pacific Northwest National Laboratory, Richland, Washington.

Fairbrother F., The Chemistry of Niobium and Tantalum, Elsevier Publishing Company, New York (1967).

Fernald, E.A., Purdum, E.A., Anderson, J.R. Jr., and P.A. Kraft. 1992. <u>Atlas of Florida</u>. University of Florida Press, Gainsville, Florida. 280 p.

Fetter, C.W., 1988, <u>Applied Hydrogeology</u>, 2nd ed. McMillan Publishing Co., New York.

Flanders, R.B., "Try Tantalum for Corrosion Resistance," Chem. Eng., 17 Dec. 1979.

Gibalo, I. M., Analytical Chemistry of Niobium and Tantalum, Ann Arbor-Humphrey Science Publishers, Ann Arbor (1970): 49.

Hayes, L.R., and D.E. Barr. 1983. Hydrology of the Sand and Gravel Aquifer, Southern Okaloosa and Walton Counties, Northwest Florida. US Geological Survey Water-Resources Investigations Report 82-4110, 43 p.

Johnson, B.A., 1969, "Corrosion of Metals in Deionized Water at 38°C," Technical Memorandum TM X-1791, National Aeronautics and Space Administration, 10 March, 1969.

Johnston, R.H., and J.A. Miller. 1988. Region 24, Southeastern United States. In Back, W., Rosenshein, J.S., and P.R. Seaber, eds., Hydrogeology: Boulder, Colorado, The Geological Society of America, The Geology of North America, Volume O-2, p.229-236.

Kester, D.R., I.W. Duedall, D.N. Connors, R.M. Pytkowicz, 1968. Preparation of Artificial Seawater. Lymnology and Oceanography V.12, p. 176-179.

Lanyon, W.E. 1995. Eastern meadowlark. *The Birds of North America* 160: 1-23.

Laskey, J.W. and F.W. Edens. 1985. Effects of chronic high-level manganese exposure on male behavior in the Japanese quail (*Coturnix coturnix*). *Poultry Science* 64: 579-584.

Laskey, J.W., G.L. Rehnberg, J.F. Hein, and S.D. Carter. 1982. Effects of chronic manganese (Mn_3O_4) exposure on selected reproductive parameters in rats. *Journal of Toxicology and Environmental Health* 9: 677-687.

Lassner E. and R. Püschel, **Zur Chemie der Wässrigen Lösungen von Niob und Tantal**, Journal of the Less-Common Metals, **12**, 1967: 146-161.

Mehring, A.L., Jr., J.H. Brumbaugh, A.J. Sutherland, and H.W. Titus. 1960. The tolerance of growing chickens for dietary copper. *Poultry Science* 39: 713-719.

Meijer, A., Report in progress: Corrosion studies with metallic alloys in artificial preparations of sea water, surface water and ground water, 2019 Ridgecrest NE, Albuquerque NM, 87110 (May- August 1997).

Miessler, G. L., Tarr, D. A., Inorganic Chemistry, Prentice Hall, Englewood Cliffs (1991).

Miller, G.L., Tantalum and Niobium, Butterworths Scientific Publications, London (1959).

Miller, J.A., 1988. Coastal Plain Deposits. In Back, W., Rosenshein, J.S., and P.R. Seaber, eds., Hydrogeology: Boulder, Colorado, The Geological Society of America, The Geology of North America, Volume O-2, p.315-322.

Mineau, P., B.T. Collins, and A. Baril. 1996. On the use of scaling factors to improve interspecies extrapolation of acute toxicity in birds. *Regulatory Toxicology and Pharmacology* 24: 24-29.

Nagy, K.A. 1987. Field metabolic rate and rood requirement scaling in mammals and birds. *Ecological Monographs* 57: 111-128.

National Academy of Sciences, 1973, Manganese, Committee on Biologic Effects of Atmospheric Pollutants.

National Academy of Sciences, 1977, Copper, Committee on Biologic Effects of Atmospheric Pollutants.

National Atmospheric Deposition Program/ National Trends Network, 1991. Precipitation-weighted means, Colorado State University, Fort Collins, Colorado.

Orlov, D. S., Humus Acids of Soils, Oxonian Press, New Delhi (1985).

Phelan, J.P. and R.H. Baker. 1992. Optimal foaging in *Peromyscus polionotus*: the influence of item-size and predation risk. *Behaviour* 124: 95-109.

Pourbaix, M. et al., 1966. Atlas of Electrochemical Equilibria In Aqueous Solutions, (Translated from the French by James Franklin), Pergamon Press & CEBELCOR, Brussels, Belgium. Reimpression by NACE and CEBELOR.

Prager, J.C., 1995, Environmental Contaminant Reference Data Book, Van Nostrand Reinhold, New York.

Quarrell, A. G., Niobium, Tantalum, Molybdenum, and Tungsten, Elsevier Publishing Company, New York (1960).

Ringelman, J.K., M.W. Miller, and W.F. Andelt. 1993. Effects of ingested tungsten-bismuth-tin shot on captive mallards. *Journal of Wildlife Management* 57: 725-732.

Registry of Toxic Effects of Chemical Substances (RTECS). 1998. *On-line*.

Sample, B.E., D.M. Opresko, and G.W. Suter II. 1996. *Toxicological Benchmarks for Wildlife: 1996 Revision*. ES/ER/TM-86/R3. Risk Assessment Program, Health Sciences Research Division, Oak Ridge National Laboratory, Oak Ridge, TN.

Schussler, M., C. Pokross, 1985. Corrosion of Tantalum, in Metals Handbook, Ninth Edition, V. 13, Corrosion, ASM International, Metals Park Ohio p. 725-739.

Seiler, H.G., H. Sigel, 1988. Handbook on Toxicity of Inorganic Compounds. Marcel Dekker Inc, New York.

Sittig, M., 1985. Handbook of Toxic and Hazardous Chemicals and Carcinogens, 2nd ed., Noyes Publications, Park Ridge, New Jersey.

Sittig, M., 1994, World-wide Limits for Toxic and Hazardous Chemicals in Air, Water and Soil, Noyes Publications, Parkridge, New Jersey.

Smith, I.C., B.L. Carson, 1981. Trace Metals in The Environment Volume 6- Cobalt an Appraisal of the Environmental Exposure. Ann Arbor Science Publisher, Inc. Ann Arbor, Michigan.

Stephen, C.E., D.I. Mount, D.J. Hansen, J.H. Gentile, G.A. Chapman, W.A. Brungs. 1983. *Guidelines for deriving numerical national water quality criteria for the protection of aquatic life and its use.* US Environmental Protection Agency, Environmental Research Laboratory, Duluth, MN.

Streile, G.P., K.D. Sheilds, J.L. Stroh, L.M. Bagaasen, G. Whelan, J.P. McDonald, J.G. Droppo, and J.W. Buck. In press. *Multimedia Environmental Pollutant Assessment System (MEPAS): Source-Term Release Formulations.* Pacific Northwest National Laboratory, Richland, Washington.

Strenge, D.L., and A.R. Chamberlain. 1995. *Multimedia Environmental Pollutant Assessment System (MEPAS): Exposure Pathway and Human Health Impact Assessment Models.* Pacific Northwest National Laboratory, Richland, Washington.

Strenge, D.L., and S.R. Peterson. 1989. *Chemical Data Bases for the Multimedia Environmental Pollutant Assessment System (MEPAS): Version 1.* PNNL-7145, Pacific Northwest National Laboratory, Richland, Washington.

Stumm, W., Chemistry of the Solid-Water Interface, John Wiley & Sons, Toronto (1992).

Suter, G.W. 1993. *Ecological Risk Assessment.* Lewis Publishers, Boca Raton, FL.

Suter, G.W. 1996. Toxicological benchmarks for screening contaminants of potential concern for effects on freshwater biota. *Environmental Toxicology and Chemistry* 15: 1232-1241.

Suter, G.W., II, B.E. Sample, D.S. Jones, T.L. Ashwood, and J.M. Loar. 1995. *Approach and strategy for performing ecological risk assessments for the US Department of Energy's Oak Ridge Reservation: 1995 Revision.* ES/ER/TM-33/R2. Risk Assessment Program, Health Sciences Research Division, Oak Ridge National Laboratory, Oak Ridge, TN.

Trapp, H. Jr., C.A. Pascale, and J.B. Foster, 1977. Water Resources of Okaloosa County and Adjacent Areas, Florida, US Geological Survey, Water Resources Division, Tallahassee, Florida.

Trethewey, K.R., J. Chamberlain, 1988. Corrosion for Students of Science and Engineering. Longman Group UK Ltd, England.

US Air Force (1995), Appenix H: Soils and Geology, Final Eglin AFB Environmental Baseline Study Recources Appendices.

US Air Force (1995), Appenix I: Water Resources, Final Eglin AFB Environmental Baseline Study Recources Appendices.

US Air Force (1995), Appenix J: Air Quality, Final Eglin AFB Environmental Baseline Study Recources Appendices.

US Air Force (USAF). 1972. *Animal survey studies of Test Area C-52A, Eglin AFB Reservation, Florida.* AFATL-TR-72-72. Air Force Armament Laboratory, Elgin Air Force Base, FL.

US Air Force (USAF). 1976a. *Aquatic baseline survey of selected test areas on Elgin AFB Reservation, Florida.* AFATL-TR-76-4. Air Force Armament Laboratory, Elgin Air Force Base, FL.

US Air Force (USAF). 1976b. *Species diversity indices of the fish populations of streams draining selected test areas on Elgin AFB Reservation, Florida.* AFATL-TR-76-145. Air Force Armament Laboratory, Elgin Air Force Base, FL.

US Air Force (USAF). 1983. *Benthic macroinvertebrates of Bull Creek and Ramer Branch, Elgin AFB Reservation, Florida.* AFATL-TR-83-24. Air Force Armament Laboratory, Elgin Air Force Base, FL.

US Air Force, 1995. Final Eglin AFB Environmental Baseline Study Resource Appendices. Air Force Development Test Center, Eglin AFB, FL.

US Department of Health and Human Services, 1993. Toxicological Profile for Nickel.

US Environmental Protection Agency, 1988. *Hazardous Substances Priority List, Toxicological Profiles; Second List.* Federal Register, 41280.

US Environmental Protection Agency (USEPA). 1988. *Recommendations for and documentation of biological values for use in risk assessment.* EPA/600/6-87/008. US Environmental Protection Agency, Office of Criteria and Assessment, Cincinnati, OH.

US Environmental Protection Agency (USEPA). 1989a. *Risk assessment guidance for superfund, Volume I. Human Health Evaluation Manual (Part A).* EPA/540/1-89/002. US Environmental Protection Agency, Office of Emergency and Remedial Response, Washington, DC.

US Environmental Protection Agency (USEPA). 1989b. *Risk assessment guidance for superfund, Volume II. Environmental evaluation manual.* US Environmental Protection Agency, Office of Emergency and Remedial Response, Washington, D.C. EPA/540/1-89/001.

US Environmental Protection Agency (USEPA). 1992. *Framework for ecological risk assessment.* US Environmental Protection Agency, Risk Assessment Forum, Washington, DC. EPA/630/R-92/001.

US Environmental Protection Agency (USEPA). 1993. *Wildlife exposure factors handbook, Volume I of II.* EPA/600/R-93/187a. US Environmental Protection Agency, Office of Research and development, Washington, DC.

US Environmental Protection Agency (USEPA). 1996. *Ecotox thresholds.* EPA/540/F-95/038. Eco Update Intermittent Bulletin 3(2): 1-12. US Environmental Protection Agency, Office of Solid Waste and Emergency Response, Washington, DC.

US Environmental Protection Agency (USEPA). 1998. *Proposed guidelines for ecological risk assessment.* EPA/630/R-95/002B. US Environmental Protection Agency, Risk Assesment Forum, Washington, DC.

US Environmental Protection Agency (EPA). 1988. Superfund Exposure Assessment Manual. OSWER Directive 9285.5-1, Office of Remedial Response, Office of Solid Waste and Emergency Response, US Environmental Protection Agency, Washington, D.C.

US Environmental Protection Agency (EPA). 1995. Compilation of Air Pollutant Emission Factors. AP-42, Section 13.2, Fugitive Dust Sources, Office of Air Quality Planning and Standards, Research Triangle Park, North Carolina.

Vecchioli, J., Tibbals, C,H., Duerr, A.D., and C.B. Hutchinson. 1990. Ground-Water Recharge in Florida: A Pilot Study in Okaloosa, Pasco, and Volusia Counties. US Geological Survey Water-Resources Investigations Report 90-4195, 16 p.

Venugopal, B. and T.D. Luckey. 1978. *Metal toxicity in mammals. Volume 2: Chemical toxicity of metals and metalloids.* Plenum Press, New York, NY. 409 pp.

Verbal communication with Dr. P. Brassard, McMaster University, November 1997.

Watkin, G.E. and M.E. Stelljes. 1993. A proposed approach to quantitative assess potential ecological impacts to terrestrial receptors from chemial exposure. Pages 422-439. In: J.W. Gorsuch, F.J. Dwyer, C.G. Ingersoll, and T.W. LaPoint (eds.), *Environmental toxicology and risk assessment: 2nd volume.* Special Technical Publication 1216. American Society for Testing and Materials, Philadelphia, PA.

Whelan, G., and J.P. McDonald. 1996a. *Multimedia Environmental Pollutant Assessment System (MEPAS): Surface Hydrology Formulations.* PNNL-11178, Pacific Northwest National Laboratory, Richland, Washington.

Whelan, G., and J.P. McDonald. 1996b. *Multimedia Environmental Pollutant Assessment System (MEPAS): Overland Pathway Formulations.* PNNL-11177, Pacific Northwest National Laboratory, Richland, Washington.

Whelan, G., and J.P. McDonald. 1996c. *Multimedia Environmental Pollutant Assessment System (MEPAS): Riverine Pathway Formulations.* PNNL-11176, Pacific Northwest National Laboratory, Richland, Washington.

Whelan, G., J.P. McDonald, and C. Sato. 1996d. *Multimedia Environmental Pollutant Assessment System (MEPAS): Groundwater Pathway Formulations.* PNNL-10907/UC-630, Pacific Northwest National Laboratory, Richland, Washington.

Whelan, G., Buck, J.W., Strenge, D.L., Droppo, J.G., Hoopes, B.L., and R.J. Aiken. 1992. *Overview of the Multimedia Environmental Pollutant Assessment System (MEPAS).* Hazardous Waste and Hazardous Materials, Vol. 9: Number 2, pp 191-208.